1-1-2002

Molecular and nanoscale reinforcement of polymers.

Adam S. Zerda
University of Massachusetts Amherst

MOLECULAR AND NANOSCALE REINFORCEMENT OF POLYMERS

A Dissertation Presented

by

ADAM S. ZERDA

Submitted to the Graduate School of the
University of Massachusetts Amherst in partial fulfillment
of the requirements for the degree of

DOCTOR OF PHILOSOPHY

September 2002

Polymer Science & Engineering

MOLECULAR AND NANOSCALE REINFORCEMENT OF POLYMERS

A Dissertation Presented

By

ADAM S. ZERDA

Approved as to style and content by:

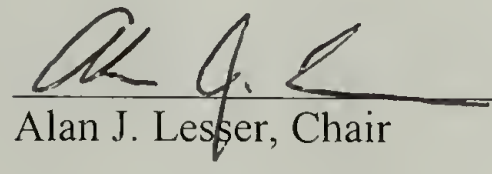

Alan J. Lesser, Chair

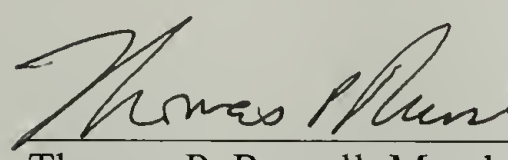

Thomas P. Russell, Member

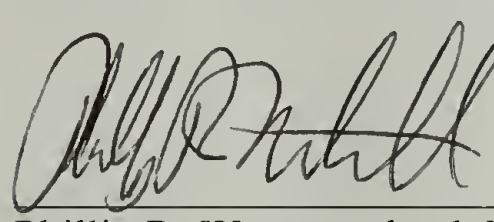

Phillip R. Westmoreland, Member

Thomas J. McCarthy, Department Head
Polymer Science & Engineering

DEDICATION

For my parents, who challenge me;

for my brother, who motivates me;

for my sister, who inspires me.

ACKNOWLEDGEMENTS

A number of people must be aeknowledged for their numerous, and varied, eontributions to the eompletion of this dissertation.

First and foremost, my parents for instilling in me the drive to sueeeed and the eagerness to learn. My father, as an aeademie inspiration, and my mother, as a spiritual ground, form the basis through whieh I approaeh not only my educational eareer but life in general. My brother, Miehal, provides a friendly eompetitiveness and has done his best to remind me of my motivations. His lamentations of being "the unedueated one" in the family have always been happily aeeepted as eomedie relief. And finally, my sister, Basia, who appears to be slowly heading down this road herself. She has kept me mindful of my early enthusiasm in times of frustration.

My advisor, Professor Alan Lesser, has been an ineredible person to work with and to work for. He has been an advisor in every sense of the word, guiding my research endeavors, not direeting them. This freedom to explore new areas has lead to the investigation of a number of interesting tangents. Although often of varying degrees of sueeess, I feel these avenues might have remained unexplored in different environments. These experienees have only added to the value of my education and I am very grateful for them! My other eommittee members, professors Tom Russell and Phillip Westmoreland, have also been very helpful, in terms of both time dedieated and guidance given. Professor Russell was one of the major reasons I applied to and joined the Polymer Seienee and Engineering department in the first plaee. I must also point out professor Westmoreland's attention to the details of this dissertation. I truly believe that

his comments have not only made this dissertation a better-written document, but also contributed to making me a more polished writer.

As always, the research in this dissertation could not have been completed without financial support. Most of the work has been conducted under the support of the CUMIRP program, specifically Clusters C and F. The many members of these Cluster groups are therefore acknowledged. Specifically, I would like to graciously thank my early lab partner, Huiqing Zhang, for the many discussions I have had with her on the topic of fire retardation and characterizations thereof. Additionally, the fellowships, which I received from the Society of Plastics Engineers PMAD and Composites divisions, helped validate my progress and instill confidence during the final stretch.

Finally, I must mention the people responsible for the many fun memories of graduate life. Particularly: Kathryn Wright, my officemate, with whom I have been able to work, debate, study and have many a full-filled lunch; Richard Nause, my roommate and great friend, responsible for many of my extracurricular adventures here in Amherst; and Terry Caskey, whom I will sorely miss for the academic help, social excitement and many philosophical discussions he has always made available to me. I will likely miss these friends the most!

ABSTRACT

MOLECULAR AND NANOSCALE REINFORCEMENT OF POLYMERS

SEPTEMBER 2002

ADAM S. ZERDA, B.S., TEXAS CHRISTIAN UNIVERSITY

M.S., UNIVERSITY OF MASSACHUSETTS AMHERST

Ph.D., UNIVERSITY OF MASSACHUSETTS AMHERST

Directed by: Professor Alan J. Lesser

The reinforcement of polymers using additives of dimensions below one micrometer is presented: those acting at the molecular and nanometer scales. This thesis will describe new additives and morphologies exhibiting high levels of mechanical reinforcement. It is the focus of this work to chronicle the range of physical and material properties that are altered upon inclusion of these modifiers. Additionally, this thesis will establish how these physical-property changes affect the mechanical behavior of the resulting composite.

In the area of molecular reinforcement, a new class of additive, the organophosphate, is shown here to enhance modulus and yield strength in epoxy polymers once cured. Initially, the effect on the physical and thermal properties of the polymer system is investigated as a function of additive molecular weight, solubility, and

concentration. The altered properties include T_g, density, thermal stability and initial epoxy viscosity. The mechanical properties of the modified epoxy are demonstrated to be a result of the physical changes made to the matrix polymer through the addition of the organophosphorous additive. By increasing the density of the polymer and reducing or eliminating sub-T_g relaxations, the modulus and yield strength of the polymer can be greatly enhanced. These property changes are investigated in a variety of epoxy polymer systems in order to elucidate the effects of both the additive and polymer chemical structure on final mechanical properties.

Polymer modification using nanometer-scale additives and modifiers has been the focus of intense study recently. Heretofore, these studies have focused on the exfoliated, or delaminated, clay morphology to impart the property enhancements, effectively isolating the particulates within the matrix. This thesis focuses on polymer modification at the nanometer scale such that the added clays interact and positively change the composite fracture toughness. By introducing this clay-clay interaction, modulus and strength can be increased together with the toughness. Such a property combination is highly desirable, as most toughening agents reduce modulus and strength. Initially, the intercalated morphology is investigated in an epoxy system. Additionally, new routes to synthesizing intercalated morphologies of clay concentrations approaching 50 % are developed.

TABLE OF CONTENTS

LIST OF TABLES

Table Page

LIST OF FIGURES

CHAPTER 1

INTRODUCTION

This research investigates the effects of reinforcement at the nano- and molecular scales on the basic physical and mechanical behavior of glassy, amorphous polymer systems. In order to appreciate how polymer reinforcement at these length scales may affect material properties, a brief review of macro- and microscale reinforcement is presented, addressing specifically the effect of particle size scale in dictating material properties. Duc to the wide variety of approaches to sub-micron reinforcement, the current work on intercalated silicate nanocomposites and phosphate antiplasticizers is differentiated from ongoing efforts in related fields, including exfoliated silicate nanocomposites and fortification of linear polymers.

Modification of polymeric materials through additives and fillers is the predominant method by which polymer manufacturers tailor behavior to fit sometimes complex material requirements. Although synthetically altering the nature of the polymer structure can result in new materials of interesting properties, this method is unattractive due to the high costs of new monomer production, changeover, etc. New products utilizing existing polymers, however, continue to be introduced by taking advantage of the fact that aesthetic, thermal, mechanical and other material properties of polymers can easily be altered through the use of additives.

1.1 Length scales in polymer reinforcement

Microscale reinforcement of materials through fillers and composites has been a focus of intense academic and industrial interest for decades.[1] These interests focus on

understanding the mechanisms for synergistic property enhancement to aide in the development of new polymer composites or blends. For example, the use of coupling agents in enhancing adhesion, and of diblock and triblock copolymers in attaining compatibility, grows out of this increased understanding. The limitations of synergistic reinforcement must, however, also be recognized. These include shape and geometry, the structure of the reinforcement and the size scale over which it acts. It is well known, for example, that the lay-up architecture of a polymer-matrix composite dictates the loading conditions to which such a material can be exposed. This allows engineers to predict the conditions under which the composite is expected to fail.[2] Fiber-reinforced composites are designed such that tensile loads are carried primarily by the fiber component of the composite (i.e. carbon-fiber reinforced epoxy). Under compressive loading, however, the composite fails, or yields, as the fibers cooperatively microbuckle.[3] This behavior demonstrates the existence of a matrix-dominated response under compressive loading, and must be addressed when designing materials. In reinforced polymers, filler dimension can also dictate the range of applicability.

Microscale composites are, generally, those where the filler material is of the size scale of one micrometer. At these dimensions, continuum methods can be used to model mechanical behavior based on the properties of individual components (provided the properties of the constituents and interfacial adhesion can be measured at this length scale). Continuum treatments of composites rely on the concept of effective homogeneity in heterogeneous materials at length scales typically one or two orders of magnitude greater than the scale of the inhomogeneity. Effectively, the properties of the composite material are taken as an average of the two or more components present within

the body while accounting only for parameters, which are thought to be implicitly important. End effects in chopped-fiber reinforcement are an example of a case where the continuum approach predicts declining composite properties because of decreasing fiber aspect ratio. Other important parameters not discussed here include interfacial adhesion and anisotropy. Of course, there does exist a size scale of the inhomogeneity which cannot be treated as statistically additive. When the inclusions decrease in size below a critical dimension, the mechanics of deformation can change significantly. This can occur when the additive or filler fundamentally alters the properties of the constituent members.

Recently, additives of dimensions closer to the molecular scale have been developed. Composites made from these materials have demonstrated enhanced properties. The mechanics of reinforcement at these length scales, however, have yet to be fully investigated. Although it is known that nanoscale materials and molecular additives exist which can enhance modulus, strength or fracture toughness, it is unknown whether continuum-level treatments of these materials apply. Rather, it is understanding how these materials behave close to the molecular level in prescribing material properties which is important.

As alluded to above, reinforcing mechanisms apply only over some defined length scale. In appreciating the limits imposed by such critical length scales, a review of toughening approaches is presented. Here, the impact of critical length scales is well demonstrated. Materials incorporating nanoscale reinforcement often fall outside of the length scales responsible for increased toughness. They may, however, be designed such that these limitations are overcome (Section 1.4.2).

1.2 Toughening mechanisms

Epoxy thermosets are commonly used in composite applications where the tensile properties are provided to the composite through the use of filler materials. Examples include carbon fiber, glass bead and chopped fiber composites. Here, the matrix resin encases the modifier, providing shear and compressive performance. Epoxy thermosets have excellent thermal stability and provide good compressive strength and stiffness. Their impact strength, however, typically requires modification, as a well-known inverse relationship between toughness and strength exists. In applications where the toughness or impact strength is of critical importance, toughening of the polymer is typically achieved through the use of elastomeric particles composed of carboxyl-terminated butadiene-acrylonitrile (CTBN) rubber. A number of other toughening mechanisms for epoxy have also been identified and the most important of these are described below. These mechanisms include 1) crack bridging, 2) micro cracking, 3) shear banding and 4) crack-trajectory deflection.[4] All of these toughening methods act over well-defined length scales. If the toughening agent, such as CTBN, is made smaller or larger than this critical scale, the toughening mechanism breaks down. Each of the toughening mechanisms will be briefly discussed with emphasis on particle size effects. A trait common to all of these mechanisms, however, is the net increase in energy required to propagate the crack. This is the fundamental philosophy behind fracture toughening: by increasing the total energy consumed upon failure, toughening can be achieved.

The *crack-bridging* mechanism (Figure 1.1) relies on large particle sizes capable of bridging or spanning the crack and is an example of a crack-wake mechanism. The crack-wake region includes those areas active behind the propagating crack tip. Crack-

bridging particles can be either chopped fiber or large rubber particles through which the crack is allowed to propagate. These materials effectively stitch the crack, limiting the crack-opening displacement at a given load. Particle sizes greater than 25 μm are typically required for this type of mechanism to occur. Crack bridging is often observed together with cavitations and shear banding mechanisms in epoxies containing polydisperse rubber-particle distributions.[5]

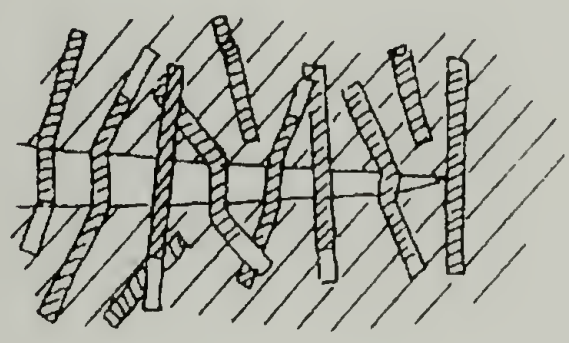

Figure 1.1 Crack-bridging mechanism.

Microcracking in front of the crack tip results in the creation of new surface area. This additional energy consuming mechanisms requires a greater energy input for crack propagation. Microcracking occurs in the process zone, which is the region active in front of the main crack. Energy is consumed in front of the main crack tip through the formation of microcracks or crazes within the process zone. Process-zone mechanisms rely on means of increasing the amount of material which is involved in fracture. Microcracks can interact cooperatively, leading to an overall reduction of the stress intensity in front of the main crack and requiring greater stresses for propagation. This reduction of the stress-intensity field further reduces the potential for crack growth. Microcracking can be initiated through the use of additives which act as crack-initiation sites. Here, small inclusions (< 10 μm) have been demonstrated to act as nucleating agents for microcrack formation.

Shear banding at the crack tip predicts an increased plastic deformation zone in front of the crack tip.[6] Shear banding (Figure 1.2) occurs due to a reduction in the yield stress of the material in front of the crack tip allowing for greater shear deformation. As a result of this shear deformation, more energy is required to propagate the main crack. Shear banding relies on small interparticle distances, ensuring particle-particle interaction.[7] Particle cavitation has also been discussed as an important step in toughening through shear banding.[8] Although it has been argued that the creation of new surface area during particle cavitation would lead to energy consumption, it is rubber-particle dilatation that initiates shear-band formation. This occurs by allowing the material to first flow and then form shear bands. The critical length scales (0.1 μm – 50 μm) required for shear-band formation are a result of the rubber-particle cavitation requirement. The lower bound (approximately 0.1 μm) defines the smallest rubber particle which is capable of cavitation. Rubber particles smaller than 0.1 μm are inefficient toughening agents because they exhibit cavitation resistance.[9] At these length scales, the strain energy within the rubber particles is insufficient to overcome the energy required to create new surface area.

The upper bound for cavitation/shear-band formation is dictated by the size of the process zone of the matrix material.[10] The size of the plastic zone can be estimated to be:

$$r_p = \frac{1}{6\pi}\left(\frac{K_{IC}}{\sigma_y}\right)^2 \qquad \text{Eq. 1.1}$$

where r_p is the radius of the plastic zone, σ_y is the yield strength of the material and K_{IC} is the critical stress-intensity factor, or fracture toughness, with units of $MPa\cdot m^{1/2}$. For a typical, glassy epoxy, the plastic zone size is approximately six μm. Particles larger than

the size of the plastic zone are not completely exposed to the hydrostatic stresses present in front of the crack tip and therefore do not cavitate. Large rubber particles can only toughen the polymer through a crack-bridging mechanism, described above, which is less effective than cavitation/shear banding.

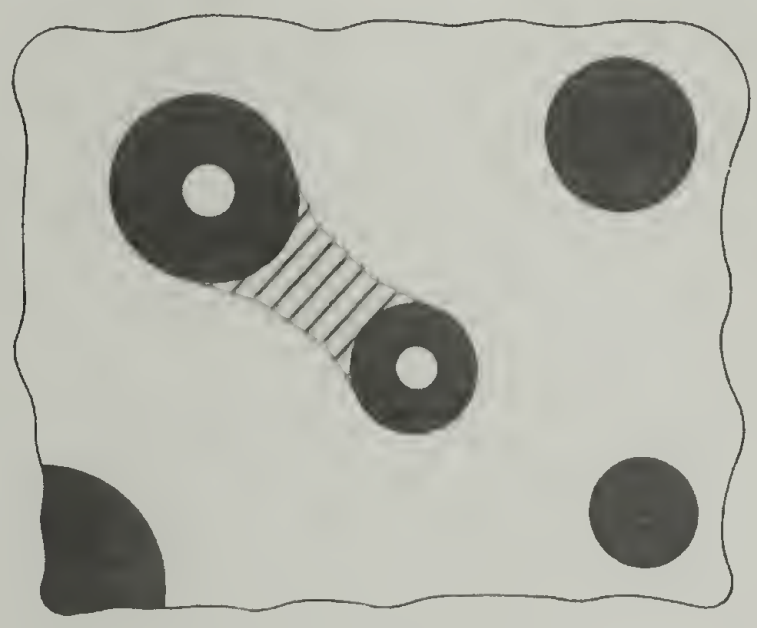

Figure 1.2 Shear-banding mechanism.

Finally, *crack deflection* has been observed for fillers which alter the trajectory of a propagating crack (Figure 1.3). The increase in toughness is a result of crack opening in mode II rather than mode I. As most polymeric materials are more resistant to mode II crack opening, the result is an increase in the overall critical stress-intensity factor, K_C. This mechanism does not rely on particle size but rather on spacing and distribution leading to crack deflection. Nevertheless, the additional surface area, which is generated through tortuous crack propagation, leads to materials with higher apparent toughness.

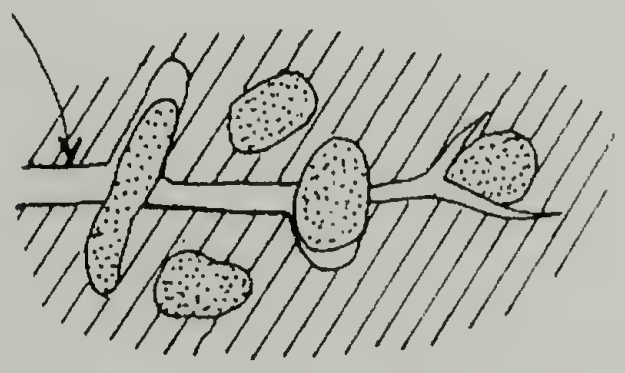

Figure 1.3 Crack deflection around particles.

The impact of length scale in polymer reinforcement is thus illustrated using the case of toughening in epoxy. Other areas of polymer reinforcement demonstrating the importance of understanding appropriate length scales include modulus reinforcement through the use of chopped fibers and creation of polymer blends exhibiting single glass transition temperatures. In the latter case, incomplete blending of two polymers results in microphase separated materials of undesired properties. When introducing additives which explore reinforcement at novel length scales, the effect of those length scales will obviously be of great interest. The remainder of this chapter focuses on nanoscale and molecular reinforcement of polymers, multiple orders of magnitude below the lengths described above.

1.3 Molecular fortification

Molecular reinforcement, or fortification, requires an understanding of the chemical and physical properties of polymers at the molecular scale. The fundamental idea of molecular fortification is based on physical interactions between two polymers, or between polymer and additive, altering the mechanical response of the system on a continuum level. One example of molecular reinforcement is the incorporation of specific functionalities along the polymer backbone to generate an inherent stiffness within the polymer. This is an example of internal fortification, since the properties of the polymer are chemically altered. Liquid-crystalline polyamides, such as Kevlar, demonstrate how molecular stiffness of the backbone leads to high tensile modulus. Incorporating functionalities into a polymer, which generate additional internal bonding, can also lead to enhanced mechanical properties. Examples here are hydrogen bonding in cellulose and polar-polar interactions between nitrile groups in cyanoacrylates.[11,12]

Fortification of polymers through external means includes the blending of dissimilar polymers with the goal of achieving a hybrid product of improved overall performance. Blending poly(vinyl chloride) with chlorinated polyolefins to enhance impact strength is an industrially important example. Hundreds of others exist. Recently, fortification through the addition of molecular additives has been described.[13,14] Because molecular additives already enjoy widespread use in polymer modification, expanding the role of these diluents, plasticizers or stabilizers into mechanical reinforcement would render their use more diverse. However, a fundamental understanding of the mechanisms for such molecular reinforcement should be formed to better predict this behavior.

1.3.1 Antiplasticization

At low concentrations, some plasticizers have been shown to increase, rather than decrease, the stiffness and strength of polymers. Such additives are termed antiplasticizers. Well known in thermoplastic polymers such as polycarbonate (PC),[15-18] polystyrene[19] and poly(vinyl chloride) (PVC),[20-22] antiplasticization has also been demonstrated in thermoset epoxy resins with a variety of additives.[23-25] The antiplasticization effect, so called because the mechanical response is opposite that of a plasticized material while still exhibiting a depressed glass transition temperature, has been related to reduced mobility on the molecular scale. By reducing molecular mobility, the polymer is effectively stiffened at a molecular level. In order to impart this molecular-level stiffening to the polymer, antiplasticizers for PVC and PC have been shown to require 1) strong interactions between polymer and additive and 2) inherent stiffness of the antiplasticizer.[14] These criteria ensure cooperative action between the additive and resin. Using dynamic mechanical methods, the reduction in mobility has

been attributed to an amplitude decrease in the sub-T_g β-relaxation peak of a number of polymers.[20,26,27] This decrease in sub-T_g relaxations corresponds with increased stiffness of the backbone and is manifested by enhanced mechanical properties. Although the storage modulus is not significantly affected through antiplasticization, the relaxations in the loss-modulus spectrum are decreased. The complex modulus is a function of both the storage, E', and loss, E'', moduli:

$$E = E' + iE'' \qquad \text{Eq. 1.2}$$

As a result, the mechanical properties measured statically are observed to increase.

In the case of antiplasticized amine-cured epoxy, the β-relaxation affected by the presence of the antiplasticizer is related to the mobility of the hydroxypropylether group, $[OCH_2CH(OH)CH_2]$, in the polymer backbone. It has been postulated that antiplasticization is, therefore, a result of strong hydrogen bonding between the hydroxyl moiety in the epoxy and the antiplasticizers, all of which contain hydrogen-bonding acceptors.

The increase in mechanical properties is also usually accompanied by an increase in the density of the material. This increase is strongly related to the reduction in molecular mobility.[28-31] The densification which is observed is often greater than that predicted by simple additivity of the densities of the two component systems. By binding with the hydroxypropylether group, the antiplasticizer reduces the free volume of the polymer. It is this reduction of the free volume that results in the increase in density of the mixture. The densification is often greater than that predicted by a simple rule of mixtures. Vrentas et al.[30] present a model predicting the density of antiplasticized resins based on the additive density of each phase in the equilibrium liquid state. At its core,

this model assumes that the density deviation from simple additivity is a function of the glass transition temperature mismatch between the polymer and additive. This mismatch allows the system to form a non-equilibrium mixture below the T_g of the pure polymer, resulting in a lower specific volume of the polymer-additive mixture. In the case of epoxy, the equilibrium liquid density is taken as the density of the polymer at T_g. By then extrapolating the density at T_g to the test temperature using a coefficient of thermal expansion term, the density of the mixture can be predicted. The thermal expansion coefficient of the pure polymer and the polymer-additive mixture are assumed to be equal. The proposed models can then be used to estimate the mode of polymer densification in antiplasticized systems.

Currently, antiplasticization is used within industry as a method for enhancing tackiness in adhesives. Presumably, by introducing an antiplasticizer into a rubbery polymer and thereby enhancing its modulus and strength, the adhesion can be enhanced. In applications where plasticization (to enhance ductility and impact strength) is the desired result, as in PVC and PC, antiplasticization is viewed as an undesired property. As a result, the concentration range over which antiplasticization occurs is characterized by a "concentration threshold." This concentration represents a minimum plasticizer content required to result in reduced modulus and strength.[32] In applications where high modulus and strength are sought, antiplasticization sees potential applicability. Epoxy, particularly as a matrix resin, can be such an application.

Antiplasticizers for epoxy have been developed recently based on the understandings gleaned from work in PVC and PC. The example from Daly et al.[24] (Figure 1.4) represents the chemical architecture generally required for efficient

antiplasticization, including compatibility with the polymer backbone and some degree of stiffness. High levels of enhancement with this complicated additive have been achieved. The work in the current study is based on initial observations of antiplasticization for epoxy without, seemingly, requiring the types of architectures that have previously been alluded to.[33] Dimethyl methyl phosphonate is a small, molecular additive which, in addition to imparting flame-retarding potential and improved processibility to the epoxy, enhances the modulus and strength of the matrix as a function of the additive concentration. The dimethyl methyl phosphonate antiplasticizer seemingly relies only on strong interactions with the polymer backbone to impart enhanced strength and stiffness. This observation raises the question of true chemical requirements for antiplasticization.

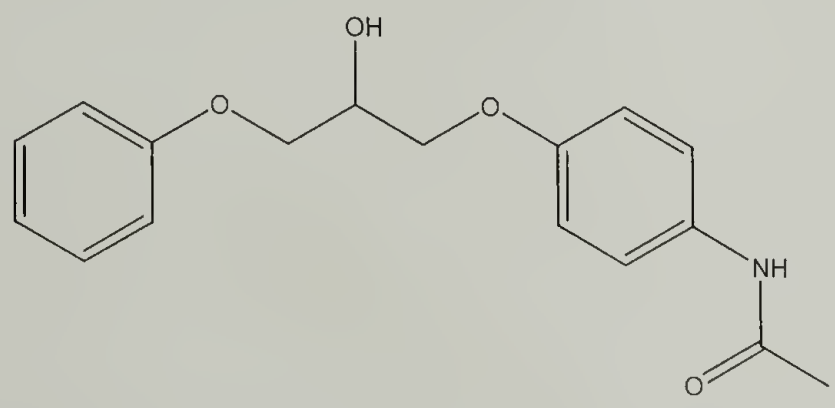

Figure 1.4 Reaction product of 1,2-epoxy-3-phenoxypropane and 4-hydroxy-acetanilide; an antiplasticizer for epoxy.

This study, therefore, is concerned with examining the molecular architectures leading to antiplasticization in crosslinked epoxy, believing them to be different from those required for linear polymers such as PVC and PC. Understanding the mechanism of antiplasticization in crosslinked epoxy, one can perhaps optimize mechanical enhancements through molecular fortification.

1.4 Silicate nanocomposites

Within the last decade, the emergence of nanotechnology has excited both academic and industrial institutions with promise of new material advances. Although the field of nanotechnology expands to a variety of applications including electrical and optical materials, the development of new composite materials utilizing nanometer-scale fillers has raised questions as to their mechanism of reinforcement. Research is currently focusing on the exfoliated morphology, which has been demonstrated to impart good thermal, mechanical, and barrier properties at low filler concentrations. Our interest lies with the intercalated morphology, and the opportunity to enhance fracture toughness through the use of this structure.

Polymer nanocomposites are defined as containing filler with at least one dimension in the nanometer scale. A common nanoscale filler for such applications is a surface modified aluminosilicate clay such as montmorillonite. Montmorillonite is a naturally occurring aluminosilicate with the general structure $Na^{+}_{0.86}[Mg_{0.86}Al_{3.14}Si_{8.0}O_{20}H_4]^{-}$. These clays form as platelets, with individual sheets measuring approximately 250 nm in length and 10 Å in thickness. During their natural formation, defects in the crystal structure of the clays result in the formation of a net anionic surface charge. These defects are the result of Mg^{2+} substitution for Al^{3+} in the crystalline lattice. The resulting charge is then countered through the adsorption of surface cations such as sodium and calcium. The dry silicates tend to stack together, but can be exfoliated, or delaminated, by using appropriate solvents. Upon delamination, materials such as polymers can be made to enter into the silicate gallery spacing. The unmodified clays are hydrophilic and to facilitate their incorporation into organic

polymers, the surface must be modified in some manner. This modification is typically achieved through an interchange of the surface cations with alkyl ammonium surfactants, also of a positive charge. By suspending the clays in water and introducing an excess of the alkyl ammonium salt, the clay surface is rendered organophilic. The alkyl ammonium salts reduce the enthalpic barrier to polymer intercalation by rendering the clays organophilic. Likewise, by using long alkyl chains, the d-spacing of the clays can be increased, reducing the entropic penalty of polymer confinement. The initial d-spacing of the organically-modified layered silicates can be controlled by virtue of the surfactants bound to the surface. For example, using a $C_{12}H_{25}NH_3Cl$ surfactant salt results in a d-spacing of 14 Å. Adding six methylene groups, as in $C_{18}H_{37}NH_3Cl$, results in a d-spacing of 18 Å. Of course, this change does not significantly alter the surface enthalpy.

Exfoliated nanocomposite materials require careful synthetic or processing routes to achieve high degrees of dispersion. This is due to the large entropic cost of polymer confinement. However, it is this complete dispersion which leads to efficient improvements at low clay concentrations. The intercalated morphology requires less rigorous production techniques and is therefore more easily manufactured. More importantly, we believe that the intercalated, silicate nanocomposites have the potential of providing much improved mechanical properties unattainable via the exfoliated systems, namely high degrees of toughness. As described in Section 1.1.1, toughening mechanisms in glassy polymers are limited in dimension. The intercalated morphology allows for some enhancements in toughness through interactions near this lower bound. Because the exfoliated morphology results in complete delamination, no toughening

mechanisms exist which can be exploited. Each of these nanocomposite morphologies (Figure 1.5) is described in further detail below.

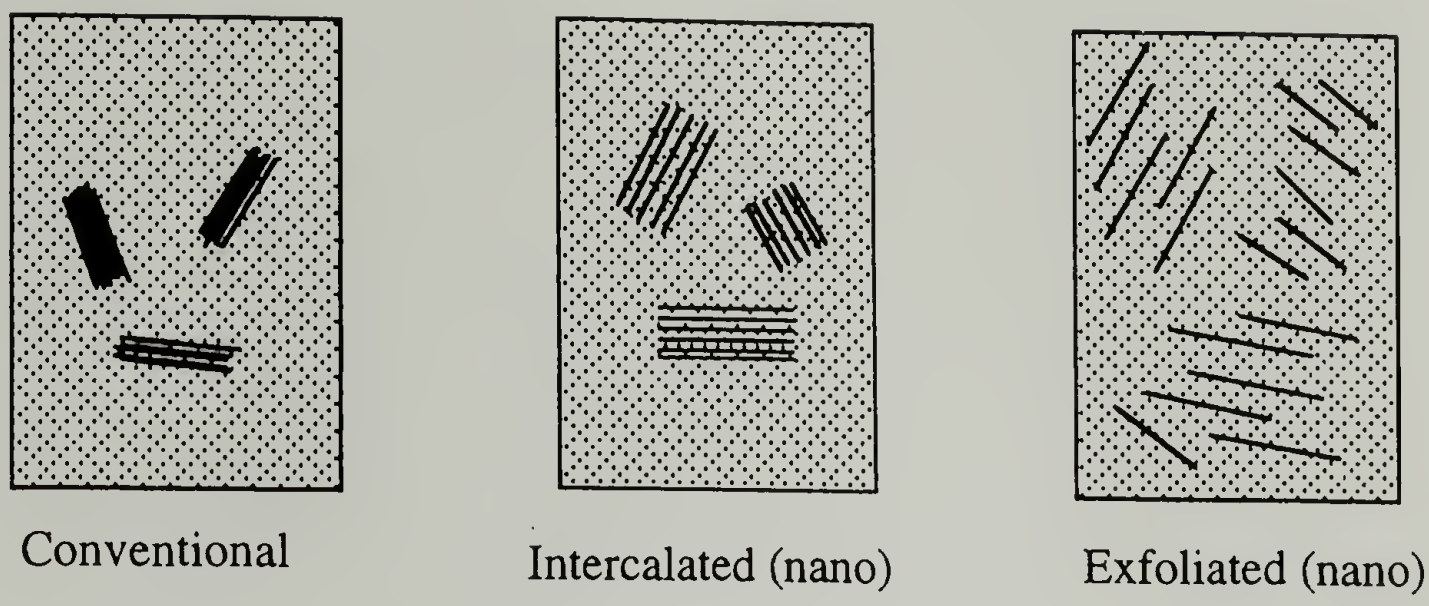

Figure 1.5 Composite morphologies including conventional, intercalated and exfoliated composite morphologies.

1.4.1 Exfoliated nanocomposites

The exfoliated morphology of aluminosilicate nanocomposites is characterized by the level of dispersion of the clay platelets. Here the silicates are homogenously dispersed throughout the polymer matrix with little or no interaction between individual platelets. The surface area of exfoliated montmorillonite platelets is approximately 700 m^2/g. A microscale platelet such as boron nitride, for example, only has a surface area of 0.66 m^2/g. The exfoliated morphology takes advantage of the incredibly high surface area to effectively modify the entire volume at very low concentrations. Using modified silicates, organic-inorganic clay hybrids have been produced with various engineering polymers including epoxy thermosets,[34,35] polyamide,[36,37] polyimide,[38] polystyrene,[39] polyurethane[40,41] and polypropylene.[42,43] In all cases, the exfoliated morphology, wherein the clay platelets are completely dispersed in the polymer matrix, is sought with the

expectation of providing the most improved mechanical properties. These include improved barrier properties,[44] higher stiffness and strength,[34] better heat stability[36,37,45] and enhanced viscoelastic behavior.[46] However, such improvements are usually only reported for glassy epoxy thermosets or amorphous elastomers such as polyurethane.[47] In glassy epoxies and semicrystalline polymers, as with most particulate filled systems, increased stiffness results in a corresponding decrease in toughness and strength.[37,48]

It is known, however, that toughening occurs over a specific size range and effective toughening may not be energetically favorable at nanometer length scales. Rather, toughening generally requires a filler size greater than 0.1 μm.[8] The silicate nanoparticles are often of sizes too small to provide toughening through a crack bridging mechanism and cannot effectively enhance crack trajectory tortuosity; they are simply invisible to the propagating crack. Therefore, the extremely reduced scale of a fully exfoliated nanocomposite does not lend itself to a toughening application. However, in an intercalated system (Figure 1.5), where polymer has entered into the galleries between silicates but has not fully delaminated them into the completely exfoliated structure, there is considerable interaction between silicate layers which might alleviate this concern.

1.4.2 Intercalated nanocomposites

The intercalated morphology is characterized by a distinct peak in the X-ray diffraction (XRD) pattern, signifying the presence of a lamellar structure and retention of order within the silicate domains (Figure 1.6). Such a peak disappears in the case of an exfoliated material. It is thought that the intercalated morphology exists where one or two polymer chains have entered into the gallery spacing, increasing the d-spacing. In the case of *in situ* polymerized composites, order is retained via a difference in the

reaction kinetics inside and outside the silicate galleries. If the reaction rates outside the silicate domains are faster than those within the galleries, exfoliation does not occur.[49] This is a result of a slow transport of monomer into the silicate galleries. Exfoliation, however, is achieved when the reaction kinetics within the galleries are slower than the diffusion of additional monomer into the silicate galleries.

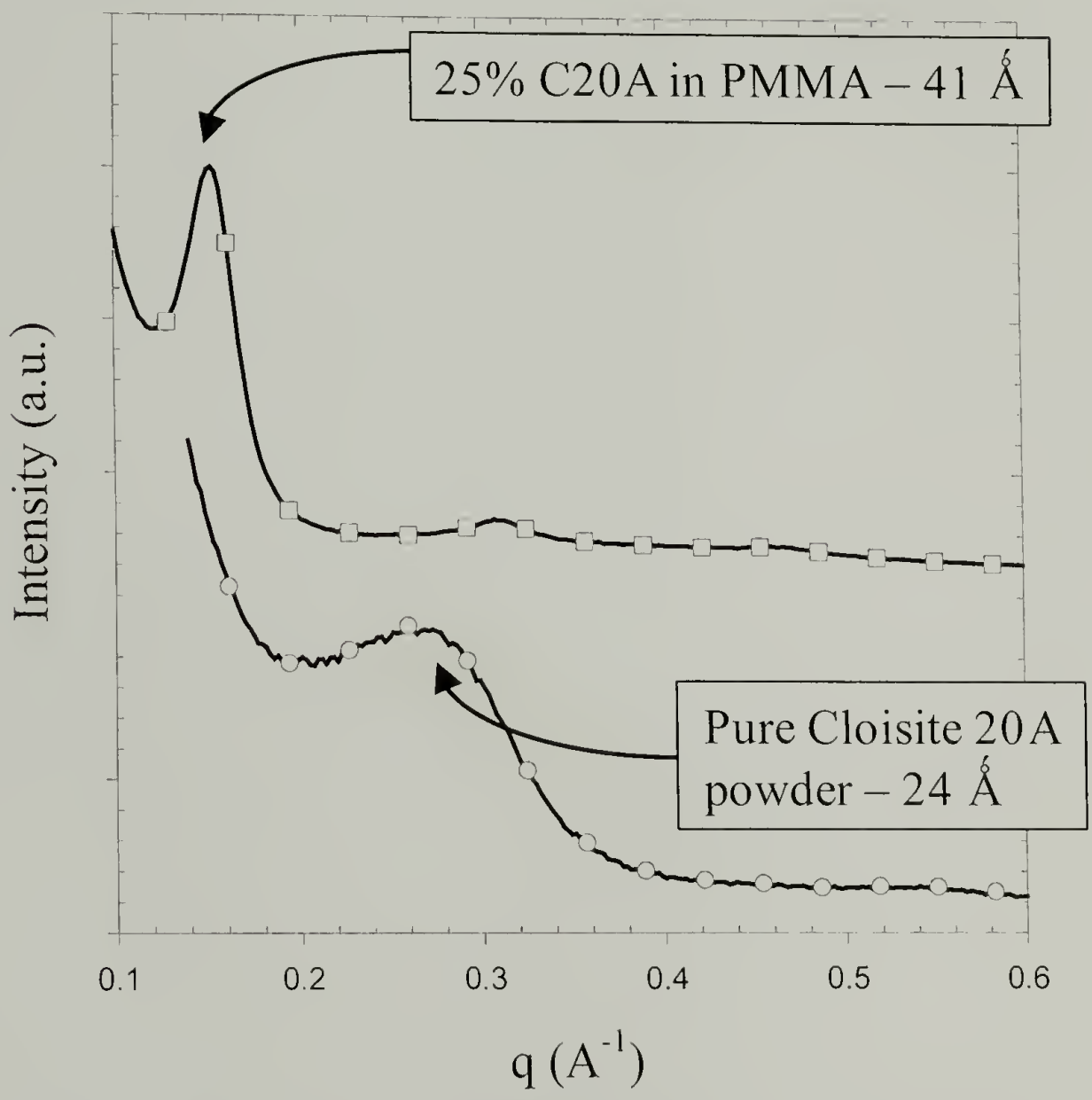

Figure 1.6 Intercalation results in an increase of the d-spacing (from 24 Å to 42 Å in the case above). A distinct peak in the XRD remains, indicative of a stacking architecture.

Based on the length-scale arguments, presented above, describing the limitations of the exfoliated morphology, it is thought that the intercalated nanocomposites may provide a means to achieve mechanical improvements unavailable to the exfoliated systems. Here, by acting cooperatively, the nanoclay displays an effective micrometer

length scale. In the case of fracture toughening of silicate nanocomposites, this intercalated morphology can serve to enhance the toughness of such a material only when the silicates are able to interact cooperatively. Such interaction is not available to the fully dispersed exfoliated morphology. Kachanov[50] has shown that in the case of microcracked materials, the orientation, alignment and separation between microcracks within an array can result in a decrease of the stress intensity factors in front on the crack tip. This ultimate reduction in the stress intensity factors is dependant on the distance between parallel cracks (a) as well as the separation between those which are out of plane with each other (b) as seen in Figure 1.7. The formation of such microcrack arrays has been observed in fatigued materials and is thought to contribute to the retention of service life of such materials.[51] It is proposed that similar materials can be manufactured artificially to study the effects of interacting 'microcracks' and the relative contributions of tip and platelet separation. However, rather than including regular arrays of microcracks, ordered structures of nanosilicates can be manufactured. When considering platelets rather than cracks in the work of Kachanov, the physics of interaction remain the same. Simply the boundary conditions on the silicate surfaces change. The proposed work will investigate techniques to manufacture such ordered materials.

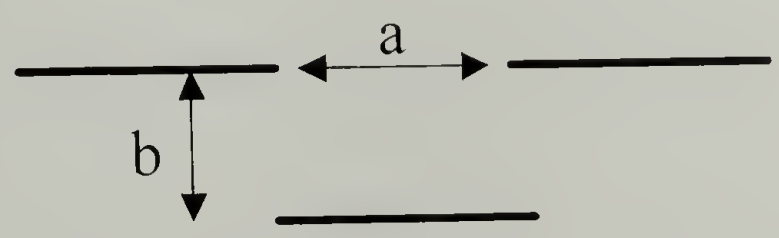

Figure 1.7 Microcrack array resulting in a decrease of the overall stress intensity at the crack tips.

1.5 Conclusion

The study below builds on the ideas presented above. Molecular fortification of polymers is investigated in the case of a new class of additives, which are effective antiplasticizers for epoxy. The mechanisms of this antiplasticization are investigated in terms of the additive chemistry and polymer architecture. Molecular additives can fundamentally alter the properties of the polymer through chemical interactions.

Nanoscale reinforcement through the use of an intercalated morphology is also examined. Materials containing a wide range of silicate concentrations are developed, and investigated for their effect on modulus, strength, failure mechanisms and fraction toughening. The research characterizes the mechanisms for reinforcement of epoxy thermosets on sub-micron length scales. This is accomplished through the design of new materials containing both nanoscale filler and chemical fortifiers.

These materials reinforce mechanical properties on close to the molecular level. As a result, the mechanisms of reinforcement may differ from continuum level effects of traditional fillers. Understanding the mechanisms for molecular fortification can lead to more conscious development of reinforcement agents. Likewise, a basic investigation into the properties of intercalated clays and the manufacture of these materials is necessitated by the lack of existing results concerning this particular nanocomposite morphology. The intercalated morphology is studied particularly for its effects on the fracture toughness of the reinforced polymer. Materials of high clay concentration can be used to investigate polymer-clay composites of true hybrid properties.

CHAPTER 2

MOLECULAR FORTIFICATION – PHYSICAL PROPERTIES

2.1 Introduction

Molecular fortifiers, unlike other plasticizers, are low-molecular weight additives, which increase the modulus and yield strength of a polymer after curing. Molecular fortification, or antiplasticization,[13,14] has previously been observed in epoxy thermosets.[25,52,53] To date, a number of fortifiers have been developed and patented for the specific purpose of achieving high enhancements in engineering properties.[23,24,54] A thorough literature search, however, has revealed a lack of information regarding the role of the additive and, more importantly, the role of the polymer in dictating the level of fortification achievable through antiplasticization of epoxy thermosets. A number of studies have focused on the effect of additive molecular weight in the antiplasticization of PVC and PC resins[15,16,18,20,55,56] but these polymers differ significantly from crosslinked polymers so a thorough investigation is warranted. Indeed, the conclusions based on the investigations of PC-reinforcement[14] are completely at odds with those based on amine-cured epoxy, as will be discussed in the following chapter. The fundamental differences between linear polymers, such as PC and PVC, and crosslinked epoxy result in the behavior observed. The presence of crosslinks allows smaller additives to function as molecular reinforcement agents.

Increasingly, additives are introduced to impart specific changes into the polymeric matrix. However, such modifications rarely occur without consequence and often one property is adversely affected when enhancing another. This behavior often

leads to the use of a variety of additives, each counteracting the negative effects of the other while, hopefully, adding a small benefit of its own. An example is the use of diluents to aid in processing of reinforced polymers. Diluents are commonly used to reduce the resin viscosity in highly filled composites and laminates. However, removal of the diluent following processing is often difficult, if not impossible. Any trapped diluent then acts to decrease properties of the polymer matrix by depressing the glass transition temperature and lowering mechanical strength and stiffness. These effects are inconsequential only if a plasticized polymer is the desired final product, as is the case for many PVC applications. For epoxy resins, the thermal stability and mechanical integrity are the desired characteristics and plasticizers should only be used if they do not significantly interfere with the final properties. Because complete removal of diluents is very difficult, an alternative approach is to employ diluents capable of imparting desired property enhancements. Employing a single additive to achieve a number of property enhancements minimizes the opportunity for competing, and conflicting, material-property alterations. A class of additives, which exhibit such multifunctionality, is the focus of this investigation.

The first portion of this investigation into molecularly reinforced polymers looks at the physical properties of the modified polymer as contrasted against the properties of the initial, unmodified matrix. From this study, a basis is formed for evaluating the material properties of the system. Additionally, this investigation leads to an understanding of mechanical performance. This chapter covers a full material characterization, ignoring for now the engineering properties that are attained upon

fortification. The effects on engineering properties are specifically addressed separately in Chapter 3.

In the present study, dimethyl methyl phosphonate (DMMP) and a family of related phosphates is considered for their ability to enhance the final mechanical and thermal properties of a crosslinked epoxy resin when used principally as a diluent during thermoset formulation. Additionally, due to the high phosphorous content of the additives, an investigation into the flame-retarding potential of the fortifiers is also presented.

2.2 Materials

In developing an investigation of the role of polymer and additive architecture on the mechanical properties of epoxy thermosets, a family of closely related fortifiers was identified. In this way, the role of the additive chemistry can be investigated in a systematic manner. The phosphonate and related phosphates used (Table 2.1) were chosen specifically to monitor the effects of additive molecular weight, density, van der Waals volume, V_w, and Hildebrand solubility parameter, δ_H. By investigating additives that incorporate such a large range of properties, it is possible to draw correlations between the final properties of the mixture and the properties of the molecular additive itself. The additives in Table 2.1 are listed in order of increasing molecular weight. All organophosphate additives were obtained from Aldrich Chemical and used as received.

Table 2.1 Organophosphorous additives for use in epoxy resins

Phosphonate [$P(O)(CH_3)(OR)_2$] R=			**Mol. Wt. (g/mol)**	**Density (g/cm^3)**	**V_w (cm^3/mol)**	**δ_H $(MPa)^{1/2}$**
Dimethyl methyl phosphonate	DMMP	CH_3	128	1.154	59	---
Phosphate [$P(O)(OR)_3$]		**R=**	**Mol. Wt. (g/mol)**	**Density (g/cm^3)**	**V_w (cm^3/mol)**	**δ_H $(MPa)^{1/2}$**
Trimethyl phosphate	TMP	CH_3	140	1.197	63	19.6
Triethyl phosphate	TEP	CH_2CH_3	182	1.072	94	17.9
Tripropyl phosphate	TPrP	$(CH_2)_2CH_3$	224	1.012	124	17.6
Tributyl phosphate	TBP	$(CH_2)_3CH_3$	266	0.979	155	---
Triphenyl phosphate*	TPhP	C_6H_5	326	1.266	159.5	17.6

In order to compare unambiguously the effect of each of the additives on material properties, most of the following results are presented as a function of additive molar percent (mol %). Such a comparison normalizes the weight percent of the additive by its molecular weight. Most commercial formulations, however, are reported as function of weight percent or, more commonly, parts-per-hundred resin (phr). As a matter of reference, most of the following formulations lie within a 25-phr range, similar to that used for plasticizers in PVC and diluents in epoxy. When reporting the effects of a single additive on a single property, the more common phr concentration is used (see Figure 2.9).

In the second portion of this investigation, the polymer network architecture is varied. By altering the polymer backbone structure, the physical properties of the polymer will also be changed. Although related to the discussion here of the physical

property effects of antiplasticizers, this discussion is more germane to the discussion of mechanical properties. It is therefore presented in Chapter 3.

2.3 Experimental

The crosslinked network investigated in this chapter is a reactive product of a high purity diglycidyl ether of bisphenol A (EPON 825 from Shell, Figure 2.1) cured with an aliphatic diamine curing agent (Huntsman D230, Figure 2.2). This resin exhibits a T_g of approximately 90 °C and a M_e of 500 g/mol

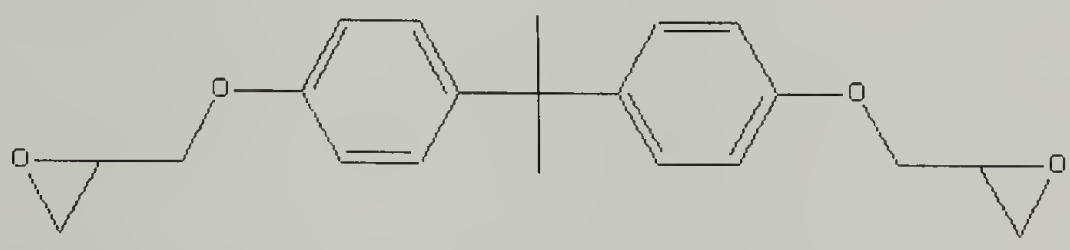

Figure 2.1 Diglycidyl ether of bisphenol A (EPON 825).

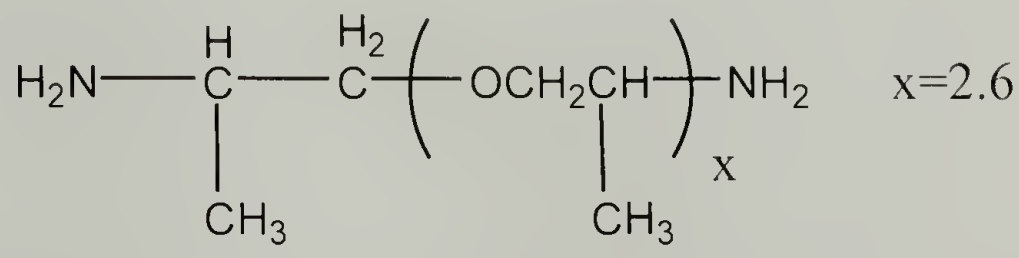

Figure 2.2 A tetrafunctional polyoxypropyleneamine curing agent from Huntsman Chemical (Jeffamine D230).

The additives in Table 2.1 were mixed with the epoxy prepolymer resin at various concentrations and combined with a stoichiometric amount of curing agent. This mixture was degassed under vacuum for a period of 15 minutes and poured into appropriate molds to form 3 mm thick plaques and 8 mm diameter tubes. All samples were cured for 3 hours at 75 °C followed by an additional 3 hours at 125 °C for postcuring. Following these reaction conditions, the epoxy is fully reacted. A complete reaction is verified by

the disappearance of epoxide functionality using Fourier transform infrared spectroscopy (FT-IR).

Rheological measurements of viscosity of the epoxy prepolymer were preformed on an RSI ARES rheometer using a Couette geometry. Viscosity measurements were made at both room temperature (25 °C) and elevated temperatures (50 °C) to simulate typical processing temperatures. The shear rate was varied from 1 Hz to 1000 Hz. The unmodified epoxy resin exhibited shear-thinning behavior at high shear rates (Figure 2.3). Diluted resins, however, exhibited constant viscosity over the entire shear range. The melting point of the EPON 825 is approximately 30 °C although crystallization is very slow. Resin processing therefore often occurs at elevated temperatures to melt any crystals and achieve an overall lower viscosity. The thermal properties of the cured resins were investigated using both differential scanning calorimetry (DSC) and dynamic mechanical thermal analysis (DMTA). The scanning rate was 10 °C/min for DSC and 5 °C/min for DMTA at 1 Hz while imposing a 0.05 % dynamic strain amplitude. Densities were measured using the buoyancy method at room temperature in degassed, deionized water (ASTM D792).

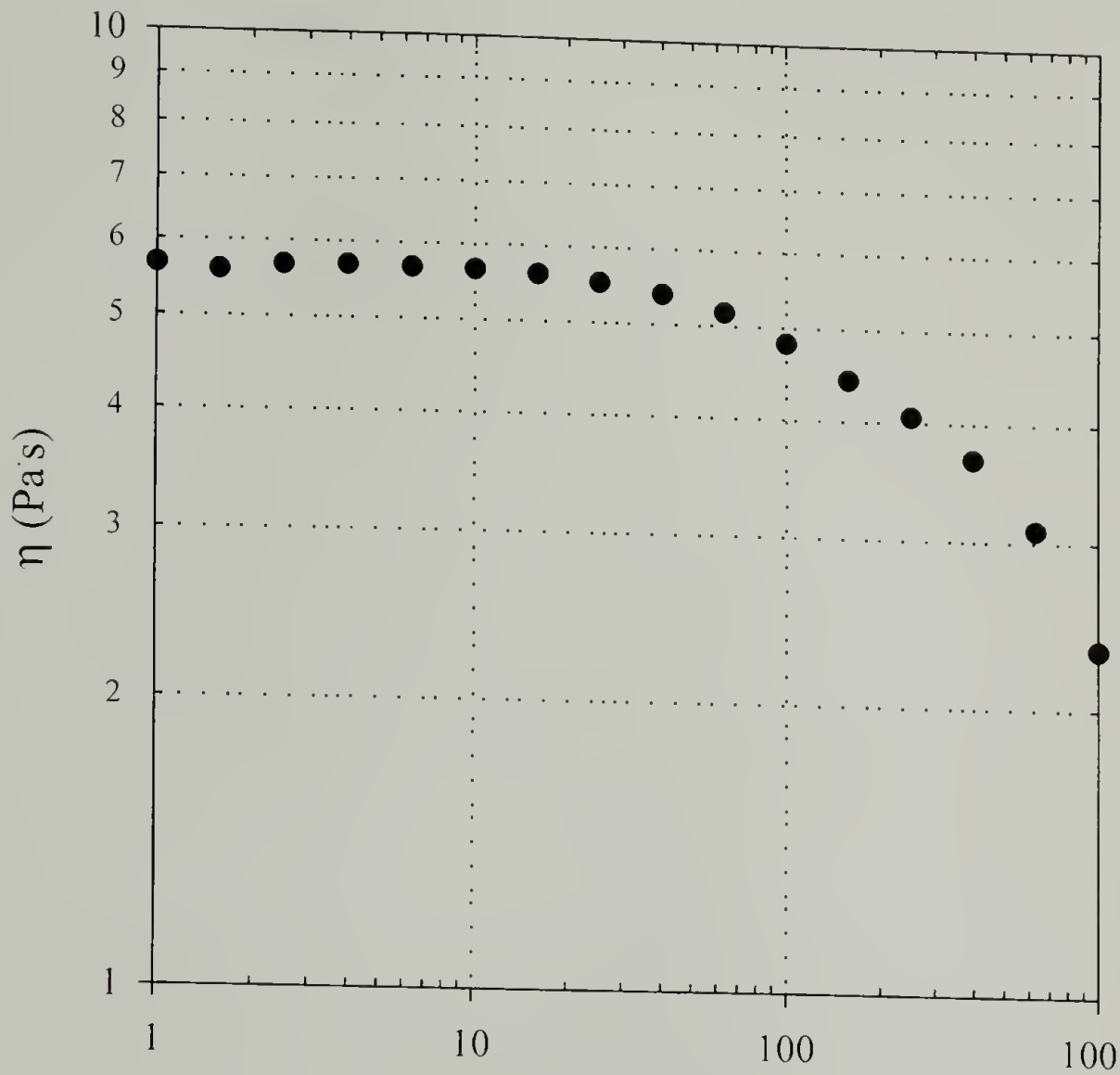

Figure 2.3 Shear thinning exhibited in undiluted 825 resin at room temperature.

Thermal degradation measurements were made employing thermogravimetric analysis (TGA) on a TA 2050 at a heating rate of 40 °C/min from ambient temperatures to 800 °C. Samples were run under a nitrogen purge, although no significant differences were apparent in char yield and degradation rate when the samples were degraded in air at these heating rates. Measurements of heat release capacity and total heat release upon degradation were made on the Federal Aviation Administration (FAA) pyrolysis-combustion flow calorimeter (PCFC) which was developed to monitor the flammability of polymers on milligram quantities.[57] In such an experiment, the sample is flashed (5 °C/s) to 1200 °C, and the pyrolysis gases are oxidized under an O_2/N_2 atmosphere. The

rate of O_2 consumption under these conditions is monitored and related to the heat release rate. This technique has been shown to correlate well with larger scale flammability tests such as the OSU fire calorimeter and cone calorimetry.[58] Cone calorimetry samples were 4"x4"x1/16" squares. The samples are oriented horizontally to the applied flame. An external heat flux of 50 kW/m^2 is then applied.

2.4 Physical properties

2.4.1 Solubility

The interactions between epoxy networks and polar additives are well understood. Various NMR[53] and dynamic mechanical[52] investigations into the molecular motions of antiplasticized amine-cured epoxy thermosets have demonstrated that polar additives interact with the hydroxypropylether [$OCH_2CH(OH)CH_2$] group (Figure 2.4) along the polymer backbone. The hydroxypropylether group is the product of nucleophilic ring opening of the epoxide ring by an amine curing agent. The R functionality in Figure 2.4 is part of the diepoxy prepolymer. The R' refers to the variety of diamine curing agents which can be used.

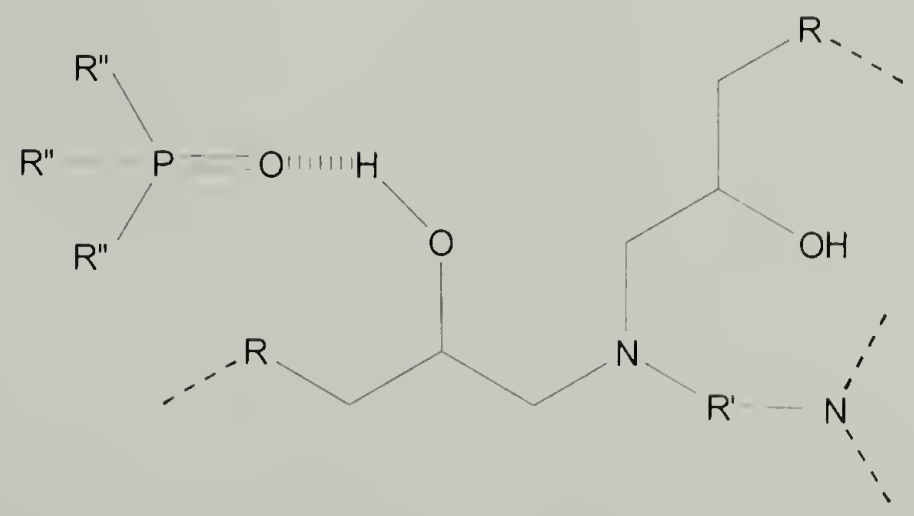

Figure 2.4 A trialkylphosphate hydrogen-bonded to the hydroxyl moiety along the diamine-cured epoxy backbone.

In the ease of additives that ean aet as hydrogen-bond aeeeptors, as is the ease for the organophosphorous compounds used in this study, the interaction is expeeted to exist between the hydroxyl and the phosphoryl moieties of the polymer and additive, respeetively. By ehanging the substituent groups, R'', of the phosphates in Table 2.1, the strength of this interaetion is varied. In the ease of the higher molecular weight speeies, steric hindranee due to the presenee of large substituent groups can lead to interferenee in the polymer-additive interaetion.

One way to prediet the strength of the additive-polymer interaetion is with the solubility parameter, δ_H. Solubility parameters are measures of the strength of interactions between like moleeules in the liquid state. Values of δ_H are obtained by measuring the enthalpy of vaporization, ΔH_{vap}, of a liquid, eorreeting for the behavior of an ideal gas and normalizing by the molecular volume:

$$\delta_H = \left(\frac{\Delta U_{vap}}{V_m} \right)^{1/2} = \left(\frac{\Delta H_{vap} - RT}{V_m} \right)^{1/2} \qquad \text{Eq. 2.1}$$

where ΔU_{vap} is the internal heat of vaporization of the liquid. Normalization of the internal heat of vaporization by the molecular volume, V_m, results in the eohesive energy density and is related to the solubility parameter. Generally speaking, the higher the solubility parameter of a liquid, the stronger its moleeular interaetions. For example, water has a δ_H of 47.9 $MPa^{1/2}$due to its high degree of hydrogen bonding. Thc δ_H of the additivcs were obtained from thc literature whcre available. Clearly, as the molecular wcights of the additivcs in Table 2.1 inerease, the strength of intermoleeular interactions of the additives is eorrespondingly inereased.

The δ_H for solids is detcrmined experimentally by using a number of solvents of known δ_H and measuring the degrcc of swclling of the polymer upon interaetion with the

solvents. The δ_H of the solvent, which results in the greatest degree of swelling of the polymer, is thereby determined to equal the δ_H of the polymer. The solubility parameter for epoxy is reported[59] to be between 18.5 and 20.5 $MPa^{1/2}$, depending on the hydrogen-bonding strength of the solvent. In such a manner, it is expected that TMP will have the greatest interaction with epoxy. This argument is important in describing the interactions between the various additives in Table 2.1 and the epoxy thermoset. References to this discussion will be made later.

2.4.2 Viscosity

One of the potential applications of molecular additives in polymers is their ability to act as diluents to aid in processibility. This is especially true for the epoxy resins. The EPON 825 used is a low molecular weight difunctional epoxy of moderate viscosity. Most commercial epoxies, however, are polydisperse oligomers of bisphenol-A of higher molecular weight. These are also often of greater viscosity, affecting their ease of processing. Epoxy resins are often used in high-performance applications where there is a strong reliance on manufacturing defect-free parts. In order to ensure ease of processibility, a low resin viscosity is desired. Elevated temperatures, therefore, are often used to achieve a significant reduction in the viscosity. At higher temperatures, the pot life of the resin is compromised. The use of diluents is reducing viscosity is, therefore, often preferred.

As seen in Figure 2.5, the viscosity of the epoxy is greatly reduced upon addition of a small amount of each of the additives DMMP, TMP and TPhP. The reduction is exponential with increasing concentrations. At room temperature and 35 mol % additive, for example, the viscosity of the epoxy is on the order of the undiluted epoxy at 50 °C.

This kind of viscosity reduction eliminates the need for elevated temperatures. The higher concentrations see an even more significant reduction at elevated temperatures. It is well known that such a reduction in viscosity is important to processing of highly filled composite materials.

The viscosity measurements were fit using an expression for additive viscosity:

$$\ln \eta = f \ln \eta_a + (1 - f) \ln \eta_e \qquad \text{Eq. 2.2}$$

where f is the weight fraction of the additive in epoxy, η_a is the viscosity of the additive and η_e is the viscosity of the epoxy prepolymer under the test conditions. A conspicuous absence of any effect of the additive chemistry on viscosity reduction is evident in Figure 2.5. That is to say, all of the additives reduce the viscosity of the resin equally. This result is due to the absence of any favorable interaction between the additive and epoxy prepolymer prior to crosslinking. This is not the case for the crosslinked polymer, which has introduced the aforementioned hydroxyl group through ring opening of the epoxide. By eliminating any opportunity for hydrogen-bonding or polar-polar interactions, the additives are effective diluents regardless of molecular structure.

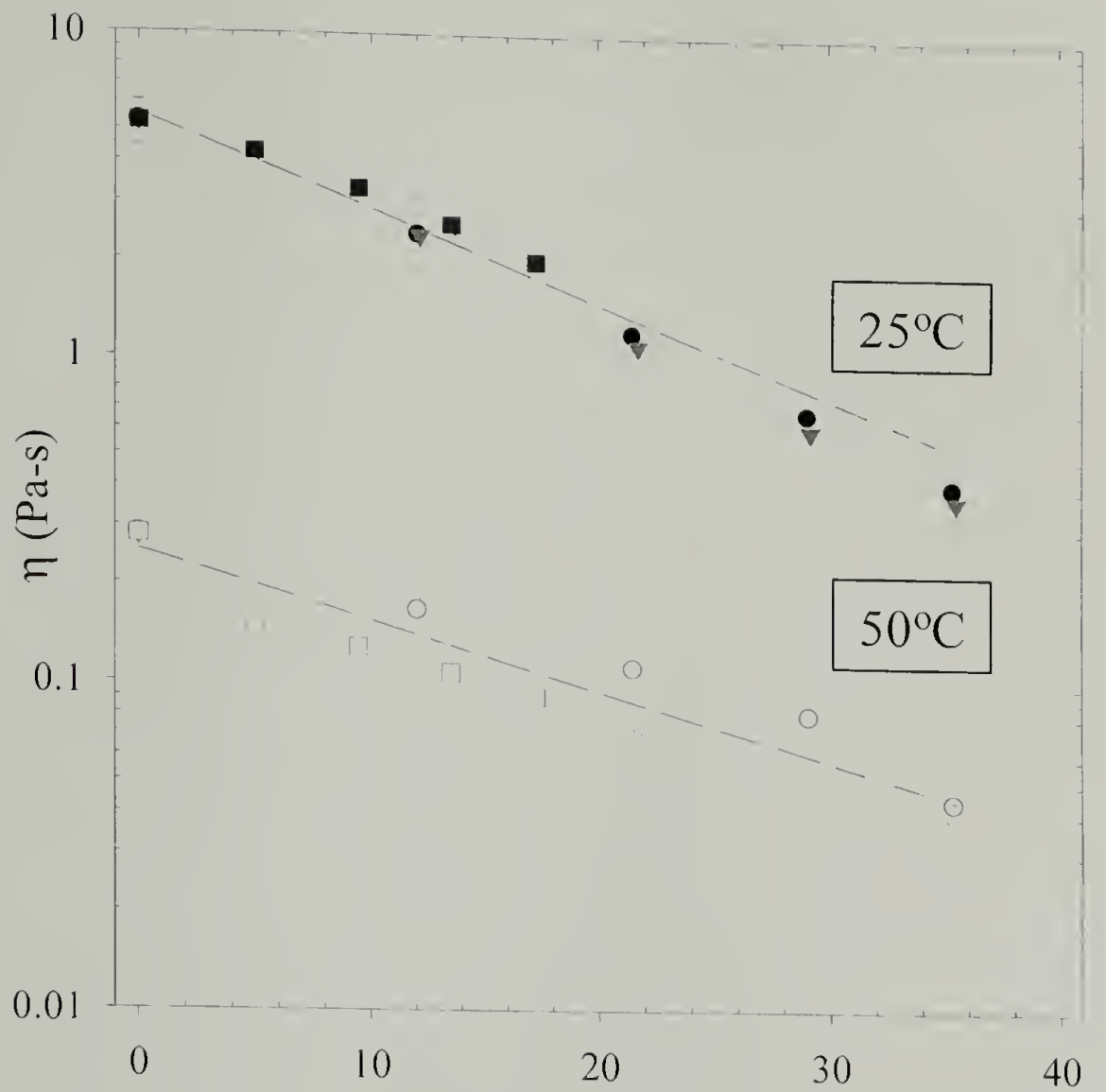

Figure 2.5 Viscosity of epoxy prepolymer with increasing additive coneentration. Linear fits represent rule of mixtures viscosity reduction. All three additives, DMMP (○), TMP (▽) and TPhP (□) reduce the viseosity similarly. Solid symbols indicate room temperature, while hollow symbols 50°C.

2.4.3 Glass transition temperature

Diluents, plasticizers and antiplasticizers alike, reduce the glass transition (T_g) of a polymer as a function of eoncentration. The addition of trialkylphosphate additives into an epoxy thermoset depresses the glass transition linearly with additive concentration (Figure 2.6). In the case of the larger additives, the deerease in T_g follows with the size of the additive, with the largest additive, TBP, having the most severe effect on the thermal properties of the polymer.

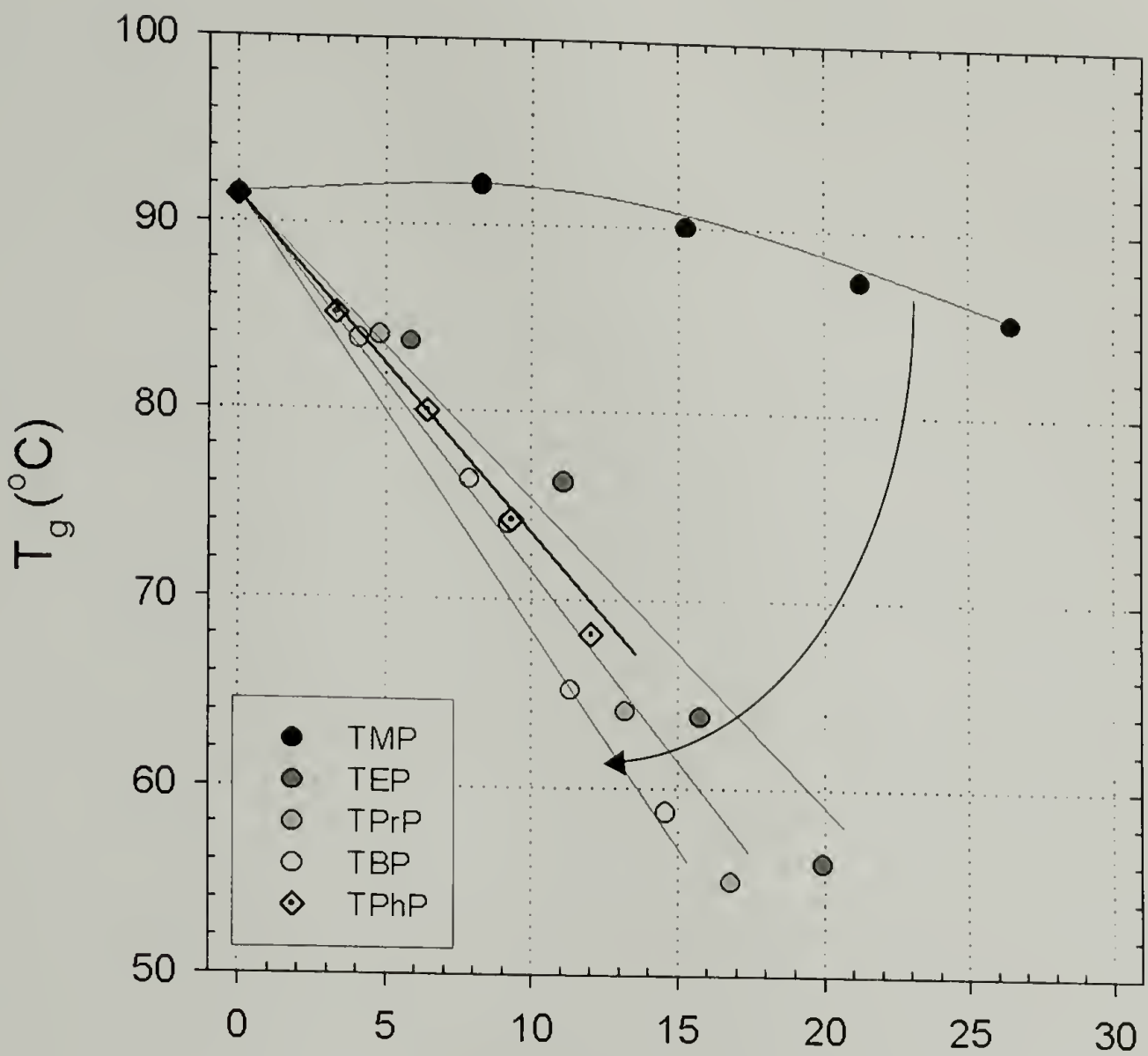

Figure 2.6 Glass transition temperature with phosphates of increasing molecular weight. As the molecular weight of the phosphate is increased, the glass transition temperature of the epoxy is further decreased.

This phenomenon is best viewed in the context of plasticization of polymers with molecular solvents. Polymers such as PVC and PC are stiffened at a molecular level by intermolecular interactions such as van der Waals interactions and hydrogen bonding. Phthalate plasticizers, however, inhibit these intermolecular interactions.[60-62] The result of this plasticization is the reduction of T_g by allowing for greater molecular flexibility. The effect of the plasticizer on T_g is strongly affected by its chemical architecture. Early work in the area of polymer plasticization demonstrates the effect of alkyl chain branching in phthalic diesters on plasticization of polymers. Here, the degree of

branching is inversely proportional to the efficiency of the additive, indicating that the volume of an additive is an important contributor to reducing T_g.[63] A similar effect is evident for triphenyl phosphate (TPhP) in Figure 2.6. TPhP behaves similarly to TBP, and in fact has a similar van der Waals volume.[64] The smallest of the fortifiers investigated, TMP, behaves decidedly outside the trend of the remaining diluents, increasing the glass transition temperature at 5 mol % and not reducing the T_g of the mixture until higher concentrations.

Measurements of the glass transition through dynamic mechanical methods, such as DMTA, are known to be more sensitive than calorimetric measurements. Although the absolute values of the T_g using these two methods are not identical, the relative trends, including any increases or decreases in the transition temperature, appear unaffected. The example of DMMP is shown (Table 2.2). Considering that these molecular additives are intended for engineering applications, dynamic mechanical measurements of T_g seem more appropriate over those performed using DSC. Observations of the T_g using DSC do not exhibit any hints of phase separation with increasing additive concentration. All of the scans show a single thermal transition. Using the DMTA measurement method, high additive concentrations do appear to exhibit a small phase separation at high concentrations (Figure 2.7). At 20 phr DMMP in 825-D230, a shoulder at 110 °C in the α-relaxation peak of the tan δ is clearly observable. It is likely that this hint of phase separation may have an effect on the resulting mechanical properties at high concentrations. It is important to note that external evidence of phase separation, such as opacity, is not evident.

Table 2.2 Glass transition as measured thermally and mechanically.

DMMP	(phr)	0	5	10	15	20
DSC	(°C)	91	86	78	70	63
tan δ	(°C)	101	96	97	90	82
peak E"	(°C)	95	87	87	81	69

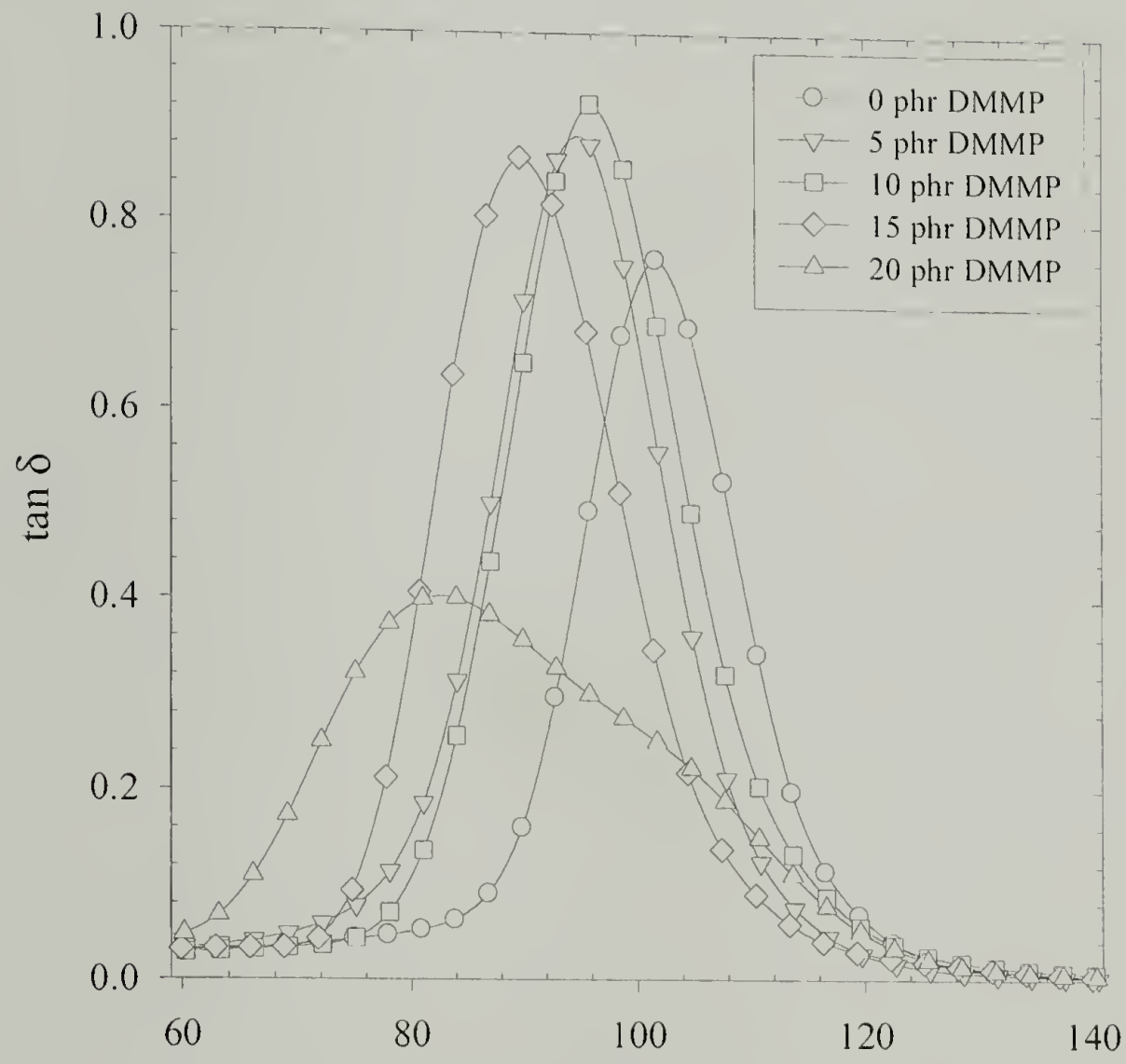

Figure 2.7 The tan δ peak at high organophosphate concentration exhibits indications of phase separation, which are not observed in the DSC measurements.

There is a strong effect of the additives on the β-relaxation of the dynamic spectrum as well. Increasing the additive concentration reduces the intensity of this relaxation (Figure 2.8). The β-relaxation peak for epoxy consists of two separate molecular relaxations.[26,27] The low-temperature relaxations within the β-relaxation peak

are thought to correspond to phenyl flips in the bisphenol-A repeat of the epoxy and occur, roughly, between –100 °C and –50 °C. These are unaffected by antiplasticization. In point of fact, antiplasticization affects only the higher-temperature portion of the β-relaxation. The high-temperature portion of this relaxation peak corresponds to cooperative motions of the aforementioned hydroxypropylether group.[52] These cooperative motions occupy the –50°C to 0°C region of the β-relaxation. Phosphonates such as DMMP are hydrogen-bonding acceptors and, as the hydroxyl moieties are hydrogen-bond donors, it is likely that the interactions occur here. The reduction in the β-relaxation peak between –50 °C and 0 °C correlates well with this conclusion.

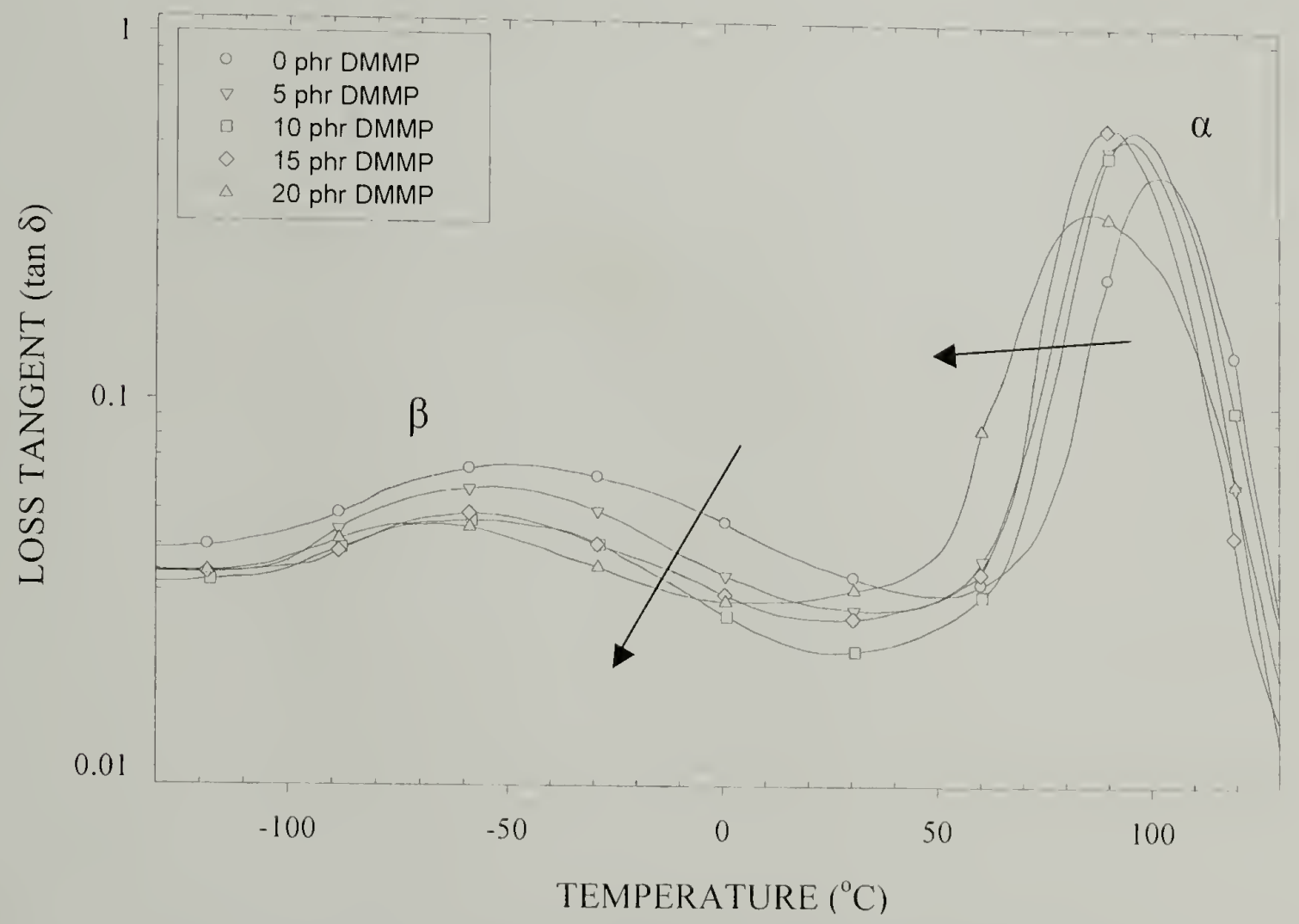

Figure 2.8 Thermal relaxations with increasing additive concentration. Increased DMMP concentration reduces the α-relaxation temperature while also reducing the intensity of the β-relaxation peak.

2.4.4 Density

A common observation of antiplasticized polymers is the apparent negative change in the volume of mixing between the polymer and the additive.[28,29] This effect is manifested through a densification, or reduction of the free volume, of the polymer in a manner unrelated to simple free volume additivity of the two constituents, as demonstrated by the results of DMMP (Figure 2.9).[30,31]

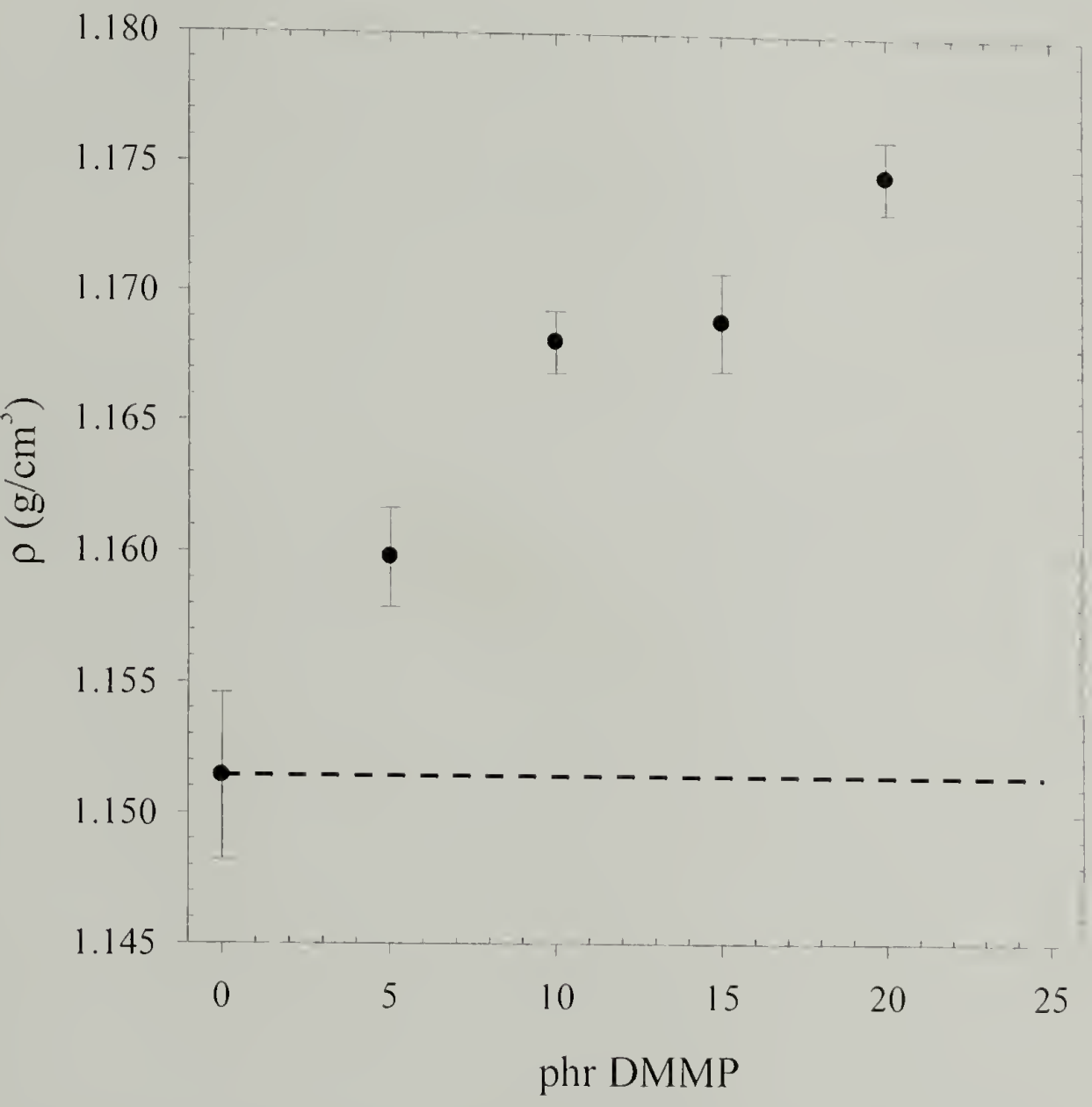

Figure 2.9 Density increase with DMMP concentration. The dashed line represents a rule of mixtures density for the system.

The physical properties of the additives themselves have a clear effect on the amount of densification of the polymer (Figure 2.10). This effect has been exhibited in

most antiplasticized polymer systems[25] and is thought to be predictive of the level of mechanical reinforcement observed.

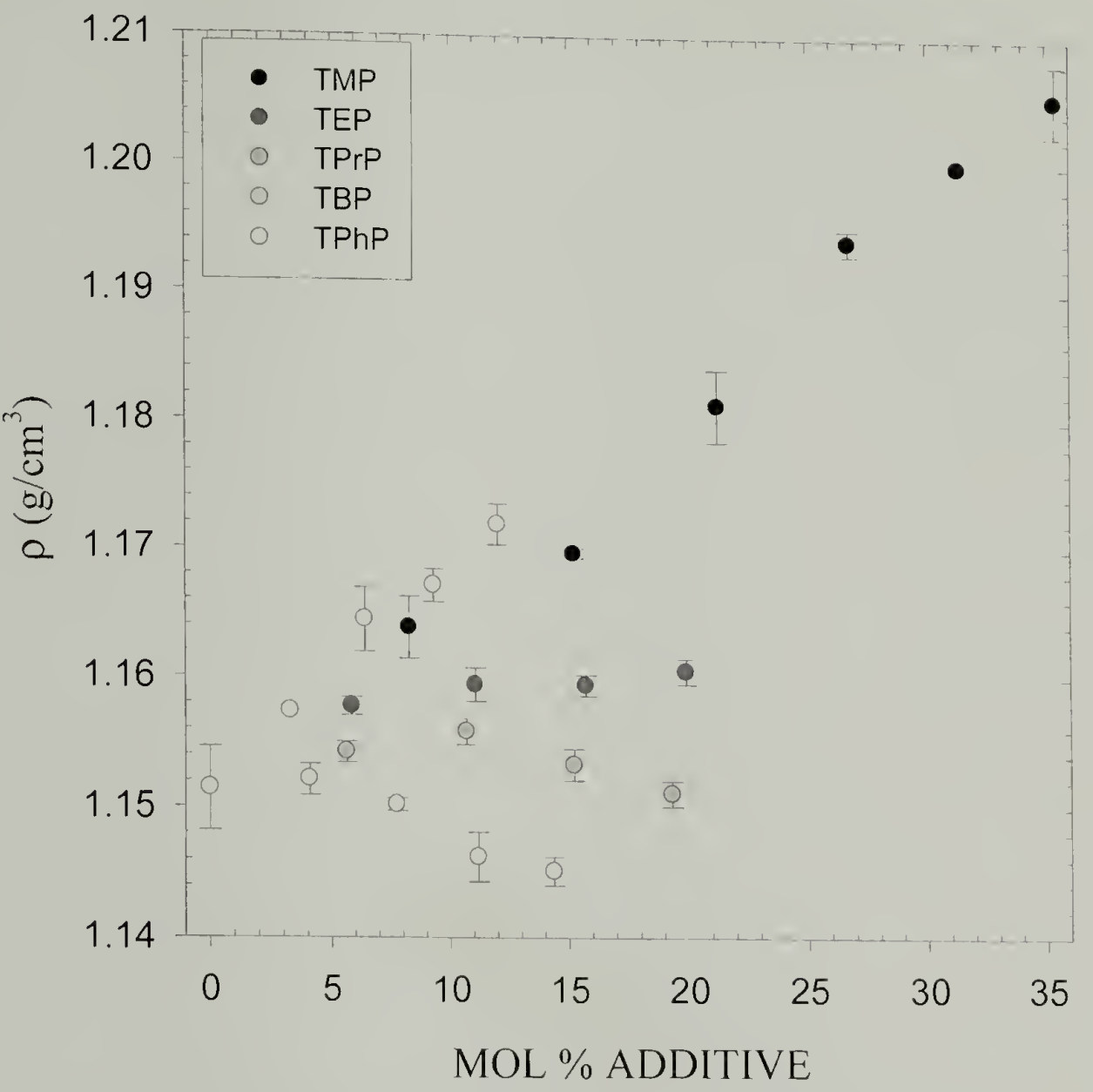

Figure 2.10 Density changes in epoxy resin with phosphates of increasing molecular weights.

Mixing of small molecules with glassy polymers can lead to a departure from specific volume additivity and a number of theoretical models exist to predict this behavior based on the equilibrium liquid-state specific volumes of polymer and diluent. One such model, proposed by Paul and Ruiz-Treviño[31] uses volume additivity of the two components, polymer and additive, in their equilibrium liquid states and incorporates a thermal expansion term which results in the departure from simple additivity (Eq. 2.3).

$$V_{mg}(T) = \omega_a V_{al}(T) + \omega_p V_{pl}(T) + \left(\frac{dV_{ml}}{dT} - \frac{dV_{mg}}{dt}\right)\left(T_{gm} - T\right) \qquad \text{Eq. 2.3}$$

The speeific volume of the mixture in its glassy state, $V_{mg}(T)$, at a test temperature T, below T_g in Eq. 2.3 is expressed as a weight fraetion rule of mixtures of the liquid speeific volume of the additivc, $V_{al}(T)$, and speeifie volume of the amorphous liquid state of the polymcr, $V_{pl}(T)$. The thermal expansion term for the mixture extrapolates the specific volume of the mixture from T_g, where V_{ml} is the liquid state speeific volume of the mixture and V_{mg} is the specifie volume of the mixture in its glass state. The model, therefore, indieates that any dcparture from density additivity is a result of a T_g mismateh between the polymer and the additives, whieh are mostly liquid at room temperature. This mismatch in the T_g of thc two eonstituents allows the mixture to reaeh a more tightly paekcd state by virtue of the thermal expansion eoeffieient. The predieted speeific volume of the matrix, $V_{mg}(T)$, can then bc translated into a density:

$$\rho_{mg}(T) = \frac{1}{V_{mg}(T)} \cdot \rho_{H_2O}(T) \qquad \text{Eq. 2.4}$$

All of the eomponents for this model ean be either experimentally obtained or estimated from literature.[64] The experimental densities measured for all of the additives, with the exeeption of TMP, follow thc predictions of thesc models elosely (Figure 2.11).

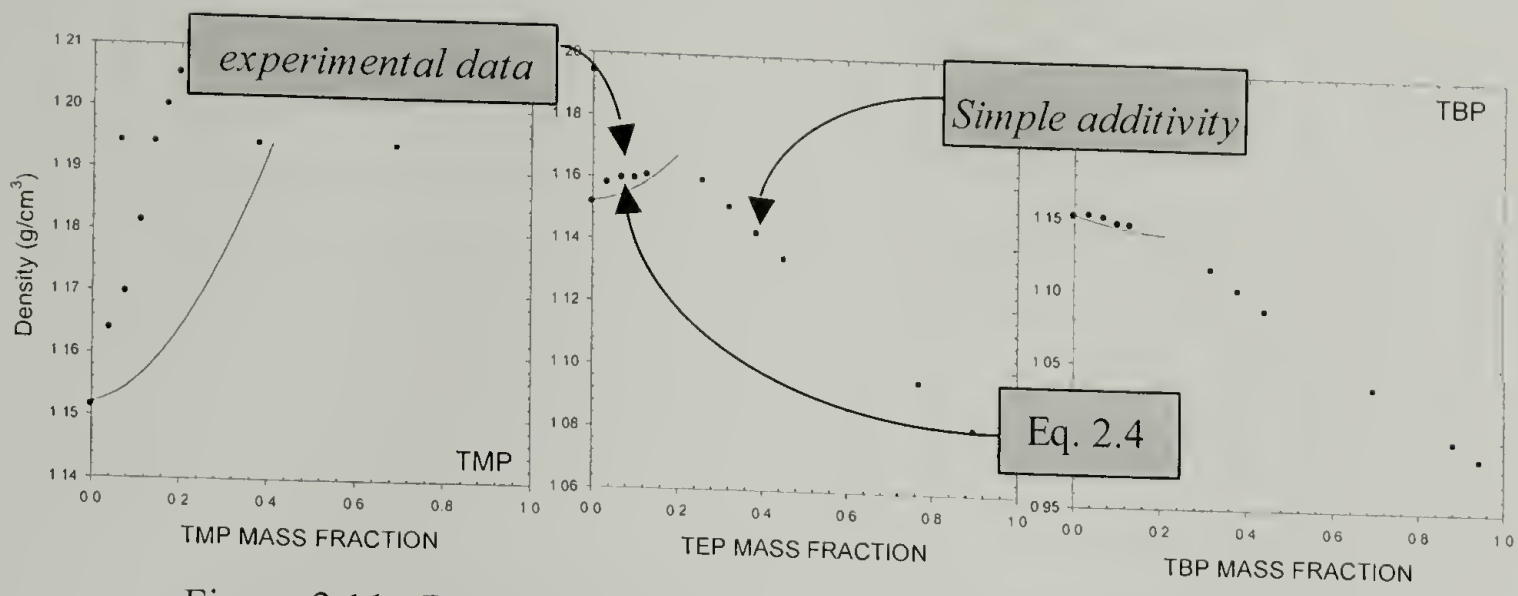

Figure 2.11 Densification upon addition of phosphate additives as compared to the Ruiz-Treviño equation, Eq. 2.4.

This latter fortifier, already shown to demonstrate unique glass transition behavior, does not fit the model to any degree of success and even exceeds the maximum density predicted by the model. Simple additivity in Figure 2.11 is defined as the density accessible at T_g.

Covalent bonding between the polymer backbone and TMP, as well as the other phosphate additives, can, however, be discounted. By subjecting the modified thermoset to 24 hours under vacuum above both the T_g of the polymer and the boiling point of the additive, significant weight loss can be observed. Selective loss of additive can be verified via elemental analysis through a reduction in phosphorous content following such a heat treatment (Table 2.3). Since the additives are not reactive with the polymer matrix, the reduction in free volume implies an interaction between the polymer and the additive which leads to a tight packing of the additive within the matrix.[53] The observation that the additives are not covalently bound plays an important role in describing the mechanism for mechanical reinforcement by discounting the presence of additional, additive-initiated crosslinks. Increasing the crosslink density would be a possible alternative method to enhancing mechanical strength.

Table 2.3 Elemental analysis of epoxy with DMMP

Weight Percent Phosphorous		
Initial	Post-heat	% change
0.00	0.00	0
0.89	0.07	92
1.72	0.90	48
2.49	1.20	52
3.22	1.60	50

The lack of covalent bonding between the additive and polymer, however, leads to a limitation in the thermal stability of the resulting polymer mixture. Whereas epoxies can be subjected to high temperatures for long periods without significant changes in material properties, the molecularly modified epoxies do exhibit material changes. As indicated in Figure 2.12, upon heating a fortified resin above T_g for 12 hours, a significant change in the glass transition temperature is observed. The apparent increase in T_g, a possible indication of an incomplete reaction between the epoxy and the curing agent, is simply a result of the DMMP additive leaching out under such conditions. Normalizing the T_g's observed in Figure 2.12 (a) with the elemental analysis data from Table 2.3 results in a collapse of the data onto the original curve Figure 2.12 (b). These observations reinforce the opinion that molecular fortifiers, although exhibiting a number of significant material enhancements, face limitations similar to traditional plasticizers. Investigations into the aging of antiplasticized epoxies would have to be carried-out prior to determining commercial applicability.

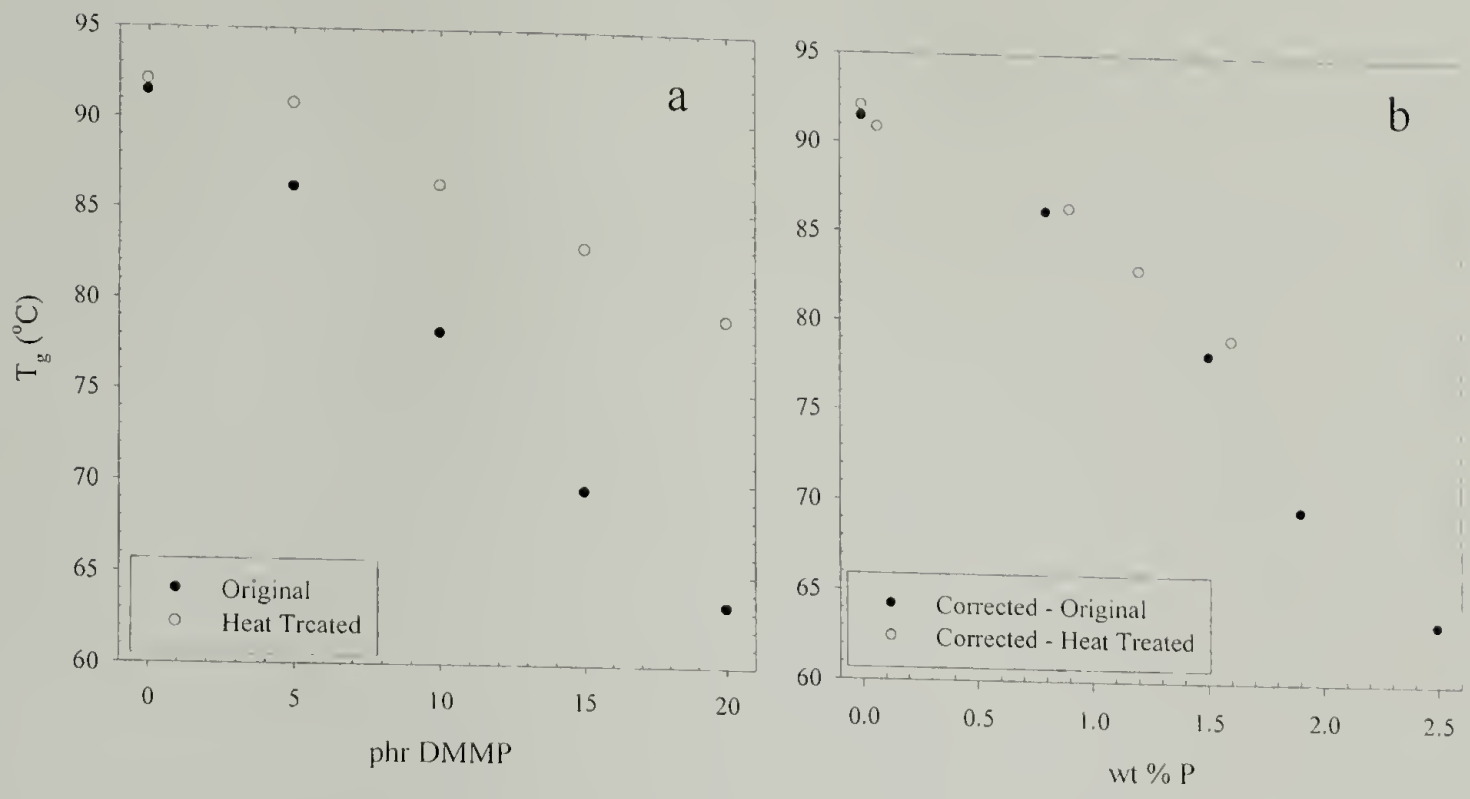

Figure 2.12 Upon prolonged heat treatment (12 hr at 125°C) of the epoxy-DMMP resin, the glass transition temperature is observed to increase (a). Correcting for loss of the additive (b) collapses the results.

2.5 Flame-retardation properties

Organophosphorous materials are well known flame-retardants. Thus, it is interesting to investigate the potential of DMMP and the related organophosphates to reduce the flammability of the epoxy network. Recently, organophosphorous additives and curing agents for epoxies have been reported which reduce the flammability of epoxy resins.[65-68] Presently, flame-retardant epoxy resins are based on brominated or chlorinated components which produce toxic emissions and corrosive fumes upon degradation. Future-generation flame retardants are meant to suppress these by-products. Organophosphorous flame-retardants produce less toxic gas and smoke than halogenated products and are seen as possible replacements with the recent push to eliminate halogenated flame-retardants.

A good initial measure for the flame retarding potential of an additive is the thermal degradation of the modified polymer as measured in a TGA (Figure 2.13). The resulting degradation plots provide information on the thermal stability and degradability of the polymer undergoing a temperature ramp. In Figure 2.13, TGA curves of the epoxy network with increasing concentrations of DMMP additive illustrate the changes in the degradation of the epoxy matrix. Although the onset of degradation is decreased with the addition of the molecular additive, the rate of degradation is likewise reduced, as evidenced by the degradation rate plot at the bottom of Figure 2.13. The degradation rate is a measure of how quickly the polymer pyrolyzes as the temperature is increased and is a good relative comparison of the flammability. By adding a small concentration of DMMP, the rate of degradation is significantly (up to 54 %) diminished.

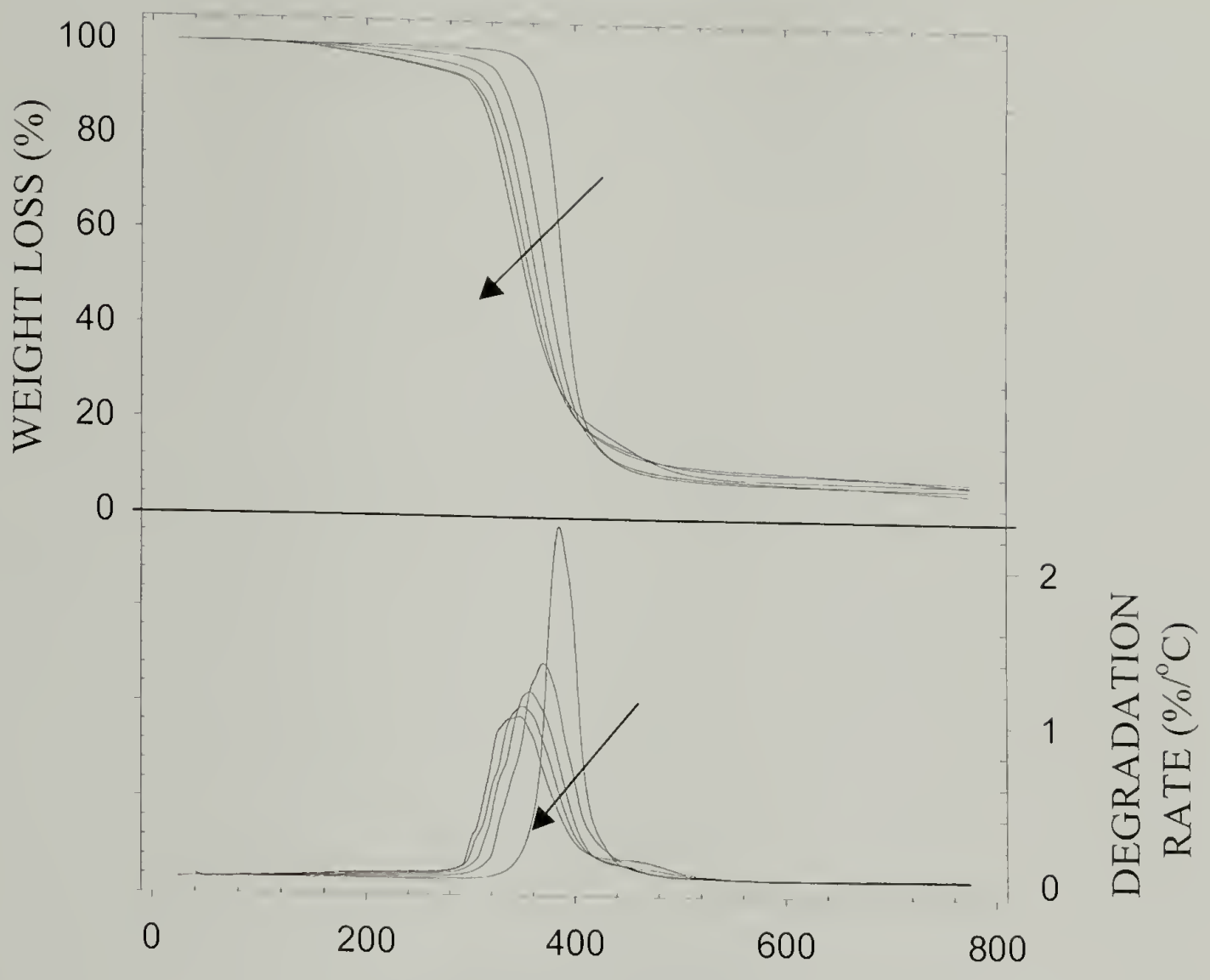

Figure 2.13 Thermal degradation of epoxy resin with increasing additive concentration. Although the onset of thermal degradation is reduced (top), the rate of degradation is likewise decreased (bottom). Arrows indicate increasing DMMP concentration.

The reduction in the onset of degradation is a result of the additive being unbound to the polymer backbone. DMMP has a boiling point of 181 °C and evaporates as the temperature increases. Similar results were obtained when comparing the effects of TMP and TPhP in addition to DMMP within the 825-D230 resin (Figure 2.14 and Figure 2.15). The rate of degradation with the three additives is unaffected by the chemical architecture of the additives themselves. All of the additives decrease the degradation rate equally with molar concentration. For example, at 10 mol % additive, the peak rate of degradation of the 825-D230 resin is reduced by 33 %. The fact that all three compounds

collapse onto the same plot with respect to their molar concentration within the epoxy demonstrates the importance of elemental phosphorous concentrations. Increasing the size of the substituent groups, as per TPhP, only limits the weight percent of the additive that can be incorporated before the other material properties suffer. For example, although 30 mol % of TPhP could significantly reduce the flammability of the resin, the glass transition temperature would suffer correspondingly, reducing the overall effectiveness of the epoxy as an engineering plastic.

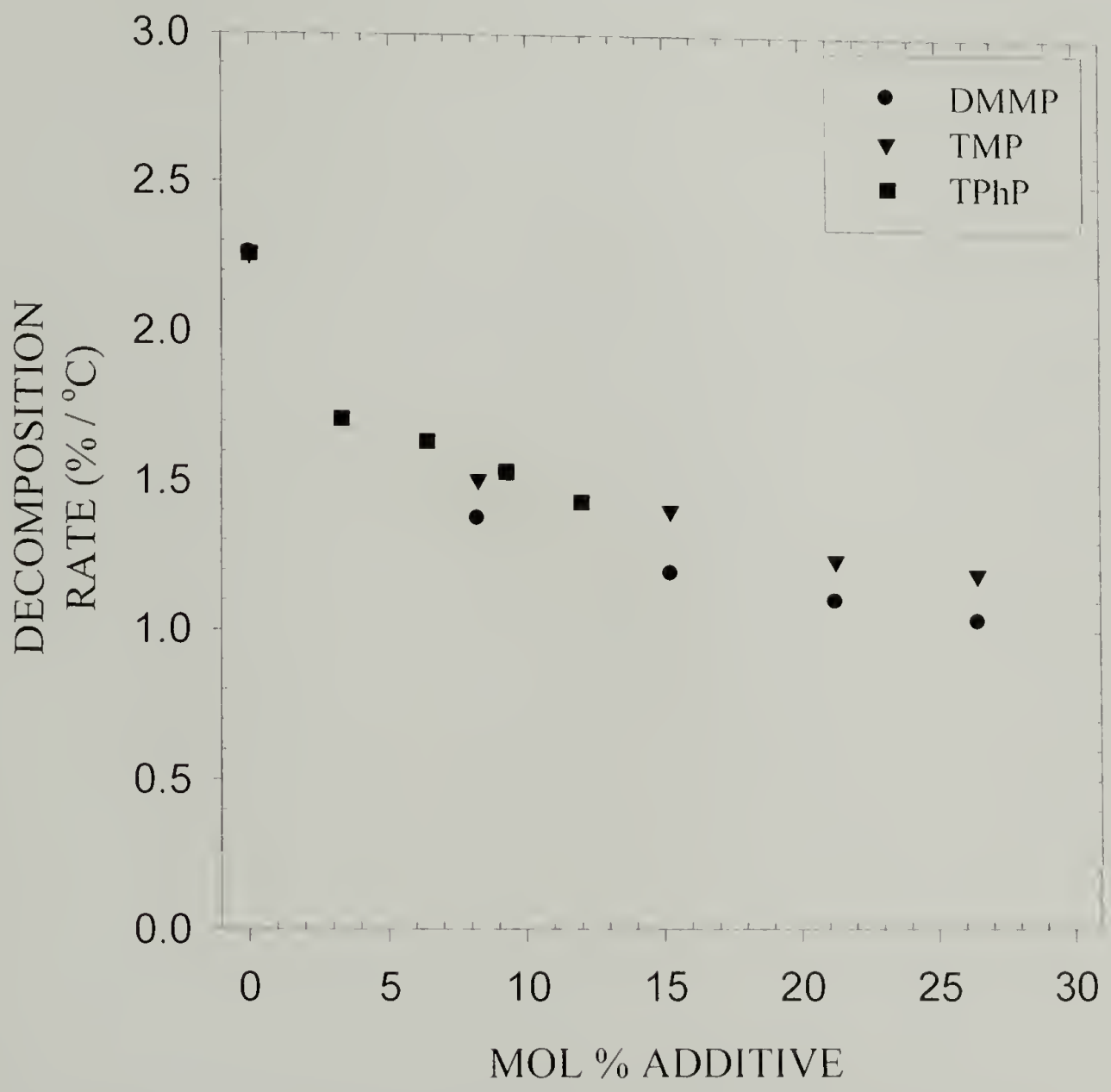

Figure 2.14 The decomposition rate, as measured by the peak mass loss, is unaffected by changing the organophosphorous additive. Rather the elemental amount of phosphorous is important.

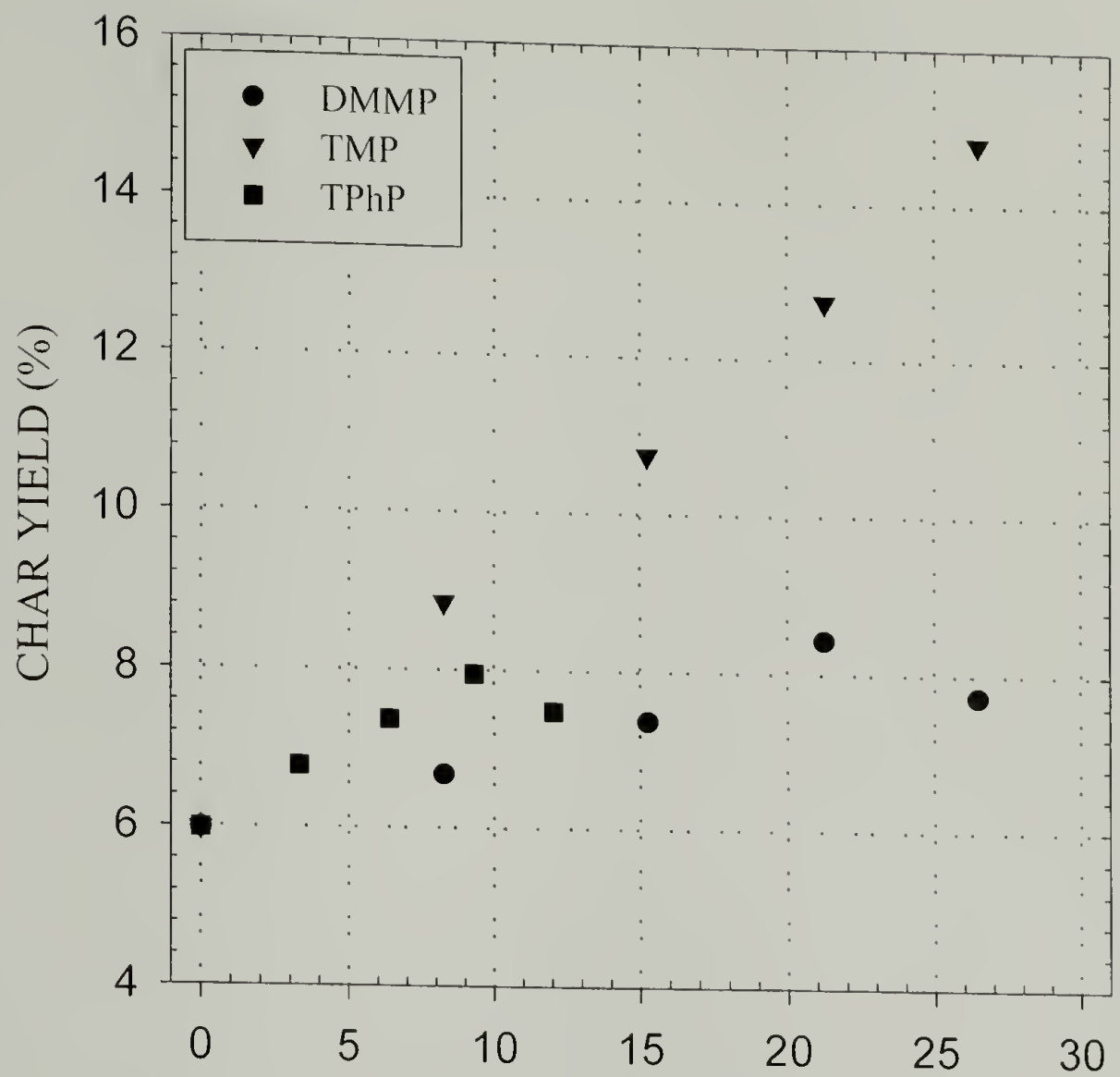

Figure 2.15 Increased char yield at 800 °C with addition of organophosphate additives.

The additive chemistries strongly affect the amount of char formed upon pyrolysis (Figure 2.15). Whereas both TPhP and DMMP each yield little change in residual mass, there appears to be a linear relationship between TMP concentration and the char yield at 800 °C. Analysis of the volatiles produced below 300 °C using a GC-mass spectrometer reveals that the additives are the major components of weight loss at this temperature (Figure 2.16). Thus, the reduction in the rate of degradation and the lack of considerable char formation for DMMP and TPhP indicates that these additives slow the pyrolysis of the epoxy network. TMP, with a strong effect on the char yield, exhibits some condensed-phase action.

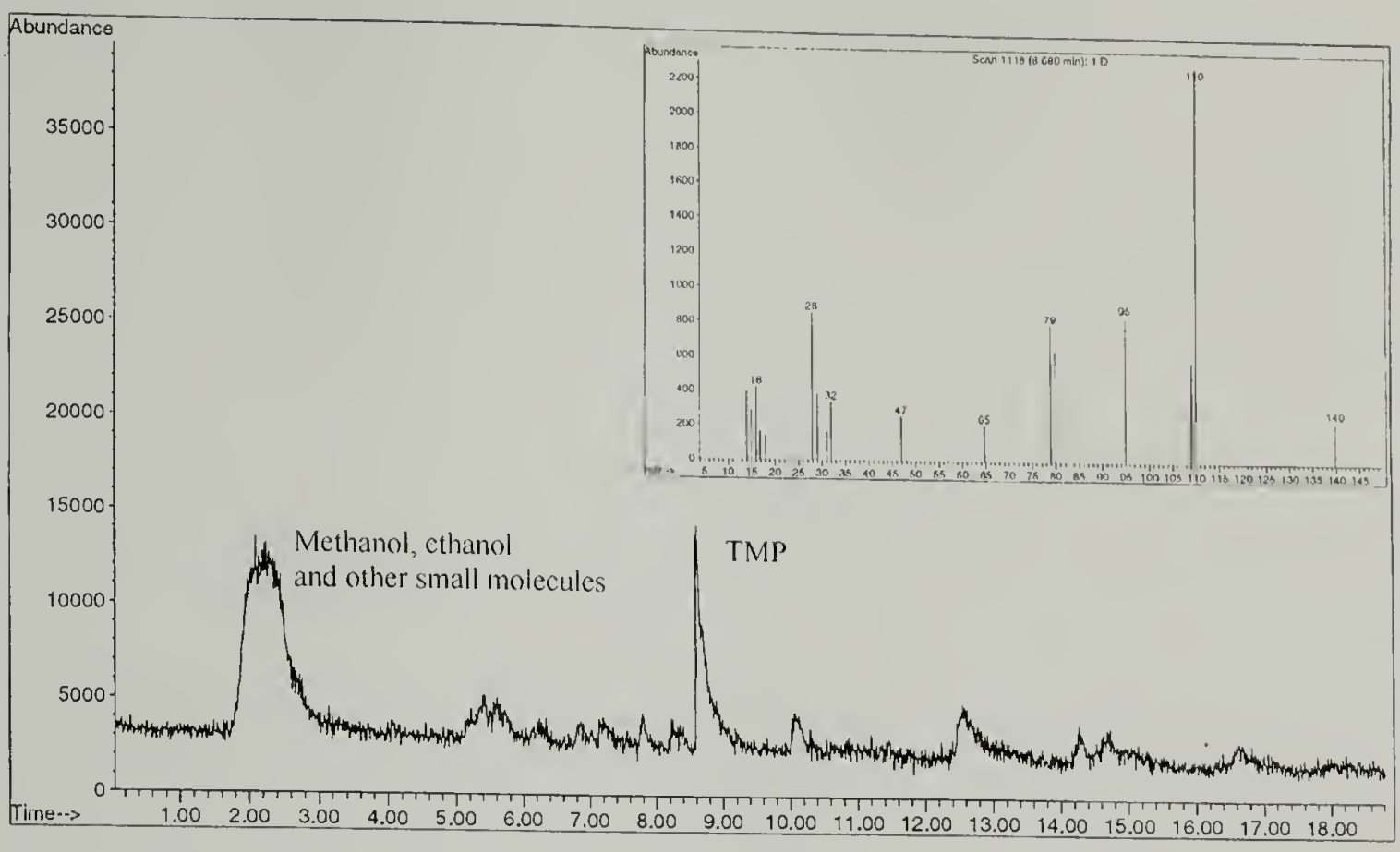

Figure 2.16 GC-mass spectrometer of low temperature (<300 °C) out-gassing products of TMP-epoxy pyrolysis. Inset: mass spectrum of TMP.

The flammability of DMMP-containing epoxy was also investigated using a PCFC microcalorimeter. This method measures the amount of oxygen consumed during pyrolysis and provides a quantitative evaluation of the heat released upon incineration. The results of this evaluation are found in Table 2.4. The total heat released is not significantly changed by the addition of the additive, and there appears to be a lack of additional char formation above that provided by degradation of the unmodified matrix. Both of these observations indicate that the DMMP additive does not alter the mechanisms of epoxy pyrolysis to a large degree. However, the heat release capacity is reduced in a manner similar to the rate of degradation seen in the TGA, from approximately 1100 J/g·K of the unmodified resin to 365 J/g·K at 15 phr DMMP (65%). Rather, the presence of the organophosphate slows the rate of degradation.

Table 2.4 Microcalorimeter heat release rates of DMMP-modified epoxy

DMMP (phr)	Rapid Wt. Loss Temp. (°C)	Heat Release Capacity (J/g·K)	Total Heat Released (kJ/g)	Char Yield (%)
0	385	1063	27.2	3.1
5	370	469	25.4	4.6
10	357	371	23.8	4.5
15	350	365	23.7	6.0
20	347	382	23.7	5.2

The data provided by the small-scale PCFC microcalorimeter are supported by cone calorimeter measurements of the 825-D230 resins modified with increasing concentrations of TMP (Table 2.5). The cone calorimeter is a large-scale measure of the heat generated upon incineration and requires samples of considerably greater dimension than those used in the PCFC. The cone calorimeter data, however, has the advantage of being a widely used, and widely accepted, measure of the flammability of a material. Regardless of the difference in the evaluation methods, the data obtained from the DMMP formulations on the PCFC and the TMP formulations on the cone calorimeter are in good agreement, with the 20 phr TMP sample reducing the peak heat release rate (HRR) by 61 % over the unmodified resin.

Table 2.5 Cone calorimeter flammability test

TMP (phr)	Peak HRR (kJ/m^2)	CO_2/CO ratio	Total heat released (kJ/m^2)
0	1324	34	43
5	1294	19	40
10	510	9	24
20	519	10	28

It should be noted, however, that the formulation being investigated here is not ideal for flame-retardant applications since the curing agent used is an aliphatic diamine with little inherent thermal stability. A stiffer curing agent with a higher aromatic content, such as 4,4'-diaminodiphenylmethane (DDM), would be better suited for exhibiting improved flammability characteristics.[69] Such formulations would yield significantly higher char upon degradation, further reducing the total heat released.

2.6 Chemical resistance

Many epoxies are used industrially because of their high chemical resistance. This is especially true for high performance applications such as matrix applications in aerospace composites. These are designed to withstand environmental attack after prolonged use at elevated temperatures and stresses. Under such conditions, attack by water is thought to be most destructive. Incursion by water into the matrix can cause swelling and internal stresses, weakening the matrix.[2] In order to investigate the effects of water on the antiplasticized matrices, each of the antiplasticized resins was subjected to a water treatment. The shape and sizes of the test specimens were kept as similar as possible to minimize geometric contributions in the analysis of results. However, the results here are normalized with respect to the original mass of the sample. All of the samples were weighed and submerged into a water bath. At select time intervals, the samples were removed, excess water was dried off and the samples weighed. Measurements of mass loss upon drying commenced after a 72-hour water submersion. The samples were laid out on a counter, and mass measurements were taken periodically.

The water-uptake data for all of the antiplasticizers, with the exception of TMP, show little evidence of water absorption. The unmodified epoxy resin, 825-D230, exhibit

a mass gain of 0.25 % after a 48 hour soak, whereas resins antiplasticized with DMMP, TEP and TPhP have mass gains of 0.4, 0.4 and 0.5 %, respectively, after similar soak periods. The TMP-antiplasticized resin, however, demonstrates a strong attraction to water under identical conditions (Figure 2.17). TMP is known to form strong hydrogen-bonded complexes with solvent water, where both the phosphoryl and alkoxy oxygens are active.[70,71] Triethyl phosphate, however, hydrogen-bonds to water only at the phosphoryl oxygen, and it is not surprising that the water affinity for these organophosphates is diminished. When used as antiplasticizers, the phosphoryl moiety of the organophosphates is engaged with the polymer matrix. This may further reduce the larger additives' affinities for water.

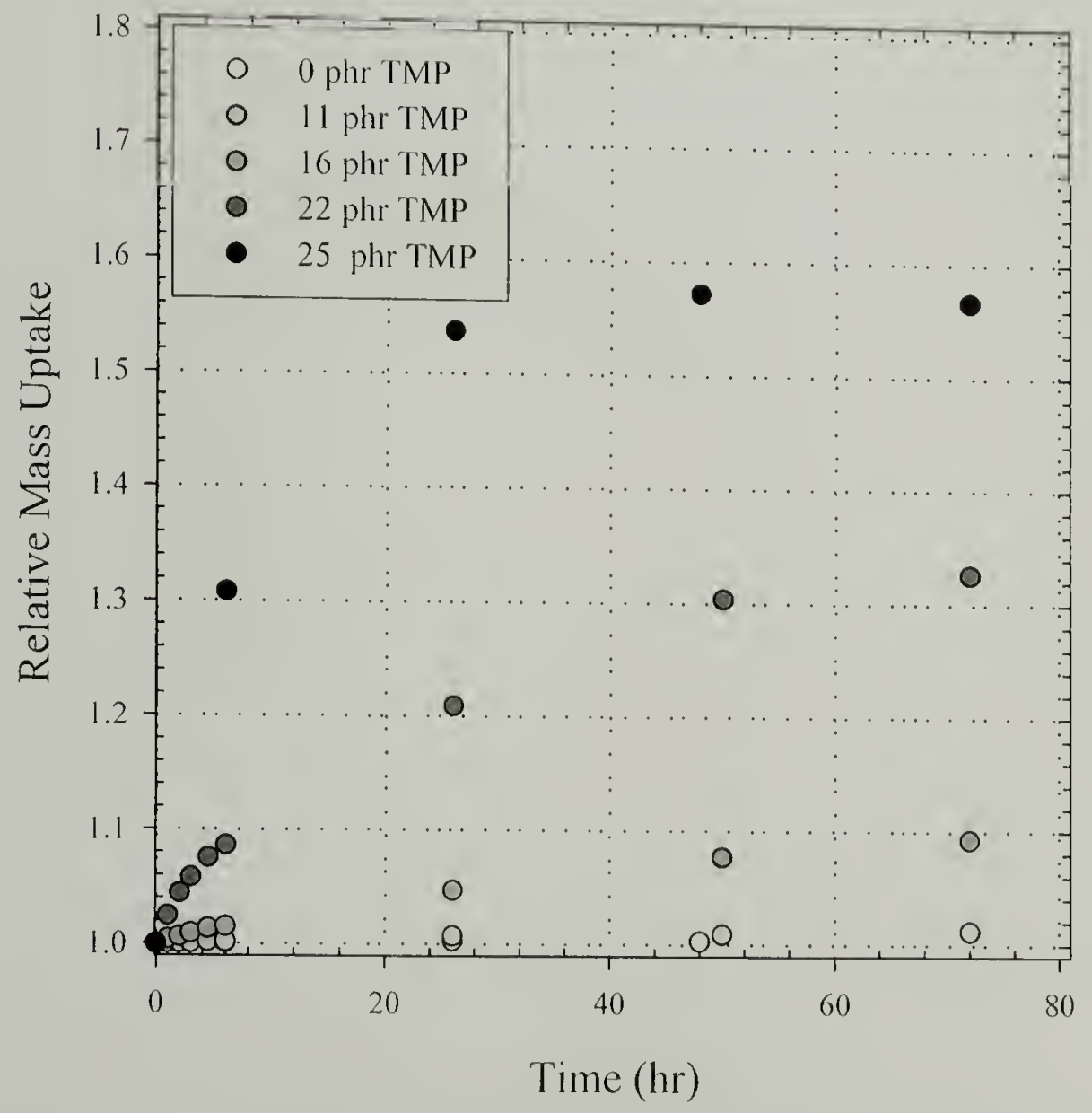

Figure 2.17 Relative mass uptake of water into 825-D230 resin modified with TMP.

The early regions of the mass-uptake curves follow Fick's law, with the slope of the curves exhibiting linearity against the square root of time (Figure 2.18). The slope of the line in such a representation is related to the diffusion coefficient. In this study, quantitative diffusion values cannot be extrapolated, as there is enough variability in sample geometry to preclude such analysis. Qualitative observations, however, can be made. That the slopes in Figure 2.18 increase with increasing TMP concentration indicates that the diffusion of water into the polymer is also increasing. Eventually a plateau is reached whereupon further mass uptake by the polymer is opposed by the physical properties of the matrix. Because the steady-state concentration of water (maximum water concentration) increases with increasing TMP concentration, this is further evidence that the water-polymer interaction is enhanced by TMP.

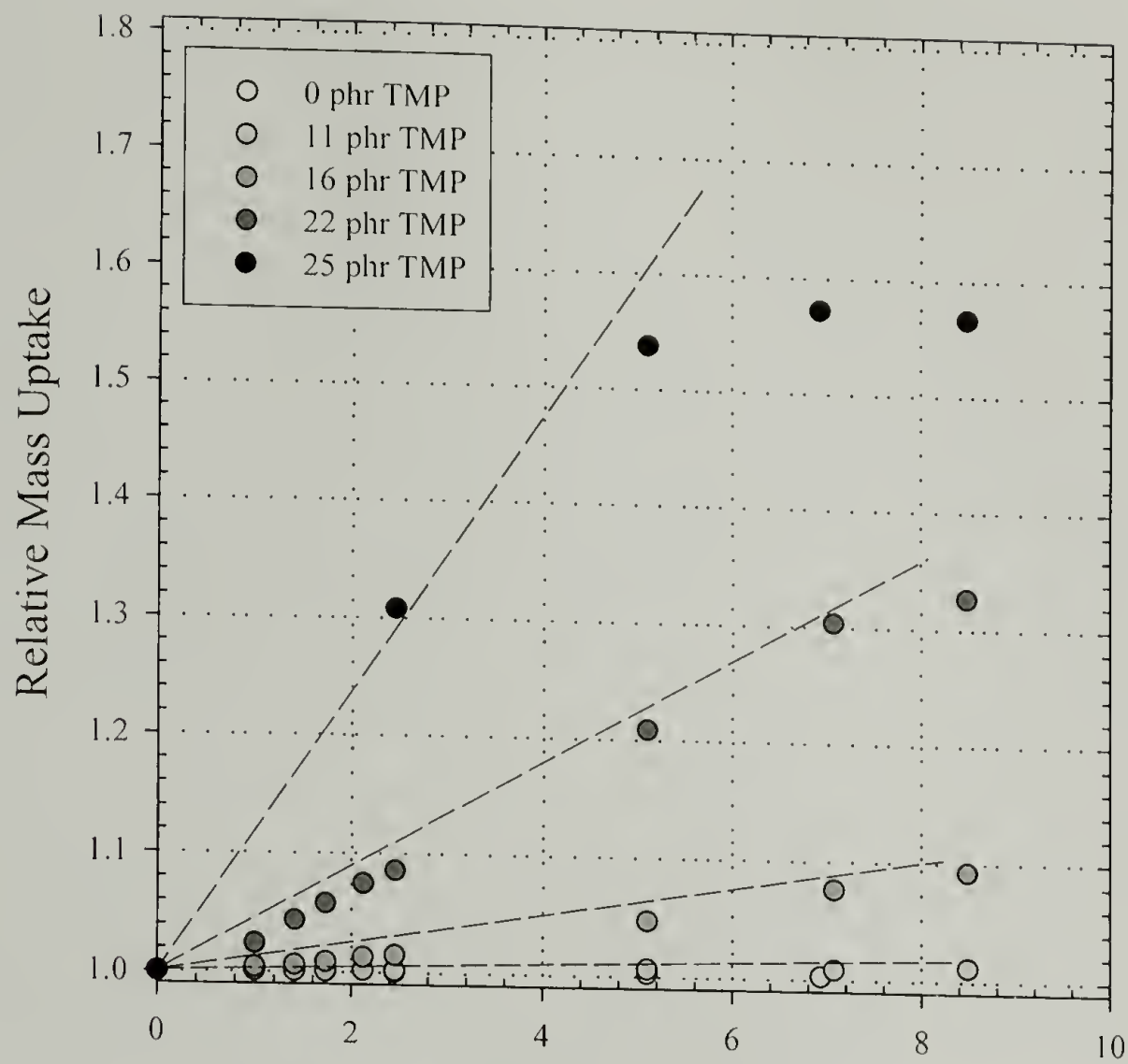

Figure 2.18 Fickian plot of mass uptake again the square root of time. (---) is used as a guide to the eye of the initial linear behavior.

Water absorption into the TMP-antiplasticized resin results in significant loss of mechanical integrity (Figure 2.19). In fact, after a 48-hour soak, a 25-phr TMP resin is completely plasticized. The modulus of the plasticized resin is 3.6 MPa, the strength to 3.8 MPa while the strain at failure is increased to almost 50 %, indicative of a rubbery polymer. These values are significantly different from the properties of unplasticized resin (modulus = 3.6 GPa, σ_y = 80 MPa and ε_y = 3 %).

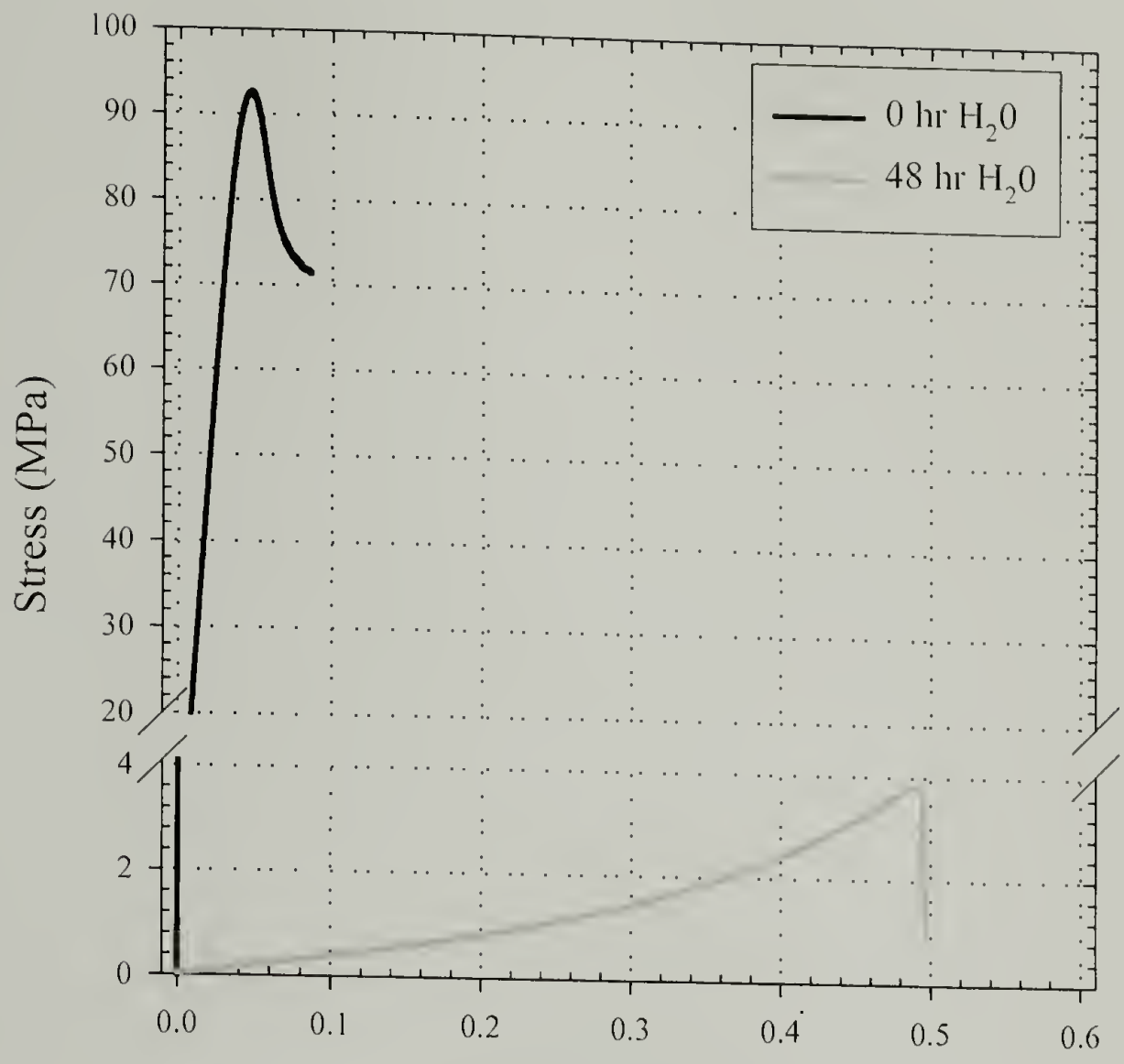

Figure 2.19 Resulting degradation of compressive mechanical properties of a 25 phr TMP in 825-D230 resin after 48 hour submersion in water. The resin is effectively plasticized.

The water-absorption is fully reversible, however (Figure 2.20). The initial mass reported is based on the mass of the fully plasticized resins. Evaporation at ambient conditions results in a loss of approximately 50 % the absorbed water. The mass-loss behavior is also Fickian (not shown), with increasing diffusion out of the resin with increasing TMP concentration. Further water removal can be accelerated by treatment of the samples in a vacuum over at 50 °C. Following 24 hours under vacuum, the samples have completely recovered their original mass. Elemental analysis, however, demonstrates that there is no evidence of antiplasticizer migration out of the resin throughout the entire submersion-evaporation cycle. This indicates that, although the

TMP does allow for water-complex formation around the alkoxy oxygens, the antiplasticizer itself is not dissolved and removed from the polymer. After complete water removal, the dry resin can again be swollen by simply submerging in water. This type of reversible behavior may have useful applications.

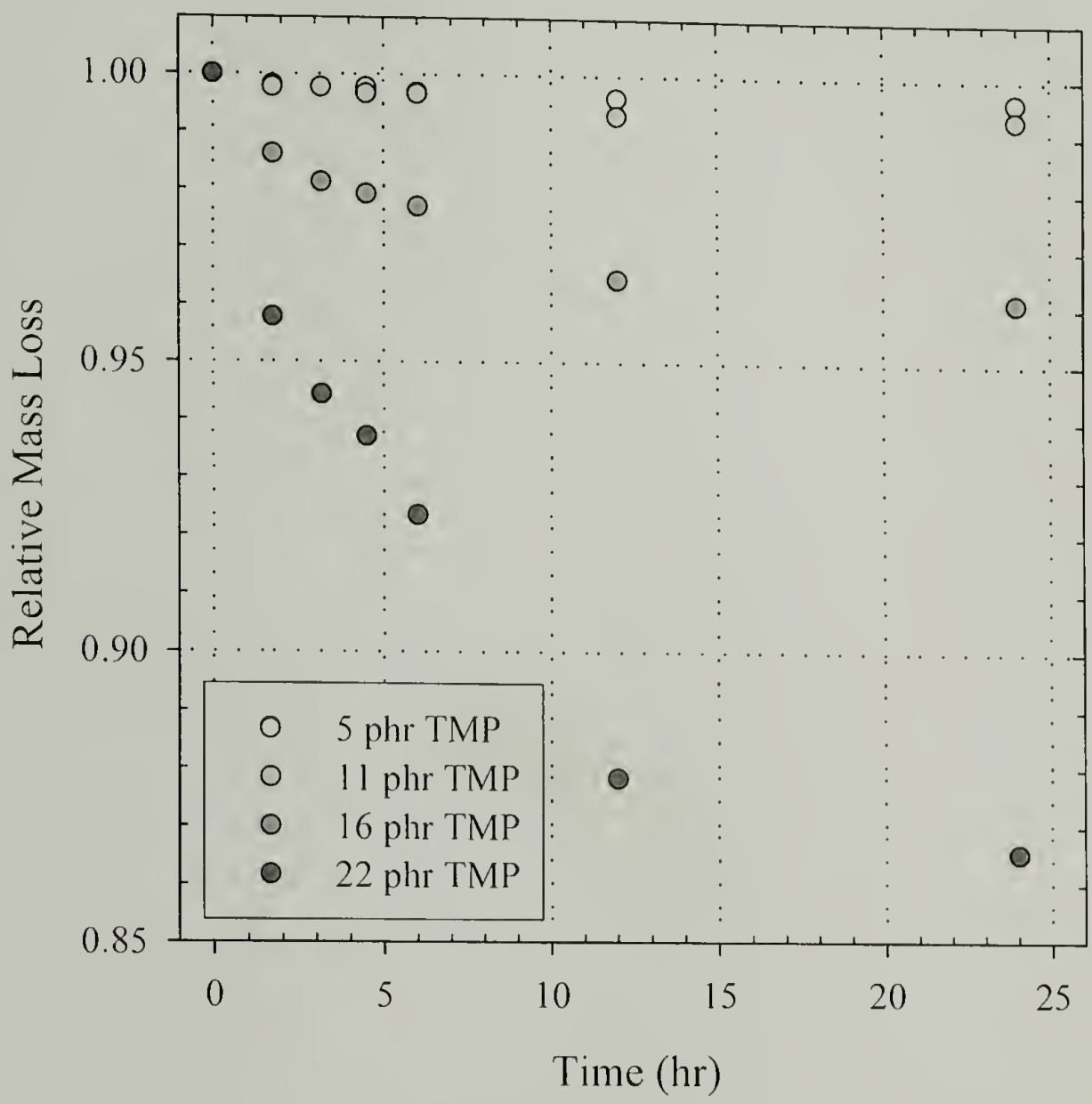

Figure 2.20 Relative mass loss of water upon ambient drying of 825-D230 resin modified with TMP.

2.7 Covalently bonded moleeular additives

In order to probe the role of eovalently bound organophosphate additives, a brief investigation was eondueted into the properties of a resin chain-extended using an amine-funetionalized phosphate. The additive, diethyl phosphoramidate (DEP) in Figure 2.21, is reaetive with the epoxy prepolymer. Beeause it is only a difunetional amine, however,

it acts only as a chain extender, increasing the molecular weight between crosslinks (M_c) of the polymer (Figure 2.22).

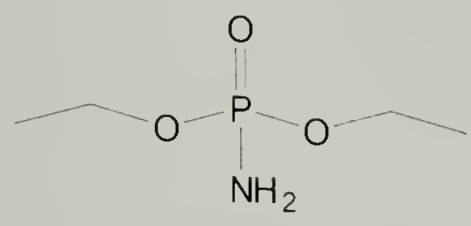

Figure 2.21 Diethyl phosphoramidate (DEP) – a reactive, chain-extending organophosphorous additive.

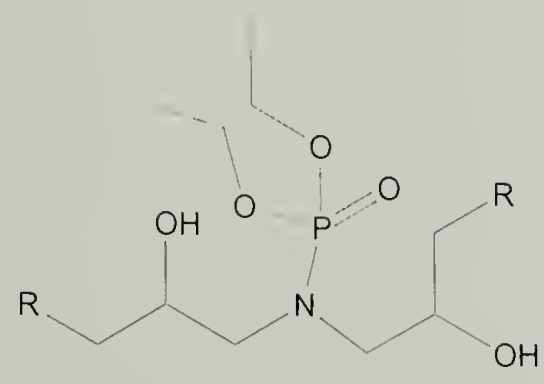

Figure 2.22 DEP acts as a difunctional, chain-extending curing agent during the reaction of the epoxy resin. After crosslinking, it behaves as a covalently bonded DMMP analogue.

The motivation for this investigation lies in previous literature evidence pointing to the greater effectiveness of covalently bound flame-retardants over blended additives.[66,68,69,72,73] By chemically binding the flame retardant species to the polymer backbone, release of the additive due to evaporation is minimized and increases the likelihood of a solid-state reaction leading to char formation. However, thermosets containing equimolar amounts of phosphorous result in almost identical thermogravimetric response (Figure 2.23).

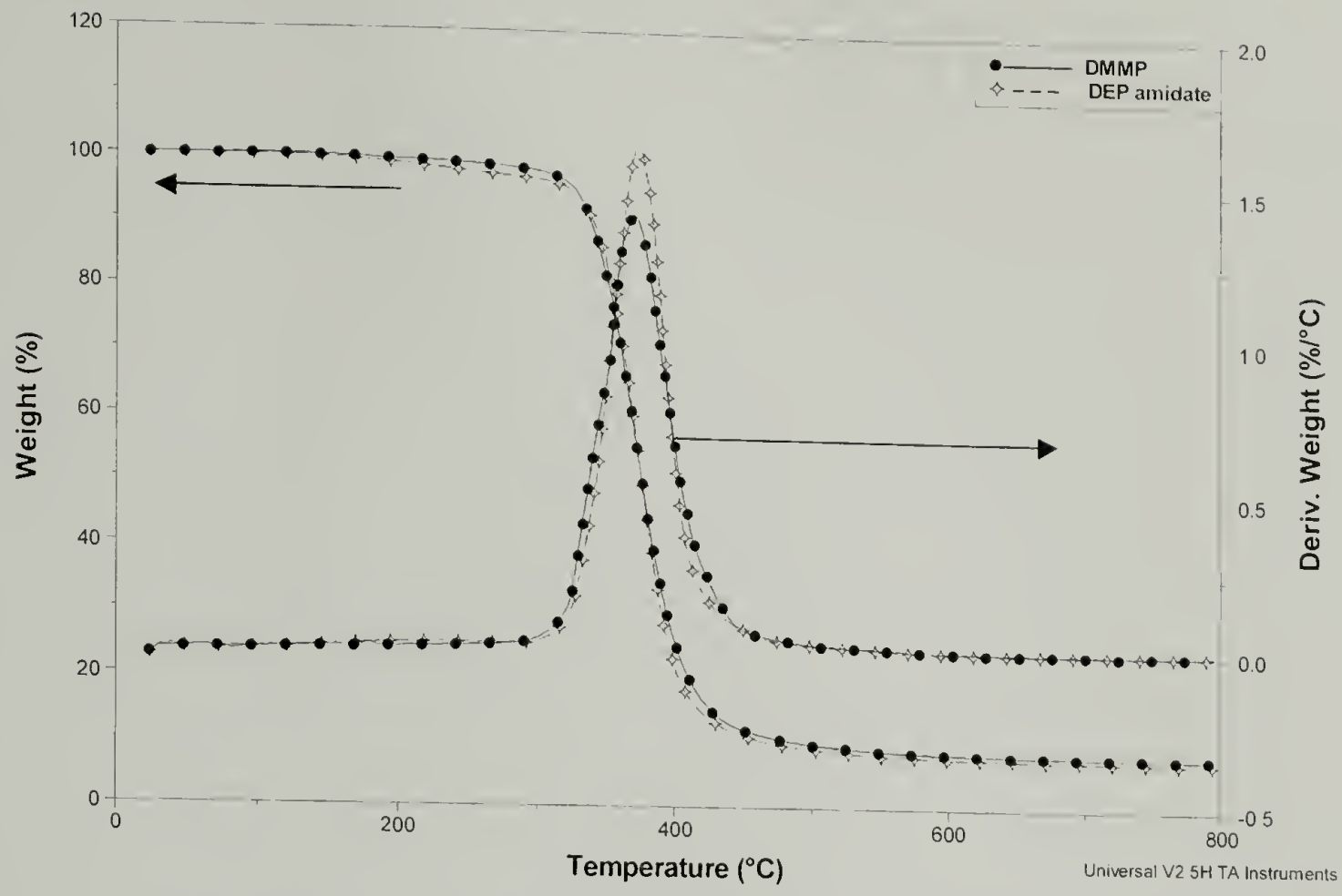

Figure 2.23 The thermal degradation of an epoxy resin containing equimolar amounts of organophosphorous additive does not display an effect of covalent bonding.

This result is likely due to the pendant nature of the DEP along the polymer backbone, leading to facile scission of the N-P bond. Rather, incorporating a diamine-functionalized organophosphate such as $P(O)(OR)(NH_2)_2$ could prove more efficient. Nevertheless, it was found that the covalently bound organophosphate behaved similarly to the unbound DMMP additives while restricting the concentration range over which such an additive would be applicable. With increasing concentration of DEP, the molecular weight between crosslinks of the thermoset would increase, thereby reducing the glass transition temperature of the matrix. This reduction in the T_g would reduce the overall mechanical properties of the matrix without significant benefit to the flammability behavior, and it diminishes the interest in such an additive.

The mechanical properties of the resins containing covalently-bonded phosphate analogues were compared to those provided by the DMMP additive. Because DEP acts

as a chain extender, resins containing identical M_c were compared. In order to increase the M_c of the DMMP-reinforced resin, aniline was used as a chain extender. Equimolar concentrations of DMMP and DEP were then used to compare identical antiplasticizer concentrations. The results (Figure 2.24) demonstrate that the mechanical performance of the covalently bonded phosphate is very similar to the conventional additive. Again, the disadvantages to using DEP over DMMP are evident. These include a decreased T_g with increasing the M_c, and only marginal enhancements to the final mechanical properties.

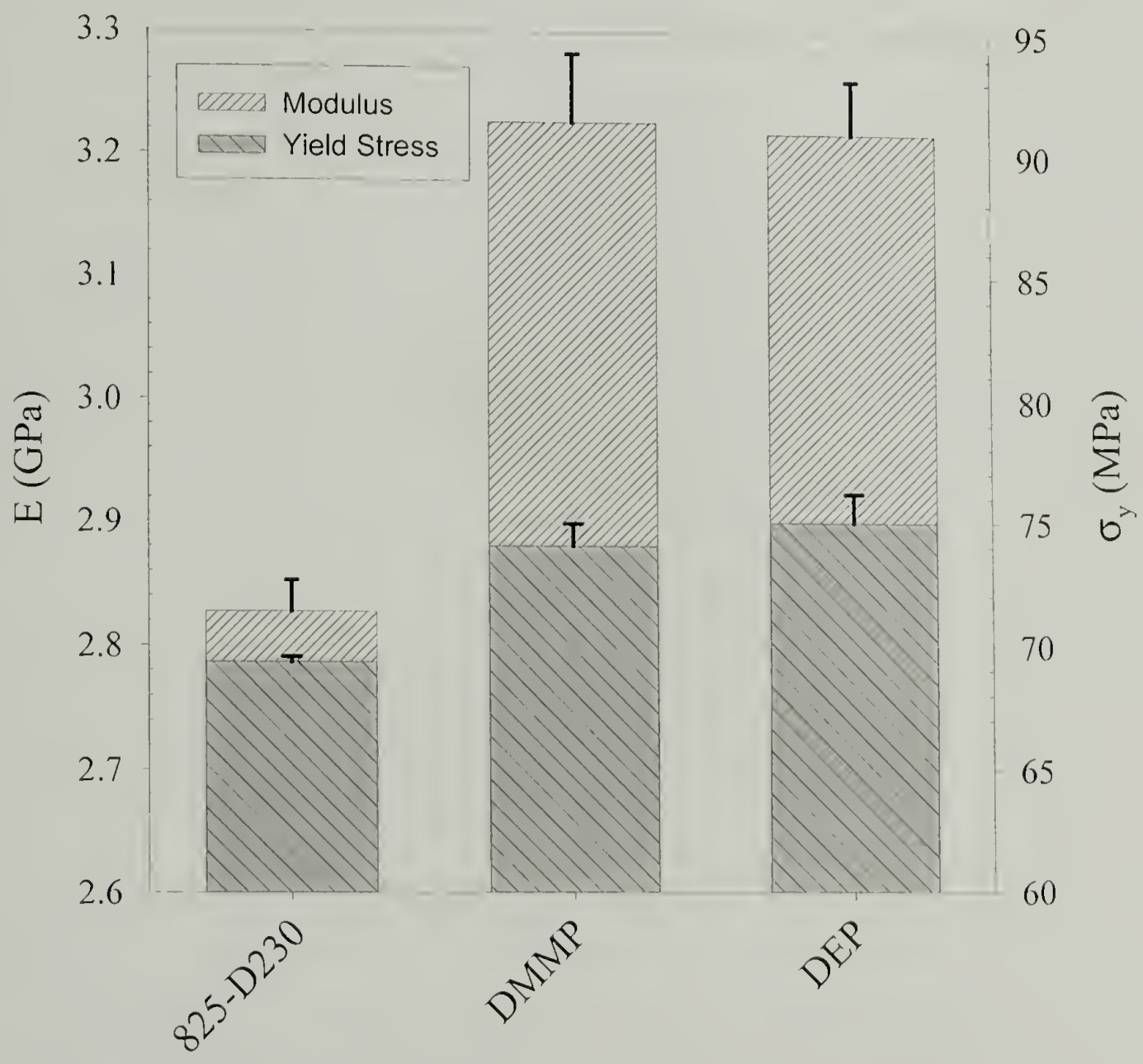

Figure 2.24 Mechanical properties of resins reinforced with equimolar concentrations (4 mol %) of DMMP and DEP as compared to an unreinforced resin (825-D230).

2.8 Conclusions

The effects of molecular additives on non-engineering physical properties are investigated. The chemical structure of the additives used strongly affects the thermal and physical characteristics of the resin, either by reducing the glass transition temperature or by increasing the density. The changes in material properties can often be related to the engineering behavior of a polymer. Mechanical properties are the focus of Chapter 3.

The T_g of a molecularly fortified resin is seen to be inversely proportional to the molecular weight and volume of the additive introduced. A similar observation is made of the effect of additive size on the density of the resin. Although all of the additives succeed in increasing the density of the resin, the efficiency of this densification is typically reduced with increasing alkylphosphate molecular weight. As a result, it is expected that the mechanical properties upon fortification may exhibit a similar trend in reinforcement potential.

A number of other material properties unrelated to mechanical performance have also been detailed. A potential advantage of using molecular fortifiers over typical reinforcement agents such as glass beads or mica is the effect of the additive on the viscosity and processibility of the resin. Traditional reinforcement agents lead to large increases in viscosity. Molecular fortifiers, on the other hand, can reduce viscosity, effectively acting as diluents in the early stages of resin processing. Order-of-magnitude reductions of viscosity were obtained by the organophosphates studied here.

The additives at the focus of this investigation contain high elemental concentrations of phosphorous with potential applicability as flame retardants. The

flammability of phosphate-containing resins is observed to decrease as the heat release capacity of the material upon incineration is significantly (greater than 60%) reduced. In order to improve the flame-retarding character of the additives, a covalently bonded analogue to the organophosphates was studied. No improvements in degradation reduction and char yield formation were observed, however.

A number of limitations exist with regards to applicability of such organophosphates as multifunctional additives for reinforcement of epoxy resins. Because the additives are not covalently bonded to the polymer network, it is possible to remove the additive at high temperatures through evaporation. Some of the additives have also been demonstrated to increase the affinity of the network to aqueous attack, resulting in significant swelling and plasticization of the polymer network. Epoxies are often used as structural components in engineering applications where resiliency to chemical environments is of great importance. Such applications appear to be inappropriate for TMP-reinforced resins, which exhibit a high affinity for water-absorption.

CHAPTER 3

MOLECULAR FORTIFICATION – MECHANICAL PROPERTIES

3.1 Introduction

The previous chapter addresses the effects of antiplasticization on the physical and thermal properties of fortified epoxy thermosets as a function of the additive chemistry. In light of these material property changes, the role of the additive and polymer network on the mechanical reinforcement of epoxy thermosets is explored.

Initially, the focus of this investigation is on the role of additive chemistry in dictating the level of mechanical enhancement. To complete our understanding of molecular fortification, the effect of the crosslink density and polymeric structure on antiplasticization is investigated by using a host of different curing agents in forming the epoxy matrix. This added complexity into the system can, if approached in a systematic manner, be used to add new insight into the mechanism for molecular fortification.

The goal of the following discussion, therefore, is to tie the preceding observations of the physical and thermal properties of an antiplasticized system with the resulting enhancements in mechanical properties. Consequently, the focus is not limited to the mechanical properties of antiplasticized epoxy thermosets. Rather, the culmination of this investigation is understanding the mechanisms for antiplasticization and the manner by which the fortification potential can be dictated using appropriate additives and thermoset architectures.

3.2 Materials

A number of curing agents are used in this investigation to control the molecular weight between crosslinks, M_c, as well as the chemical structure of the polymer backbone. Two diamine curing agents (EDA, PDA) are used to formulate model networks of a well-characterized, small M_c. This is due to the low molecular weight of these curing agents. The polydispersity of these curing agents is not of great consequence; rather, it is their effect on the continuum properties of the resin, as dictated by the M_c. The commercially cured systems (D230, D400), by contrast, result in loosely crosslinked networks. Simply by changing the curing agent, and thereby R' in Figure 2.4, the M_c of the epoxy is altered:

$$M_c = M_e + \frac{M_{ca}}{2} \qquad \text{Eq. 3.1}$$

The molecular weight of the epoxy, M_e, remains constant (370 g/mol) as the same reagent (EPON 825) is used throughout. Polydispersity is not taken into account. The four diamine curing agents result in the type of polymer-additive interaction discussed previously (Figure 2.4). The nature of the polymer-additive interaction is not altered. In addition to the four diamine curing agents, an anhydride curing agent was investigated, hexahydrophthalic anhydride (HHPA), (Table 3.1).

Table 3.1 Curing agents for use in epoxy resins

Curing Agent		Structure	Mol. Wt. (g/mol)	M_c (g/mol)
Ethylene diamine	EDA	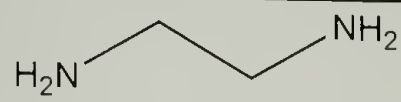	60	400
Propylene diamine	PDA	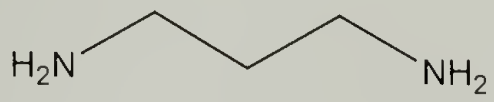	74	410
Jeffamine D230 (x=2.6)	D230	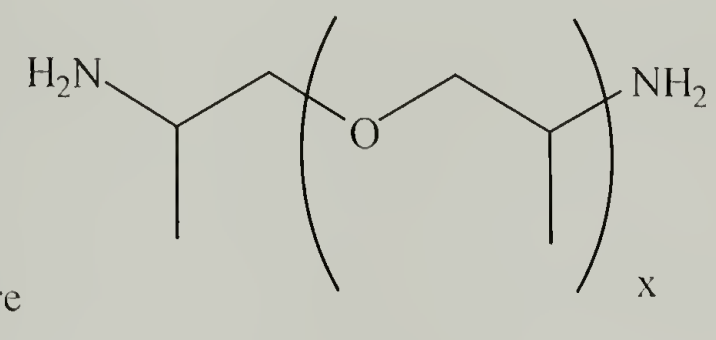	241	500
Jeffamine D400 (x=5.6)	D400		453	600
D230-D400	mixture		N/A	550
Hexahydrophthalic anhydride	HHPA	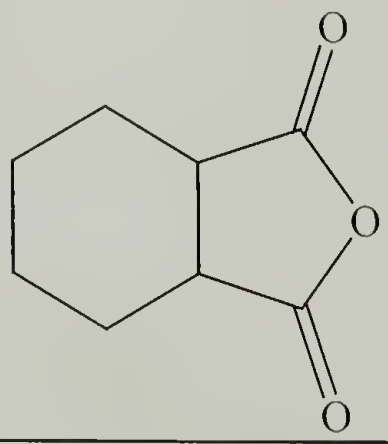	154	450

The network formed by crosslinking with an anhydride, rather than a diamine, results in a backbone lacking the characteristic hydroxypropylether functionality. Instead, the linkages (Figure 3.1) are carboxylic esters formed by opening of the anhydride of the curing agent. The R'-groups, above, form the cyclohexyl moiety of the HHPA curing agent and result in a rigid polymer backbone characterized by a high glass transition temperature. This type of network is not capable of sustaining the type of polymer-additive hydrogen-bonding interaction described in Section 2.2. The organophosphates can only interact with the anhydride-cured network through polar-polar interactions.

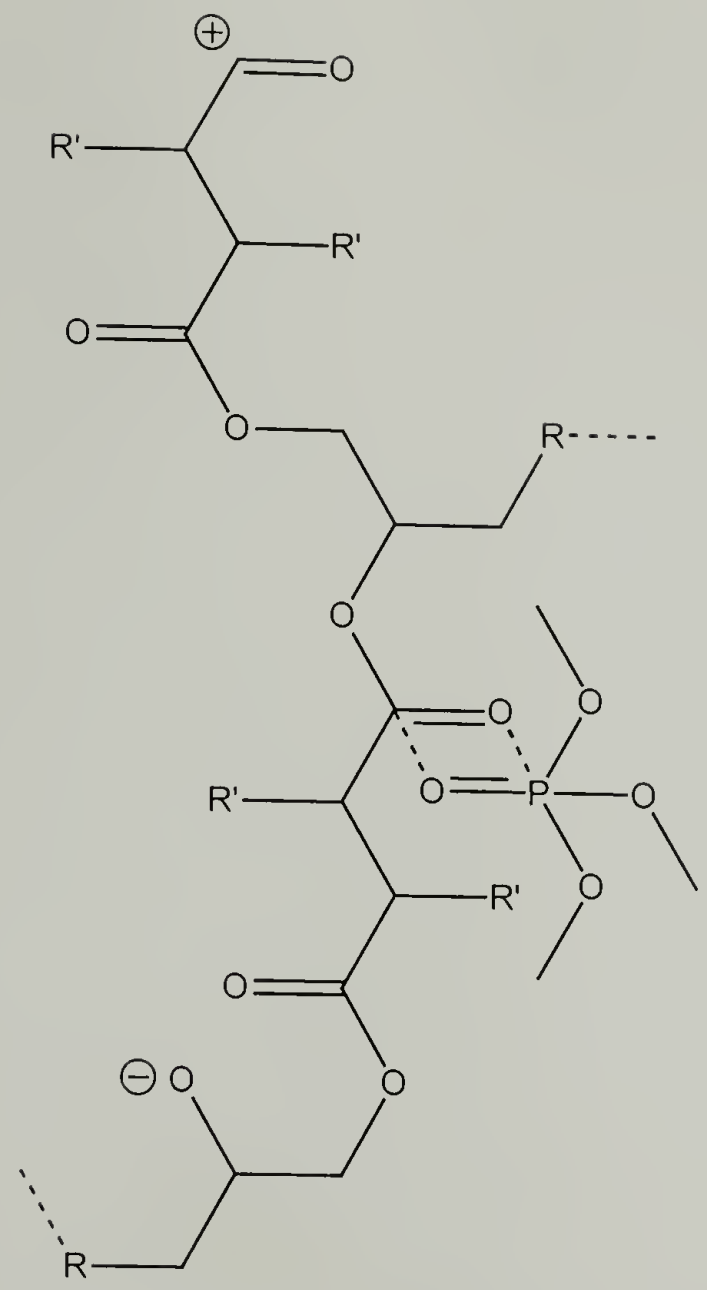

Figure 3.1 Possible interaction between organophosphate (TMP) and moieties along the backbone of an anhydride-cured epoxy resin.

3.3 Experimental

The fortified polymers are made by blending a given antiplasticizer into the epoxy resin (EPON 825) at 50 °C and mixing with a stoichiometric amount of curing agent. In the case of the D230-D400 system, a 50-50 molar mixture of the D230 and D400 curing agents is used to crosslink a stoichiometric amount of epoxy. The epoxy prepolymer is a purified diglycidyl ether of bisphenol A (DGEBA) of known molecular weight. After degassing under vacuum for fifteen minutes at 50 °C, the mixture is transferred into

molds for curing. Plaques are made by pouring into Teflon molds between glass plates treated with a silating release agent, Surfasil (Pierce Chemical). Samples for compression testing are cured in 8mm diameter glass test tubes. The amine samples are cured at 75 °C for 3 hours followed by an additional 3 hours at 125 °C. The anhydride-cured epoxy includes 1 phr (parts per hundred) accelerator, 2,4,6-tris-(dimethylaminomethyl) phenol, and is reacted for 3 hours at 75 °C followed by 2 hours at 200 °C. This reaction is completed under a nitrogen blanket to minimize oxidation of the polymer at such high temperatures. Complete cure is verified using differential scanning calorimetry (DSC), whereupon further curing does not result in an increase to the T_g of the resin.

Measurements of modulus and strength are conducted both in tension and in compression. Samples are prepared according to ASTM D638 and ASTM D695 for tension and compression, respectively. All samples are tested on an Instron 1123 machine. Tension and compression samples are loaded at constant crosshead speed of 2 mm/min and extensometers used where appropriate for measurements of strain. Densities are measured using a buoyancy method at room temperature in degassed, deionized water (ASTM D792). The thermal properties of the cured resins are investigated using DSC and a scanning rate of 10 °C/min.

Results are reported as a function of the molecular percent of additive. This calculation is based on the initial molar amounts of epoxy resin, fortifier and curing agents used to make the thermoset. A molar-based comparison allows for additives of different molecular weights to be compared more easily and without ambiguity. It should be noted, however, that the additives never exceed 30 weight percent and that optimal

conditions, although varying by additive, are achieved at 10 to 20 weight percent additive.

3.4 Properties of TMP in variable M_c systems

The physical and thermal properties of the fortified resins with changing curing agent are briefly discussed below. This discussion follows that presented in Section **2.4**. The fortifier in the following remains trimethyl phosphate (TMP). The role of the M_c in dictating the initial (0 % additive) T_g of the resin is evident (Figure 3.2).

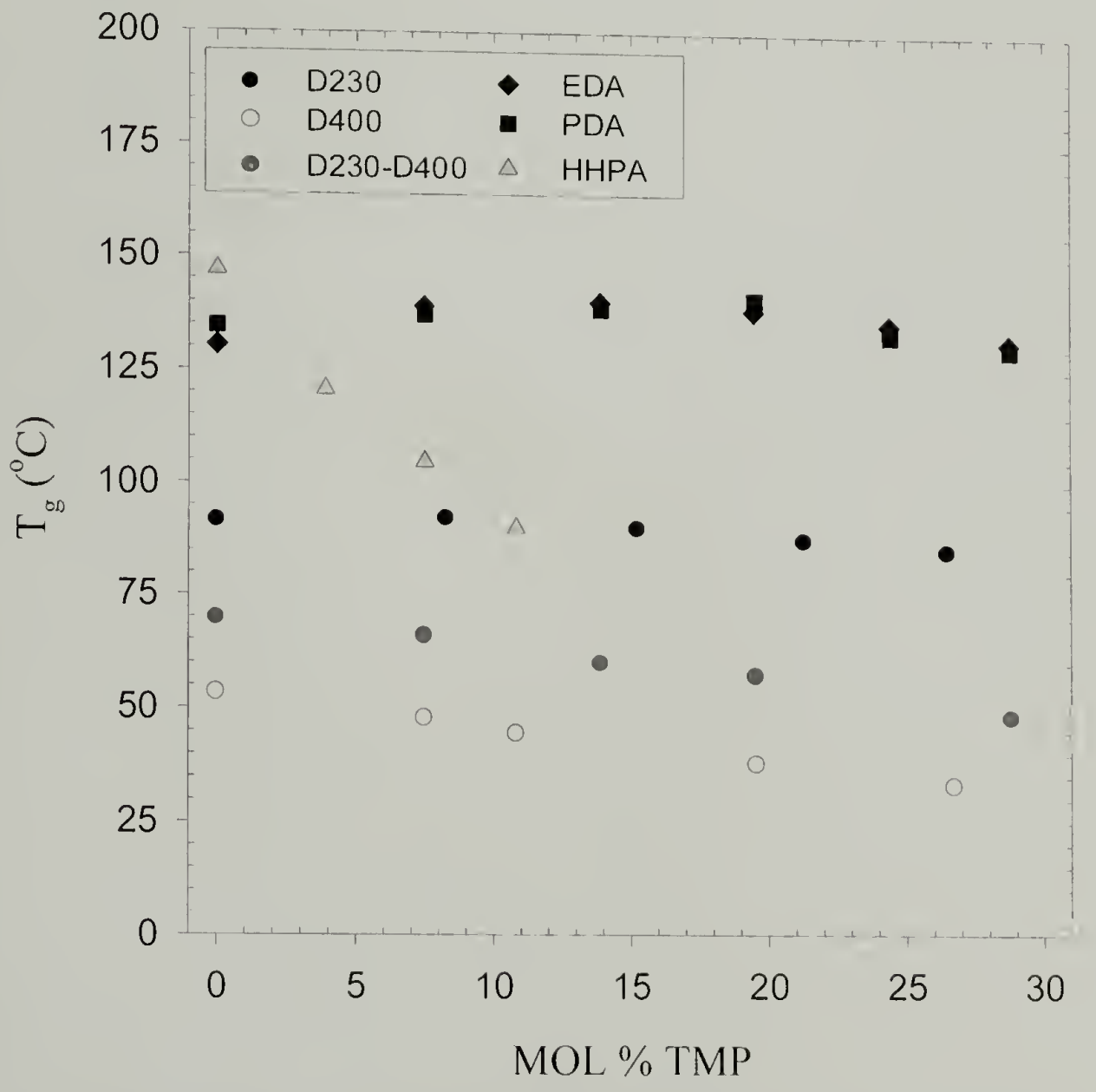

Figure 3.2 Glass transition of epoxy resins cured with a number of curing agents as a function of TMP concentration.

As expeeted, the glass transition of the unmodified, amine-eured resin is inversely proportional to the M_c of the polymer.[74] Addition of TMP into the resins has a profoundly different effeet on the T_g depending on the ehemieal structure of the polymer. For the case of the four diamine-eured epoxies, the addition of TMP does not signifieantly alter the T_g response. The anhydride-eured resin, on the other hand, is of a different chemieal structure and therefore falls outside this general trend. As previously seen for TMP in 825-D230 (Figure 2.6), the T_g is initially inereased slightly and subsequently deereased with higher additive eoneentrations. A similar behavior is observed for the remaining diamine-cured materials, indieating that the polymer-additive interaetion is preserved. A small effeet of M_c on the thermal behavior is evident, as the resins with smallest M_c exhibit the greatest (10 °C) inerease in T_g. The most loosely erosslinked networks (D230-D400 and D400) deercase the T_g at all TMP coneentrations, although the amount is not as signifieant as that observed for the larger organophosphates in 825-D230.

The HHPA-eured epoxy behaves thermally in a signifieantly different manner from the diamine-eured epoxies. At all concentrations, the T_g is depressed (almost 60 °C at 10 mol % TMP). With regards to phase separation, the DSC seans exhibit only one transition tempcrature at all eoncentrations for all networks, indicating a homogenous dispersion of the phosphate within the matrix.

Similar observations to those of T_g can be made as to the effeet of the phosphate on the density of different networks (Figure 3.3). This time, however, the density increases monotonically for all M_c's regardless of chemical structure. The rate of density inerease, represented by the slope of each plot in Figure 3.3, does seem to be affected by

the M_c, however. The more tightly crosslinked epoxies (EDA and PDA) have more dramatic increases in density (4.4 % and 3.4 % respectively) than does the least crosslinked D400 (2.4 %). The D230-D400 system represents an average of the D230 and D400 systems, in terms of both M_c and density and T_g.

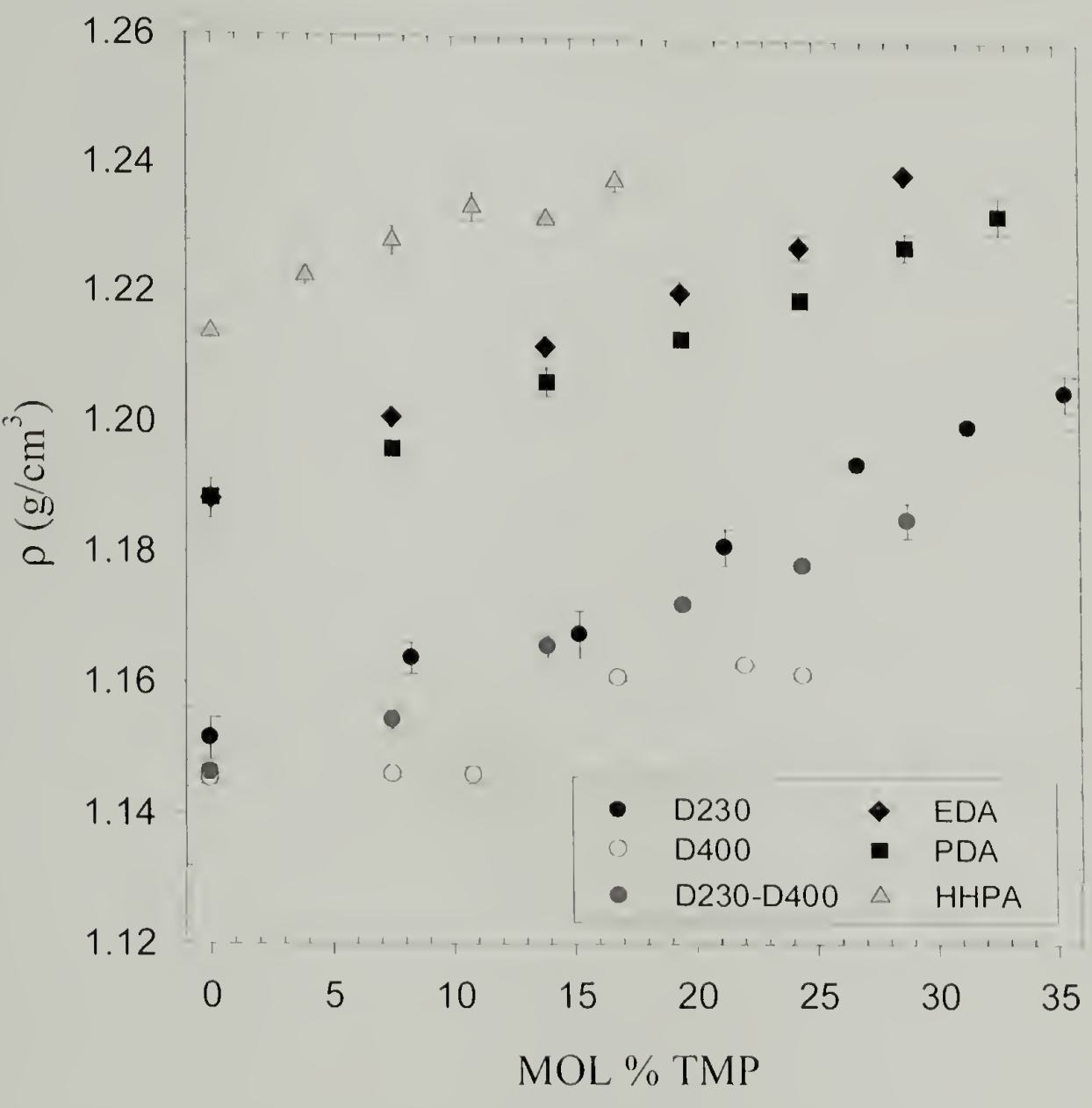

Figure 3.3 Increase in density for all epoxy networks fortified with TMP.

3.5 Mechanical properties

3.5.1 Dimethyl methyl phosphonate in 825-D230

Static mechanical properties of the DMMP-antiplasticized amine-cured epoxy networks were characterized in uniaxial tension and compression (Figure 3.4 and Figure

3.5). Under optimal concentrations (i.e. those resulting in the greatest enhancement of material properties), both the tensile modulus and yield strength increase 12% over unmodified epoxy. The compressive modulus improves 17%, while the compressive yield stress increases by 15% over the unmodified resin. The greatest enhancements in mechanical properties occur at a concentration of 10 phr DMMP, regardless of the loading condition.

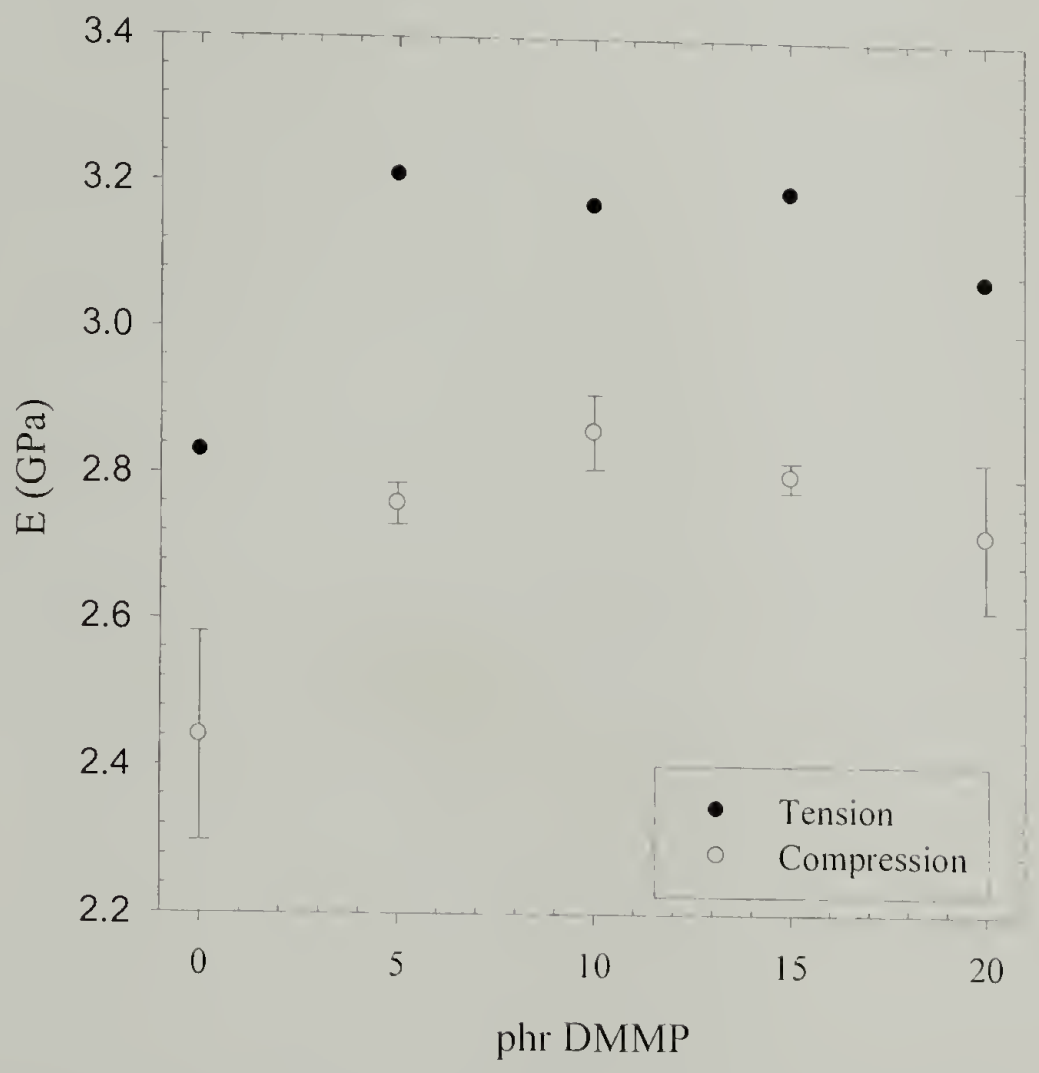

Figure 3.4 Tensile and compressive modulus of 825-D230 epoxy resin fortified with DMMP.

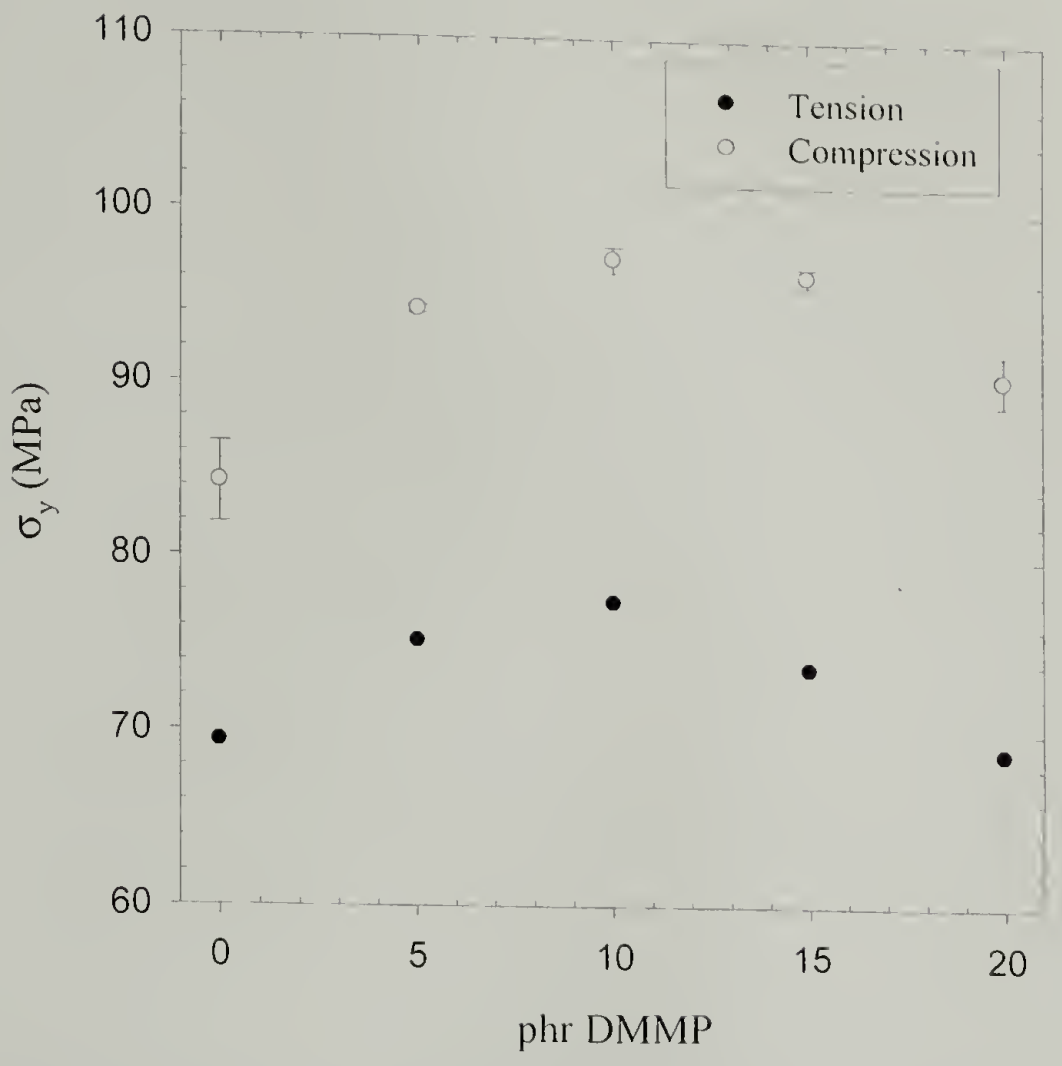

Figure 3.5 Tensile and compressive yield stress of 825-D230 epoxy resin fortified with DMMP.

The yield strain (Figure 3.6) is also affected by the presence of the antiplasticizer. At 10 phr DMMP, for example, the average strain at yield in tension and compression is reduced by 9.4% and 13.8%, respectively, over the unmodified resin. It should be noted, however, that the materials realize a zero-slope regime in the stress-strain curve, undergoing yielding before subsequent failure. Therefore, although there is a loss in ductility, the material does not undergo a ductile-to-brittle transition in its yield response.

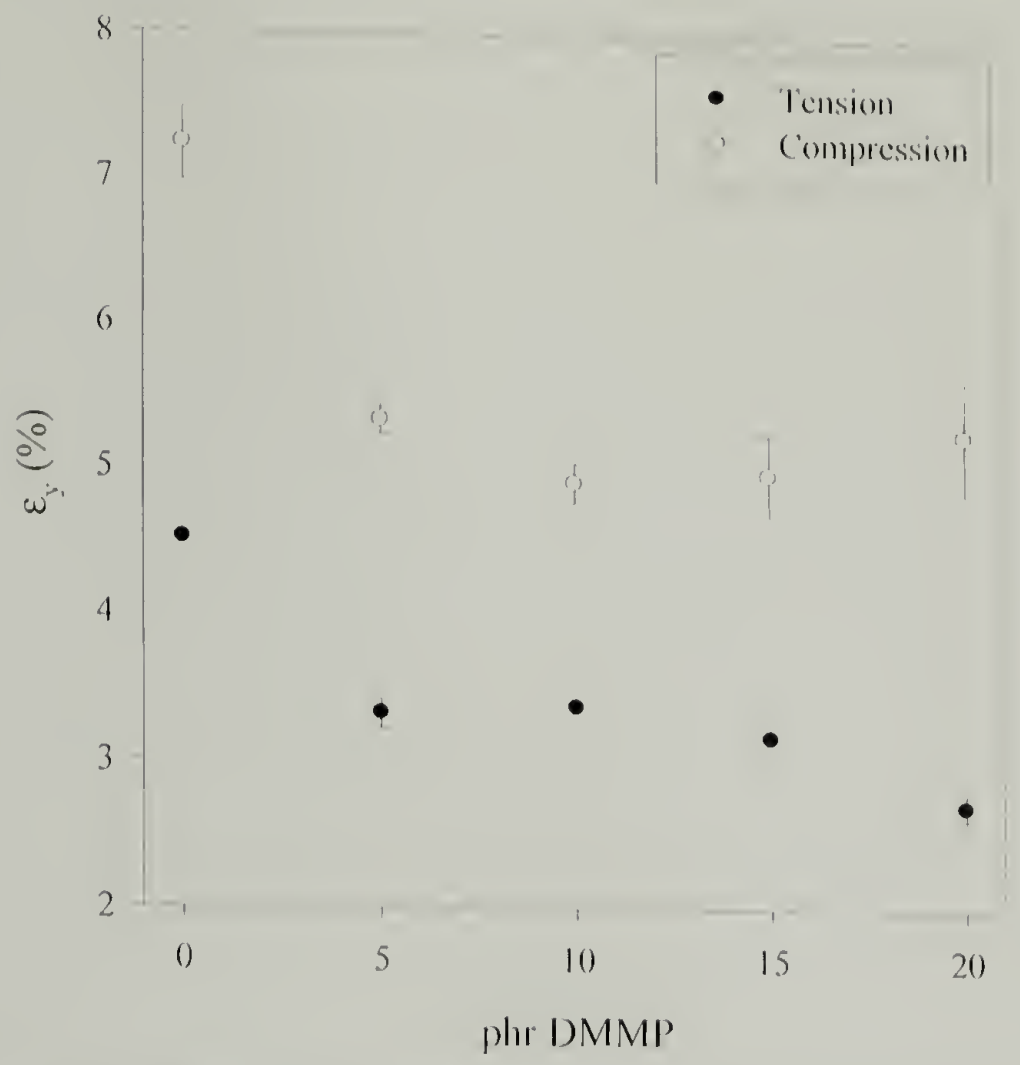

Figure 3.6 Tensile and compressive elongation at yield of 825-D230 epoxy resin fortified with DMMP.

The effects of DMMP on the Young's modulus, E, (Figure 3.4) and yield strength, σ_y (Figure 3.5) hint at the presence of a critical concentration of the additive above which the antiplasticizer ceases to fortify the network. Further addition of the antiplasticizer above 20 phr, for example, results in a reduction of the modulus and strength of the material until it can be said that the network is plasticized (its strength, stiffness and T_g are all below that of the unmodified sample). This concentration threshold has previously been reported for PVC and is a characteristic of small molecule antiplasticizers.[32] In the case of traditional plasticizers, this threshold is recognized as a minimum concentration, usually around 5 wt. %, of plasticizer that must be added. In this investigation, the concentration threshold is treated as a maximum concentration of additive that can be introduced while retaining some level of reinforcement.

The effect of DMMP on the fracture toughness was also investigated (Figure 3.7). An increase in the strength and stiffness of a material through the addition of an additive is often accompanied by a decrease in the fracture toughness of that material. In other words, materials are often embrittled as they are reinforced.

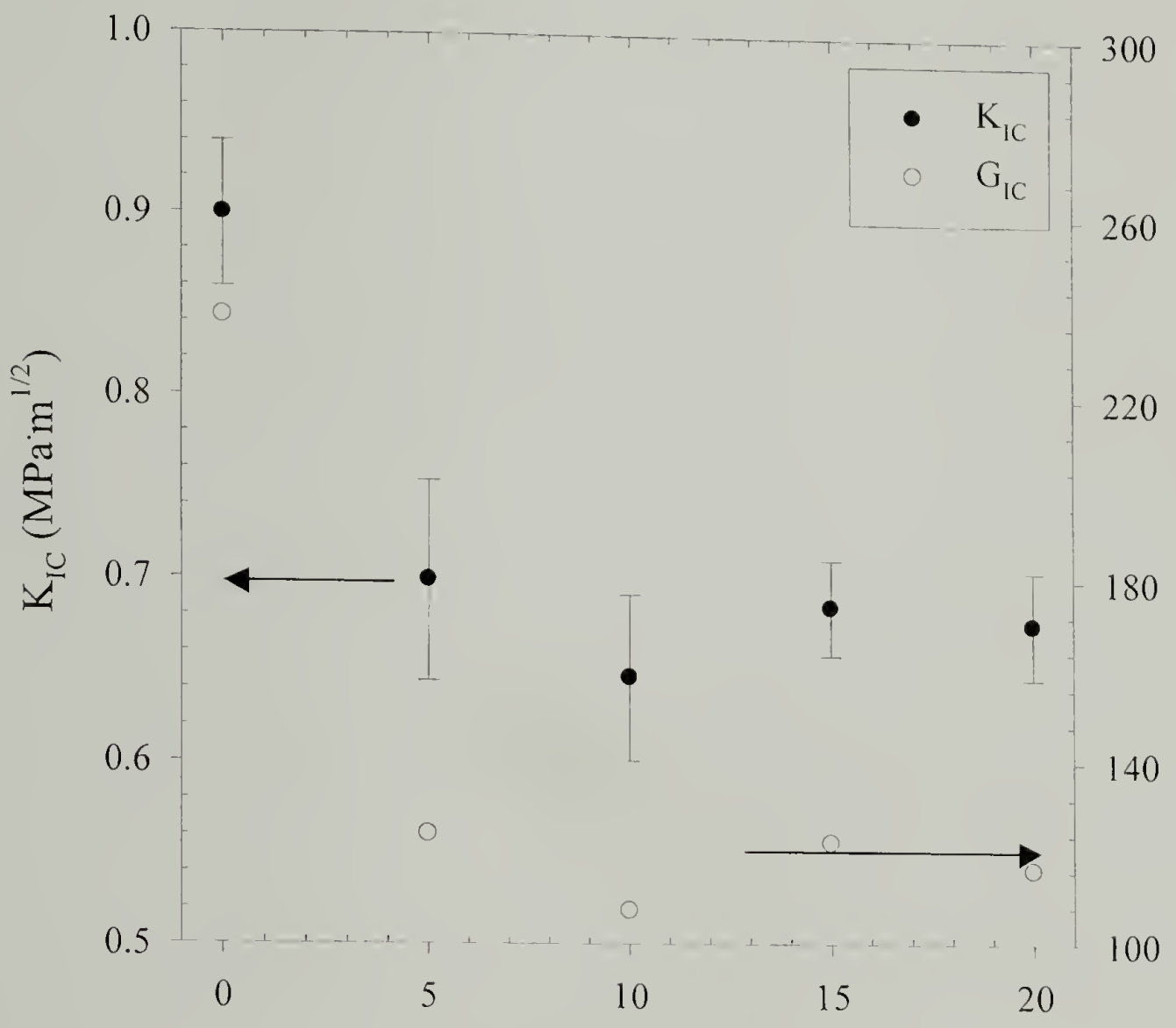

Figure 3.7 Fracture toughness of 825-D230 epoxy resin fortified with DMMP. Both the critical stress-intensity factor, K_{IC}, and critical energy-release rate, G_{IC}, are shown.

One approach to understanding this behavior is with cohesive-zone models to predict the behavior in front of the crack tip. Cohesive-zone models have successfully been used to describe the fracture toughening of thermosets through localized yielding at the crack tip as a function of the modulus and strength of the material.[75] The localized

yielding can lead to crack blunting, changing the radius of curvature of the crack tip and increasing the fracture toughness. This effect can be expressed as:

$$\rho \propto \delta_t = \frac{K_{Ic}^2}{E\sigma_y} \qquad \text{Eq. 3.2}$$

where ρ is the crack tip radius. This radius can be approximated to be proportional to the crack-tip opening displacement, δ_t. Equation 3.2, therefore, demonstrates that, for a constant δ_t, when increasing either modulus or σ_y, K_{IC} must be reduced. This inverse relationship between strength and toughness is well known, especially in rubber-modified systems. In fact, many approaches to toughening utilize this approach by sacrificing the strength of a material to gain in fracture toughness. As can be seen in Figure 3.7 for DMMP fortification, this initial trend is as predicted by Eq. 3.2. Both the stress intensity factor, K_{Ic}, and energy release rate, G_{Ic} (Eq. 3.3), are reduced with increasing E and σ_y of the matrix.

$$G_{Ic} = \frac{K_{Ic}^2(1-\upsilon^2)}{E} \qquad \text{Eq. 3.3}$$

where υ is the experimentally determined Poisson's ratio. The Poisson's ratio, υ, remains virtually unchanged for all DMMP concentrations.

At higher fortifier concentrations, however, the fracture toughness remains depressed, even though the tensile yield strength has been reduced. This is contrary to the response predicted above (Eq. 3.2). Upon closer inspection, it appears that only the initial introduction of fortifier is necessary to reduce the fracture toughness. At 5 phr DMMP and above, the fracture toughness remains statistically equivalent, whereas the tensile properties change dramatically.

In developing a complete understanding of the molecular fortification, a wider investigation into the reinforcement mechanisms was initiated. The role of various additives in enhancing the modulus and strength of a single polymer network is detailed below, followed by the action of the polymer network in dictating behavior.

3.5.2 Organophosphates in 825-D230

In the investigation into the role of the additive on mechanical reinforcement, the polymer network (the same 825-D230 from the DMMP study) is kept constant and only the organophosphate is changed. Both the tensile modulus and yield strength of the 825-D230 system are increased upon incorporation of the organophosphates (Figure 3.8). These improvements follow the general trends already observed for the diluents' effects on thermal and physical properties, wherein increased additive size leads to a decrease in the efficiency with which the additive antiplasticizes the matrix. The smallest of the additives, TMP, increases the strength and stiffness to a more significant amount over the other additives (34% increase in tensile modules, 29% increase in tensile yield strength). The larger additives show decreased efficiency with increasing molecular weight, such that TBP, the largest of the alkyl phosphates, results in only a 6% increase in tensile modulus and 5% increase in tensile yield stress at optimal concentrations.

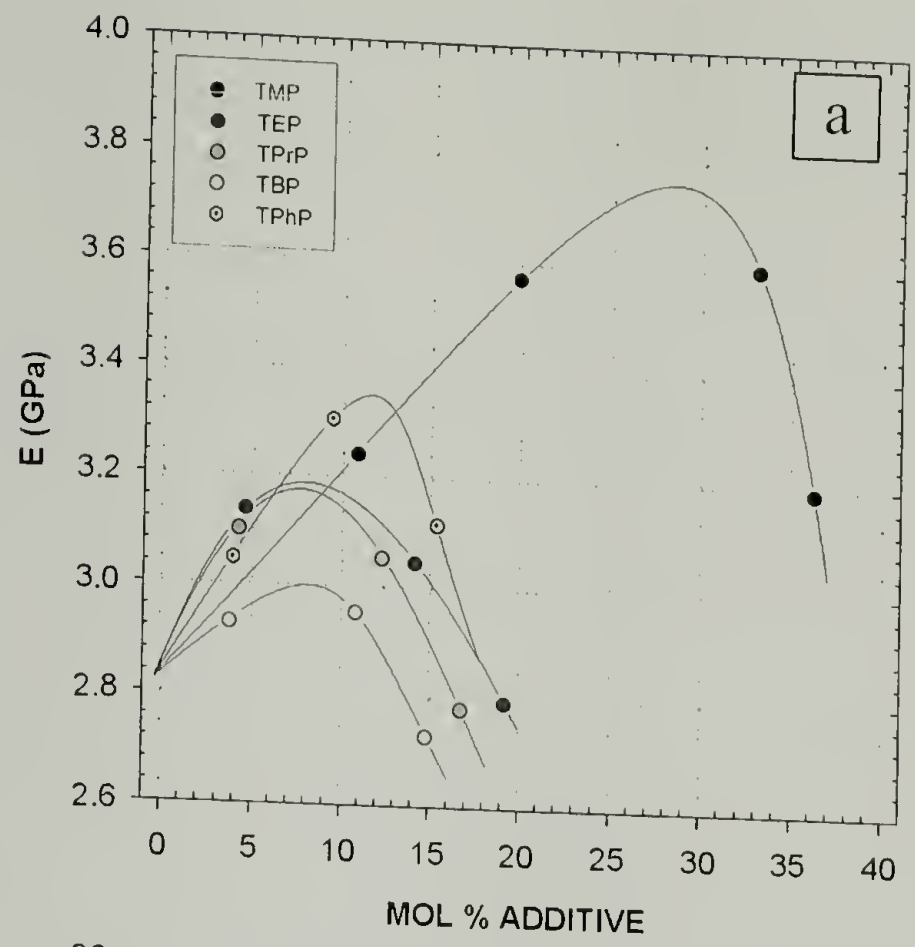

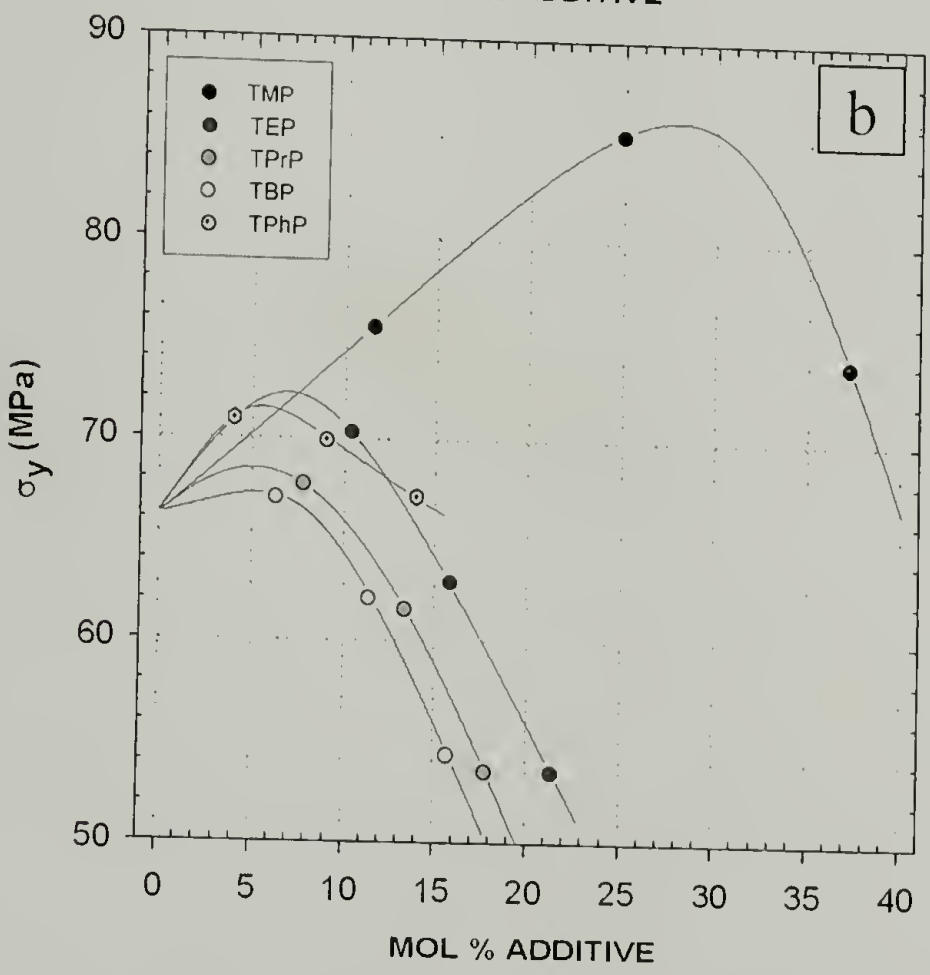

Figurc 3.8 Tensile modulus (a) and yield strength (b) of organophosphates in 825-D230 resin.

The threshold concentration is also affected. Here the threshold concentration is dcfined as that required for the material to return to thc tensile modulus of the unmodified resin. A yield-stress thrcshold can be similarly defincd. Thc maximum concentration

resulting in improved mechanical properties decreases with increasing additive molecular weight. Because antiplasticizers lead to improved strength and modulus over a well-defined concentration range, the threshold concentration proves to be a good comparative tool for antiplasticizer efficiency. Beyond the threshold concentration, the additive behaves as a plasticizer, decreasing mechanical performance. The threshold concentration is 36 mol % for TMP, and decreases to 18, 15, 13 and 18 mol % for TEP, TPrP, TBP and TPhP, respectively. Although these numbers differ slightly for compressive modulus and yield strength, the general trend remains the same, with a significant difference between TMP and the other, larger phosphates.

Note the performance of TPhP in increasing the modulus and yield strength. Whereas TPhP behaves similarly to TBP is reducing the T_g (Figure 2.6), it is a more efficient antiplasticizer in terms of density increases (Figure 2.10) and mechanical fortification (Figure 3.8). This difference in mechanical behavior for volumetrically similar additives demonstrates the importance of an additive's effect on the density of the resin. Although TPhP depresses the epoxy T_g similarly to TPrP and the larger organophosphates, its effect on density is more akin to TMP. The fact that the mechanical reinforcement realized through fortification with TPhP falls between both of these extremes demonstrates the importance of both increasing density and retaining a high degree of thermal stability.

Previous discussions of antiplasticization in the literature have focused on the ability of the fortifier to reduce or eliminate cooperative motions (as evidenced in the β-relaxation, Section 2.4.3) and thereby lead to an increase in the material's strength and stiffness.[52] Both Figure 2.8 and Figure 2.9 illustrate that the β-relaxation peak and the

free volume decrease linearly with fortifier concentration. The modulus and strength should therefore reflect such a trend through a continuous increase in these properties. The trends observed in the mechanical performance (Figure 3.4, Figure 3.5 and Figure 3.8) do not exactly match the trends set forth by the physical properties, which purportedly initiate the mechanical enhancements. This indicates that another mechanism is present limiting the enhancements in modulus and strength. A number of observations touched on in the previous chapter ought to be recalled here. These include the evidence for phase separation at the highest fortifier concentrations, the reduction in the glass transition temperature of the mixture and the apparent effect of the additives on the shape and size of the tan δ relaxation peak. These concepts are discussed in detail below in relation to the mechanical properties of the antiplasticized resins.

Phase separation observed in the DMTA (Section 2.4.3) at high fortifier concentrations may be responsible for the decline in mechanical properties at those concentrations. As the concentration of the additive is increased and the epoxy resin becomes saturated, additional organophosphate would act as a typical solvent. It is difficult to quantify the amount of phase separation using the DMTA data, however, as only the highest phosphate concentration exhibits a strong shoulder. Nevertheless, a crude approximation might be attempted using the solubility parameters of both the epoxy (~20 $MPa^{1/2}$) and additive. These can be used to approximate a Flory-Huggins parameter, χ, for the polymer-solvent interaction and predict the concentration range for solubility. Knowing the solubility parameters involved, as well as the molar volume of the solvent, V_1, χ is approximated:[76]

$$\chi = \chi_s + \frac{V_1}{RT}(\delta_1 - \delta_2)^2 \qquad \text{Eq. 3.4}$$

In the ease of DMMP, where δ_H is unknown, the solubility parameter is approximated using the van Krevelen[64] group contribution values to be ~18.7 $MPa^{1/2}$. The entropic component, χ_s, is typically taken to be constant and often taken as 0.34. Miscibility of two-component solvent-polymer systems is related to the change in the chemieal potential, $\mu_1 - \mu_1^0$, of that system, typieally with change in temperature.[77] However, miscibility ean also ehange with solvent/solute concentrations:

$$\mu_1 - \mu_1^0 = RT\left[\ln(1-v_2) + \left(1 - \frac{1}{x}\right)v_2 + \chi v_2^2\right] \qquad \text{Eq. 3.5}$$

where v_2 is the volume fraction of polymer, and x is the number of chains, T is the temperature and R is the gas eonstant (8.3145 J mol^{-1} k^{-1}). A system is known to be miseiblc when the ehemieal potential of the binary system is deereased upon mixing. Therefore, if it can be shown that $\mu_1 - \mu_1^0$ undergoes a sign-change over the additive eoncentrations investigated, phase separation is expected and can be quantified.

The first approximation outlined above, however, is valid only if 1) there are no favorable interaetions between the polymer and the solvent, and 2) there is no volume ehange upon mixing. Obviously, neither of these eriteria applies for the case of a strongly interacting additive that has been demonstrated to decrease the free volume of the polymer upon mixing, as is the case for DMMP. Even with these qualifications, however, Eq. 3.4, yields a χ value of 0.41, well within the critical value of χ=0.5, dietating miscibility over the entire eoncentration range. Strong interactions in this system would only enhanee miseibility. As a result, the phase separation observation in the tan δ is likely an artifact of the DMTA measurements. Thus, phasc separation as a

route to decreased mechanical properties at higher additive concentrations can be ruled out.

The strength of the polymer-additive interaction, however, can be used to predict the effective concentration range for each additive (Figure 3.9). The solubility parameter of epoxy networks in strongly hydrogen bonding solvents is reported as 20 $MPa^{1/2}$. The results in Figure 3.9 are plotted against the solubility parameter difference between that of the epoxy, δ_e, and additive, δ_a. Given that the antiplasticized materials behave slightly differently when observing the increase in modulus and the increase in σ_y, the concentration ranges obtained from each plot are presented above. Ideally, the slope of each would be identical. The explanation lies in the thermal properties of the antiplasticized resins.

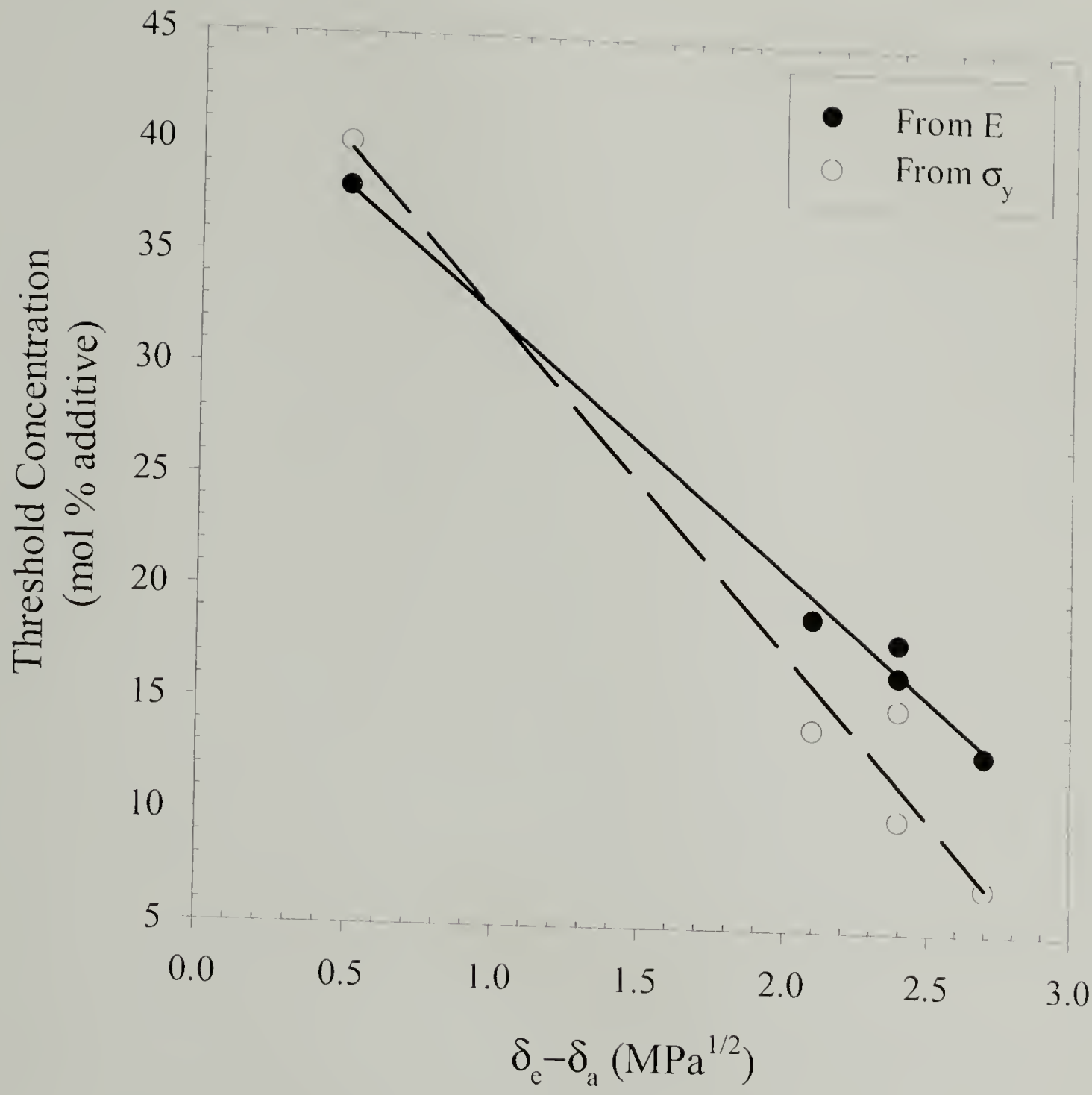

Figure 3.9 Correlation between the effective concentration range for additives in 825-D230 and the solubility difference between the resin, δ_e, and additive, δ_a.

The yield behavior of epoxy thermosets is known to be highly dependent on the thermal properties, or T_g, of the resin.[78,79] Then, because the T_g is known to be highly dependant on the M_c, one can demonstrate the dependence of σ_y on M_c.

$$\sigma_y \propto T_g = T_{g\infty} + \frac{\zeta}{M_c} \qquad \text{Eq. 3.6}$$

The T_g of a crosslinked resin is inversely proportional to its M_c, taking into account $T_{g\infty}$ of the uncrosslinked, linear polymer and the free-volume contributions to crosslink formation, ζ, which capture the entropic penalty for crosslink formation. It is not surprising, therefore, that the correlation between δ_a and the concentration range (Figure 3.9) is steeper when using the σ_y range than for the modulus-related data. Whereas σ_y changes with T_g, the modulus does not. The modulus of a crosslinked epoxy is not significantly altered upon increasing the M_c if the backbone stiffness of the polymer is kept constant.[74] Because the T_g of the resins antiplasticized with low δ_H additives (TPrP and TBP) is decreased with increasing additive concentration, the σ_y that is measured is likewise slightly depressed (low T_g usually translates to a low σ_y). The T_g of the TMP-antiplasticized epoxy is not depressed, even at high concentrations, and the effective concentration range for the TMP-fortified resin can be considered unaffected by T_g. As a result, the correlations in Figure 3.9 based on the yield strength measurements include the effect of depressed T_g and threshold concentrations are slightly reduced. The modulus-based correlation is unaffected by changing T_g of the resin.

Finally, using the dynamic-mechanical data obtained for the different additives (see Figure 2.7 for example), the yield strength of the polymer can be related to the energy required to undergo a glass-rubber transition. The DMTA experiments were conducted using a constant frequency oscillatory strain while ramping the temperature of the sample. The dissipative energy density per cycle of a system under oscillatory strain can be expressed as:

$$\frac{W(T)}{V} = \oint \sigma \frac{\partial \varepsilon}{\partial t} dt = \oint \sigma_o \varepsilon_o \sin(\omega t + \delta) \cos(\omega t) dt \qquad \text{Eq. 3.7}$$

which reduces to

$$\frac{W(T)}{V} = \sigma_o \varepsilon_o \pi \sin \delta(T) \qquad \text{Eq. 3.8}$$

δ(T) is the phase-lag angle between the imposed strain, ε, and corresponding stress, σ, at a given temperature, T, and frequency, ω. The instrument used to obtain the dynamic relaxation spectrum, however, provides only the storage and loss moduli. The dissipative energy, therefore, must be expressed in terms of the loss modulus

$$E''(T) = \frac{\sigma_o}{\varepsilon_o} \sin \delta(T) \qquad \text{Eq. 3.9}$$

as follows:

$$\frac{W(T)}{V} = \sigma_o \varepsilon_o \pi \sin \delta(T) = \varepsilon_o^2 \pi E''(T) \qquad \text{Eq. 3.10}$$

The total energy dissipation for the thermal α-transition can be treated as the integral of the loss modulus, E", with temperature. The greater the area under the loss-modulus curve, the greater the thermal energy required to undergo the transition at constant oscillatory strain.

As seen in Figure 3.10, this treatment results in a good correlation with the measured yield strength of the antiplasticized polymers. Qualitatively, the DMTA results support the observation that the antiplasticizer initially increases the energy required to yield the material. Whether this increase in total energy consumption is due to an increase in the activation energy for yielding or an increase in the activation volume cannot be determined from this analysis.

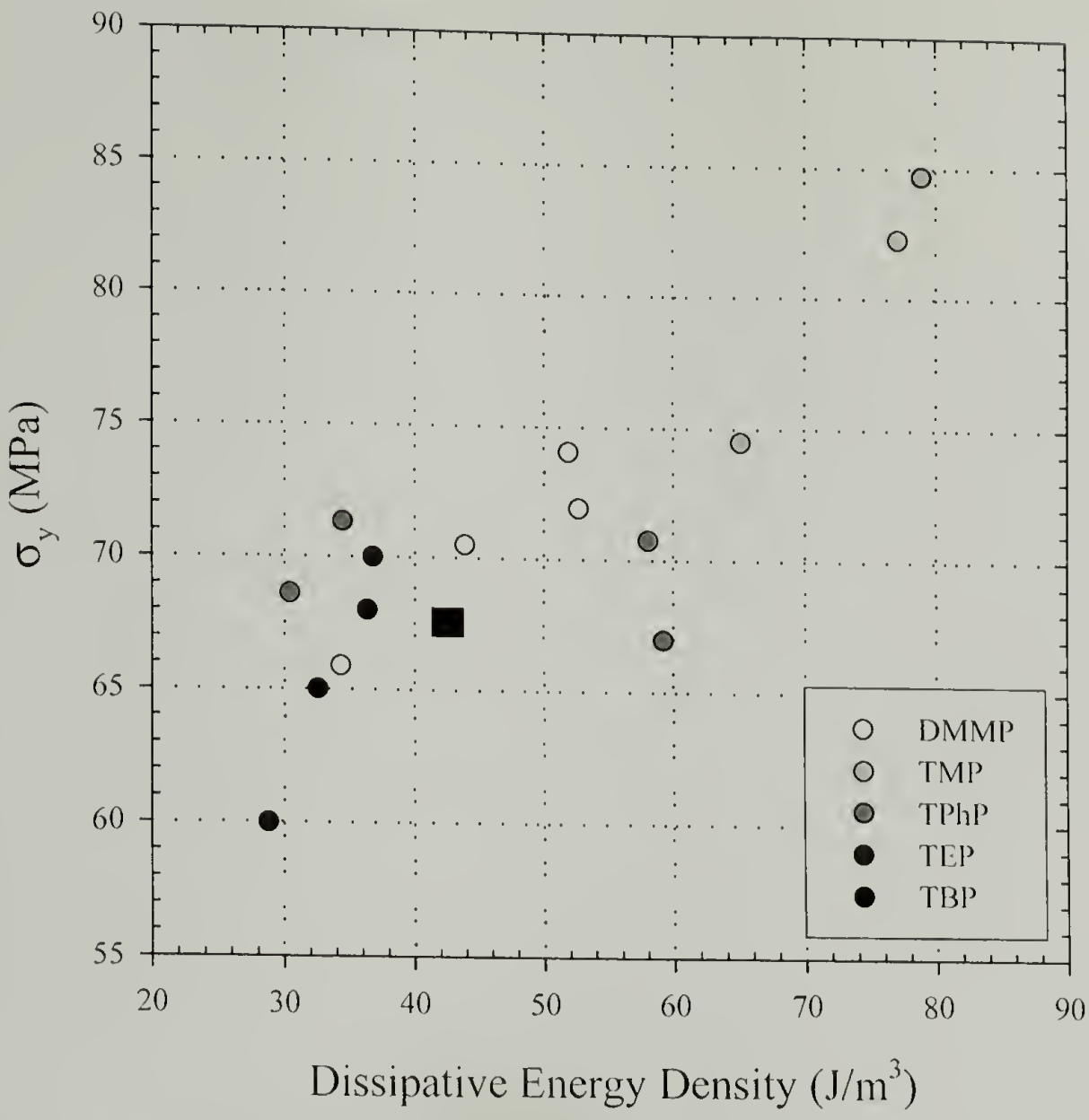

Figure 3.10 Correlation between thc yield strength of antiplastieized 825-D230 thermosets and the energy per unit volume (J/m^3) dissipated around the α-transition T_g±50 °C. The (■) eorresponds to thc σ_y and dissipative energy of the unmodified 825-D230 resin.

The observations of moleeular reinforcement with changing additive chemistry dcmonstrate that, for a constant epoxy network eapable of sustaining hydrogen bonding, the additivc dictatcs the level of reinforcement, E and σ_y, as well as the eoneentration range of additivc over which the fortification is sustainablc. A number of compcting effects arc observed in this investigation: thc effect of the additive on the T_g of the resin and its ability to increasc the density, or rcduec the free volume, of the resin with inereasing eoneentration. Inereasing density enhanees the fortification, whereas

decreasing T_g dampens the effect. However, to fill out this picture of organophosphate fortification of epoxy, the role of the epoxy thermoset must be investigated.

3.5.3 Antiplasticization of variable M_c systems

In understanding the role the polymer plays in molecular fortification, a single organophosphate was used to probe a number of different epoxy networks. This is accomplished by changing the curing agents used to crosslink the network. The most obvious effect of changing the curing agent in an epoxy thermoset is the molecular weight between crosslinks of the system. As seen in Figure 3.11, the mechanical properties of the antiplasticized networks do in fact differ significantly with M_c. As the M_c of the network increases, the efficiency of the antiplasticizer is decreased. The D400-cured network, which has the largest M_c, is simply plasticized by TMP with no apparent mechanical enhancements at any concentration. The most tightly crosslinked materials, however, produce the greatest increases in both strength and stiffness. The EDA and PDA systems both exhibit increases in modulus and strength of approximately 50% at TMP concentrations of 25-30 mol %.

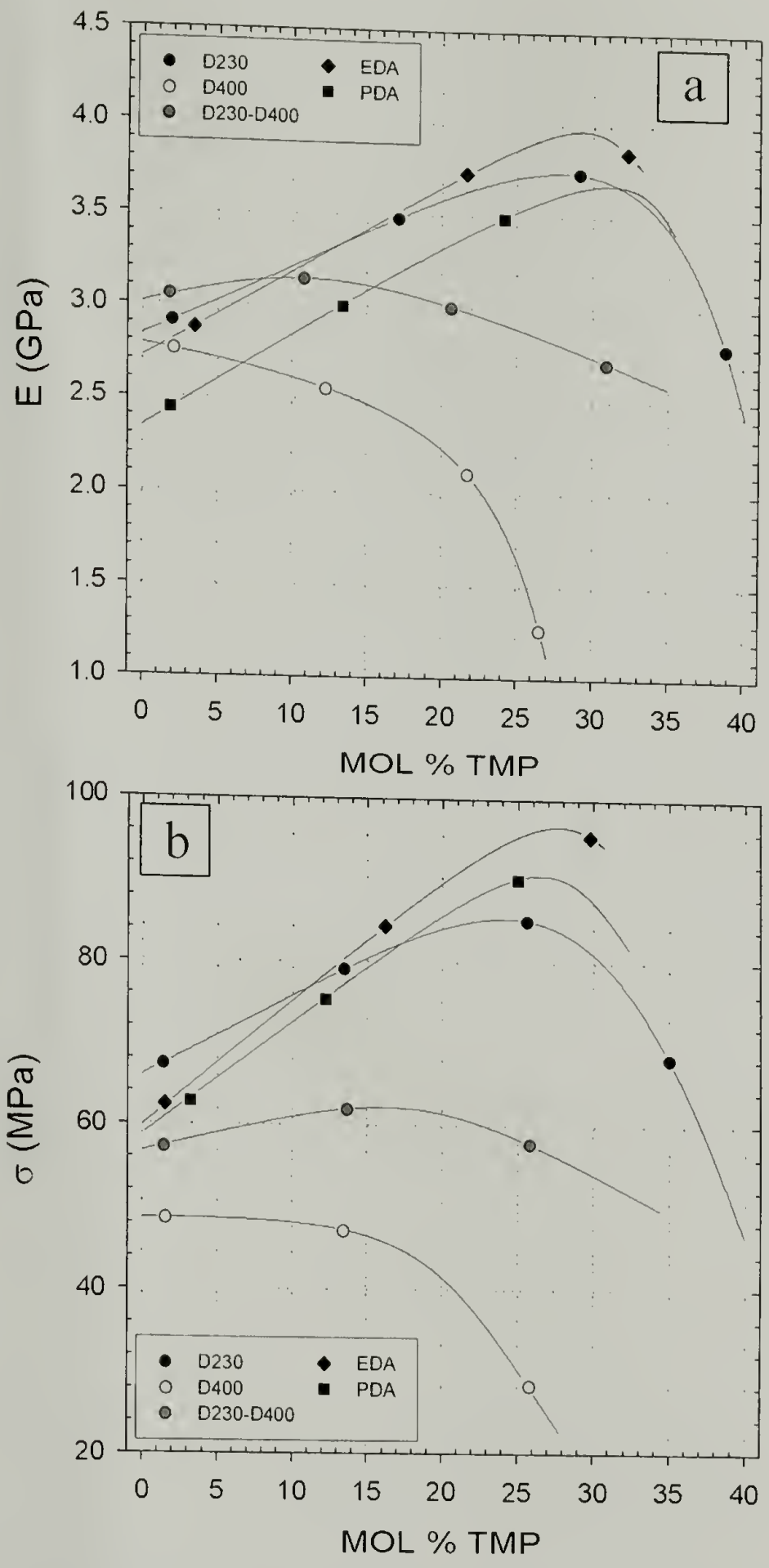

Figure 3.11 Tensile modulus (a) and strength (b) of TMP in 825-resins cured with various curing diamine curing agents. The resins cured with D230, D400 and D230-D400 yield before failing and their yield stress is presented. Both the EDA and PDA-cured resins fail in a brittle fashion and their ultimate strength is shown.

It should be noted, however, that the EDA and PDA cured networks fail in a brittle fashion under tension and the failure stress, σ_f, rather than the yield stress, for these materials is reported. Nevertheless, the increases in modulus and strength as a function of M_c clearly show that, for diamine-cured epoxy networks antiplasticized with TMP, a smaller M_c yields higher returns.

The significant departure from expected behavior for the D400 network prompted a need for a thermoset with M_c between that of the D230-cured system and the D400. In order to achieve this M_c, a mixture of equal molar amounts of D230 and D400 was used to cure the epoxy. The resulting network, D230-D400, has a M_c of 550 g/mol When TMP was used to antiplasticize this network, the mechanical response is an average of the D230 and D400 responses, indicating a competition between antiplasticization of the network, and plasticization of the same. This observation points to a critical M_c required for achieving fortification through this mechanism.

A number of other interesting observations can be made from the antiplasticization of the various networks with TMP. For the case of the low M_c networks (EDA, PDA and D230) the effective concentration appears constant. Each of these networks has a high initial T_g that is not depressed by the additive,. That is, all three of these networks exhibit a peak modulus and peak σ_y at approximately 25-30 mol % additive. This observation is consistent with the solubility parameter correlation presented above, as the δ_H of the polymer is not expected to change significantly with M_c.[80] In the case of the loosely crosslinked resins (D230-D400 and D400), each of which has a low initial T_g that is significantly depressed with TMP, the concentration threshold for TMP is observed to decrease substantially. Again, because the δ_H of the polymer is

not expected to change, the decrease in the effective concentration is more likely the effect of a depressed glass transition.

Trimethyl phosphate has been demonstrated to be an ideal molecular fortifier for amine-cured epoxy resins when compared with other trialkyl phosphates of larger molecular weight. However, as demonstrated by the case of TMP in 825-D400, a loosely crosslinked resin, trimethyl phosphate does not enhance the modulus and strength of all resins equally. In order to examine the possibility that TMP does not sufficiently fill the available free volume of a resin with large M_c, the larger organophosphates were also investigated in the D400-cured resin (Figure 3.12). A free-volume argument for increased mechanical performance would result in increased efficiency for additives of larger molecular weight. This is obviously not the case, as the larger organophosphates reduce the mechanical properties to an even larger degree than does TMP. Rather, this observation supports the view that antiplasticization is a molecularly localized event. The additive interacts strongly with only the hydroxypropylether functionality, reducing its mobility, but leaves the rest of the polymer backbone largely unaffected. By increasing the M_c, the local immobility induced by antiplasticization is diluted by the increase in degrees of freedom for the remainder of the chain.

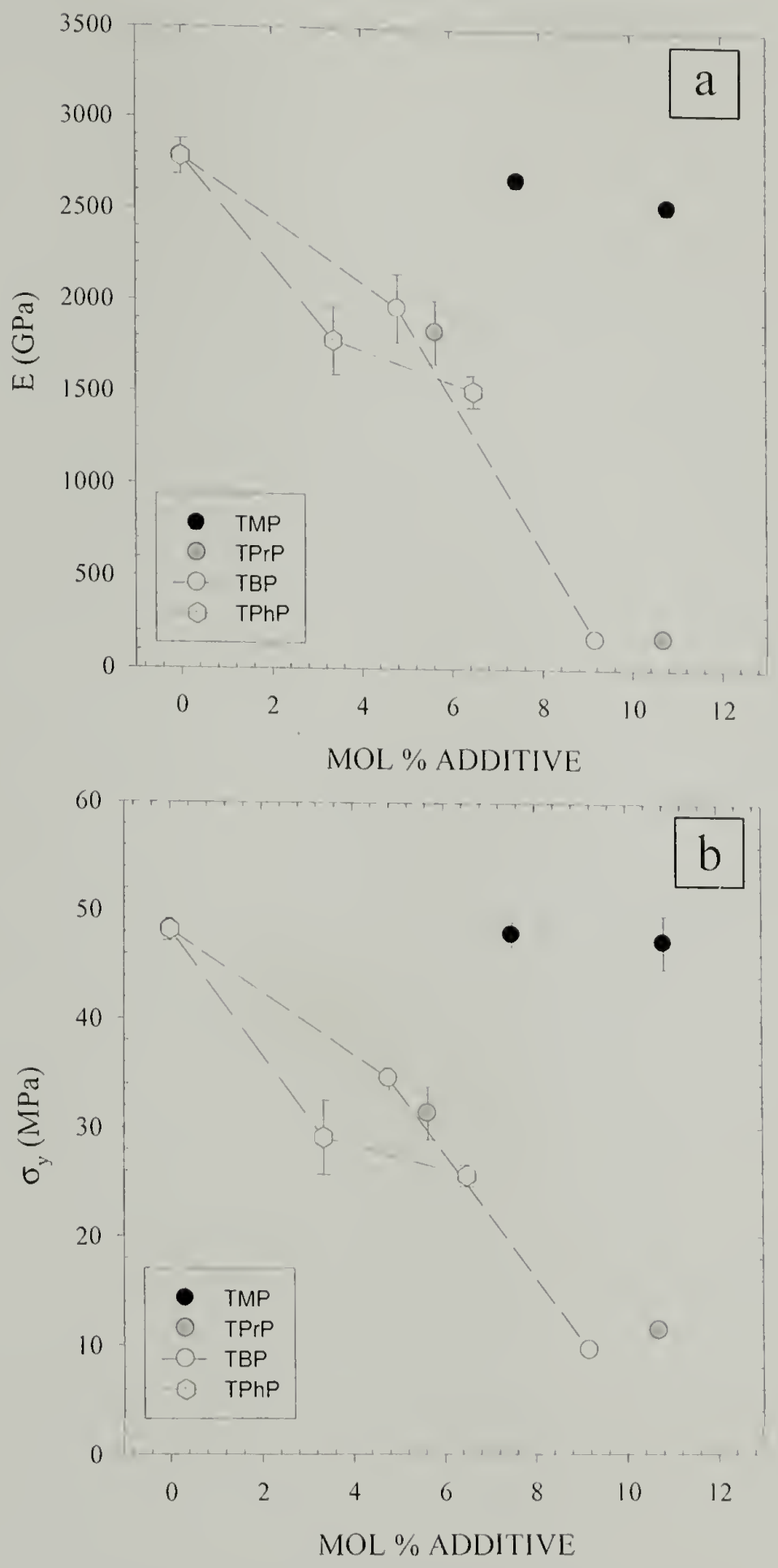

Figure 3.12 Comparison of effeet on the tensile modulus (a) and yield stress (b) D400-eured epoxy resins. None of the additives demonstrates mechanical fortifieation of this loosely-erosslinked resin.

In investigating the effect of the polymer network in dictating organophosphate fortification, one can also change the chemistry of the crosslinks formed upon curing (i.e. using an anhydride as the hardener). The resulting thermoset does not contain hydroxyl moieties and therefore eliminates the possibility for forming strong hydrogen bonds between the additive and polymer, however. This does not fully eliminate additive-polymer binding. Opportunity does exist for polar-polar interactions along the backbone (Figure 3.1). The strength of these interactions is nonetheless reduced from approximately 20 kJ/mol to less than 10 kJ/mol (general values are reported). The fortifier for the 825-HHPA resins is again TMP.

Anhydride-cured epoxies are extremely brittle materials. In order to measure accurately the strength of these materials, the mechanical properties are evaluated only under compressive loading. This minimizes the possibility for brittle failure. The effects of TMP fortification on the HHPA resin are presented in Figure 3.13. The fact that the anhydride resin is antiplasticized by TMP leads to the conclusion that hydrogen bonding between additive and polymer is not a necessary condition for antiplasticization of epoxy networks. Increases of 17% and 5% to the compressive modulus and compressive yield stress were observed. It is therefore demonstrated that dipole-dipole interactions between the additive and polymer are sufficient to ensure antiplasticization. The small increase in the yield strength, however, may be a result of the decrease in the T_g of the TMP-modified HHPA resin (Figure 3.2). The concentration threshold for the anhydride-cured resin is approximately 10 mol %, as compared to 30 mol % for the amine-cured resin. Here, by fundamentally changing the backbone chemistry, the δ_H of the anhydride-cured epoxy is expected to change.

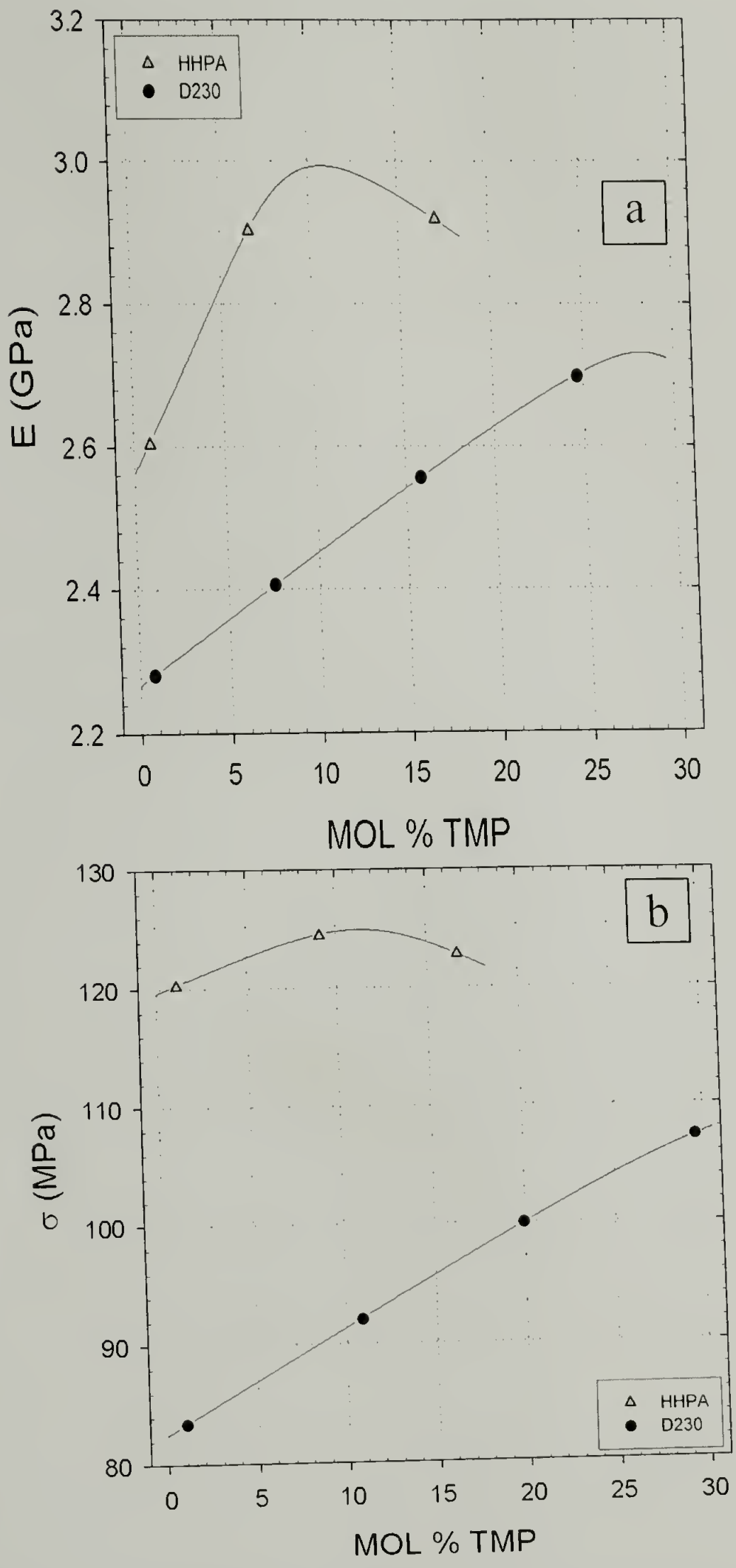

Figure 3.13 Comparison of compressive modulus (a) and yield stress (b) of TMP-fortified epoxy resins cured with HHPA (▲) and D230 (●).

3.6 Conclusions

Having related the chemical structure and properties of the additives to changes in the thermal and physical properties of a resin in Chapter 2, the mechanical properties of the fortified resins have been investigated. These changes to the material properties of epoxies modified with various organophosphates have been related to the level of reinforcement, which is realized upon incorporation of these materials into the resin. The importance of maintaining a high T_g upon fortification while increasing density is demonstrated in the fortification potential of TPhP as compared to additives of comparable molecular volume. A large enhancement in both modulus and strength is realized when the size of the additive is approximately that of the antiplasticizable region of the polymer backbone. In the case of diamine-cured epoxies, this is the hydroxypropylether functionality. As the molecular weight of the additive is increased, the strength of the polymer-additive interaction is reduced, resulting in a decrease in mechanical properties as well as a reduction in the additive's effective concentration range. This observation is captured in the correlation between concentration threshold and the solubility parameter of the various additives (Figure 3.9).

The network architecture is also instrumental in controlling the maximum levels of interaction attainable through molecular fortification. As the reinforcement mechanism is related to a reduction or elimination of β-relaxations, a low thermoset M_c is required to maximize the effect of this local chain immobilization. As observed for TMP-antiplasticization of resins with progressively larger M_c, a dilution effect of the antiplasticization mechanism is observed. To this end, a critical M_c is described.

Finally, the strength of the polymer-additive interaction can be tuned by using appropriate curing agents. An anhydride curing agent results in a polymer network lacking hydrogen-bond donating groups, reducing the strength of this interaction. As a result, the level of reinforcement for an anhydride-cured resin is lower than that attainable for amine-cured thermosets. Likewise, the concentration threshold is strongly reduced.

CHAPTER 4

FRACTURE MECHANICS OF INTERCALATED NANOCOMPOSITES

4.1 Introduction

Over the last 10 years, the area of nanocomposite materials has garnered much attention, both in the academic fields as well as industry and government.[81] It is hoped that nanotechnology can lead the way to better materials in many applications, from nanowires and nanodots in electronics, to nanoblends and composites in engineering applications. Often reported are the multitude of improvements nano-sized particles afford over their macroscopic counterparts. In the area of polymer nanocomposites, strides have been made to incorporate a large number of diverse inorganic substituents into workable materials, thereby enhancing their mechanical or physical properties.[82] Of great current interest is the use of layered silicates as nanoscopic filler materials. By modifying their surface through the use of organic surfactant molecules, high aspect ratio platelets can be incorporated into a polymer matrix. The surface modification of the clays both increases their basal spacing, thereby increasing the ease of entry of polymer or prepolymer, and serves as a compatibilizer between the hydrophilic clay surface and the, typically, hydrophobic polymer. Using such organically modified layered silicates (OMLS), organic-inorganic clay hybrids have been produced with various engineering polymer systems including epoxy thermosets,[34,35] polyamide,[36,37] polyimide,[38] polystyrene,[39] polyurethane[40,41] and polypropylene.[42,43]

In general, there are two idealized structures that can be synthesized from clay fillers: intercalated and exfoliated. The latter morphology, the focus of the majority of

literature available in this area, is defined by delamination of the individual platelets to form a homogenous dispersion of randomly distributed clay in the polymer matrix. Complete delamination of a small volume of clay (typically less than 5 %) is the goal of exfoliated nanocomposite synthesis, with the expectation that this homogeneous dispersion will provide the most-improved mechanical properties. This expectation also holds true for most materials syntheses, as heterogeneity at any length scale often leads to a reduction in properties.

Exfoliated clay nanocomposites can be synthesized through a number of different routes, including *in-situ* polymerization,[36,37] melt intercalation,[39,44] and silicate crystallization from polymer-silicate gel precursors.[83,84] Nevertheless, many systems do not achieve this ideal exfoliated structure, and a partially exfoliated morphology is normally achieved, containing a finite number of uniformly dispersed layers. The remainder of the clay remains undispersed, stacked together in agglomerates. The partially exfoliated morphology is the result of incomplete delamination, resulting in a mixture of exfoliated and intercalated structures. The intercalated morphology consists of well ordered, alternating layers of polymer and silicate. The d-spacing of these hybrids is easily recognizable using X-ray diffraction (XRD) with typically a few nanometers separating individual platelets in a lamellar stacking. In most cases, the exfoliated morphology, wherein the clay platelets are completely dispersed in the polymer matrix, is sought. Property enhancements afforded include improved barrier properties,[44] higher stiffness and strength,[34] better heat stability[37,45] and enhanced viscoelastic behavior.[46] However, such improvements are usually only reported for above T_g epoxy thermosets or amorphous elastomers such as polyurethane.[47] In glassy

epoxies and semicrystalline polymers, as with most particulate filled systems, increased stiffness often results in a corresponding decrease in toughness and strength.[48]

Nanocomposite materials garner most of their material improvements from interactions on the molecular scale, influencing physical and material parameters at dimensions inaccessible by traditional filler materials. This results in the property enhancements characterized above. However, from length-scale arguments it is known that toughening occurs over a specific size range and effective toughening may not be energetically favorable at nano-length scales. This generally necessitates a filler size greater than 0.1 μm.[8] The sizes of the nanoparticles are generally too small to provide toughening through a crack bridging mechanism and cannot effectively enhance crack trajectory tortuosity. Therefore, the extremely reduced scale of a fully exfoliated nanocomposite does not lend itself to a toughening application.

A few systems have exhibited toughening using exfoliated clays. The first example is of exfoliated silicates in rubbery polymers, such as above-T_g epoxy.[87] Here the silicates enhance the modulus of the polymer, thereby increasing the energy to failure. The second example is of exfoliated silicates in some semicrystalline polymers, such as polyamides.[37] In these nanocomposites, the impact strength of the polymer can be increased by increasing the modulus and strength of the nanocomposite. In an intercalated system, however, there is the potential for using the interaction between individual silicates for a toughening application. Once the polymer has entered into the galleries but has not fully delaminated them into the completely exfoliated structure, there is considerable interaction between silicate layers.

The goal of the present study is to characterize the mechanical behavior and toughening mechanisms of an intercalated clay-polymer nanocomposite, based on a crosslinked glassy epoxy system. Mechanical properties such as uniaxial tension, compression and fracture toughness are presented and discussed. A mechanism by which the intercalated clays provide property-enhancing characteristics is presented. The morphological impact on stiffness and toughness is also discussed, specifically with respect to its impact on the fracture mechanisms.

4.2 Materials

Unmodified montmorillonite was obtained from the University of Missouri Source Clay Minerals Repository. Modified clays were obtained from Nanocor. The clay, Nanomer I.28E, is a surface modified montmorillonite for dispersion into epoxy resins. The clay surface modification utilizes a cation-exchange, wherein sodium from natural montmorillonite is replaced by a long alkylammonium salt. This exhange serves two purposes: to render the surface organophilic and to further increase the d-spacing for the clays.

In the following discussion, all nanocomposite materials are compared on a weight percent inorganic clay basis, rather than the more common weight percent modified clay. This basis eliminates any confusion which is introduced when comparing clays modified with surfactants of various molecular weights. The weight percent clay is calculated as the fraction of the organically modified layered silicate (OMLS) that is purely inorganic. These values are determined from the residue mass upon incineration of the OMLS in a TGA. The inorganic clay makes up approximately 66 % of the mass of the OMLS. Although in the current chapter this basis is not necessary due to the use of a

single OMLS for all nanocomposite formulations, it is introduced now in order to form a basis of comparison with the following chapter.

The epoxy resin EPON 825, obtained from Shell Co., is a low-viscosity diglycidyl ether of bisphenol A with low molecular weight (epoxy equivalent 175). The epoxy was cured with a Jeffamine polyoxypropyleneamine curing agent from Huntsman Chemical. Results presented here are for the system cured with Jeffamine D230, which results in a moderately high T_g material. Similar trends to those presented here were likewise observed for epoxies cured with other diamines, such as Jeffamine D400 and T430, as well as m-phenylenediamine and ethylenediamine. Of particular importance is the low viscosity of all ingredients, as these systems become very difficult to process at clay concentrations approaching 10 wt. % clay. All chemicals were used as received.

The unmodified montmorillonite clay (Figure 4.1) is a naturally occurring aluminosilicate, the general chemical structure and properties of which are discussed in Section 1.4. In order to manufacture clay-polymer nanocomposites, these unmodified clays must be modified to facilitate polymer interaction between the silicate stacks (Figure 4.2). The montmorillonite clay is initially organically modified through a chemical exchange reaction whereby the cationic species of the montmorillonite, typically sodium or calcium cations, are exchanged with alkylammonium salts (a and b). The OMLS is then characterized by an increase in the basal spacing of the layered silicates (Figure 4.3). Additionally, the surface of the clay has been rendered organophilic through the incorporation of the alkyl surfactants, thereby reducing any enthalpic penalty for organic polymer intercalation between the silicates.

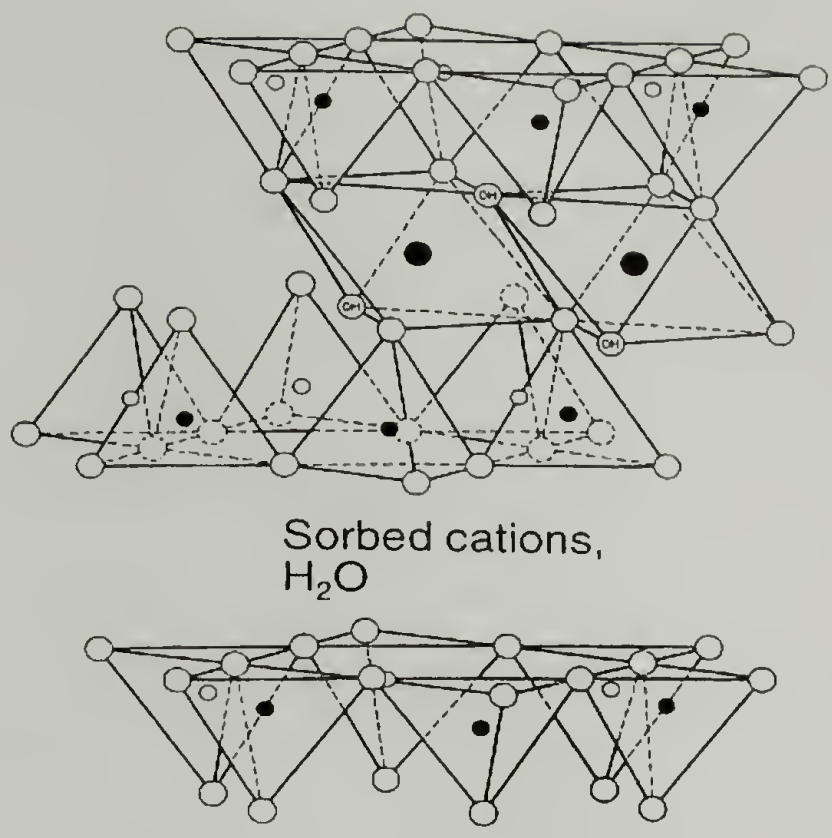

Figure 4.1 Crystalline structure of sodium montmorillonite, a naturally occurring aluminosilicate clay.

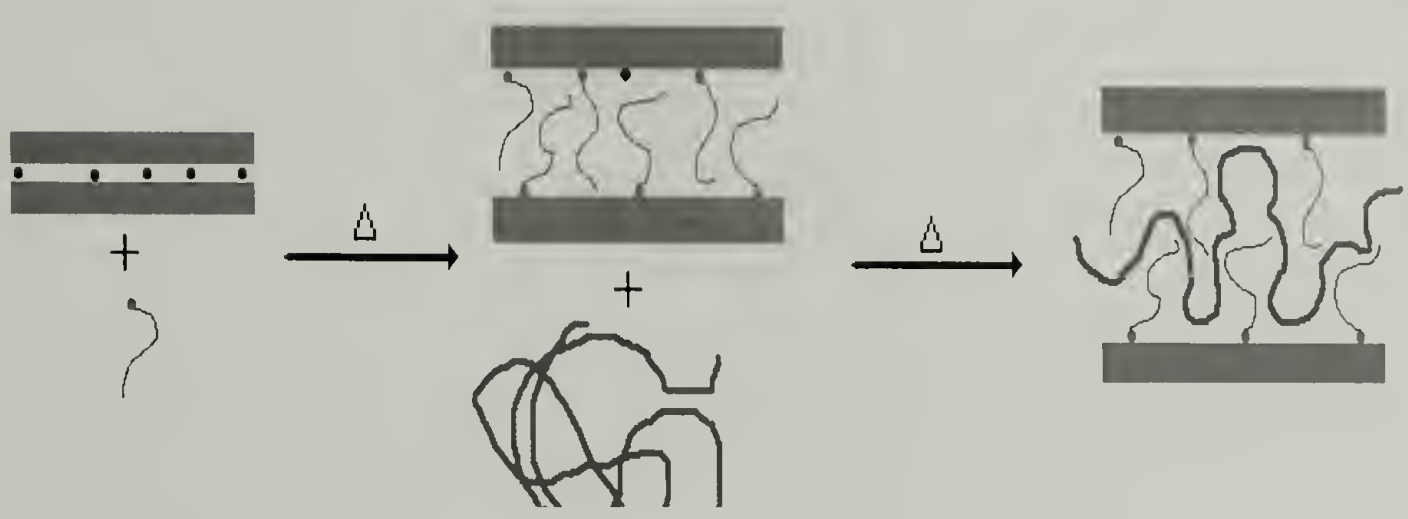

Figure 4.2 Schematic representation of silicate modification and polymer intercalation leading to a silicate-polymer nanocomposite structure: (a) unmodified sodium montmorillonite is suspended in an excess of alkylamine surfactant; (b) the resulting organically modified silicate is then combined with monomer or polymer (c) to form the nanocomposite.

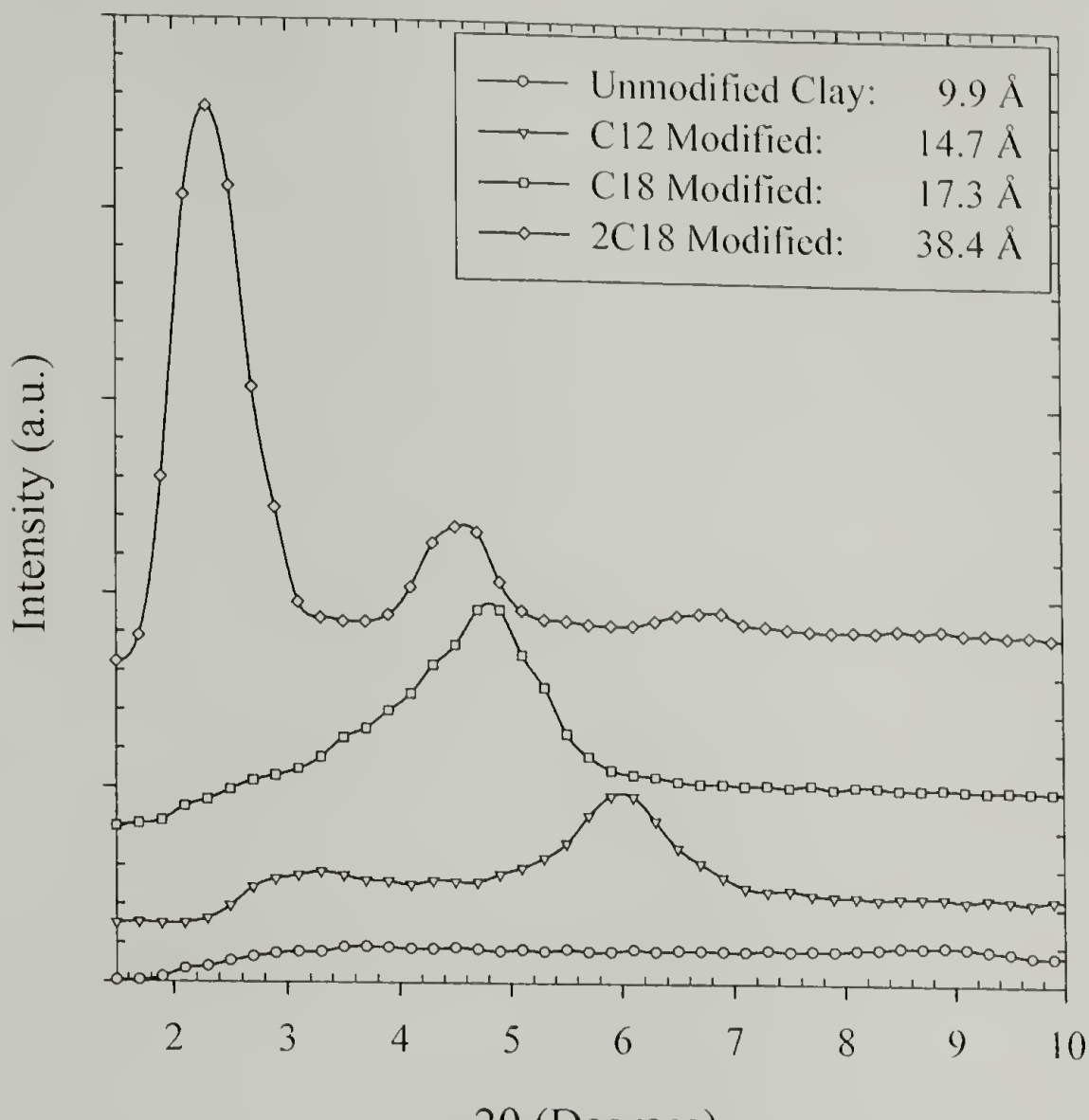

Figure 4.3 Effect of alkylamine modification on the d-spacing of OMLS.

The d-spacing of the OMLS is dictated by the length of the surfactants on the surface as well as their packing density. By using different aluminosilicates, montmorillonite being but one example of a wide variety of both natural and synthetic clays, the charge density of the clays can be altered. Montmorillonite has a charge density of approximately 100 meq/g, or 0.1 mol Na^+ counter-ions per one gram of clay. Organic modification of the clays then proceeds by suspending an amount of the silicate in acidic water and stirring in a 2:1 excess of the alkylammonium salt. Filtration and washing of the clays result in a purified OMLS characterized by the basal reflections above.

Having succeeded in producing modified clay capable of supporting polymeric intercalation, a nanocomposite is formed by blending in an appropriate amount of monomer or polymer and processing to achieve the desired morphology. The intercalated morphology is self-assembling, with the final d-spacing of the composite being dictated by the length of the alkyl surfactants. A lattice model developed by Vaia and Giannelis[85] based on intercalation of PS and related polymers into various OMLS demonstrates the need for both favorable enthalpic interactions and overall entropic gain to realize an intercalated, hybrid structure. Polymer intercalation, resulting in a finite clay separation upon introduction of the polymer, can only occur on decreasing the free energy, ΔF, of the system:

$$\Delta F = \Delta E - T\Delta S < 0 \qquad \text{Eq. 4.1}$$

where ΔE relates the energy change from intermolecular interactions and ΔS the entropic contributions from configurational changes of the polymer and surfactants. In order for polymer intercalation to take place, the enthalpic interactions have to be favorable ($\Delta E < 0$) because polymer confinement in the intragallery region always results in a loss of entropy ($\Delta S < 0$). If ΔE is negative and large with respect to TΔS, intercalation is self-promoting. However, if ΔE is negative but small, entropic arguments limit the degree of intercalation and subsequent exfoliation. Intercalation occurs while there is sufficient entropic gain in the alkyl surfactants. This limitation is evident in the constant d-spacing which results for intercalated nanocomposites. Intercalated d-spacings are often on the order of fully extended alkyl chains.

4.3 Experimental procedures

Reinforced samples were made by mixing the desired amount of clay with the epoxy prepolymer, weighing, and degassing at 65 °C. At higher clay concentrations, a foam of tiny bubbles would appear upon degassing and was removed. The mixture was then reweighed and a stoichiometric amount of curing agent was added (37 wt. % of EPON 825 for samples cured with D230). The mixture was again mixed for five minutes and subsequently degassed at 65 °C for 15 minutes. Samples were then transferred into surface-treated glass test tubes for compression bullets or between surface-treated glass plates for curing into 3 mm thick plaques. All samples were cured for three hours at 75 °C, followed by an additional three hours at 125 °C for postcuring.

4.3.1 Physical measurements

X-ray measurements were obtained on a Rigaku RU-200 rotating anode diffractometer with Fuji AS-Va image plates, and were used to characterize d-spacing in reinforced samples during the cure process. Thin sections (500 Å) were cryomicrotomed from existing samples for use in the Tunneling Electron Microscope (TEM). TEM micrographs were obtained using a JEOL 200CX using a 200 kV accelerating voltage. Scanning electron microscope (SEM) images were obtained on a JEOL-35CF. Atomic force microscopy (AFM) images were obtained on the Digital Instruments Dimension 3100 in tapping mode.

4.3.2 Mechanical measurements

Tensile specimens were cut according to ASTM D638 on a TensilKut router into Type IV test specimens. Compression bullets were cut according to ASTM D695 with

average length of 16 mm and a slenderness ratio of 2:1. Compact tension (CT) specimens were cut to ASTM D5045 and were precracked by tapping a fresh razorblade into the notch. (Figure 4.4).

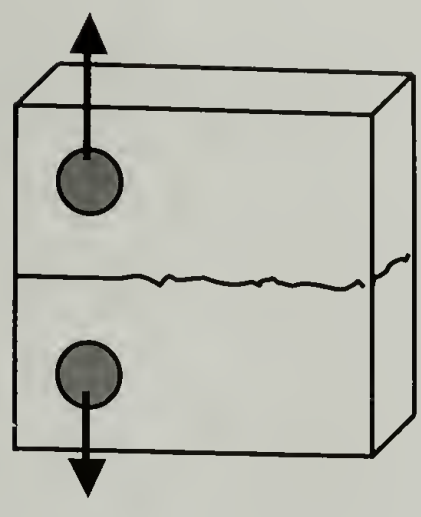

Figure 4.4 Schematic of compact tension (CT) sample geometry.

In order to monitor a crack which has been subcritically loaded, a double-notched four-point-bend (DN-4PB) specimen was cut (Figure 4.5).[86]

L/3

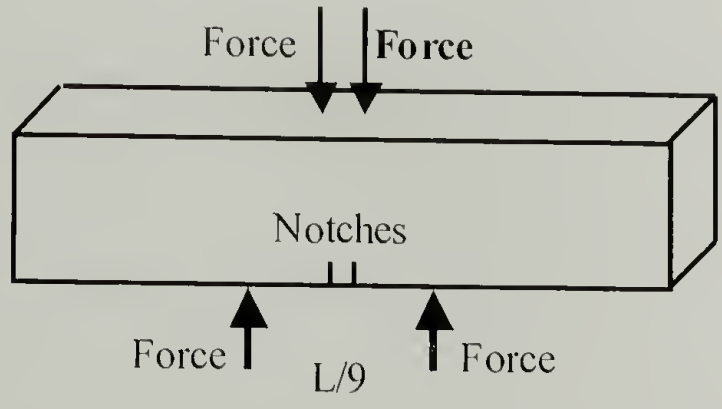

Figure 4.5 Double notch four-point bend (DN-4PB) sample geometry for generating sub-critically loaded cracks.

All samples were tested on an Instron 1123. For tension and compression, a crosshead speed of 2 mm/min was used. For fracture toughness, a crosshead speed of 10 mm/min was used to minimize the amount of plastic deformation ahead of the crack tip in the compact tension sample.

4.4 Morphological characterization

The necessity of surface modification for intercalated nanocomposite formation was verified. Natural montmorillonite was added to neat epoxy resin and cured. The unmodified clay quickly precipitated out of solution and failed to form a homogeneously dispersed composite. X-ray diffractometry (XRD) of both the unmodified clay-resin mixture and a cured sample showed that the characteristic d-spacing of the clays remains unchanged upon addition of epoxy. This d-spacing of 10 Å is identical to that determined from XRD of the clay powder. Therefore, no monomer is capable of entering into the gallery spacing of the unmodified clay.

For the formulation of intercalated nanocomposites, surface-modified clay is used and a typical two-stage cure process follows. This process follows the cure schedule recommended by both Shell Co. and Huntsman Chemical for aliphatic amine cured epoxy resins. In order to verify complete cure and stoichiometry, a measure of the glass transition is necessary. Incompletely cured epoxies exhibit T_g's lower than those expected for fully cured samples. Samples were scanned at 10 °C /min in a TA Instruments DSC 2910. All nanocomposites produced have T_g's within 2 °C from unmodified sample. This result indicates the presence of very similar cure states.

To verify that the epoxy prepolymer enters the clay galleries, the cure process was followed using X-ray diffraction at key points during the reaction (Figure 4.6). The original surface modified clay has a characteristic XRD pattern corresponding to a d-spacing of 22.8 Å. Upon introduction of epoxy prepolymer, this spacing increases to 34.2 Å, consistent with previously reported results, and indicates successful wetting of the clay with prepolymer. The epoxy resin-clay mixture also remained in suspension,

indicating a good dispersion. No precipitate is observed for up to two hours. Upon addition of the curing agent and conclusion of the first cure stage (3 hrs at 75 °C), the d-spacing remains unchanged from the epoxy solvated clays as seen in XRD.

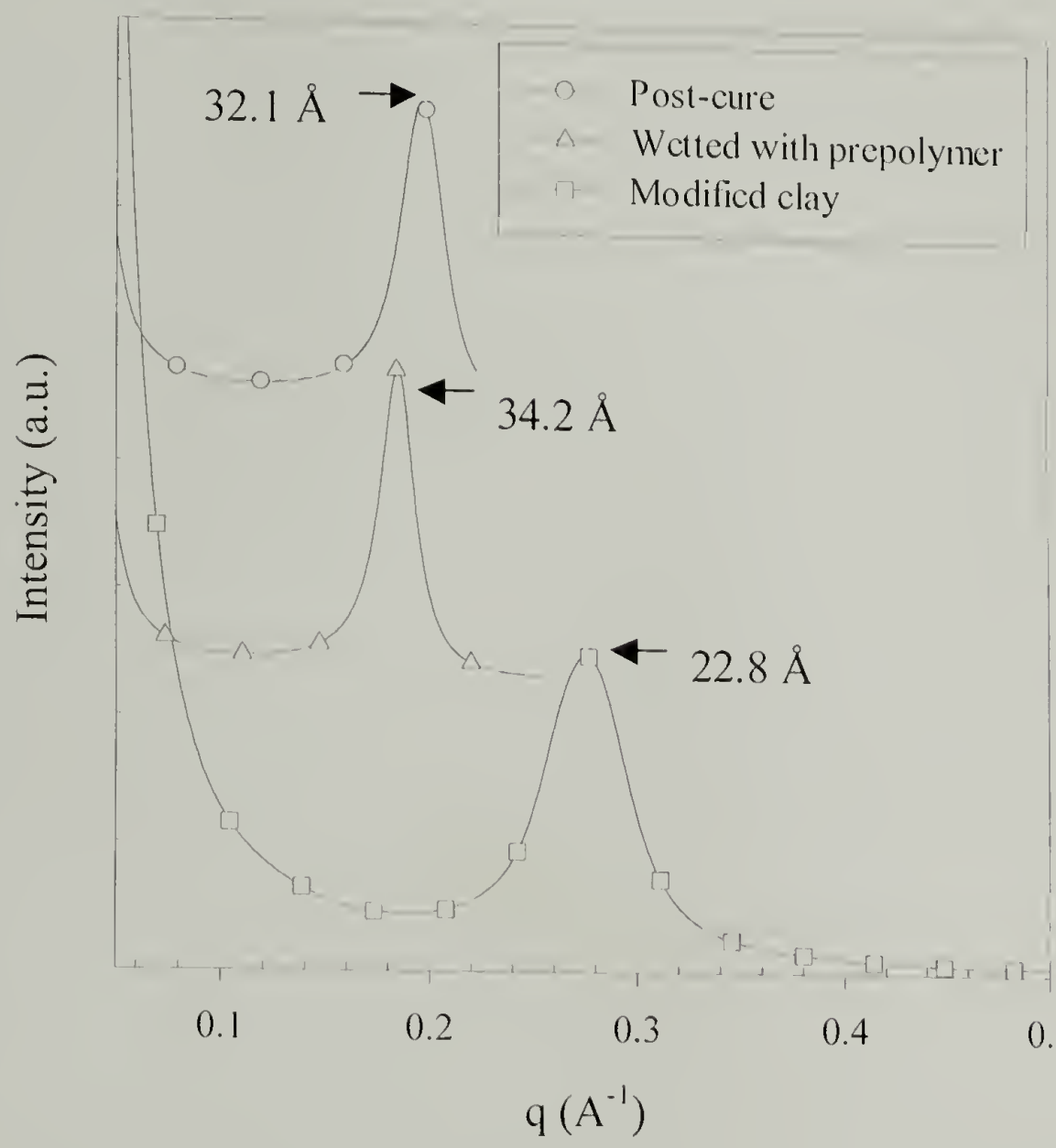

Figure 4.6 Characterization of the gelation process for intercalated clay nanocomposites using WAXS at different stages of the cure process.

Following the conclusion of the second stage (3 hrs at 125 °C), the d-spacing is slightly reduced, from 34.2 Å to 32.1 Å. This observation is not clay-concentration dependent, as XRD measures the d-spacing between platelets and is not indicative of the size of clay aggregates. The d-spacing reduction (~5 % in the transverse direction) is higher than the typically reported linear shrinkage in similar unfilled epoxy systems (3 %). The absence of curing within clay domains would likely demonstrate a d-spacing

reduction closer to 3% as the shrinkage comes only from outside the aggregates. The larger shrinkage suggests that crosslinking occurs within the clay domains, and is not isolated to the matrix regions. There is also no indication of a peak at 22.8 Å, suggesting that the clay platelets have been completely wetted with epoxy prepolymer. The radial symmetry in the XRD pattern for all samples suggests that there is no preferential orientation of clay platelets within the sample.

Although XRD is by far the simplest method to measure the d-spacing of the intercalated silicates, TEM was also employed to visually evaluate the degree of intercalation and the amount of aggregation of clay clusters (Figure 4.7). In the intercalated systems, the silicates retain much of their face-to-face alignment and can be seen to cluster together in large domains ranging from a few hundred nanometers to microns in size. TEM also indicates that a small amount of the clay does indeed exfoliate although the majority retains their face-to-face orientation and registry.

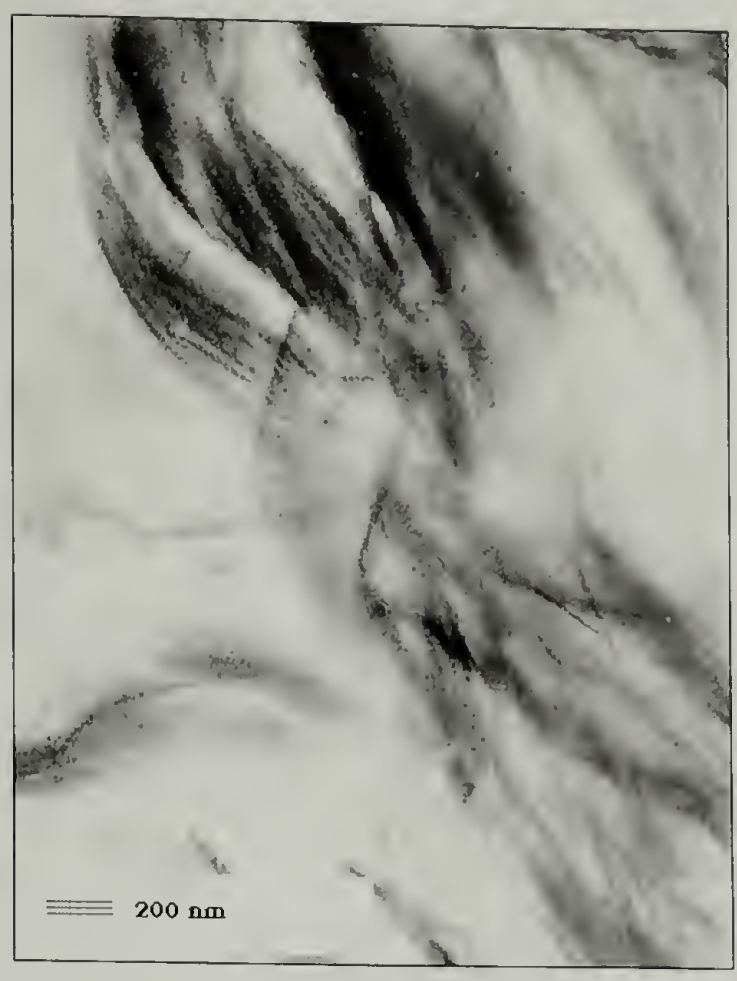

Figure 4.7 Tunneling-electron micrograph (TEM) of fully cured intercalated nanocomposite containing 6.6 wt. % clay. Clay platelets are visible as dark lines.

Using both SEM and TEM, the clay aggregate morphology can be characterized. Due to the difference in scattering density between the clay and epoxy, large clay aggregates can be easily imaged in SEM. The microscopic morphology of intercalated clays is observed in Figure 4.8. As the clay concentration increases from 1.0 wt. % clay to 4.5 wt. % clay, the particle sizes increase and interparticle distance decreases as the clay fills the available volume. Each clay concentration exhibits a single, broad size distribution. At the highest clay concentration (8.3 wt. %), there is a marked departure from this trend. There now appears to be two distinct particle sizes present: large domains, 10-30 μm in size, surrounded by sub-micron particles. Note that this morphology is not observed at the lower concentrations. This space filling leads to a decrease in interparticle distance, which has relevance to the toughening mechanism.

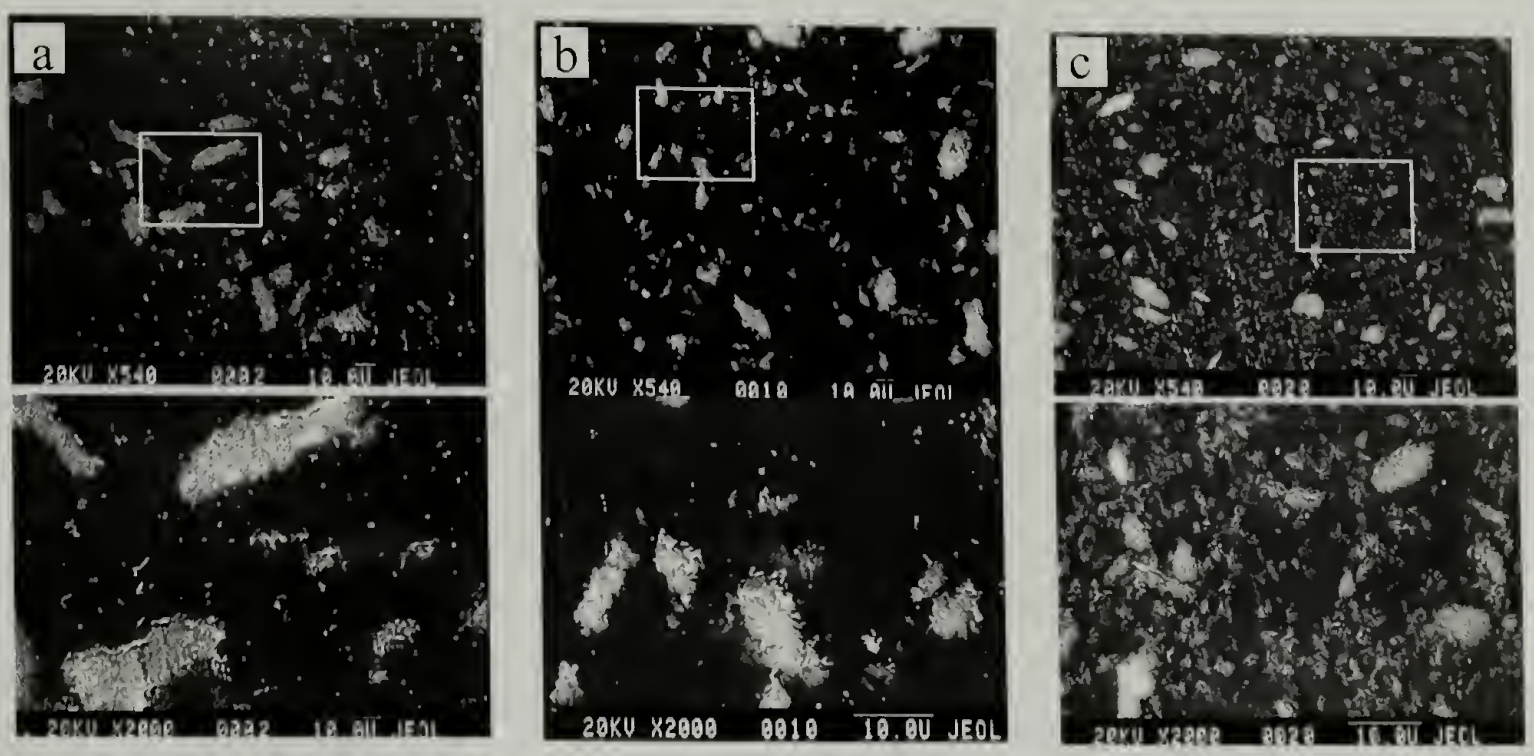

Figure 4.8 Scanning-electron micrographs of samples containing (a) 1.0 wt. %, (b) 4.5 wt. % and (c) 8.3 wt. % clay. Boxed regions in the top row indicate images of enhanced magnification in bottom row.

The amount of clay, which can be incorporated into the epoxy composites manufactured via this process, is limited by the processing technique itself. High clay concentrations (> 10 wt. % clay) result in mixtures that cannot successfully be degassed under vacuum. Shear mixing of clay with epoxy/curing agent results in trapping of air within the viscous fluid that cannot be removed by common methods (Figure 4.9).

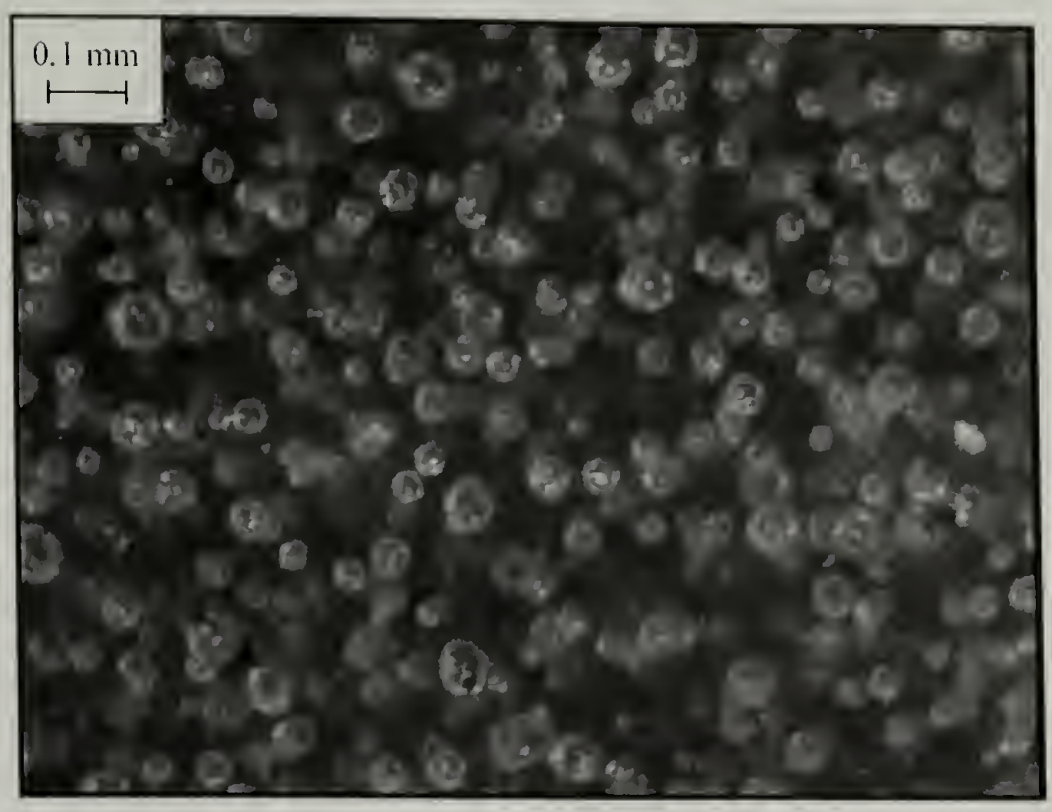

Figure 4.9 Optical image of an epoxy-clay composite containing 20 wt. % clay. Bubble formation occurs during the degassing stage of material synthesis.

These bubbles, when trapped within the final composite plaque, act as defects, concentrating applied stresses and leading to premature failure due to stress amplification (Figure 4.10). Attempts were made at manufacturing nanocomposites containing greater than 20 wt. % clay through non-standard means, including mixing the clay/epoxy/curing agent system in a twin-screw extruder and injecting the mixture into a plaque for final curing. This procedure, however, results only in decreasing the bubble size and is not capable of completely eliminating the presence of defects. In using the extruder to mix the clay/epoxy mixture, only low temperatures and short processing times were used. This is necessary to prevent gelation from occurring within the extruder itself.

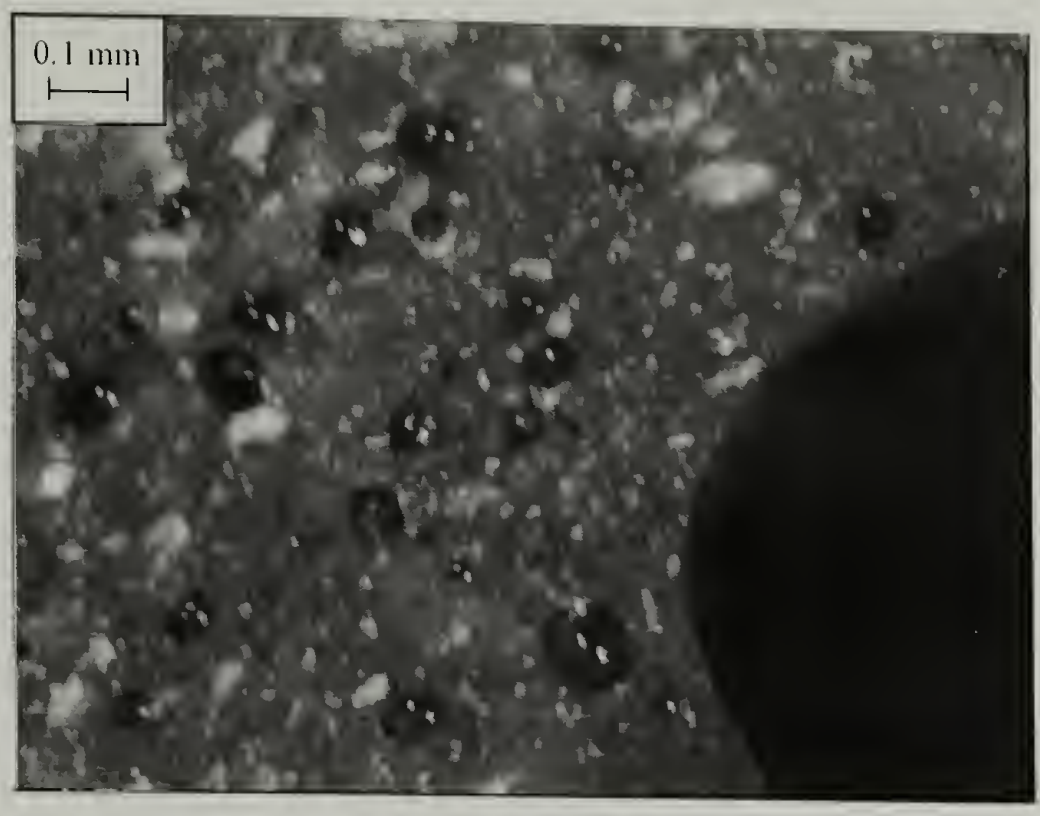

Figure 4.10 Optical image of 20 wt. % clay sample broken in tension. Failure is initiated at large defects such as the large void in the bottom-right corner of the image.

4.5 Mechanical characterization

4.5.1 Tensile properties

As shown previously for exfoliated nanocomposites in a glassy epoxy matrix, there is a significant improvement in tensile modulus with increased clay concentration.[34] This is likewise true for the intercalated morphology, although to a lesser extent. One does not see significant increases in modulus over the unmodified system until concentrations of 10 wt. % are achieved (Figure 4.11). At 10 wt. % clay, however, the modulus increase is comparable to that achieved by higher concentrations of conventional micron sized fillers, demonstrating the advantages of a nanoscopic, high-surface area filler. The enhancement in modulus comes with a reduction to both ultimate stress and strain at break (Figure 4.12), resulting in a loss of ductility. The strain at break is almost 50 % of the unmodified material at a clay concentration of only 1.5 wt. %. At the highest concentrations, a decrease of over 75 % is observed.

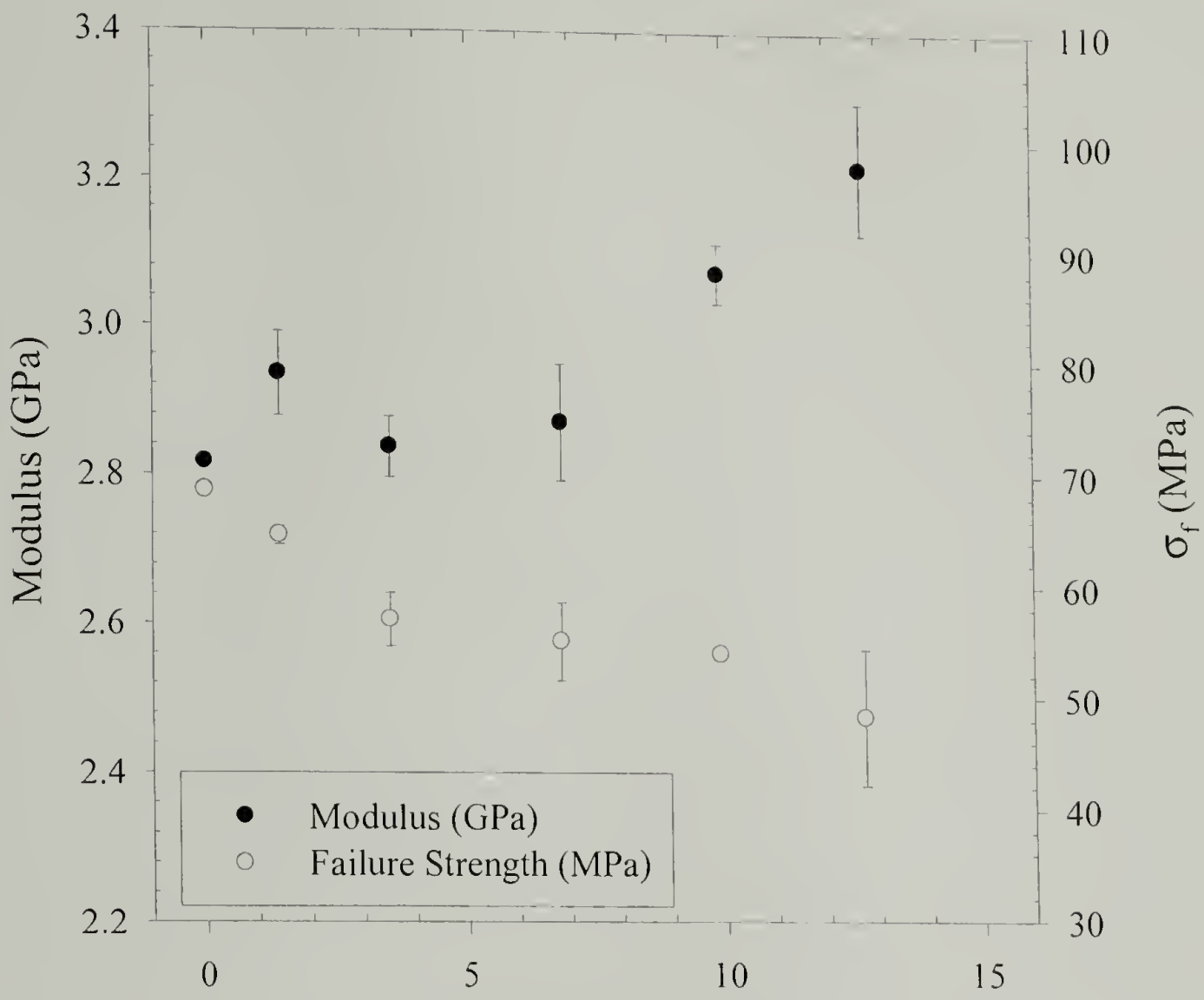

Figure 4.11 Tensile behavior of intercalated nanocomposites in epoxy matrix. Trend of data represented by dotted line (···).

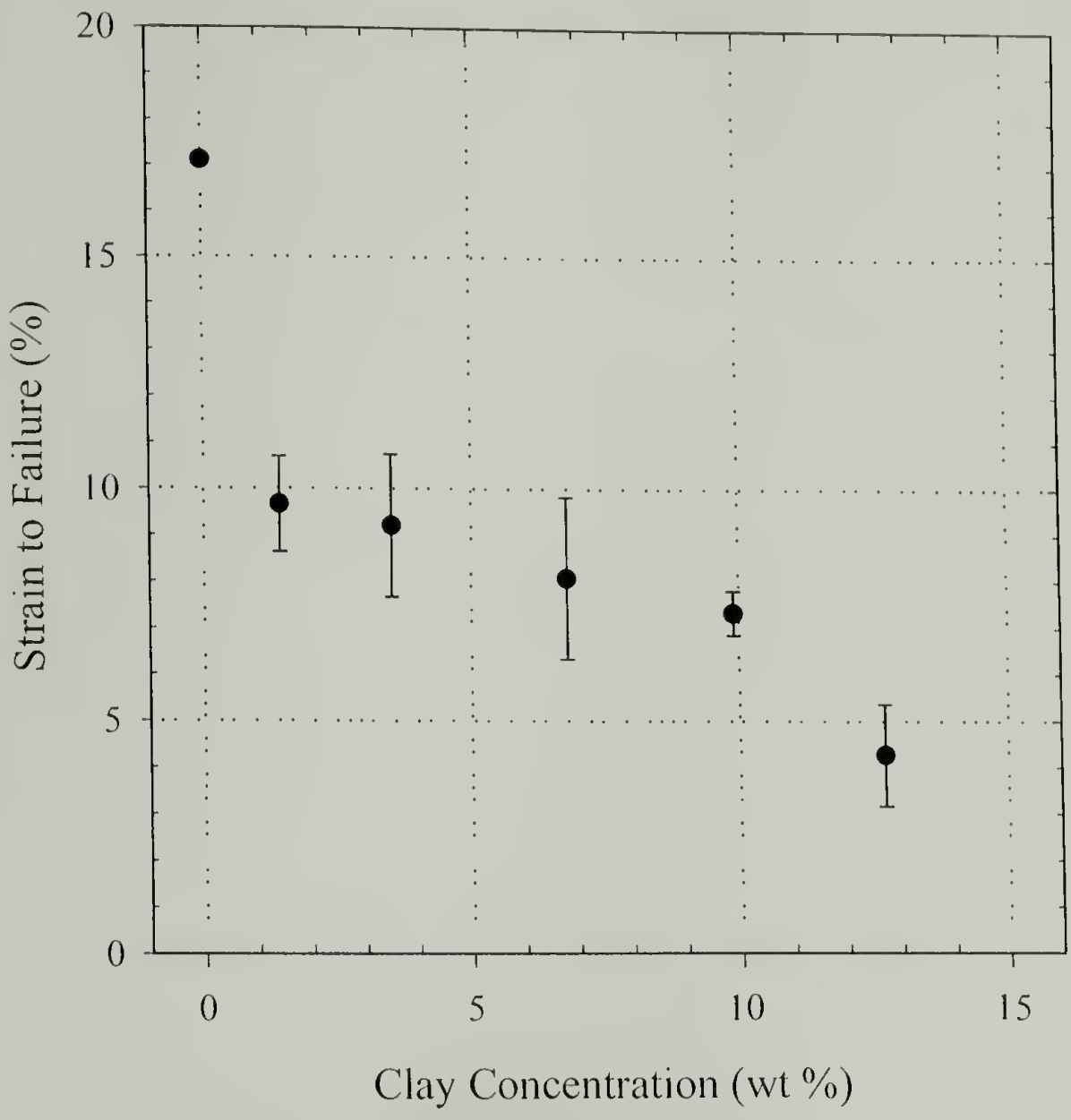

Figure 4.12 Tensile strain at failure for intercalated nanocomposites with increasing clay concentration.

This response is characteristic of materials reinforced with stiff filler materials and is particularly noticeable for the intercalated morphology. As observed in SEM, large aggregates (> 10 μm) form. These aggregates can act as load-concentrating defects, reducing ductility. As these large aggregates are present for all clay concentrations, it follows that increasing clay concentrations would lead to increased reductions in ductility.

4.5.2 Compressive properties

Limited improvements have been reported on the compressive behavior for exfoliated nanocomposites in a glassy epoxy matrix.[87] However, the intercalated

morphology does not demonstrate any measurable difference in either overall strength or compressive modulus (Figure 4.13). The apparent ductility was also unaltered, with little change in the strain at yield with increasing clay concentration.

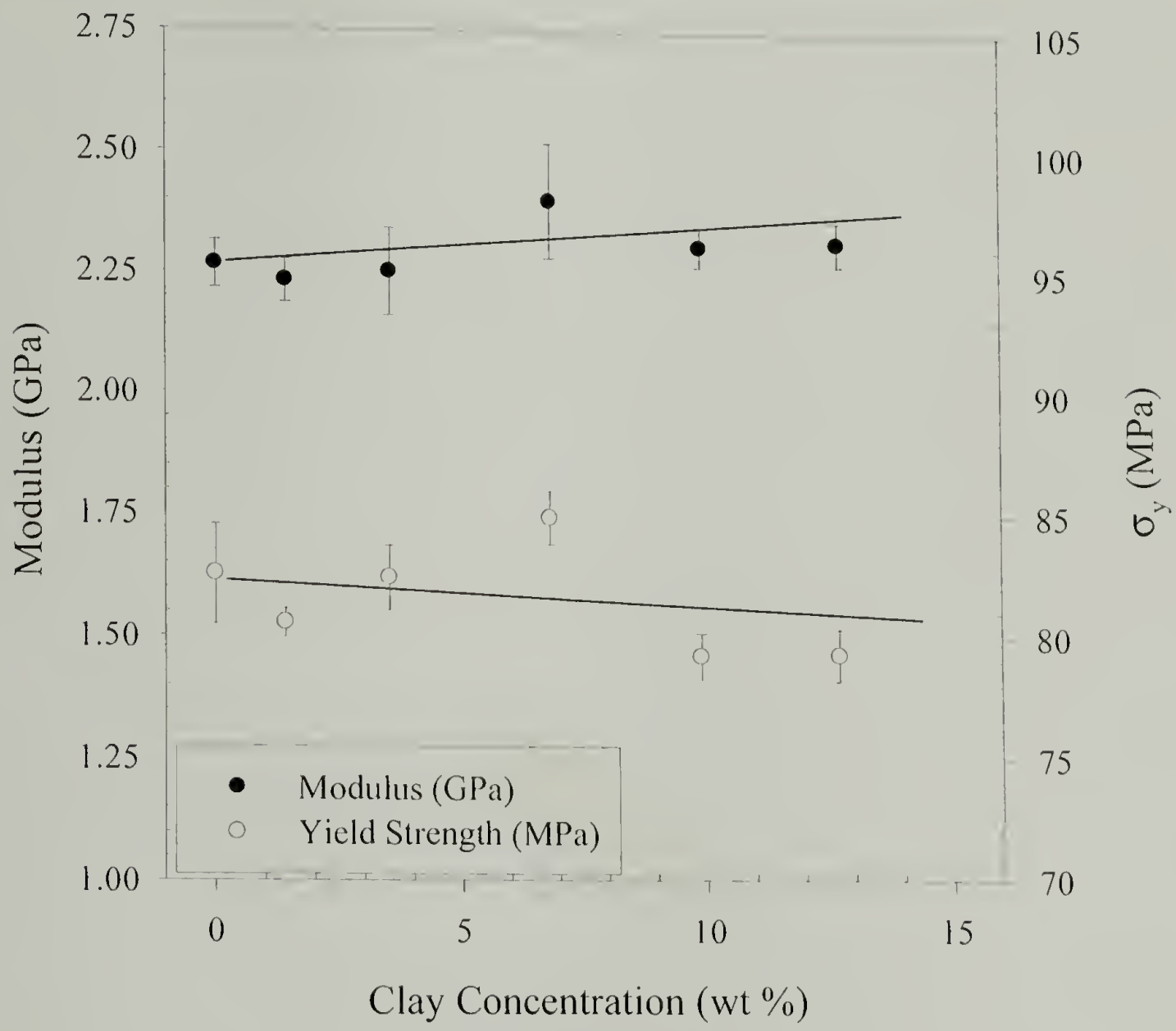

Figure 4.13 Compressive properties of intercalated nanocomposites with increasing clay concentration. Trend lines (---) represent linear fits of data.

The unfilled system exhibits a gross yielding behavior in compression, with no apparent void formation. A dramatic difference was observed in the yielding mechanism, however, upon introduction of intercalated clay as compared to the unfilled epoxy. The filled systems yield in shear with the evolution of a visible but diffuse shear-banded zone (Figure 4.14). There is obvious creation of new surface area in this region as evidenced by the scattering of visible light within the band.

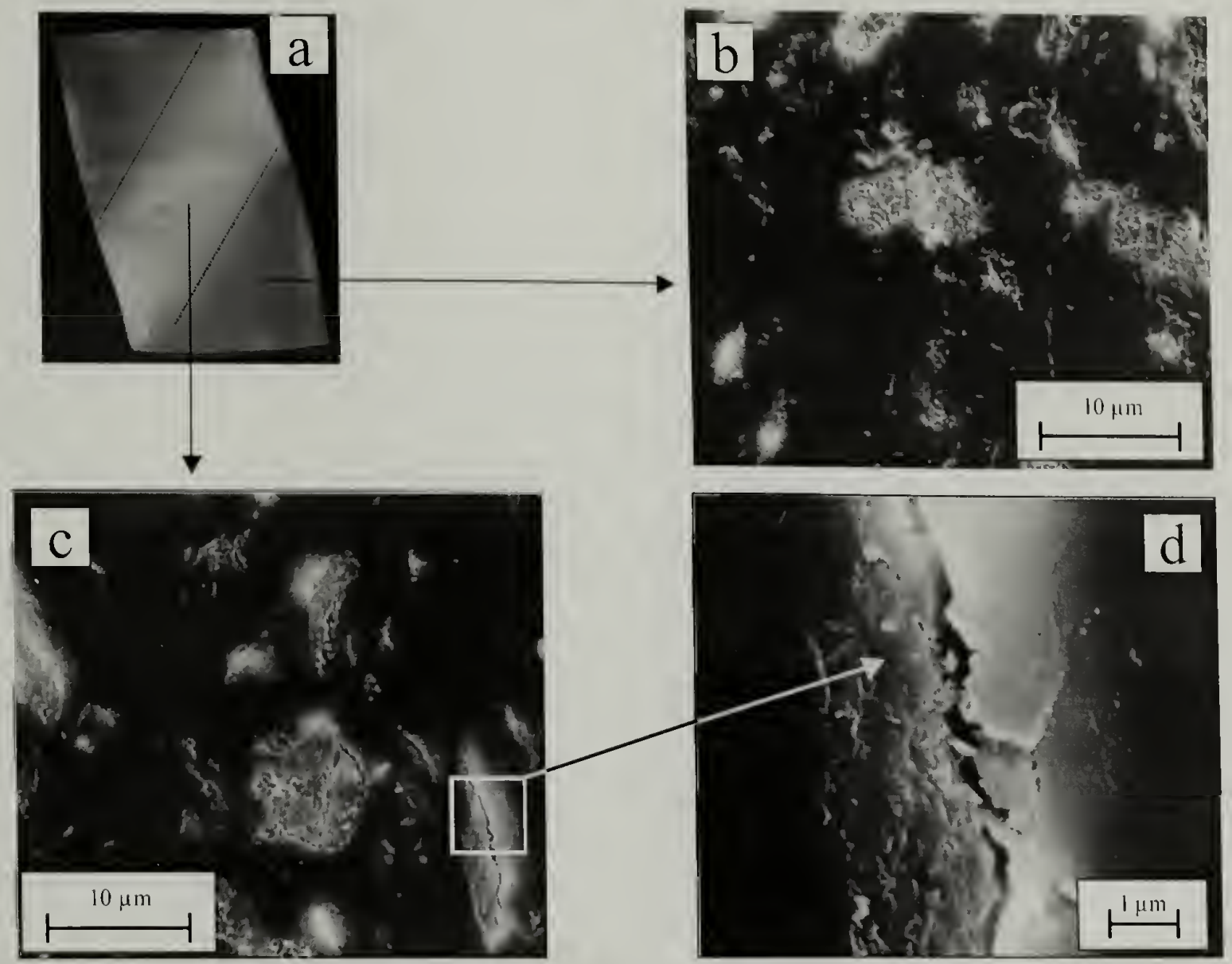

Figure 4.14 Micrographs illustrating compressive deformation and yield in a 7 wt. % clay sample: (a) macroscopic deformation resulting in diffuse shear band, (b) SEM micrograph of region outside shear band, and (c) SEM micrograph of region within shear band and (d) void detail.

Upon further compression past the yield point, the shear-banded zone expands to consume the entire sample. Optically, therefore, one can surmise that compressive loading of the samples results in void formation through shear. This shear-banded zone was further examined using SEM to verify void formation microscopically. As seen in Figure 4.14(c), voiding is confined mostly to the large clay domains (> 1 µm).

This yielding mechanism is similar phenomenologically to compressive failure of unidirectional fiber composites (Figure 4.15). When tested in tension, imbedded fibers carry the bulk of the load, and the composite exhibits enhanced mechanical properties

dictated by the tensile properties of the fibers. In compression, however, the mechanical performance is independent of the fiber volume in the composite. Rather, the long aspect ratios of imbedded fibers result in microbuckling, which is unrelated to the compressive properties of the composite. The yield strength of such composites is then matrix dominated.

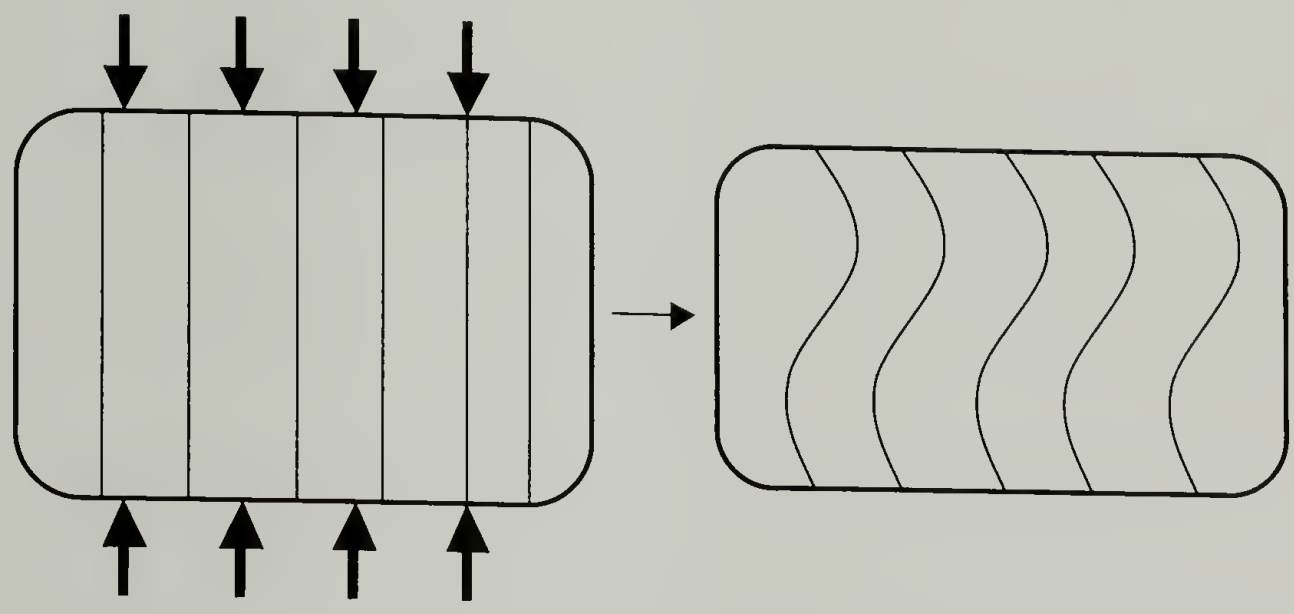

Figure 4.15 Cooperative failure in compression of fiber-reinforced composite materials.

Fiber microbuckling has been treated in the literature by a number of authors,[2,3,88] incorporating many of the observed failure modes into predictive models. Figure 4.15 represents a cooperative microbuckling scheme wherein the fibers are seen to buckle in unison, leading to the formation of a shear-dominated response. Other examples include the formation of kink-bands (sharp folds in the fiber), and extensional microbuckling resulting in the formation of compressive and tensile zones within the matrix material between individual fibers. The cooperative-buckling scheme as treated by Rosen[88] and Timoshenko[3] results in an expression for the compressive yield stress of these composites which only a function of the shear modulus of the matrix, G_m, and the volume fraction of the fiber, f:

$$\sigma_c = \frac{G_m}{1-f} \qquad \text{Eq. 4.2}$$

Although no micro-, or nano-, buckling of the aluminosilicate sheets is observed, the observations made of the compressive behavior of these nanocomposites does point to matrix-dominated shear-yielding mechanism under such loading conditions. It is hypothesized that the process of void formation is initiated by the silicate-rich intercalated regions' ability to deform preferentially in shear. Such a process, however, is observed only in compression as this stress state suppresses crack propagation responsible for brittle failure, allowing the material to behave plastically.

4.5.3 Fracture toughening

The fracture toughness of the clay-modified materials was determined using a compact tension specimen geometry. The results for a range of concentrations are presented in Figure 4.16. At low clay concentrations, less than 2 wt. %, there is little improvement in toughness. This is consistent with all other material properties reported here at low clay concentrations. The clay domains at concentrations below 2 wt. % appear isolated, thereby contributing little to the fracture toughness enhancement.

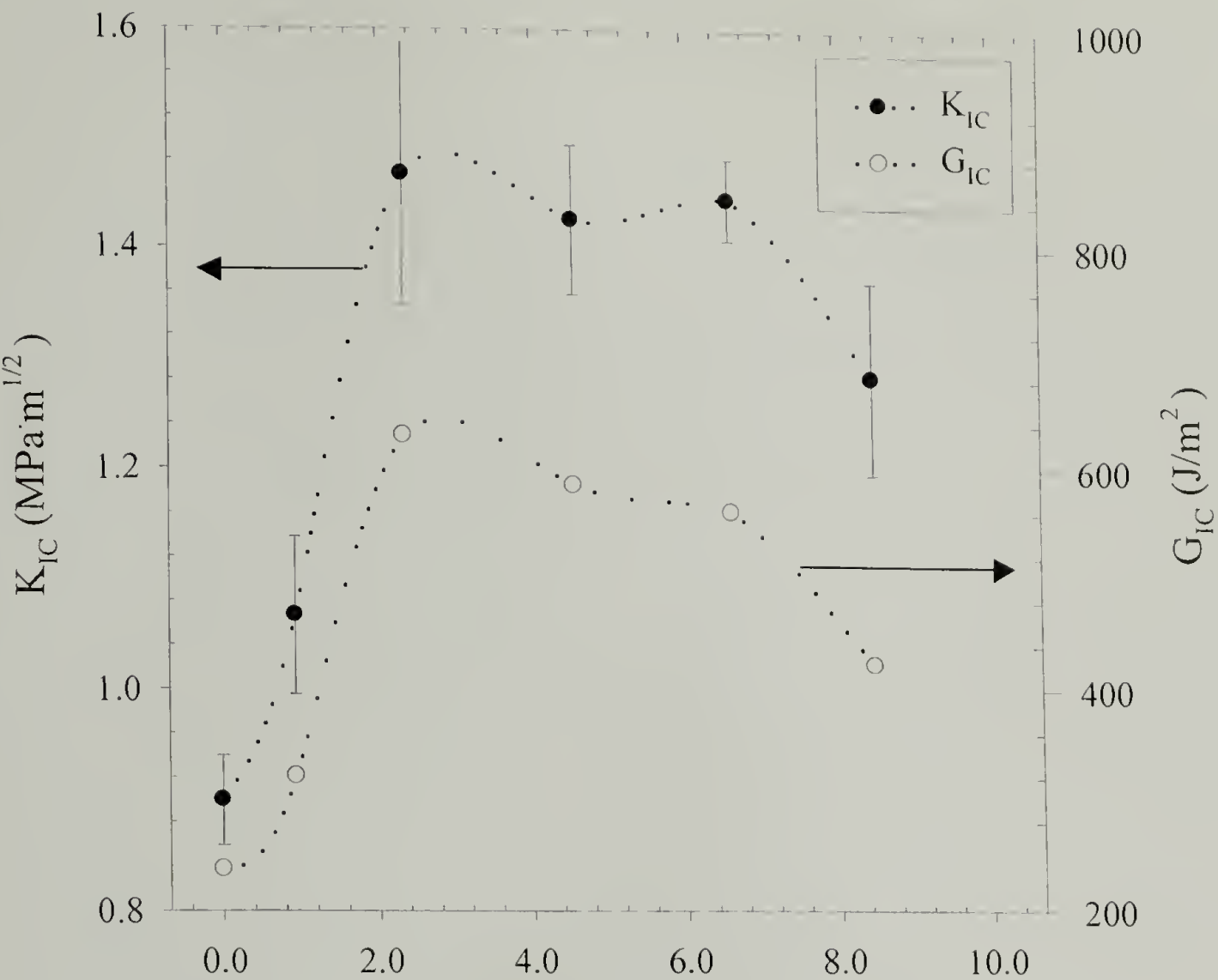

Figure 4.16 Changes in fracture toughness with increasing clay concentration. Reported are both the critical stress-intensity factor (K_{IC}) and energy-release rate (G_{IC}). Trends of data are illustrated by (···).

At 2 wt. % and above, however, there is a significant jump in the stress intensity factor, K_{IC}. Interparticle distance may play an important role in this toughening mechanism. As already seen in Figure 4.8, upon increasing the clay concentration of the sample, the interparticle separation decreases from > 50 μm in the 1 wt. % clay samples, and into the 10 μm range for 2 wt. % clay samples and above. The decrease in interparticle distance corresponds with increases in fracture behavior.

In order to investigate the fracture surface of the samples, samples were imaged using SEM (Figure 4.17). The unfilled samples all exhibited characteristically smooth

surfaces representative of brittle failure in a homogenous material. Samples of low clay concentration (1 wt. %) evidenced minimal surface roughness isolated to small regions. This is consistent with the isolation of clay domains at this concentration. At higher clay content, however, samples are extremely textured across the entire fracture surface. The roughness was seen to extend into the sub-micron regime at higher magnifications, indicating a mechanism working on a very small scale. This behavior is similar to that reported for clay nanocomposites from unsaturated polyesters.[48]

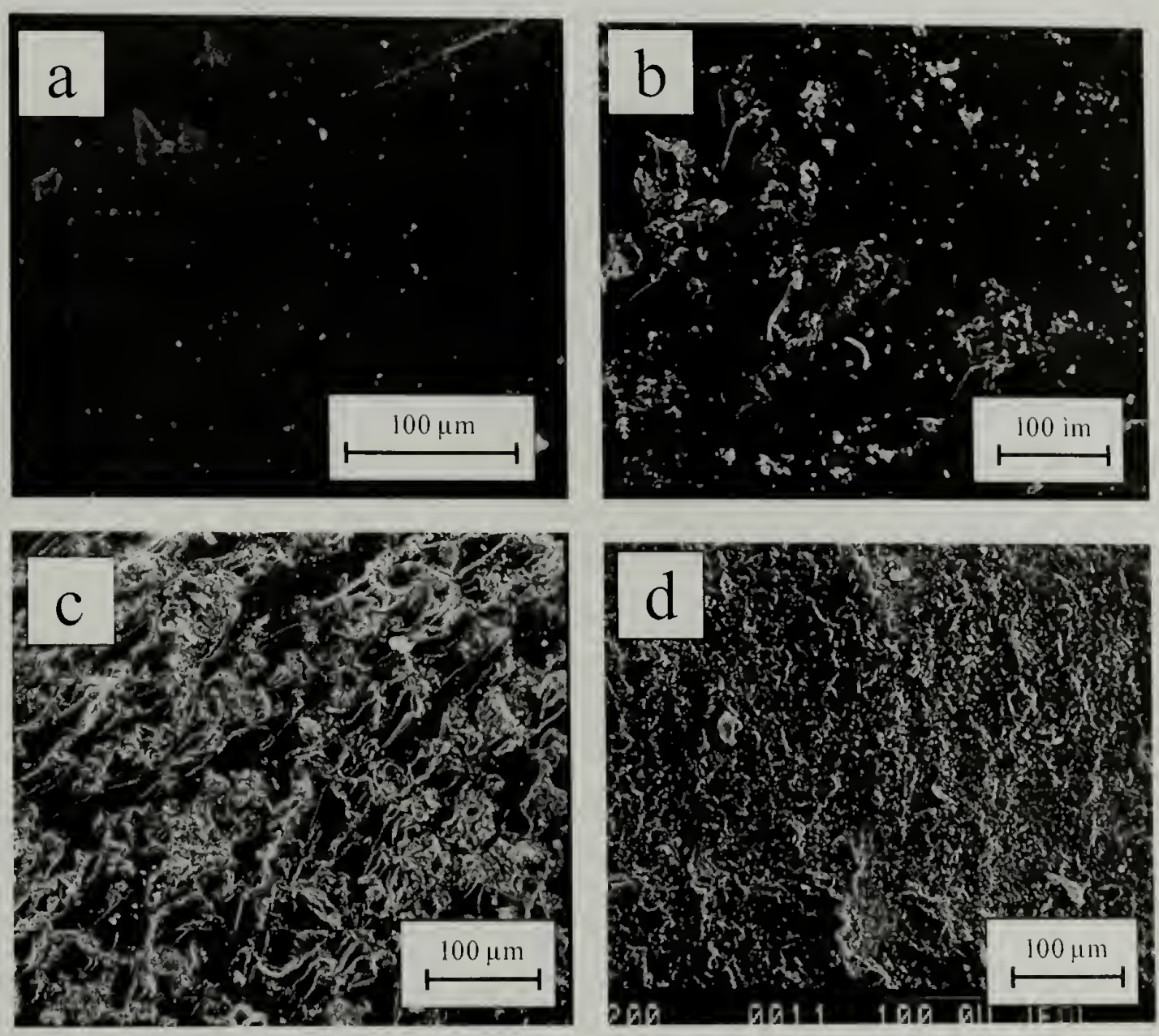

Figure 4.17 SEM micrographs of the fracture surfaces of (a) unfilled, (b) 1 wt. % clay, (c) 4.5 wt. % clay, and (d) 8.5 wt. % clay samples. Micrographs represent top-down views of the fracture surface following testing to failure of CT specimen.

Using a method introduced by Yee et al. for imaging the process zone in front of a loaded crack tip,[86] a sub-critically loaded crack was interrogated using both optical microscopy and SEM. Using the double-notched four-point bend technique (DN-4PB), two cracks or nearly equal length are introduced into a specimen and identically loaded. As one crack is taken to failure, the remaining unpropagated crack has been subjected to near the critical stress for failure. The sample can then be sanded down to a thickness of 100 μm, where it is transparent, allowing for viewing in a polarized light microscope. As demonstrated in Figure 4.18(a), the unfilled epoxy contains a smooth crack surface, whereas the intercalated nanocomposite, (b), manifests a crack trajectory that is extremely tortuous and exhibits evidence for branching along the path length. Such a progression would account for the roughness seen in the fracture surface images. As the clay concentration in the samples increases, it was shown that the distance between regions of intercalated clay decreases. This decrease likely causes the crack to take a more tortuous path, either around or between regions of high clay concentration. As the path length increases, it follows that the resulting surface roughness would also increase, consistent with the SEM micrographs of fracture surfaces.

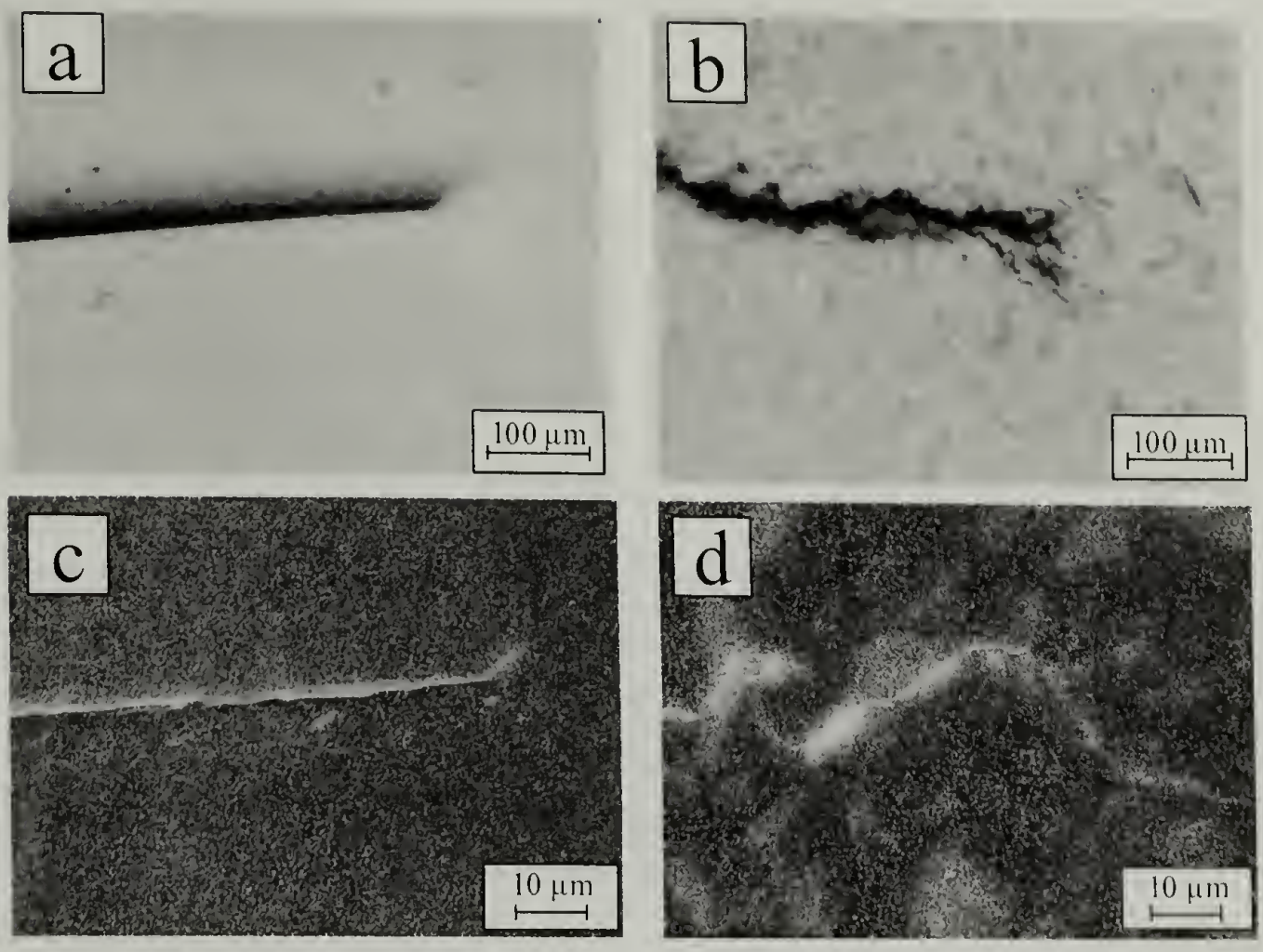

Figure 4.18 Edge-on views of cracks propagated through an unmodified epoxy resin (left) and one containing 6.6 wt. % clay (right). Images (a) and (b) are optical micrographs. Images (c) and (d) are high-magnification SEM images of the same materials. Samples represent sub-critically loaded cracks from a DN-4PB test sample.

Tapping-mode AFM was utilized to quantify the surface roughness already imaged using the SEM (Figure 4.19). This technique was used to quantify the roughness of the fracture surfaces generated by taking a number of CT specimens to failure. Quantifying the new surface created upon fracture allows for a correlation to be drawn between the fracture toughness measured mechanically and the resulting fracture roughness. Due to the highly textured topology, five scans were taken of each sample at different locations in order to characterize the surface. Multiple scans are especially necessary for the higher clay concentration samples. These exhibit the largest fluctuations in roughness. Nevertheless, the large fluctuations in measured surface area increase with clay concentration.

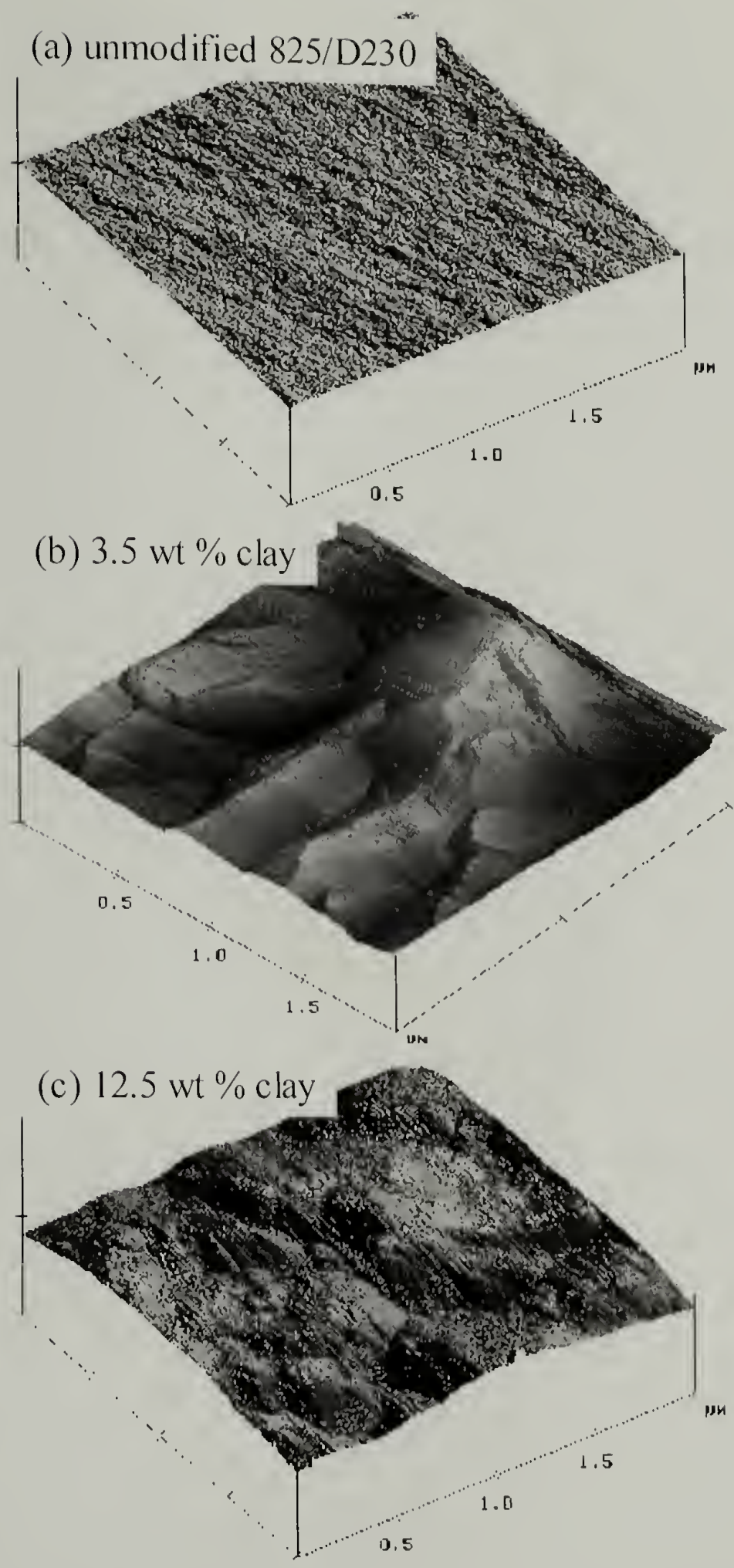

Figure 4.19 Representative fracture-surfaee maps of unmodified and modified epoxy samples obtained through 2-D atomic-force mieroscopy in tapping mode. Eaeh image is four μm^2. The z-seale in each image is one µm.

A number of methods for quantifying the roughness of a surface exist and these are presented in Table 4.1. Of these roughness correlations, the surface area difference, or Δ_S, is the only one which holds a physical meaning to be related to the fracture toughness measurements. Δ_S is the ratio of the actual surface area over the geometric surface area and relates the amount of new surface created during fracture (Figure 4.20). The surface area measured with the AFM correlates qualitatively with observations made using SEM microscopy. Here, the highest clay concentration formulations result in the roughest surfaces. Similarly, the SEM shows that the samples containing the largest amounts of clay produce the roughest surfaces.

Table 4.1. Roughness characteristics of clay-epoxy fracture surfaces.

Clay	Roughness		Surface Area Diff.	
%	Average (nm)	RMS (nm)	(%)	Error
0.0	1.9	2.4	3.0	±0
1.0	8.0	13.5	8.5	±7.8
2.3	118	150	100	±11
4.7	329	413	101	±30
6.7	193	244	100	±35
8.3	189	269	82	±62

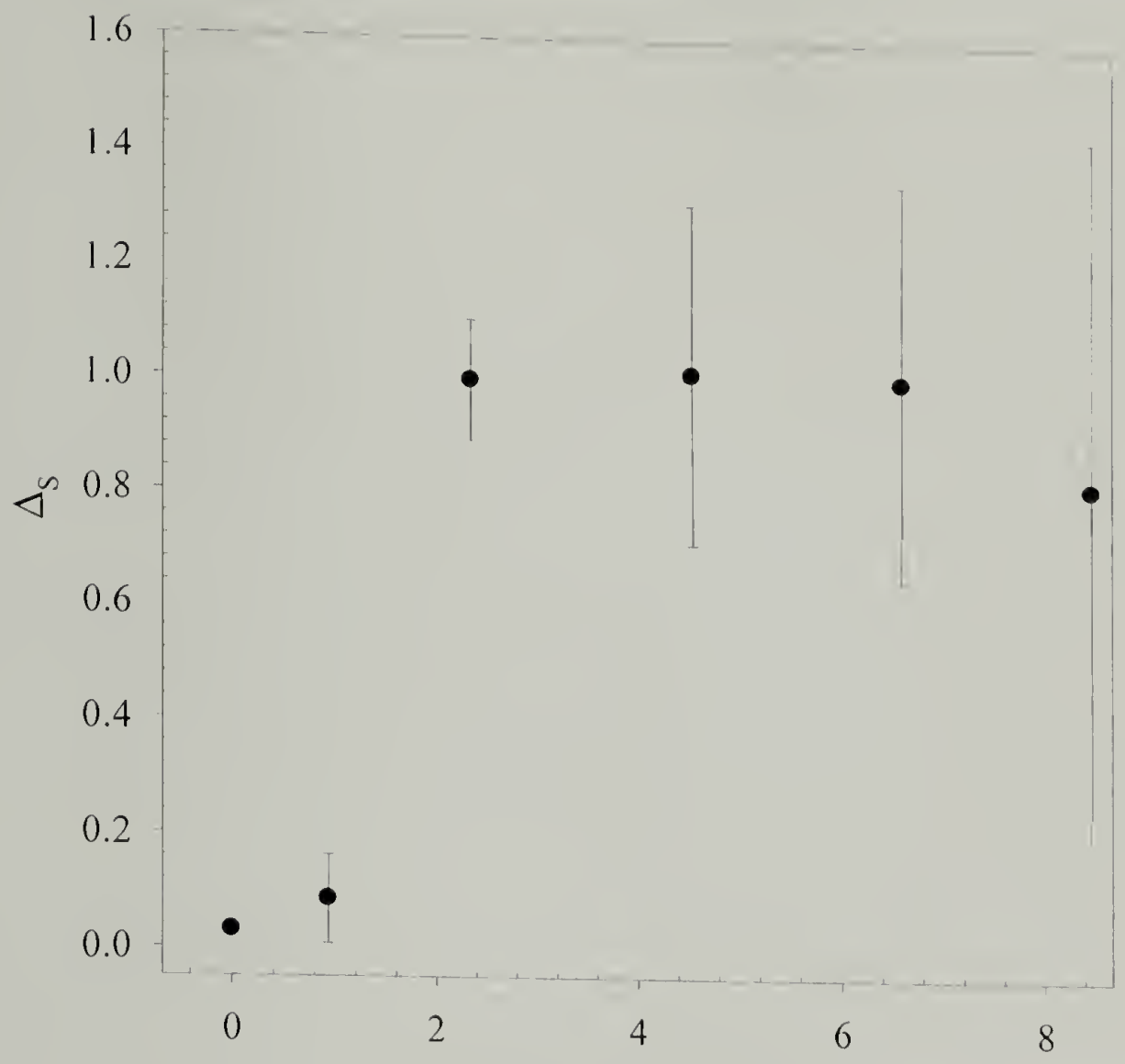

Figure 4.20 Surface area difference between the actual (from AFM) and projected surface areas as a function of clay concentration.

Quantifying these observations then allows a correlation to be made between Δ_S and the fracture toughness values measured mechanically. From Griffith, it is known that the energy release rate for brittle fracture, G_{IC}, can be related to the energy, γ, of the newly created surface.

$$G_{IC} = 2\gamma \qquad \text{Eq. 4.3}$$

In order to compare these surface energies, the measured energy release rate was normalized by the amount of additional roughness in the sample after fracture. The stress intensity factor, K_{IC}, is related to the energy release rate, G_{IC}, by:

$$G_{IC} = \frac{K_{IC}^2}{E'} \qquad E' = \frac{E}{1-\nu^2} \qquad \text{Eq. 4.4}$$

where E' is the plane stress modulus, E is Young's modulus, and ν is Poisson's ratio. The surface area ratio, Δ_S, measured in the AFM can then be used to normalize the energy release rate as follows:

$$G_{IC}^{(n)} = \frac{G_{IC}}{1+\Delta_s}. \qquad \text{Eq. 4.5}$$

This normalization effectively captures any change in surface energy upon increasing the clay concentration through Eq. 4.3. As illustrated by plotting $G_{IC}^{(n)}$ against clay concentration (Figure 4.21), normalization of the fracture toughness by additional surface area collapses the plot considerably. This is indication that the primary more of toughening is in fact the additional surface area which must be exposed in order to propagate the crack.

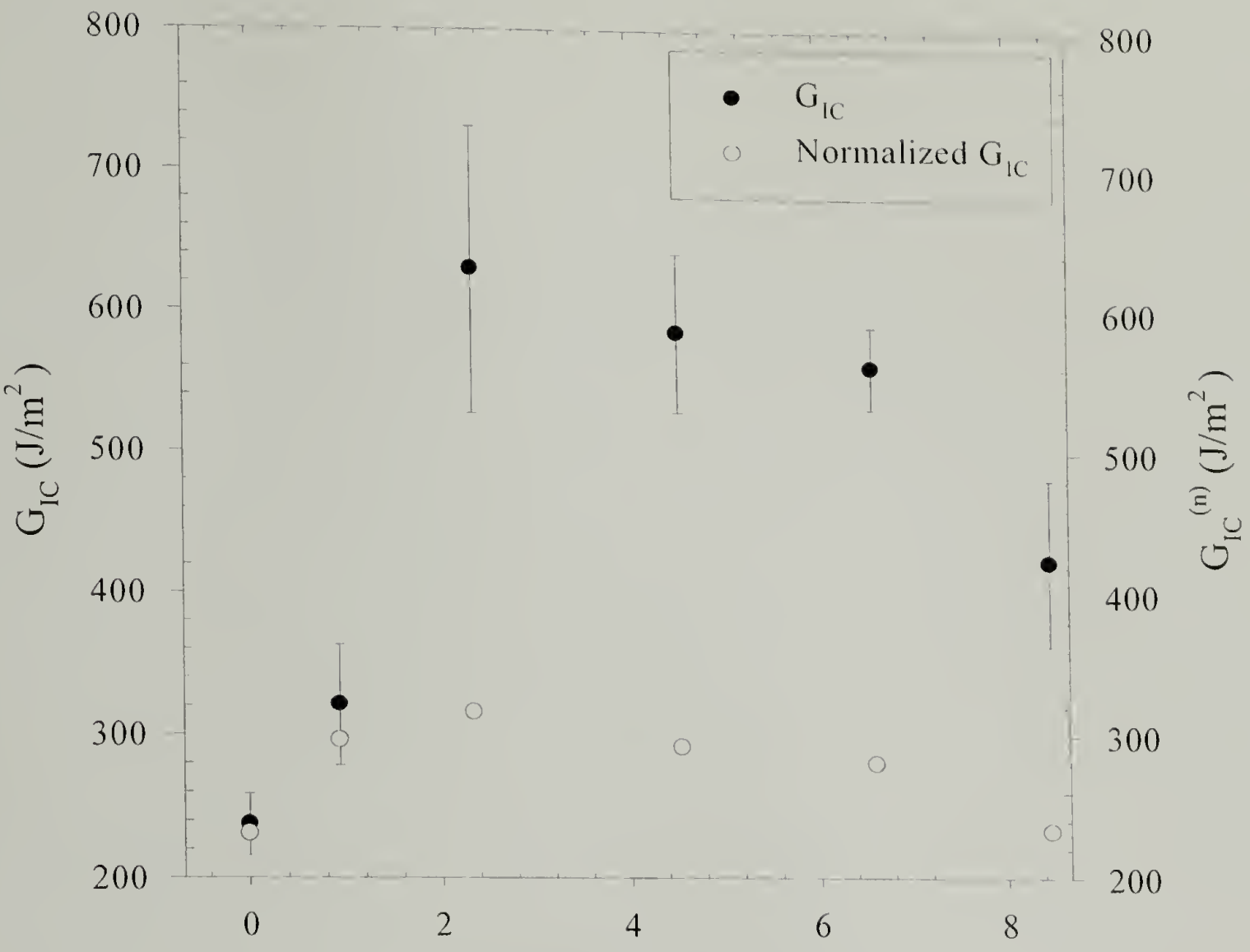

Figure 4.21 Comparison of measured and normalized energy-release rates, G_{IC} and $G^{(n)}_{IC}$ respectively, as a function of clay concentration. Following normalization of the G_{IC} by the increase in surface area, Δ_s, $G^{(n)}_{IC}$ is seen to be approximately constant over the entire range of clay concentrations.

4.6 Conclusions

The mechanical behavior for intercalated nanocomposites of layered silicates in a glassy thermoset is reported. An increase in tensile modulus is reported although the intercalated morphology appears to have a detrimental effect on the ultimate strength and ductility of the composites. Although improvements in compressive behavior for exfoliated systems have also been reported, our studies show that the intercalated morphology does not significantly improve the mechanical properties of this system under compressive stress. However, the gross yielding behavior of this system is

substantially modified, with void formation within clay aggregates leading to the evolution of a visible shear banded zone in compression samples.

The fracture behavior appears to be most dramatically improved in the intercalated system. The fracture toughness of the composites was shown to be increased by 100 % at clay concentrations of 5 wt. %. By investigating the surface roughness and crack propagation under sub-critical loading, it is hypothesized that the creation of additional surface area upon crack propagation is the primary means for toughening in intercalated systems. The morphology of this system plays an important role in the toughening mechanism as the spacing of regions of intercalated clay is important to toughening. It is believed, therefore, that the intercalated morphology can afford some property improvements that are unavailable to the fully exfoliated systems.

CHAPTER 5

SYNTHESIS OF HIGHLY CONCENTRATED, INTERCALATED SILICATE NANOCOMPOSITES

5.1 Introduction

As described in Chapter 4, the interealated morphology can be used to impart mechaniеal property enhaneements that are otherwise inaceessible to the exfoliated clay morphology. However, at low clay concentrations (below 15 wt. %) the intercalated morphology is characterized mieroscopically as multiphase. Small regions (approximately 1-10 μm in diameter) of silieate-rich polymer are surrounded by unmodified polymer (Figure 4.8). This two-phase structure leads to a microscopically heterogeneous material. As described previously, the engineering properties of this composite continue to be dominated by the properties of the resin. To appreeiate fully the potential of intercalated nanoeomposites in developing hybrid properties, the silicates must be ineorporated at high concentrations, resulting in homogeneously intercalated struetures.

Incorporation of high concentrations of nanometer-scale silicates into a composite is, however, problematic. The viscosity of a solid-liquid mixture is largely dictated by the interaction surfaee area between the two eomponents. By virtue of their small dimensions, nanoseale fillers have extremely large surfaee areas. Montmorillonite, for example, possesses 700 m^2/g of aceessible surfaee area.[89] At concentrations above 20 wt. % modified silicate, the viscosity of a monomer-silicate mixture becomes such that homogeneous dispersion is arduous and defeet formation is common. The synthetic route

described here succeeds in manufacture of defect-free intercalated nanocomposites of high clay concentrations. The challenges of high viscosity apparent at clay concentrations above 20 wt. % are overcome by using supercritical CO_2 ($scCO_2$) as a reaction medium. Homogeneous dispersion of monomer, initiation and subsequent polymerization all occur under low viscosity conditions in this medium. This route can also be used to synthesize nematic architectures where the platelets exhibit preferential order. Such ordered intercalated nanocomposites, containing upwards of 20 wt. % modified clay, exhibit true composite mechanical properties dominated by the inorganic clays.

5.2 Intercalated silicate nanocomposites through supercritical CO_2

The general methodology for synthesizing intercalated silicate nanocomposites using $scCO_2$ is based on the solvent-like qualities of the compressed gas. In this way, the process is similar to traditional solution polymerizations. Supercritical CO_2 has the added advantage, however, of exhibiting complete removal upon depressurization. Traditional solution polymerizations fail at high clay concentrations as it becomes increasingly difficult to remove residual solvent completely. Supercritical fluids have recently received attention as reaction media for polymerization of a number of polymers, especially fluorinated polymers, which are soluble in $scCO_2$.[90] In this investigation, however, the matrix material is poly(methyl methacrylate), PMMA, which is not soluble in $scCO_2$. Rather, the CO_2 is used initially as a diluent, then as a plasticizer.[91] Previous applications of supercritical CO_2 as a plasticizing medium, where the polymer is not soluble, include enhanced fiber drawability,[92,93] solvent welding[94] and phase-selective modification of multiphase systems.[95-98] Depressurization upon completion of the

polymerization results in reversible extraction of the CO_2 gas in a manner significantly superior to traditional solution techniques.

The general procedure is illustrated in Figure 5.1. The OMLS are first swollen with monomer in a $scCO_2$ atmosphere. Because the $scCO_2$ solvates the monomer, mixing of clay with monomer is not necessary. Rather, the permeability of $scCO_2$ in the entire volume is used to distribute the monomer and initiator evenly. PMMA is used as a resin material because of the ease with which radical polymerization can be initiated. The monomer is polymerized upon elevating the temperature and initiating the reaction. Depressurization removes the CO_2 from the reaction vessel.

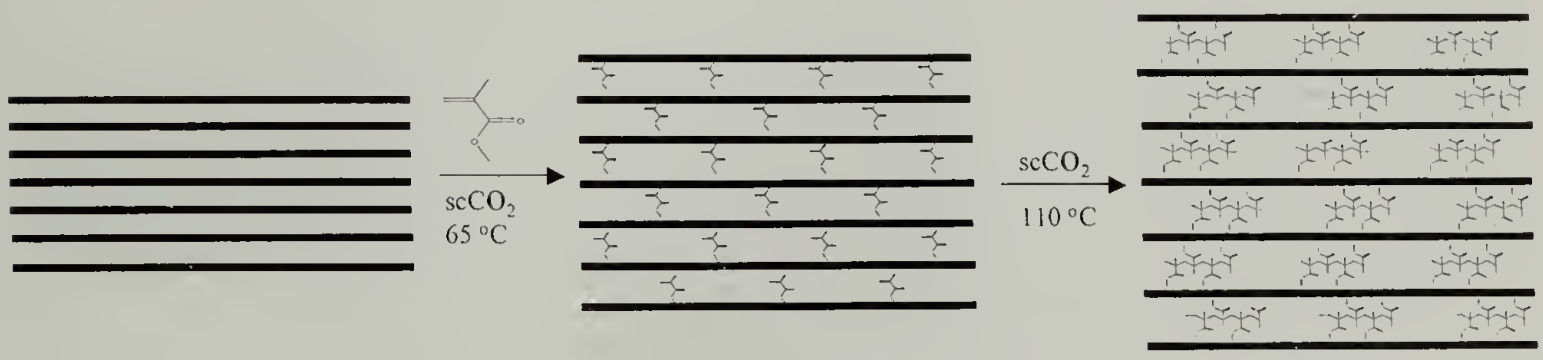

Figure 5.1 Reaction scheme for $scCO_2$ polymerization of PMMA templated by aluminosilicate clay.

5.2.1 Materials

The modified silicates used in this study are montmorillonite-based clays obtained from Southern Clay Products. The following discussion focuses on three specific organically modified layered silicates (OMLS), each with a different initial d-spacing (Table 5.1). Cloisite C15A and C20A are each modified with a dialkyldimethylammonium salt from hydrogentated tallow. The difference in d-spacing is due to the difference in the surface charge density of the base silicate. C15A has a larger charge density and therefore results in a more tightly packed surfactant layer upon

modification. Cloisite 25A is modified with an asymmetric dialkyldimethylammonium surfactant, and exhibits a smaller initial d-spacing than either C15A or C20A.

Table 5.1 Montmorillonite clays – physical data

Clay	d-Spacing (A)	Surface modification*	Surface Charge (meq/100g)
Na-mont.	10.7	none	N/A
C10A	18.3	2MBHT	125
C15A	30.6	2M2HT	125
C20A	24.2	2M2HT	95
C25A	18.6	2MHTC8	95

* HT = hydrogenated tallow (65% C18, 30% C16, 5% C14)
B = methylbenzene, 2M = dimethyl, C8 = 2-ethyl-hexyl

In order to maintain a level of comparison between the different OMLS used in this study, the results following are based on weight percent of inorganic clay. This treatment follows the brief discussion in Section 4.2. The normalization used is based on the TGA spectrum of the OMLS (Figure 5.2). The residue mass at 800 °C is taken as the mass fraction inorganic silicate, f_s. The filler weight percent, $\%_s$, is then calculated as follows:

$$\%_s = \frac{m_s}{m_{TOTAL}} = \frac{f_s \cdot m_{OMLS}}{m_{PMMA} + m_{OMLS}} \qquad \text{Eq. 5.1}$$

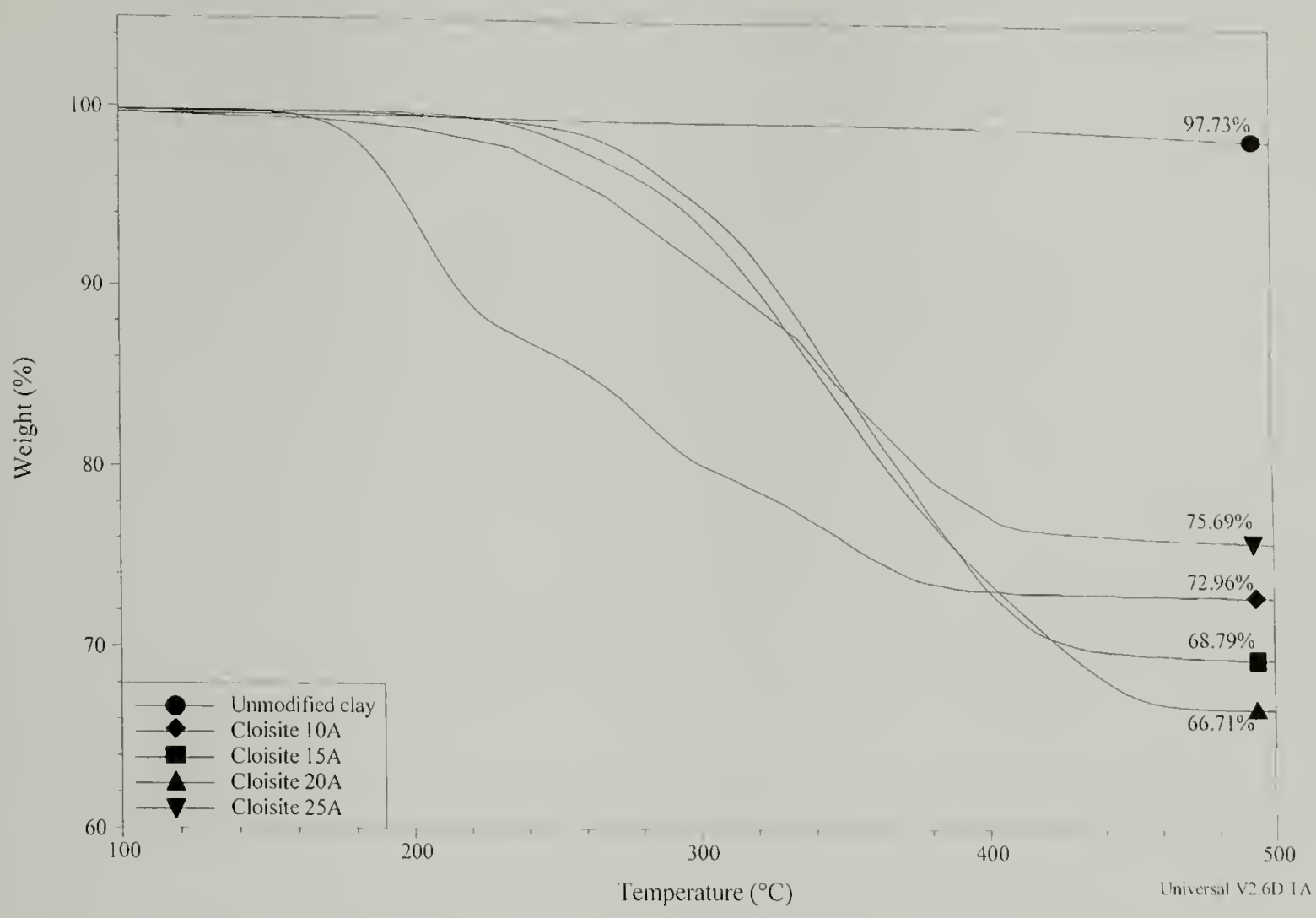

Figure 5.2 TGA of modified clays (residue upon incineration is then the inorganic percent composition).

The matrix polymer for the synthesized nanocomposites is poly(methyl methacrylate), PMMA, radically polymerized in supercritical CO_2. In order to synthesize high molecular-weight polymer efficiently, the methyl methacrylate (MMA) monomer is distilled to remove inhibitors. The radical initiator is tertiary-butyl-peroxybenzoate (TBPB), which has an activation temperature of approximately 100 °C. The half-life of the initiator is considered infinite at 65 °C. Both monomer and initiator were obtained from Sigma-Aldrich.

5.2.2 Experimental procedure and morphology

Composites are fabricated in a custom-made high-pressure apparatus (Figure 5.3) specifically designed to allow for the application of a compressive normal force to the

samples while in the presence of $scCO_2$. The normal force maintains the samples at a known volume. The details of this experimental apparatus have been discussed elsewhere, [94] but the main points of the system are reiterated here. The reaction vessel is a stainless-steel cavity, 10 cm in diameter, which is mounted in a hydraulic press. The CO_2 pressure is controlled via an electronic pressure regulator with a computer interface that allows for fine pressure control. Thermocouples penetrate the body of the vessel and allow for accurate monitoring and control of temperature. The CO_2 pressure can be dynamically controlled via an ER 3000 pressure regulator or by virtue of a back-pressure regulator. The latter allows for controlled $scCO_2$ flow through the reaction chamber and can be used to remove excess monomer. A monomer reserve is also incorporated into the design to allow for a true reaction-injection molding (RIM) synthetic route.

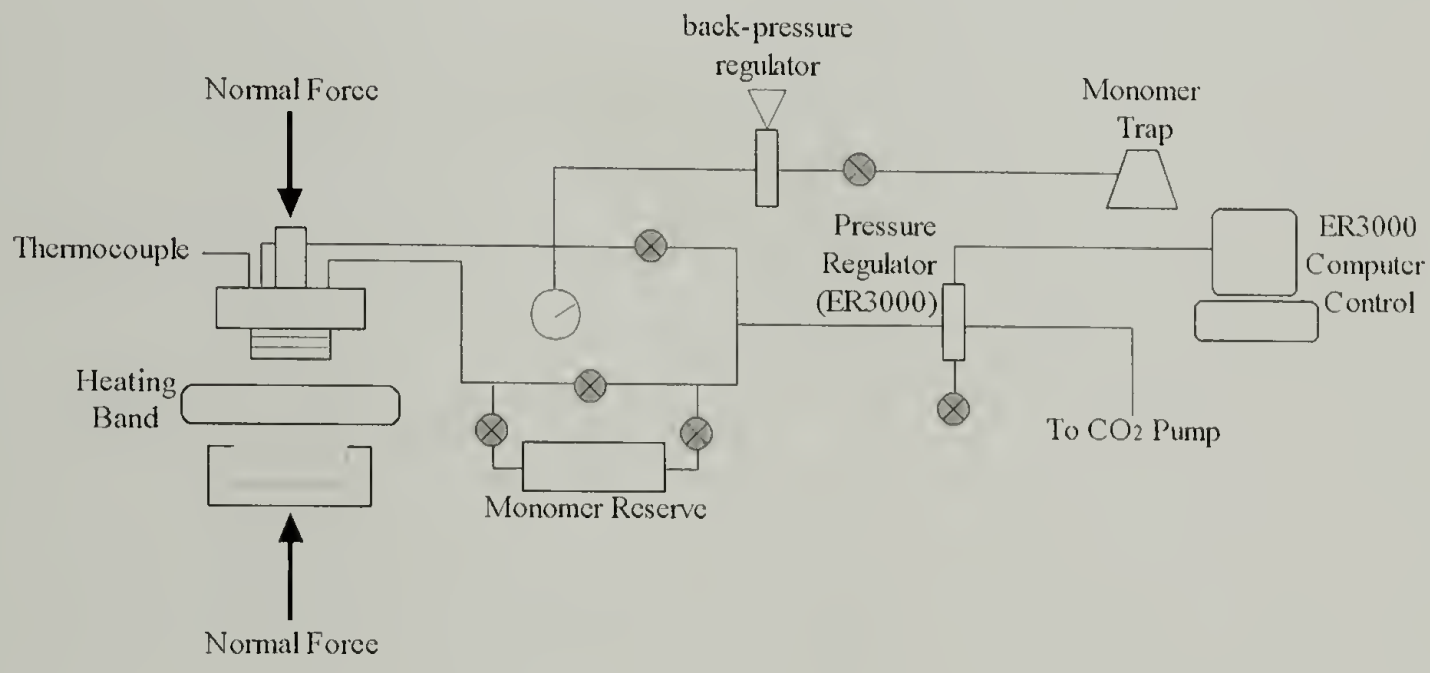

Figure 5.3 Schematic of supercritical CO_2 reaction vessel.

A number of different synthesis routes can be accomplished using this reaction design. These are summarized in Table 5.2 and will be referred to in the following

discussion. Although the other reaction schemes differ slightly, the details of Reaction Scheme A are described here.

Table 5.2 Reaction design for supercritical CO_2 polymerizations

Reaction Scheme	Reaction Summary	Soak Conditions	Polymerization Conditions	Post-polymerization depressurization
A	Standard reaction · Pre-mix known amounts of monomer and clay	10 klb_f normal force, 2 hrs, 65°C, closed vessel, 1500 psi CO_2	6 hrs, 110°C closed vessel 1500 psi CO_2	Depressurize over 15 hrs at 110°C from 1500 psi to atmosphere
B	Post-polymerization consolidation (CO_2 is forced out of the vessel)	10 klb_f normal force, 2 hrs, 65°C, closed vessel, 1500 psi CO_2	6 hrs, 110°C closed vessel 1500 psi CO_2	Depressurize over 6 hrs at 110°C to atmosphere while maintaining a constant normal force
C	Reaction-injection molding reaction (RIM) - see diagram for reaction vessel configuration	Clay is pressed to 30 klb_f then presoaked for 2 hrs, 65°C at 1400 psi CO_2. Monomer is then washed into the reaction vessel via a flow gradient from 1500 psi to 1200 psi for 3 hrs.	6 hrs, 110°C closed vessel 1500 psi CO_2	Depressurize over 15 hrs at 110°C from 1500 psi to atmosphere
D	Pre-polymerization CO_2 "dry-cleaning" (see diagram for vessel configuration)	Excess monomer in known amount of clay. Monomer is then removed from the reaction vessel through a CO_2 flow gradient from 1500 psi to 1200 psi.	6 hrs, 110°C open to reserve 1500 psi CO_2	Depressurize over 15 hrs at 110°C from 1500 psi to atmosphere

5.2.2.1 Reaetion Scheme A

The silieate nanocomposites are synthesized by adding a known amount of OMLS, MMA monomer and initiator into the reaetion vessel. Mixing is not required. The vessel is then closed and plaeed in the press with approximately 5 MPa of compressive normal pressure acting on the top of the ehamber. The mold is then pressurized to between 10 MPa and 14 MPa with CO_2 at room temperature and the main valve is closed. The chamber is then allowed to equilibrate at 65 °C for four hours at which point the temperature is increased to 110 °C for an additional six hours. The initial 65 °C stage is termed the soak stage while polymerization oeeurs at 110 °C. After reaetion, the temperature is allowed to drop and the mold is returned to dynamie pressure control from the ER 3000. The pressure is then dropped slowly to ambient eonditions over a 15-hour period. This final stage of eomposite synthesis is referred to as the eonsolidation stage as normal foree can again be applied to the top of the ehamber, compacting the sample and indueing a nematic orientation to the silieates.

Following synthesis, residual CO_2 trapped within the polymer must be removed.[99] This is done alternatively by evaeuation of the eomposite at 50 °C for a period of days or through melt-processing of the sample. The composite is heated above T_g and deliberately foamed, thereby removing all CO_2. The foam is pulverized and melt-pressed into a plaque.

5.3 Composite characterization

The composites synthesized using the above teehnique are charaeterized in terms of their morphology and the ability of the synthetic route to produee homogeneously intercalated materials. Beeause the goal of this synthesis is the produetion of

nancomposites containing a maximum clay concentrations without sacrificing homogeneity, a predictive model for such a concentration was developed.

Three different OMLS are used in this investigation in order to determine the effect of the OMLS in dictating the maximum clay concentration and degree of intercalation (Figure 5.4). At low clay concentrations, the d-spacing of the intercalated nanocomposite is constant, regardless of the amount of polymer introduced. This results in the maximum intercalated separation and is a consequence of the thermodynamics of intercalation.

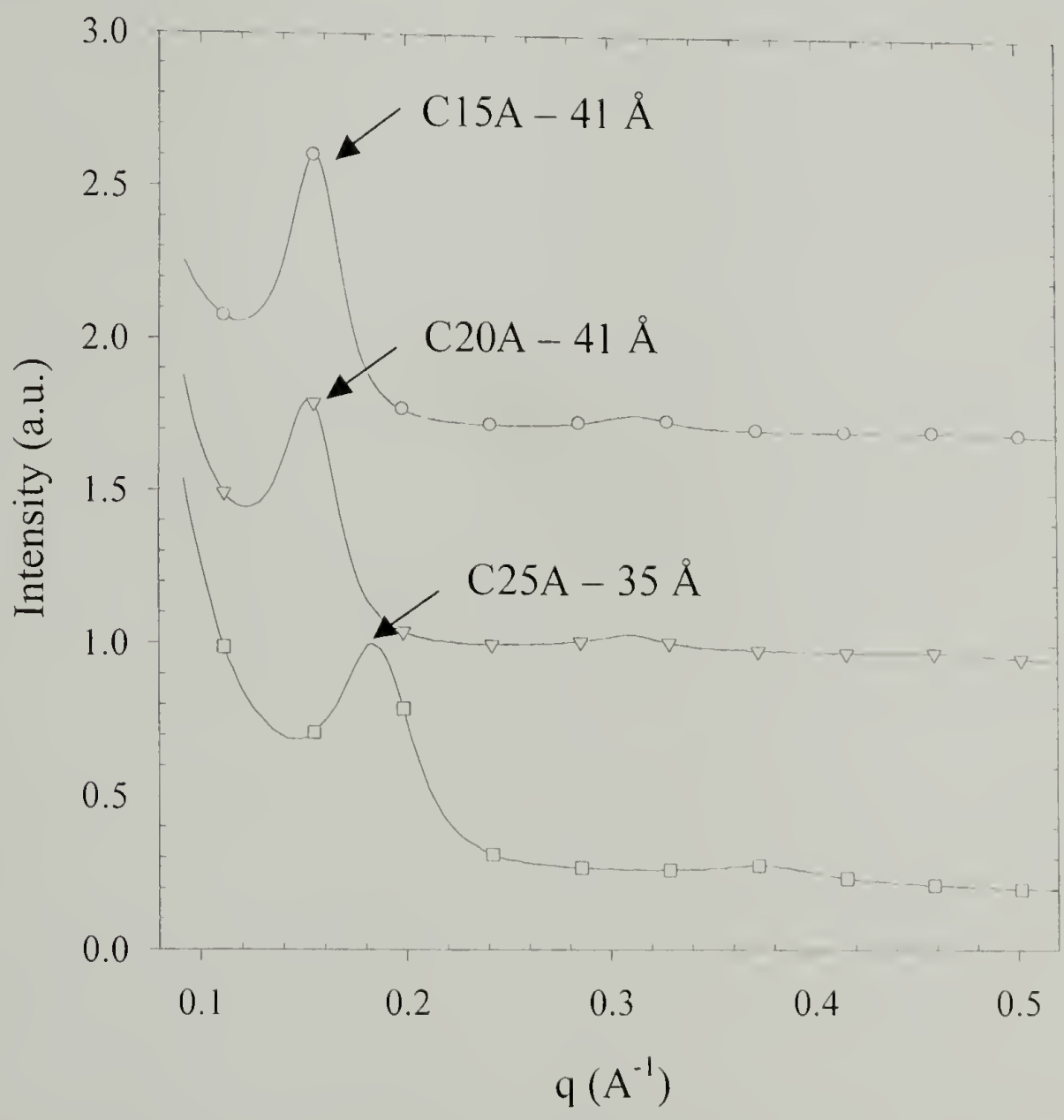

Figure 5.4 Intercalated clays in PMMA matrix. Samples all contain approximately 12 wt. % clay.

Intercalation is an enthalpically driven process which is limited by the entropic penalty for polymer confinement.[85] The enthalpic contributions during intercalation are sufficient to induce wetting of the intra-gallery regions of the OMLS. Initially, the galleries between silicates are swollen and the decrease in entropy of intercalated monomer or polymer is countered by the degrees of freedom gained during surfactant swelling. The free energy of the system is, therefore, decreased. Once the surfactants reach a maximum extension, further intercalation increases the free energy and the maximum intercalated d-spacing is maintained regardless of concentration. The d-spacing of the intercalated morphology is, therefore, strongly dictated by the architecture of the silicate modifiers. The results of this are shown in Figure 5.4, where three intercalated nanocomposites of constant clay concentration (12 wt. % clay) have been synthesized using different OMLS. The d-spacing of the nanocomposites based on the C15A and C20A, which vary in initial gallery spacing due to the difference in clay charge density, are equal because each is modified by the same alkylammonium surfactant. The d-spacing of the intercalates is therefore dictated by the extended length of the surfactants. The third composite, based on C25A, results in a small intercalated d-spacing due to its shorter surfactant length.

At these low clay concentrations, where the polymer surface area is significantly larger than that of the clays, the microscale morphology is heterogeneous with distinct regions rich in clay surrounded by a polymer-rich matrix (Figure 5.5). One can imagine, however, that higher clay concentrations would result in a homogeneously intercalated composite devoid of the two-phase morphology. At higher concentrations, the surface area of the OMLS dominates the composite and the system is starved for polymer.

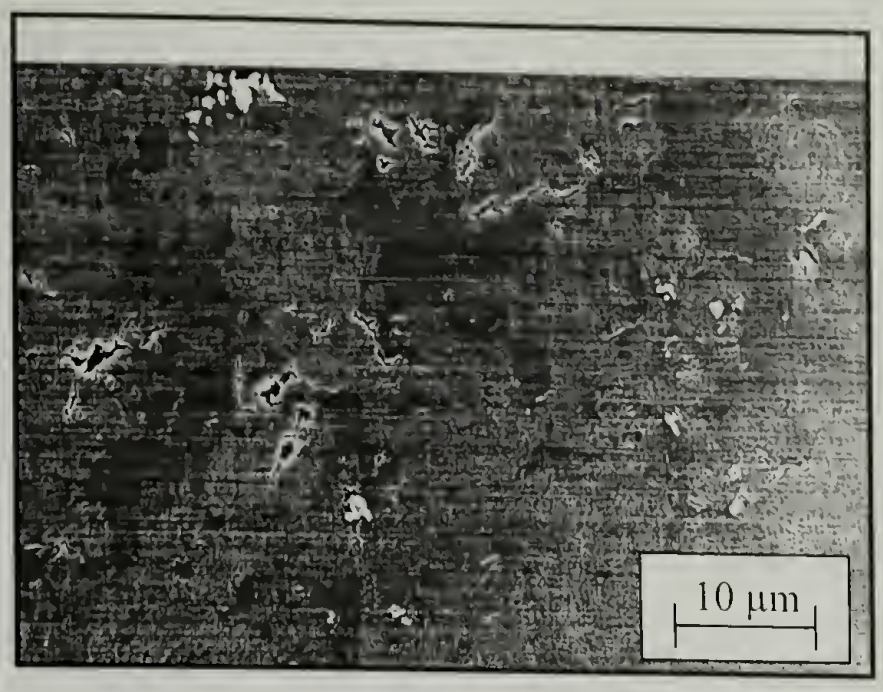

Figure 5.5 SEM micrograph of 12 wt. % clay (C20A) in PMMA. At this concentration of aluminosilicate, most of the available volume in the sample is consumed by the silicate-rich intercalated morphology.

In synthesizing intercalated nanocomposites of high concentration, it is important to estimate a polymer-clay ratio that would result in such a morphology. To this end, an estimation can be made that takes into account a number of material properties characteristic of the modified silicates, the polymer matrix and resulting nanocomposite. The polymer-OMLS ratio, f, resulting in a saturation of the modified clay surface upon blending is the product of the polymer density, ρ_p, surface area of the silicate, S_s, in m^2/g, and the polymer contribution to the intercalated composite gallery spacing, $d_c - d_{OMLS}$. This latter property is estimated as the difference between the gallery height of the intercalated nanocomposite and the initial d-spacing of the OMLS.

$$f = \frac{m_p}{m_{OMLS}} = \rho_p \cdot (d_c - d_{OMLS}) \cdot S_s \qquad \text{Eq. 5.2}$$

A number of assumptions are made. First, the increase in the gallery height upon composite formation is attributed solely to incorporation of polymer between silicate stacks. Mixing of polymer with the surfactant chains occurs with no change in the total

free volume, $\Delta V=0$. Second, the density of the polymer within the gallery is assumed to equal the bulk density of the polymer.[100,101]

5.3.1 Reaction scheme A

The simplest route to synthesizing highly filled clay composites using $scCO_2$ is the addition of known quantities of OMLS and reactive products into the reaction vessel together, and polymerizing. No post-polymerization processing is undertaken and all of the nanocomposites synthesized using this route are initially isotropic. SAXS analysis of the intercalated morphology reveals a strongly lamellar architecture (Figure 5.6). As a result, the morphology is considered to be nanoscopically anisotropic as a layered architecture is maintained within the intercalated regions. Microscopically, however, the separate intercalated regions do not retain any preferential orientation with respect to each other. Once an isotropic composite such as that in Figure 5.6 is synthesized, melt processing of the material results in a high degree of orientation (Figure 5.7). Even at clay concentrations as high as 40 wt. % clay, the synthesized nanocomposites retain a degree of melt flow, opening avenues to inducing orientation and processing the composites into more sophisticated materials. The Herman's orientation function, f_H, can be used to quantify the degree of orientation in such an anisotropic material:

$$f_H = \frac{\langle 3\cos^2\theta - 1 \rangle}{2} \qquad \text{Eq. 5.3}$$

Because a number of intrinsic material properties are known to be linear with the degree of orientation in a material, it is presumed that the mechanical properties of an oriented material are superior to the isotropic case. This concept is considered in further detail in Section 5.5.

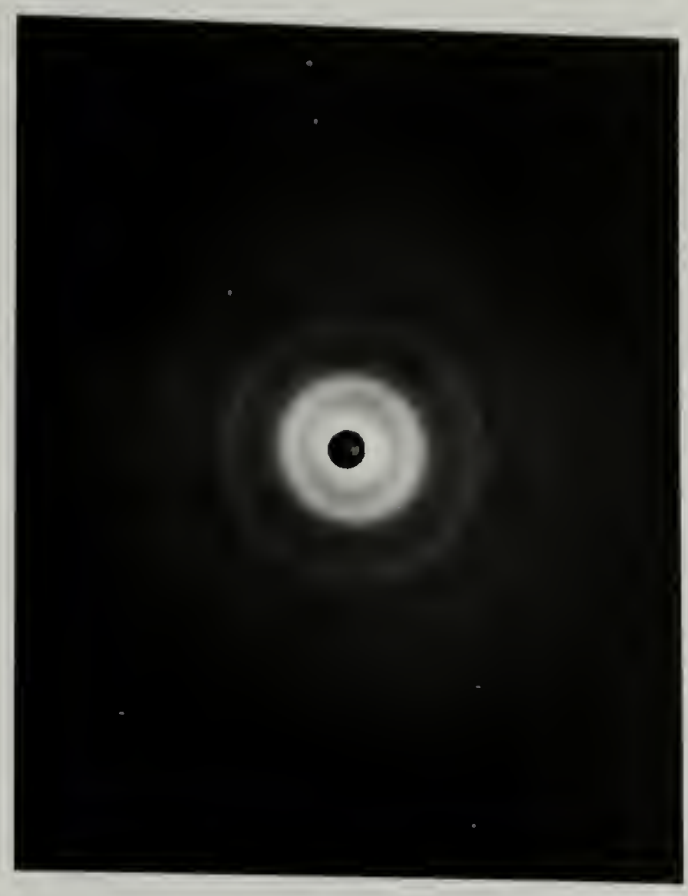

Figure 5.6 Intercalated clay-PMMA nanocomposites exhibit a strongly lamellar structure as represented in this X-ray scattering image of a 25 wt. % clay/PMMA sample.

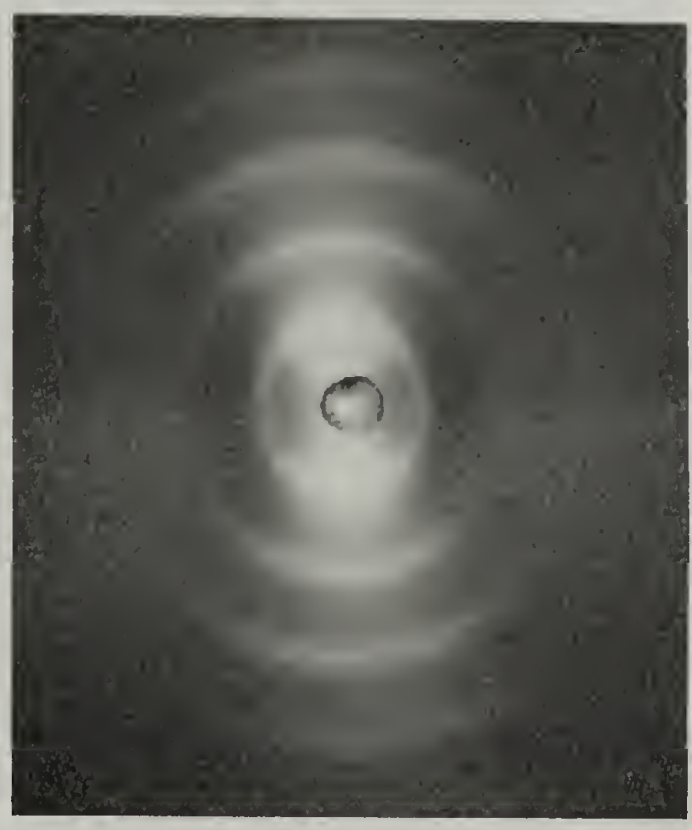

Figure 5.7 A $scCO_2$-synthesized sample can be processed following polymerization to induce orientation. This post-polymerization processing, as with the melt processed sample above, can induce a strongly anisotropic morphology ($f_{II} = 0.8$).

By changing the relative concentrations of clay and monomer, the validity of Eq. 5.2 can be verified. Given the simplicity of this model, it is nonetheless effective in estimating a maximum silicate concentration supporting a homogeneously intercalated morphology. The predicted maximum ratio in the case of a C20A-PMMA nanocomposite (ρ_p=1.2 g/cm^3, S_s=700 m^2/g, change in d-spacing = 18 Å) is approximately 1.45:1, or 27 wt. % clay. Below 27 wt. % clay, the d-spacing does not change with the amount of clay in the composite (Figure 5.8). This is in keeping with what is expected for intercalated systems. Above 27 wt. % clay, however, the d-spacing is decreased as there is not enough polymer available to further swell the clay. Rather than form a two-phase material containing both unswollen and intercalated clays, the polymer is distributed evenly throughout, resulting in a smaller intercalated d-spacing. There is no evidence of a peak at 24.2 Å (q = 0.26 Å^{-1}) corresponding to the unswollen C20A clay. This result indicates that the $scCO_2$ method does produce a homogeneous dispersion of the monomer throughout the volume prior to polymerization. Equation 5.2 has therefore been demonstrated to effectively predict a maximum clay-polymer ratio resulting in a fully intercalated structure.

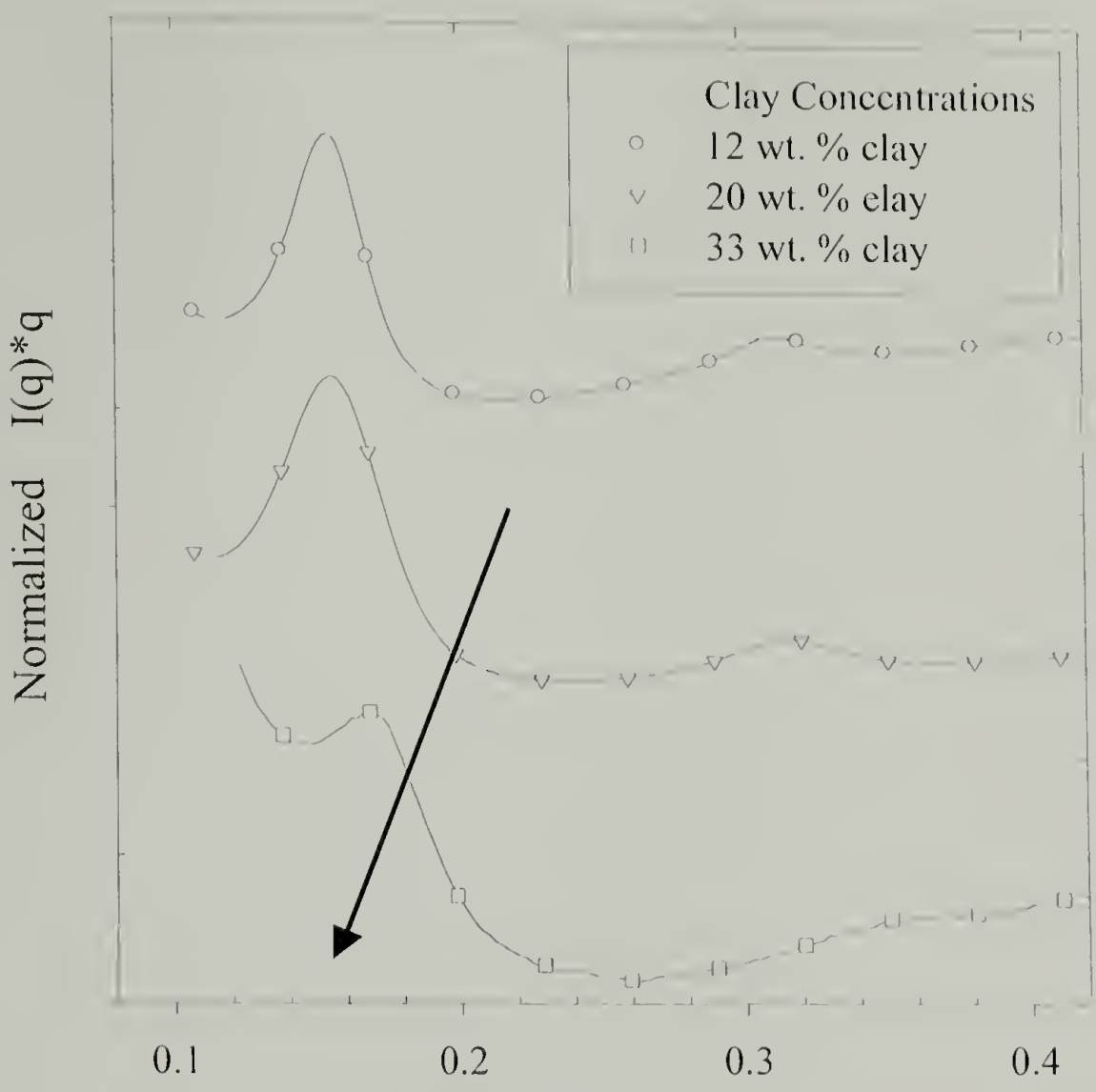

Figure 5.8 Effect of increased clay concentration on lamellar ordering and d-spacing of intercalated nanocomposite.

However, Eq. 5.2 can also be used to predict the response of an intercalated nanocomposite containing a clay concentration greater than the above estimated value. At these higher clay concentrations, the nanocomposite is starved for polymer and fully swollen gallery spacing is not achievable. The peak corresponding to the 33 wt. % clay sample is broader and less defined than those for the lower clay concentrations. This indicates a broader distribution of gallery spacings within the composite. The d-spacing has also decreased to 36.9 Å ($q = 0.17$ Å^{-1}). This value is close to that predicted by Eq. 5.2 (35.9 Å), providing an extra check for the validity of the previously made assumptions.

In order to verify a homogenously intercalated morphology devoid of clay-rich and polymer-rich phases, TEM images of a 27 wt. % clay sample were obtained (Figure 5.9). In order to obtain such images, the matrix material was changed from PMMA, which ablates readily in the electron microscope, to polystyrene (PS). The image below is representative of the entire sample volume, indicating a homogenously intercalated gross morphology. Comparison of Figure 5.9 with Figure 4.7 illustrates the difference in both clay concentration and packing density of these composites with those of lower clay concentration synthesized through more traditional means.

Figure 5.9 TEM micrograph of a 27 wt. % clay nanocomposite in PS matrix. The inset electron-diffraction pattern exhibits the characteristic isotropic lamellar ring.

5.3.2 Reaction schemes B, C and D

The remaining three reaction schemes represent more sophisticated attempts at synthesizing the types of composite structures available through Scheme A. Rather than using the experimental apparatus simply as a reaction vessel and prescribing reaction conditions, the following discussion describe attempts at achieving order and maximum clay loading through other means.

5.3.2.1 Reaction scheme B

Reaction scheme A, although very successful in synthesizing the composites of desired compositions and morphology, is nonetheless incapable of producing samples which are free from trapped CO_2 following the depressurization stage. At elevated temperature (110 °C) and pressure (1500 psi), the PMMA matrix is plasticized with $scCO_2$, which results in kind of mobility desired for producing homogeneously intercalated morphologies. As the temperature and pressure are dropped to ambient conditions during depressurization, the CO_2 dissolved in the sample is slowly removed and the matrix returns to its unplasticized state. During this process, diffusion of CO_2 out of the polymer becomes gradually slower, and ideally, at the end of the depressurization cycle, all of the CO_2 has been removed. It has been determined, however, that a small portion (approximately 3-5 wt. %) CO_2 remains trapped within the polymer. This is observed through a small mass loss in the TGA as the polymer is heated above T_g and foamed. The small amount of CO_2 results in a marked decrease in the mechanical properties of the matrix (Figure 5.10) and must be removed to achieve unbiased mechanical comparisons of mechanical properties.

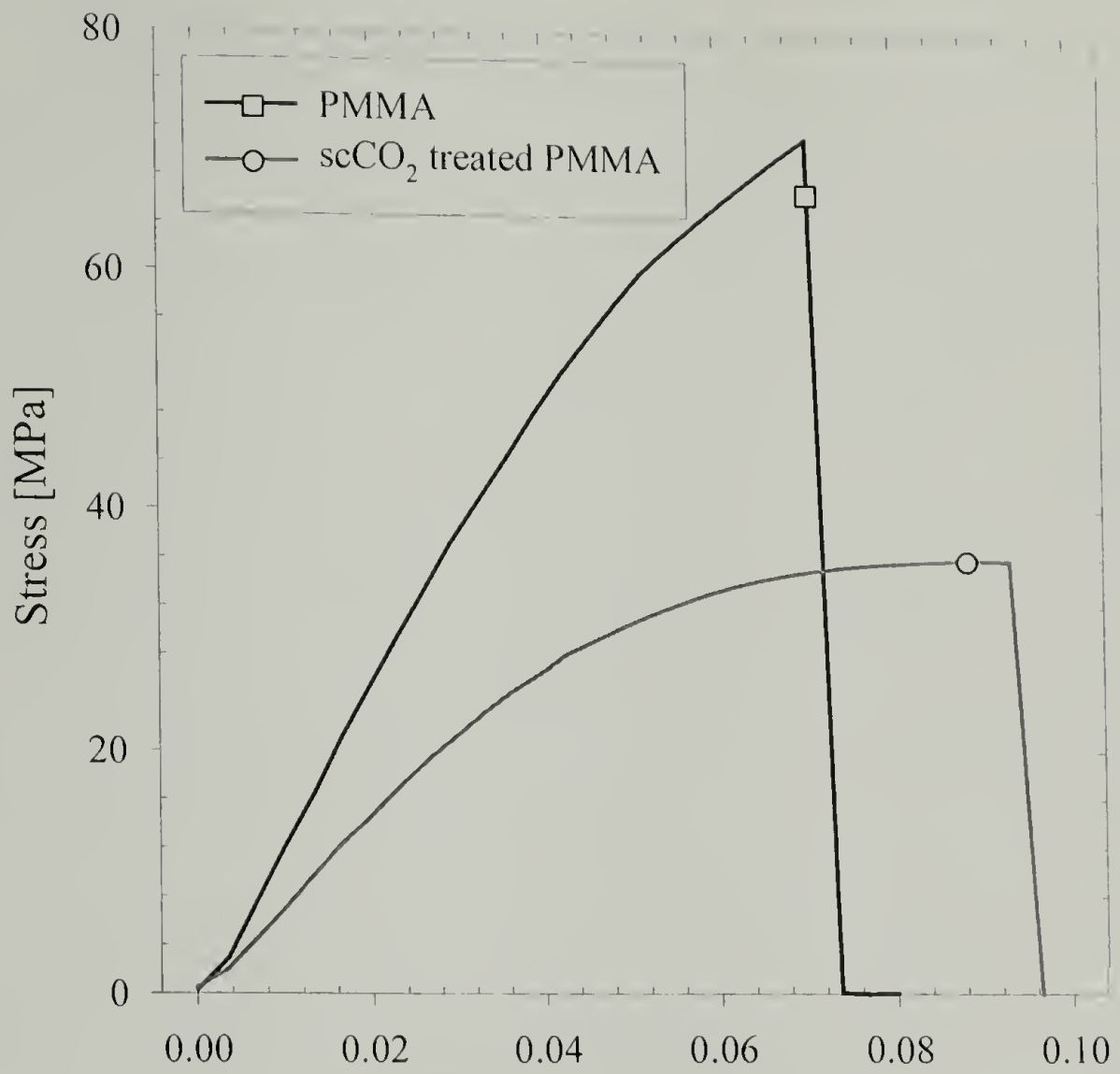

Figure 5.10 Mechanical properties of $scCO_2$-swollen PMMA (○) as compared to commercial, untreated PMMA (□).

Two methods for removing the CO_2 from the sample have been described in the experimental section (5.2.2.1) above. Both of these, however, occur following depressurization and either requires days of vacuum treatment or destruction of the sample through melt pressing. In Scheme B, a consolidation method is described which results in a significant reduction of CO_2 content and *in-situ* orientation of the sample.

Following polymcrization, the temperature of the vessel remains at 110 °C and depressurization commences as in Scheme A. Normally, the depressurization can be monitored using both the ER 3000 pressure gauge as CO_2 is removed and through a corrcsponding drop in the normal force registered on the hydraulic press. Here, however,

the normal force on the sample is kept constant (30 klb_f) for the duration of the depressurization cycle, which results in a decrease of the reaction-vessel volume with time, compressing the sample. Preferential orientation of the silicates within the sample occurs *in situ* (Figure 5.11).

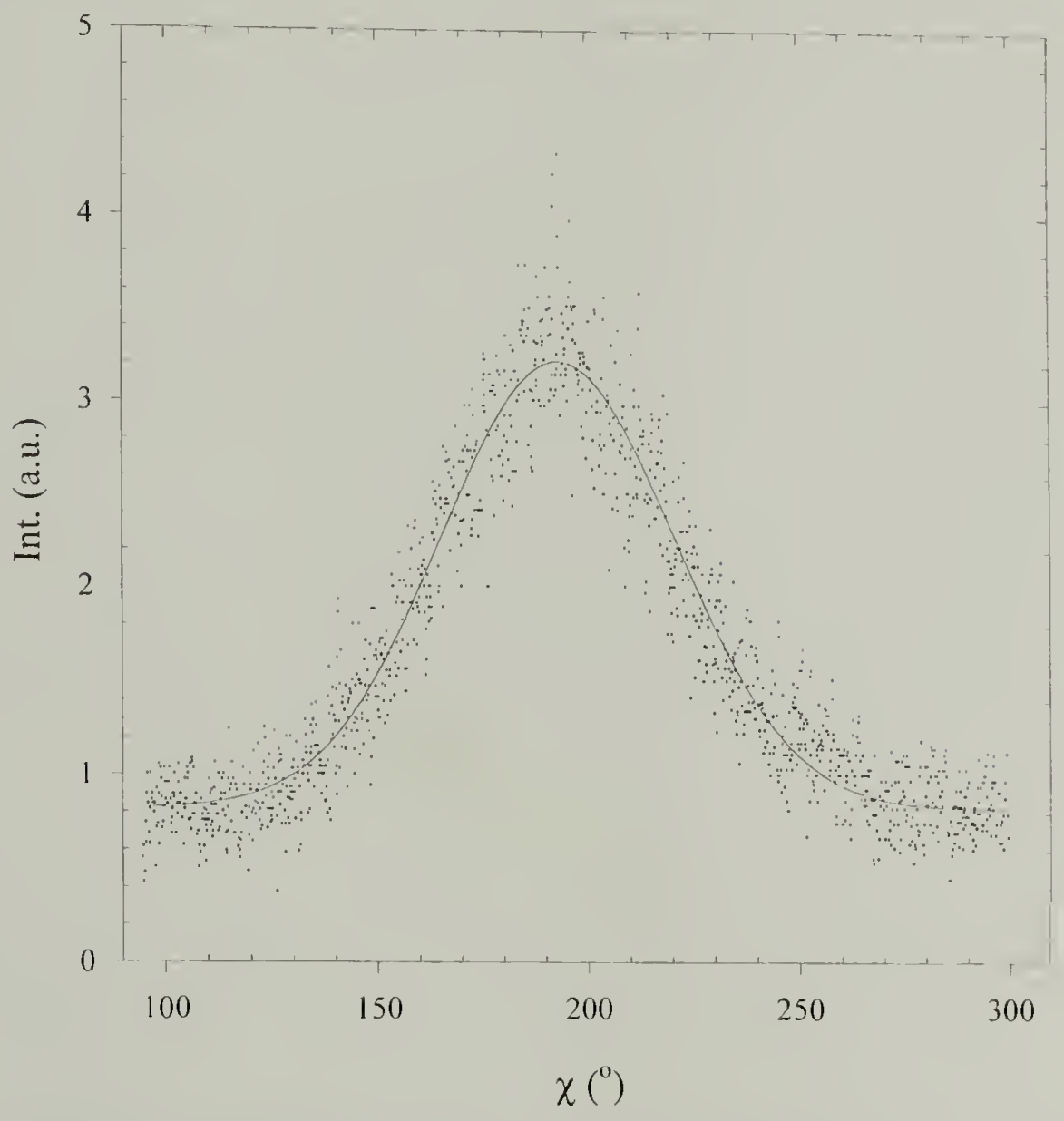

Figure 5.11 Orientation induced in sample containing 33 wt. % clay (50 wt. % OMLS) polymerized according to reaction scheme B (f_H = 0.55).

As with the melt-processed samples, orientation occurs transverse to the force direction and is uniform radially from the center of the sample. The orientation achieved in this way, however, is smaller than that achieved through simple melt processing. Consolidation in a limited volume, as is the case here, precludes massive flow of the sample. The Herman's orientation function for the sample produced in this manner is

only 0.55, as compared to 0.8 for melt processing. Nonetheless, optimization of this procedure can be envisioned which allows for a shear flow leading to orientation.

5.3.2.2 Reaction schemes C and D

Schemes C and D are attempts at synthesizing samples containing the maximum clay-polymer ratio predicted by Eq. 5.2 without prescribing known initial constituent concentrations.

Scheme C mirrors traditional reaction-injection molding (RIM). A known amount of OMLS is added to the reaction chamber, heated to 65 °C and subjected to 30 klb_f of normal force. This initial compression results in immediate consolidation of the clay such that only a small amount of free volume is available to the monomer. Without an initial compressive force, the monomer is free to fill the entire free volume of the vessel in an uncontrolled fashion. Next, CO_2 is introduced at 1400 psi and the chamber is soaked for two hours to aid in consolidation. This process results in a sample containing a high degree of orientation prior to polymerization and can be used a template. Monomer is forced into the reaction chamber by opening the back-pressure regulator to 1200 psi and creating a gradient flow of the CO_2 from the pump (1500 psi), through the monomer reserve vessel (containing 100 ml monomer) and into the reaction vessel. To prevent expulsion of monomer into the room, a trap consisting of a 2 L volume of water is added to the exit pipe after the back-pressure regulator. The CO_2 and MMA monomer are then bubbled into this trap. After a period of time, the chamber has presumably been saturated with a maximum concentration of monomer. Polymerization and depressurization follow as for Scheme A. The composite synthesized in this manner suffers from inhomogeneous dispersion of polymer (Figure 5.12).

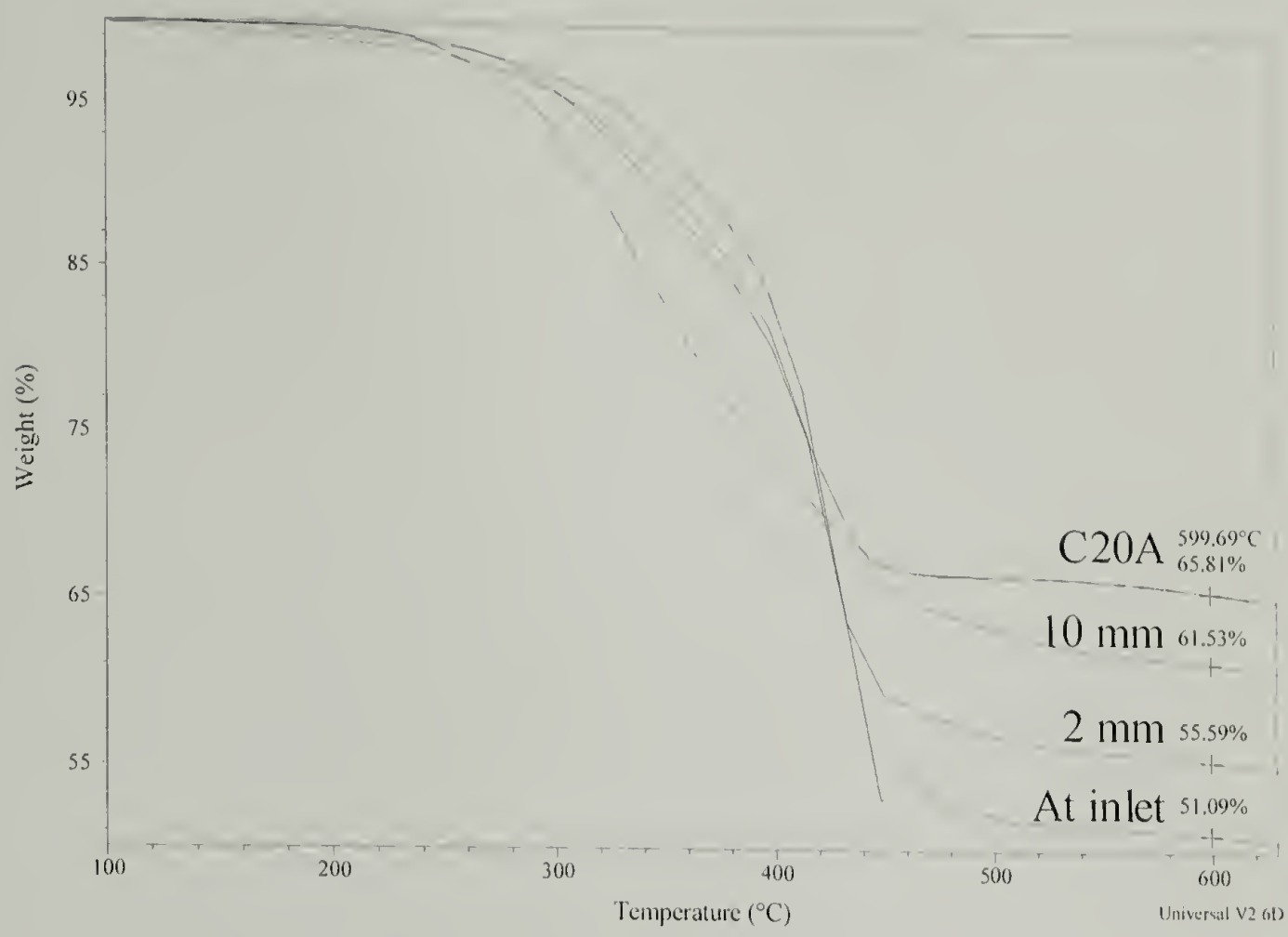

Figure 5.12 Spatial distribution of PMMA in sample made according to reaction scheme C. With increasing distance away from MMA inlet, the amount of PMMA, as represented by increasing inorganic clay concentration, decreases.

The initial compression of the clay to prevent uncontrolled swelling of the reaction volume upon pressurization also results in insufficient volume for the monomer to occupy. As exhibited in the XRD patterns of intercalated nanocomposites (Figure 5.4), swelling of the modified clay results in a 75 % increase in the d-spacing (from 24 A to 42 A in the case of C20A). If we assume a nematic structure for the clay prior to monomer incorporation, an 75 % increase in volume would be required to incorporate the necessary amount of monomer. Applying the initial high compressive pressure (greater than the pressure of $scCO_2$), swelling is prohibited volumetrically. With the current apparatus, however, this condition is unavoidable. Monitoring of the reaction volume, and thereby providing sufficient headspace of monomer injection, would alleviate this barrier.

Scheme D relies on removal, rather than introduction, of monomer from the reaction chamber. Here OMLS is added with an excess monomer volume and sealed. Again, the chamber is heated to 65 °C and pressurized to 1500 psi for two hours to allow for monomer distribution. The backpressure regulator is then opened to 1200 psi and a CO_2-flow gradient is introduced. The MMA monomer, soluble in $scCO_2$, is then removed from the reaction chamber. Polymerization and depressurization occur as with Scheme A.

Without accurate measure of the removed monomer, however, Scheme D can result in complete removal of the MMA monomer, both excess and trapped within the inter-gallery spacing. Such was the case in the initial attempts at developing this reaction scheme. Although qualitative verification of MMA removal from the vessel can be conducted by observing the water trap into which the CO_2 is bubbled, without quantitative observations Scheme D is conducted blind. One way to overcome this design flaw might be to use an IR detector at the outlet. In this way, MMA extraction may be quantified. A change in the flow rate could be indicative of the onset of MMA extraction from the interlayer spacing instead of the excess, bulk phase. Assuming this design obstacle can be overcome, Scheme D has the advantage of much easier initial monomer dispersion throughout the reaction volume. Because of the large monomer excess that is present, the OMLS surface is immediately wetted out. The $scCO_2$ is used as an extraction fluid rather than being employed as a diluent. If the design aspects can be optimized, this technique proves most efficient at producing nanocomposites of a wide range of morphologies. During the extraction stage, a gradual consolidation of the silicates would lead to an ordered architecture prior to polymerization. This would then

result in a nematic clay perform or template for composite fabrication. The difference between template formation here and in Scheme B is the use of the excess monomer as an additional fluid providing flow.

5.4 Physical properties of $scCO_2$-polymerized and melt-polymerized composites

The $scCO_2$-assisted synthetic techniques described above must be compared to simple melt-polymerization processes which can also be used to produce the type of samples desired. In the melt reaction, a known amount of MMA and initiator is added to a quantity of OMLS and compacted in a hydraulic press at 65 °C. Polymerization is initiated through an increase in temperature to 110 °C. Mixing is attempted. The high viscosity of such a mixture, however, precludes good dispersion at even low clay concentrations (12 wt. %).

As is evident in Figure 5.13, melt-produced composites suffer from a significant inhomogeneity. The starting concentrations of the samples reprcsented in Figure 5.13 were 80g C20A (53g clay) and 20g MMA. While the $scCO_2$-made composite demonstrates a 3 % scatter in composition, the melt-made material constitutes both wholly unmodified regions (66 % residue is consistent with the TGA spectrum of C20A OMLS) and overly-modified (41 % residue). The ideal concentration of the resulting composite, based on the starting concentrations of the constituents, is 53 wt. % clay. That the CO_2-made samples exhibit high clay concentrations at both extremcs is attributed to loss of monomer during some stages of the samplc preparation.

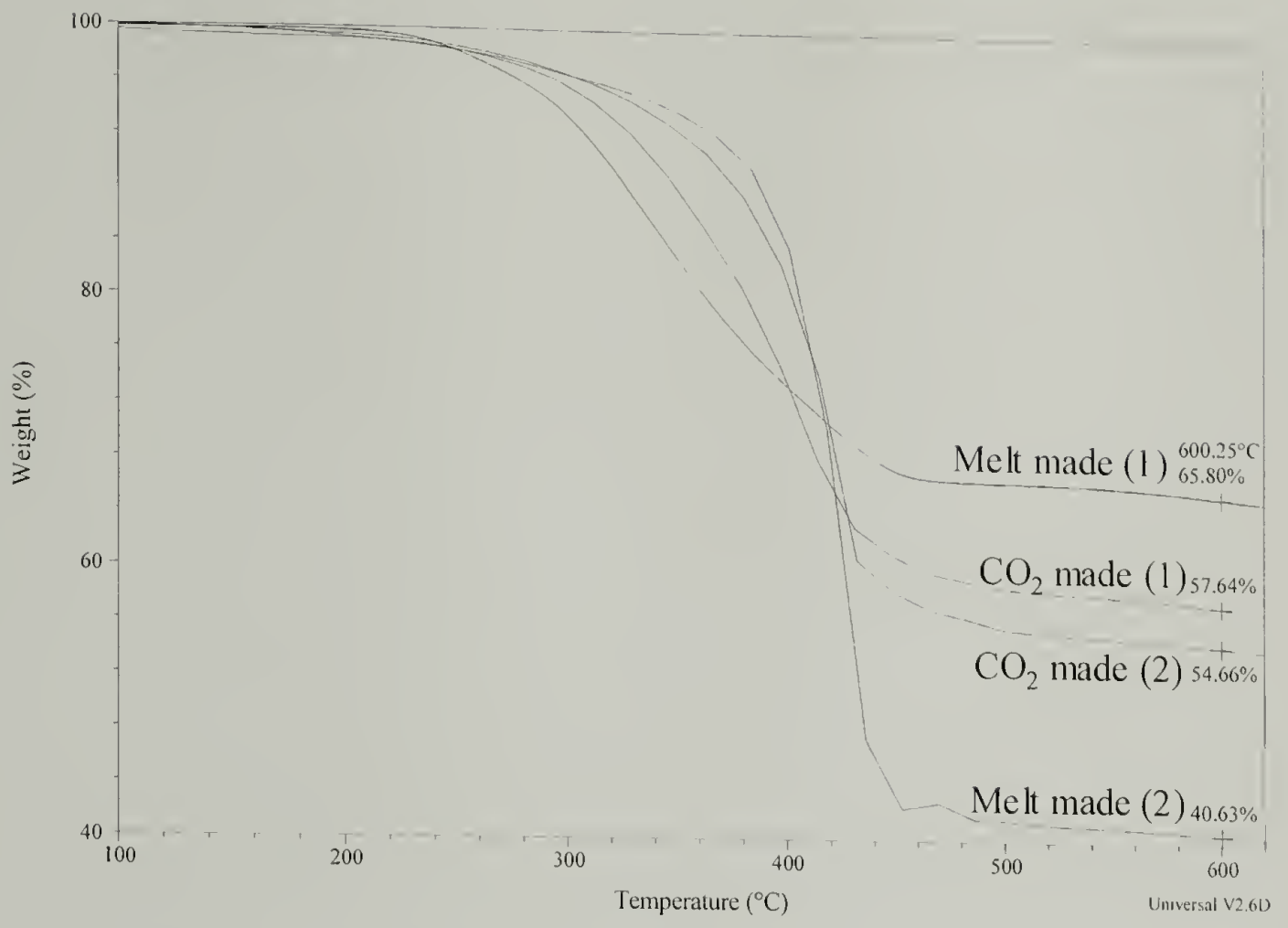

Figure 5.13 Spatial distribution of clay throughout composite samples made in $scCO_2$ and in the melt. Each set represents the extreme clay compositions in the specimen (the minimum and maximum amount of inorganic residue).

5.5 Mechanical properties of high clay concentration composites

The interest in a homogeneously intercalated morphology stems from the opportunities this system provides in terms of true polymer-ceramic hybrid properties, including significantly enhanced mechanical performance. These, as well as the thermal properties, are discussed below. Many polymer material properties, including T_g, are influenced by the molecular weight of the polymer; the polymer synthesized using $scCO_2$ was verified to be of high molecular weight ($M_w > 200{,}000$ g/mol).

The intercalated nanocomposites synthesized in this study exhibit a thermal transition near 105 °C (Figure 5.14), corresponding with the glass transition temperature of PMMA. At high clay concentrations, the transition is faint but reproducible, owing to the low polymer content in these composites. In order to analyze the thermal properties

of the composite more carefully, dynamic tensile measurements under a temperature ramp were conducted in a DMTA. These are compared to a control, a commercial PMMA sample of M_W=1,000,000 g/mol (Figure 5.15). All of the nanocomposites undergo a thermal transition (α-relaxation) at 150 °C according to the peak in the tan δ. This transition is identical to the α-relaxation peak of the PMMA control. This observation is significant in that it demonstrates the presence of molecular mobility of chains in a predominately-intercalated structure. At 27 wt. % clay, the majority of the polymer is confined to the inter-gallery spacing but continues to exhibit relaxation modes of the bulk polymer.

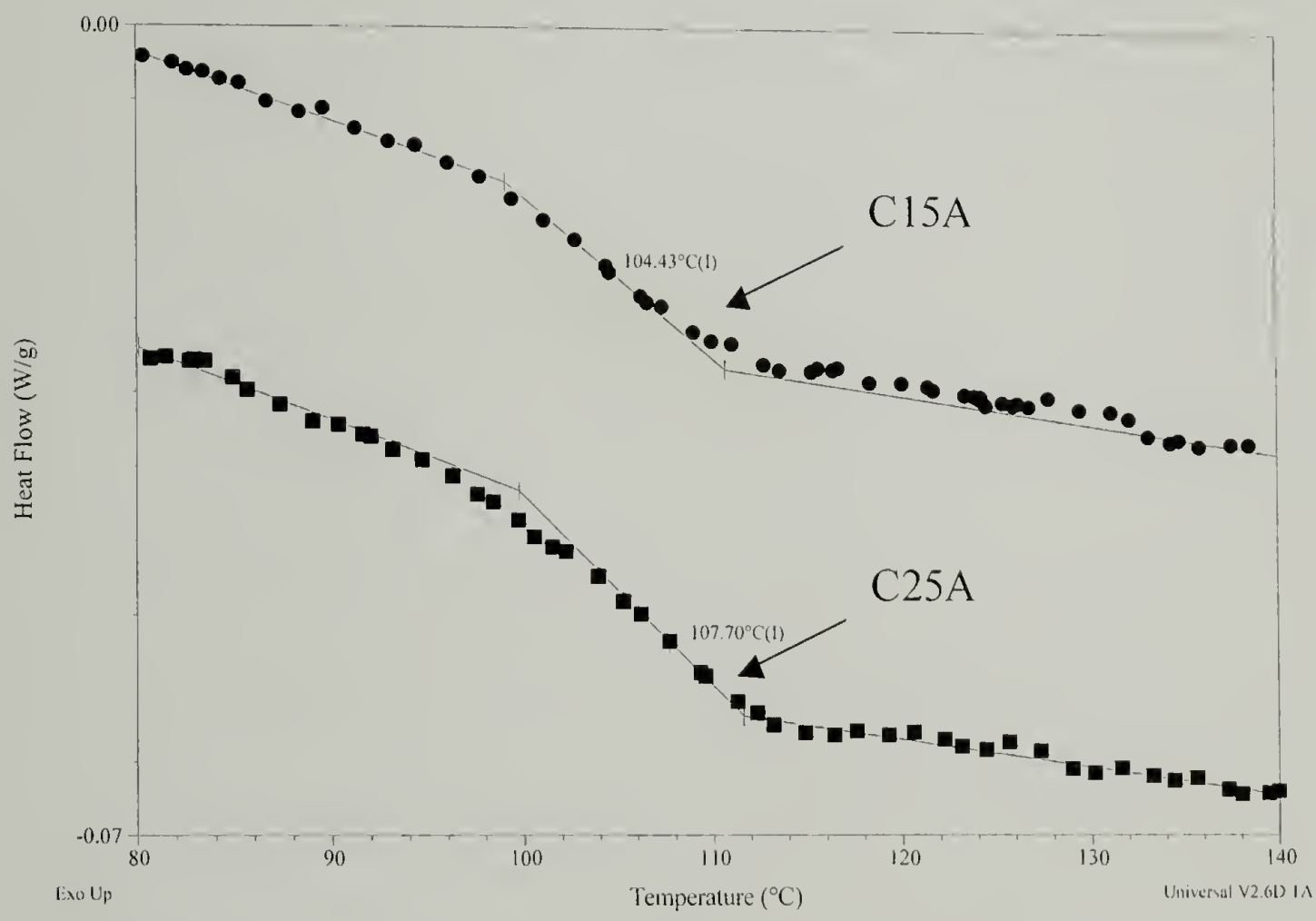

Figure 5.14 Glass transition temperatures of 12 wt. % clay nanocomposites containing both C15A and C25A clay.

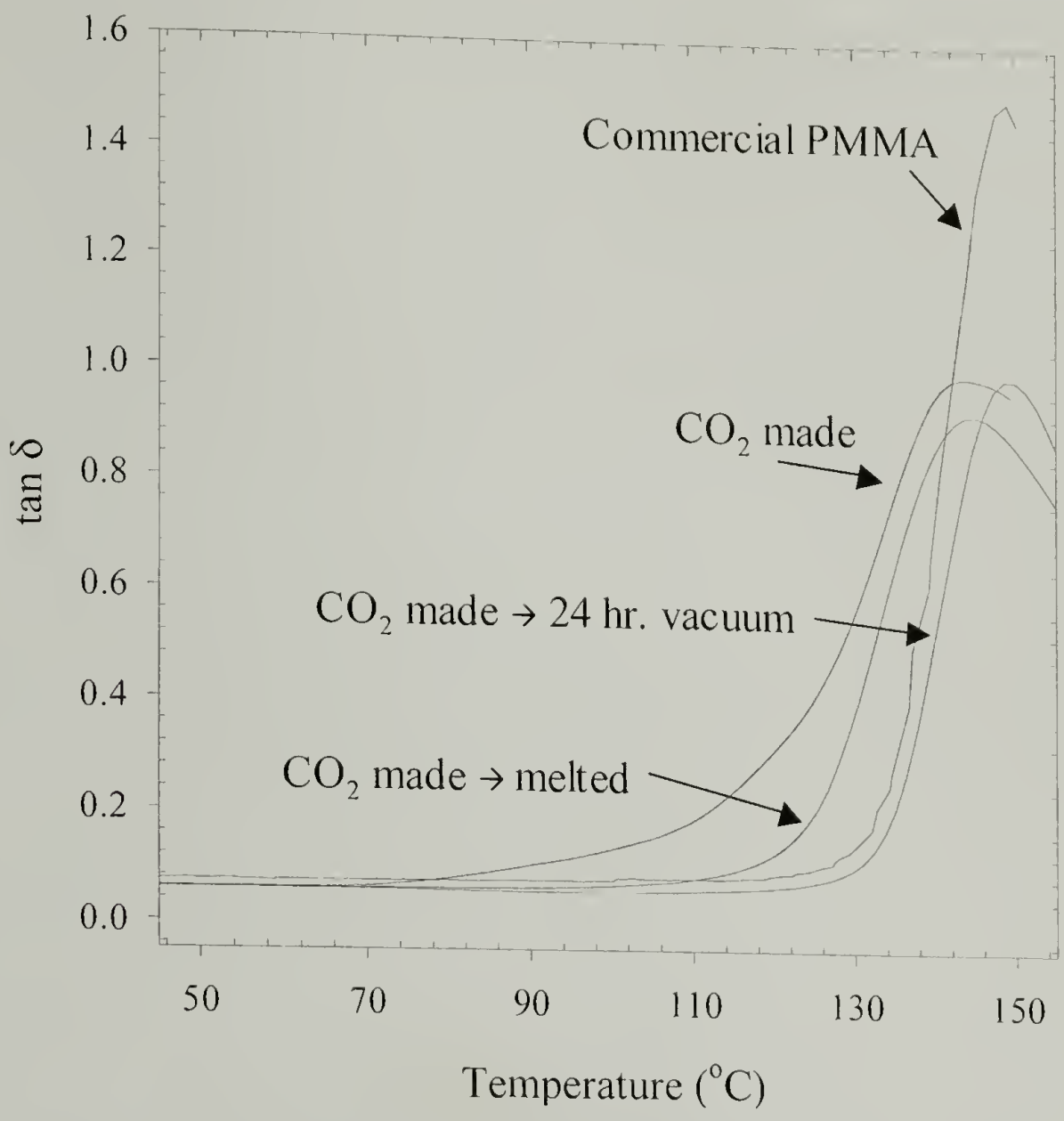

Figure 5.15 Loss tangent (tan δ) spectra of 27 wt. % C20A nanocomposites in PMMA following various post-treatments as compared to commercial PMMA. The broad peak of the CO_2-made composite illustrates the early onset of foaming prior to CO_2 removal.

The tensile modulus of 27 wt. % clay nanocomposites was determined from the storage modulus of the DMTA spectra (Figure 5.16). Under all conditions, the nanocomposites exhibit a significantly higher storage modulus. The "CO_2-made" curve demonstrates the need to completely remove residual CO_2 from the composites. A premature softening is observed at approximately 90 °C. This is a result of the CO_2 becoming less soluble in the polymer at higher temperatures, foaming the matrix. After the sample has been sufficiently evacuated, following 24 hours in a vacuum oven at 75

°C, features relating to CO_2-plasticization are eliminated. Thus far, these materials are isotropic, but both exhibit a 50 % increase in modulus. Once the composite has been oriented through melt processing, anisotropic mechanical properties are exhibited. This is observed in the CO_2-made, melt-processed sample. The curve illustrates the effectiveness of silicate orientation in achieving modulus enhancements. By inducing a nematic order to the silicates, a 220 % increase in the tensile modulus is achieved for the glassy polymer.

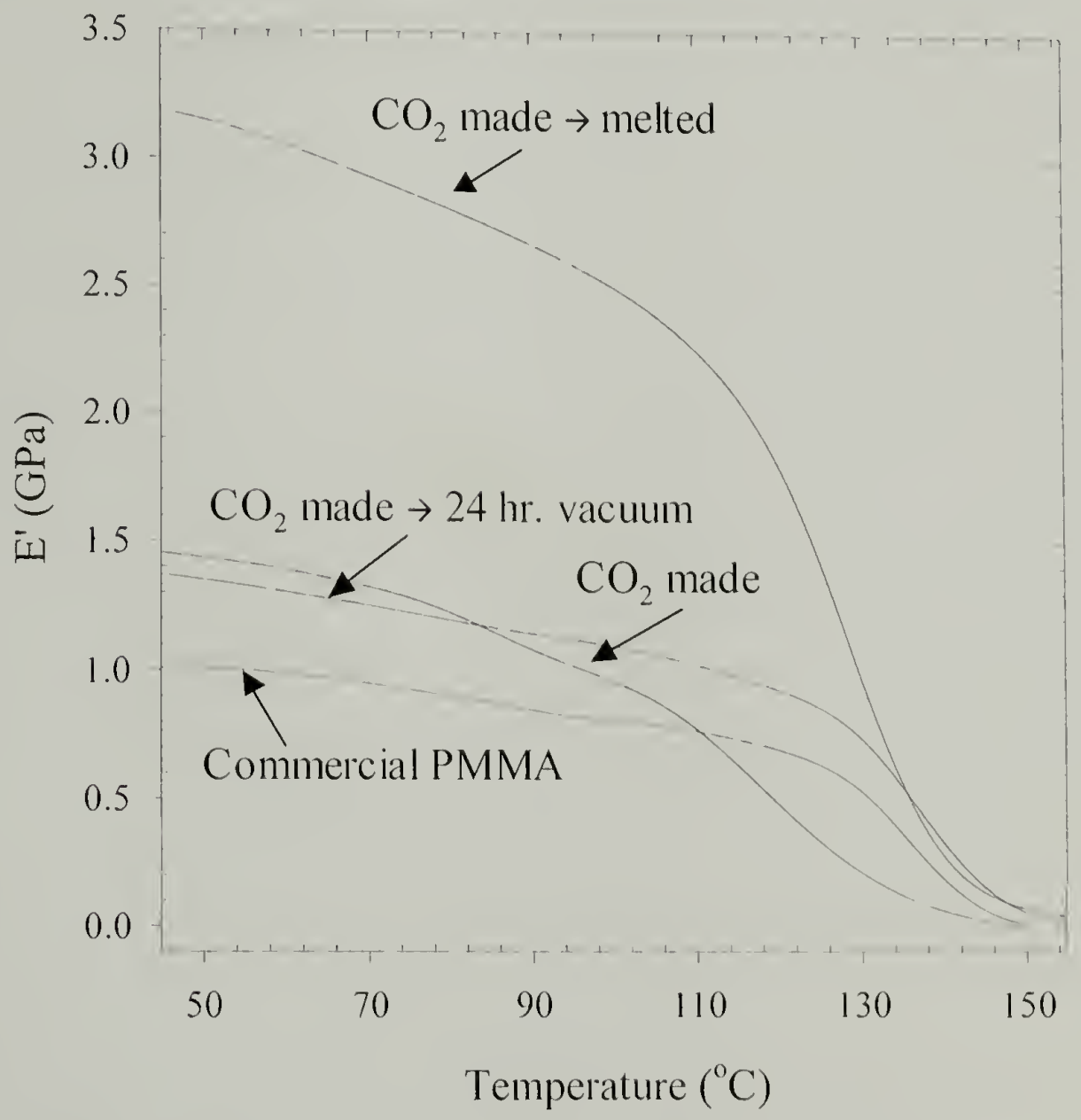

Figure 5.16 Storage modulus of 27 wt. % clay/PMMA composites as compared to commercial PMMA. Post-polymerization melt processing, which induces orientation, results in a marked increase in modulus. Removal of CO_2 from the sample negates the detrimental effects of foaming.

A traditional tensile-test specimen was made by melt pressing a 25 wt. % clay nanocomposite and cutting into a dog bone for testing (Table 5.3). The tensile modulus is increased significantly (400 %). What is also evident, however, from these results is the brittleness of the composite as compared to commercial PMMA. The oriented sample fails at less than 0.1 % strain, whereas as the commercial PMMA extends to 7 %. This behavior is consistent with ceramic properties.

Table 5.3 Traditional tensile properties

Sample	Modulus (GPa)	break strain (%)
Commercial PMMA	1.4	> 7
25% C20A - CO_2 made, melt pressed	7.5	< 0.1

5.6 Conclusions

Intercalated nanocomposites containing modified silicates in excess of 27 wt. % have been synthesized. These composites are synthesized using supercritical CO_2 as a reaction medium, eliminating the problems arising from the high viscosity of clay mixtures. At clay concentrations approaching 40 wt. %, the silicate morphology is homogeneous, with virtually the entire polymer volume present within the gallery spacing between silicates. Because the intercalated silicate structure is thermodynamically limited with regards to clay separation, high clay concentrations are required to achieve a homogeneous morphology. A simple model of the intercalated structure is used to estimate the amount of organically modified silicates required to

produce such a morphology. Using $scCO_2$, the problems associated with high viscosities characteristic of highly loaded polymers are circumvented. The $scCO_2$ is used to distribute the monomer homogeneously prior to polymerization. At clay concentrations above those predicted by the model, the intercalated gallery spacing collapses linearly as the system becomes starved for polymer.

The mechanical properties of the intercalated nanocomposites demonstrate true polymer-ceramic mechanical properties. The modulus of glassy PMMA with 40 wt. % OMLS is increased 50 % for an isotropic composite. Orientation through melt post-processing results in a 200 % increase in the tensile modulus, as measured in the DMTA. The strain at break for these hybrid materials, however, is low, consistent with properties dictated by the filler material.

CHAPTER 6

SUMMARY

6.1 Molecular-scale reinforcement

The effects of organophosphorous molecular additives on material properties are investigated. The focus is on characterization of both the physical properties of the reinforced material and the reinforcement itself. In this manner, molecular reinforcement, or antiplasticization, is described in terms of the physical response of the polymer matrix upon inclusion of the molecular additives. To broaden the scope of the study, the effects of additive chemistry and polymer network architecture are investigated. The additives used are based on the hydrogen-bond-accepting, strongly polar, phosphoryl functionality. By altering the chemistry surrounding the phosphate group, the effects of interaction strength, solubility, molecular weight and size on the fortification potential can be determined. The polymer matrix is based on a crosslinked, diepoxy thermoset. Using a variety of curing agents, the effects of matrix chemistry (anhydride-cured versus diamine-cured) and molecular weight between crosslinks (M_c) are determined.

The effectiveness of molecular fortification is largely dictated by the strength of the interaction between the additive and the polymer matrix. Because the mechanism for antiplasticization relies on a decrease or elimination in molecular mobility, decreasing the strength of this interaction reduces the range of antiplasticization as well as its intensity. Additionally, because the molecular mobility is effected only on a local scale, the molecular weight between crosslinks, M_c, can either amplify or dilute the degree of

antiplasticization. As a result, the thermosets with smallest M_c exhibit the highest degrees of fortification. Increasing the M_c dilutes the effect of the same additive. In the epoxy systems investigated, trimethyl phosphate added into an 825-PDA epoxy thermoset resulted in optimized mechanical reinforcement. The tensile modulus in this system is increased by 55 % while the failure strength increases 52 %. This level of reinforcement is attainable at 30 mol % (25 phr) incorporation of the additive.

The use of molecular additives for mechanical reinforcement has wide-ranging potential for materials applications. Using additives, rather than altering the chemistry of the polymer, is both cheaper and more easily instituted into existing systems. As described above, the diluents used in this study exhibit potential applications as diluent and flame retardants in addition to their effects on engineering performance. Future investigations may examine the applicability of related functionalities, including carbonyl- and sulfonyl-containing additives, for antiplasticization. In addition to potentially describing new chemical structures capable of molecular fortification, expanding the basic chemical structure of the additive opens the possibility of developing predictive models for antiplasticization based on chemical and physical constants.

6.2 Nanoscale reinforcement

Nanoscale reinforcement of polymers encompasses a new dimension to modifying the properties of a polymer at scales orders of magnitude smaller than traditional composite structures. In this study, polymer fracture toughening is described using the intercalated nanocomposite morphology. The intercalated morphology results in a degree of cooperation between individual nanoscale platelets, allowing a toughening mechanism that is unavailable to the exfoliated morphology in glassy polymers. The

mechanical properties of the intercalated nanocomposites are described in terms of the microscale and nanoscale morphology of these materials. A fully intercalated morphology, wherein the entire composite volume is modified, is described. Traditional synthetic techniques are unable to achieve clay concentrations which would result in such a homogeneously intercalated morphology. To this end, a novel synthetic approach using supercritical carbon dioxide ($scCO_2$) was developed. This route can be used to produce nanocomposites approaching 50 % clay concentrations. The technique is described in terms of the variety of morphologies and nanostructures which can be produced. Order, and orientation, can be achieved *in situ* through consolidation during processing, or through post-synthesis melt pressing. The latter technique results in high degrees of nematic order of the silicates. These structures then exhibit true polymer-ceramic hybrid mechanical properties. The tensile modulus for a 25 wt. % clay composite is enhanced by 200-400 % over commercial PMMA, although the strain to failure decreases from 7 % to 0.1 %.

Manufacturing composite materials incorporating high concentrations of clay filler expands more than just the scope of our understanding of nanocomposites. The silicates used as reinforcing agents can potentially be used to examine theoretical predictions of microcracked bodies. As discussed in Section **1.4.2**, microcracks can be arranged such that the overall stress-intensity factor of the material is shielded or amplified. Intercalated nanocomposites ordered into nematic arrays can be used to experimentally investigate this potential for interaction as a toughening mechanism. The work described in this dissertation introduces methods of developing this types of materials.

APPENDIX

SEQUENTIAL LAYER-BY-LAYER DEPOSITION

A.1 Introduction

A number of techniques were used over the course of this investigation into nanoscale reinforcement of polymers in an attempt to produce materials which exhibit order at the nanometer scale. As discussed in Chapter 5, the viscosity of highly filled polymers makes processing difficult. One of the techniques which was investigated, but ultimately proven unsuccessful in producing the desired materials, is described herein. Although the layer-by-layer technique is appropriate for synthesizing materials of a well-ordered repeating architecture, this structure is incapable of supporting the number of repeat units (over 200) which are necessary to obtain useful measurements of bulk material and mechanical properties.

Layer-by-layer (LBL) deposition of polymers has been demonstrated in numerous systems incorporating both organic and inorganic materials into the deposition cycles.[102-104] The technique is one of several resulting in self-assembly of polymers onto a surface. LBL of polymer-silicate complexes was first reported by Kleinfeld and Ferguson[105] as a method to produce multilayers of high order in a repeating manner. A number of other investigations have probed this technique for morphological control,[106] kinetics,[107] and applicability to a number of different polymer systems.[108] It was therefore thought that LBL was a good candidate for an automated method for producing multilayers of, at least, microscopic dimensions.

By using LBL to sheath a polymeric fiber (Figure A.1) or coat a substrate, the mechanical integrity of the multilayers can be investigated. It is known that the

multilayers formed through LBL deposition result in a stack of alternating polymer-clay layers with a d-spacing of approximately 2.4 nm. The perfectly alternating architecture allows the silicates to collaborate in a reinforcing mechanism. Due to the high modulus of aluminosilicates, multilayer sheating of a fiber can lead to improved compressive stiffness of the modified fibers. The high aspect ratio of the clays can also be employed to improve barrier properties, as the diffusion path through the sheath is made highly tortuous.

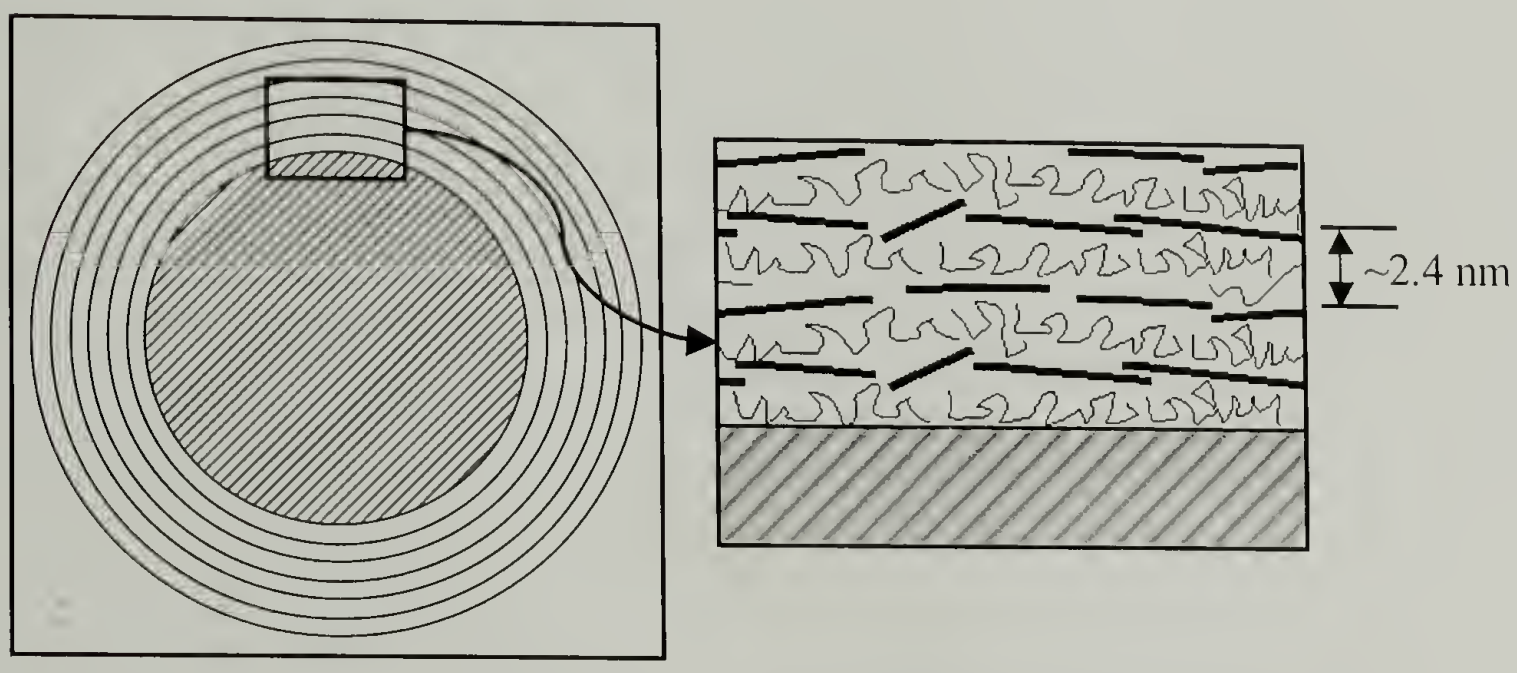

Figure A.1 Representation of alternating layers of polymer and silicate on the surface of a coated fiber.

A.1.1 Experimental

The polymer substrate used is poly(ethylene terephthalate), PET (Figure A.2). The PET substrate has the advantage of being easily hydrolyzed to form carboxylic acids and alcohols along the surface (Figure A.3).[109,110] At sufficiently high pH, the carboxylic acids can support a negative charge (PET-CO_2^-), enhancing the strength of the substrate-first layer interaction with a cationic polyelectrolyte. The PET substrate, either fiber or film, was hydrolyzed at 60 °C for 15 minutes in 1 M aqueous NaOH.

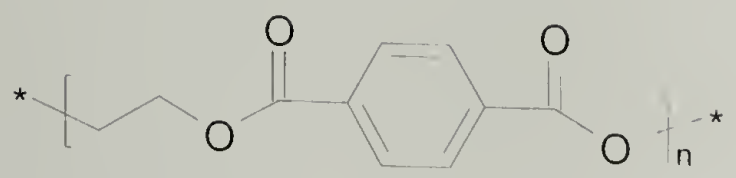

Figure A.2 Poly(ethylene terephthalate).

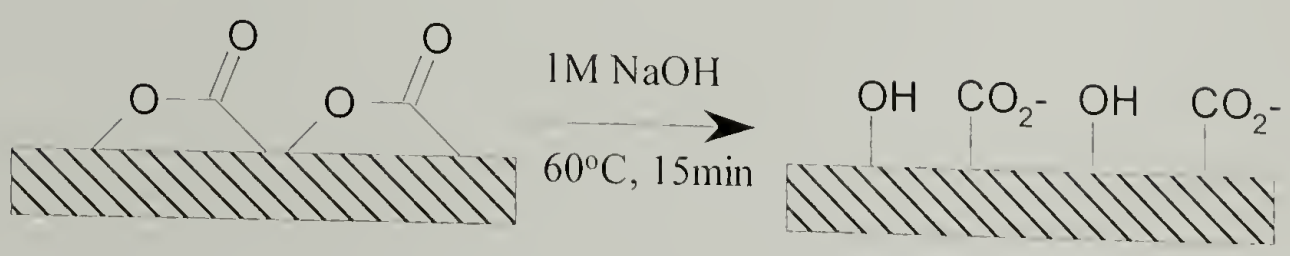

Figure A.3 Hydrolysis of PET surface resulting in a substrate that is negatively charged at pH 9 and above. This substrate is then more conducive to depositing an initial layer of cationic polyelectrolyte.

The polyelectrolyte used was cationic poly(diallyldimethylammonium) chloride, PDDA (Figure A.4). The PDDA, a 20 wt. % aqueous solution, was obtained from Aldrich. This solution was diluted to 0.2 wt. % and adjusted to pH = 9 using 0.1 M NaOH. Unmodified montmorillonite was obtained from the University of Missouri Source Clay Minerals Repository. The clays were suspended in water at 2 % by weight clay and allowed to settle for 24 hours. The supernatant, with most large impurities removed through sedimentation, was then centrifuged to result in a fine suspension of clays of approximately 0.2 wt. % as determined gravimetrically. This final suspension is very stable, with little sedimentation evident after as long as six months.

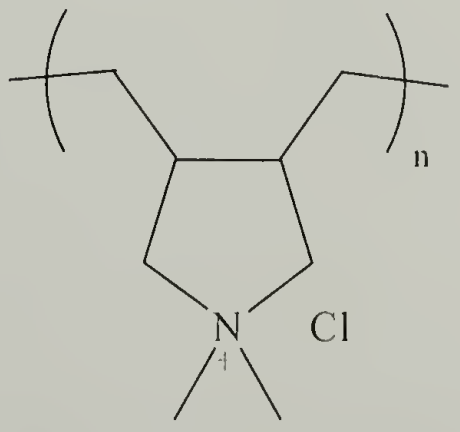

Figure A.4 Poly(diallyldimethylammonium) chloride (PDDA).

Multilayer synthesis was completely automated, as represented in Figure A.5. A motor was made to propagate the fiber or film through a number of aqueous solutions. The PET-substrate progression allowed for submersion of the polymer into, first, a solution of PDDA polyelectrolyte. The substrate was then washed in a continuously replenished water bath to remove excess polyelectrolyte, and dried under a nitrogen stream. Next, the polymer was introduced to the silicate suspension and again washed and dried. The polymer was submerged in each bath for approximately 30 seconds and a complete cycle was approximately six minutes, depending on the speed of the motor drive and the length of the polymer fiber or film. Once the polymer progression was established, the motor drive was able to maintain a stable velocity.

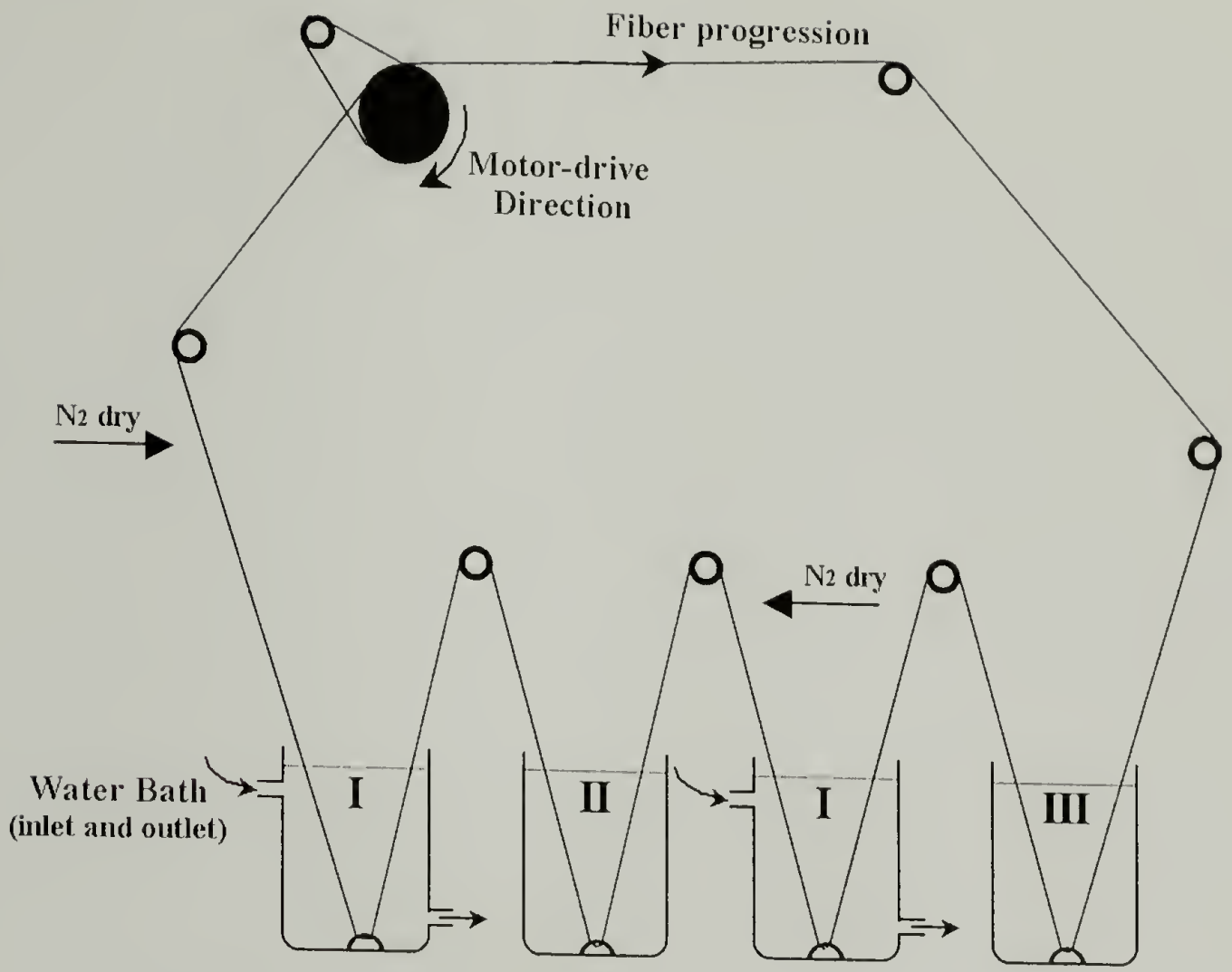

Figure A.5 Schematic of layer-by-layer deposition onto polymer fiber or film. Direction of fiber progression is represented by arrows. The aqueous baths at bottom contain (I) reverse osmosis water, (II) a 0.2 wt. % suspension of Na-montmorillonite in water and (III) a 0.2 wt. % aqueous solution of PDDA.

A.I.2 Fiber-surface morphology

Initially, fiber modification was investigated. It is thought that sheathing of a fiber with a high modulus material such as the silicate platelets may lead to potential enhancements in the compressive strength of the polymer fibers. Fiber-reinforced polymer composites have been shown to fail through cooperative buckling of the fibers under compression. This buckling, as described by Timoshenko[3] is then a function of the shear modulus, G_m, of the matrix and not affected by the properties of the fiber:

$$\sigma_c = \frac{G_m}{1-f} \qquad \text{Eq. A.1}$$

where f is the volume fraction of fiber and σ_c is its compressive strength of the composite. However, if the fiber can be made to resist buckling, the compressive strength of a fiber-reinforced composite may also be made to increase. The critical stress for fiber buckling, as described by Euler, is:

$$\sigma_c = \frac{E_f \pi^2 r^2}{L^2} \qquad \text{Eq. A.2}$$

where E_f is the fiber modulus, r is its radius and L is the fiber length capable of buckling. Eq. A.2 is valid for single-mode buckling, although expansions for this equation exist which take into account multiple buckling modes. The compressive strength of a fiber can be increased by either increasing its modulus or moment of inertia. Sheathing of a fiber with a high-modulus coating and thereby increasing its radius accomplishes both.

Fiber modification is verified using SEM. This technique allows for characterization of a new surface morphology as well as changes in fiber diameter. The surface features of an untreated PET fiber are seen in Figure A.6. Following a 60-deposition cycle, Figure A.7, there is a noticeable difference in the surface of the now-treated fiber. However, there is little change in the fiber diameter indicating that although deposition onto the fiber surface is occurring, a 60-deposition cycle has not resulting in 60 repeat layers of deposition. Fiber progressions approaching 200 cycles continue to exhibit no change in the fiber diameter, although a 1 μm increase would be expected. These observations lead to the qualitative conclusion that the multilayers deposited through LBL are subject to mechanical removal (rubbing off) as the fiber is wound around the motor drive, which consists of a number of pulleys and a rubber shaft. This

conclusion is supported through visual observation of clay being deposited onto the rubber shaft.

Figure A.6 Surface of untreated PET fiber exhibiting few features.

Figure A.7 PET fiber subjected to approximately 60 deposition cycles. There is evidence of deposition on the surface but none of an increase in fiber diameter.

Single-filament tests of the modified PET fibers do not exhibit any enhancement in mechanical properties of the fibers (Figure A.8). Representative stress-strain curves for the modified fiber in comparison with an untreated PET fiber exhibits only a lack of

micro-neeking as the filament is strained. This result, however, is likely only a result of the fiber surface being evened out as it progresses through the LBL-apparatus, eliminating features whieh may lead to stress eoncentrations and local yielding.

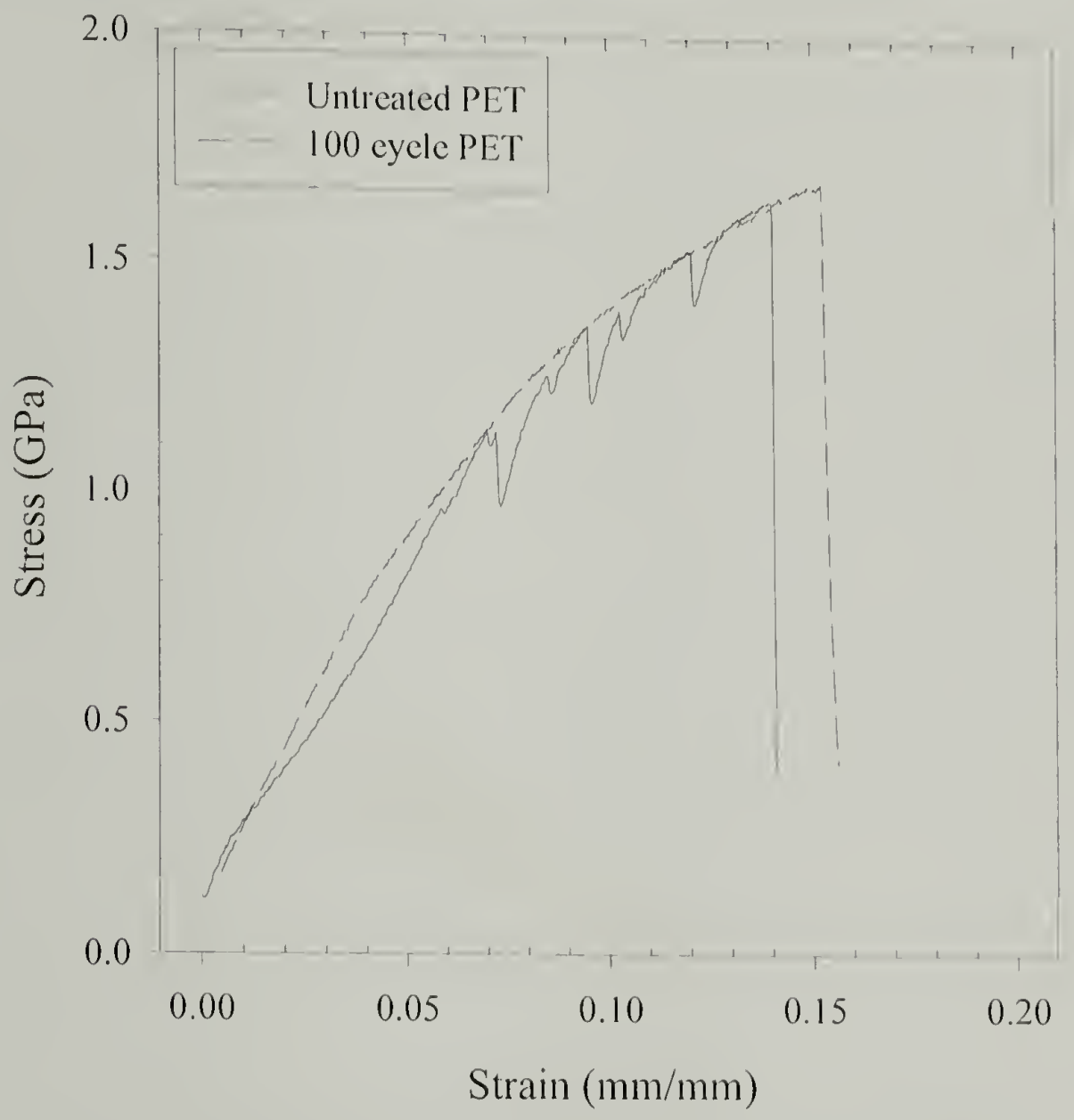

Figure A.8 Representative single-filament tests of modified and unmodified PET fibers.

A.1.3 Film-surfaee morphology

To eliminate the possibility that the fiber drive train is responsible for the laek of surface treatment, PET films were substituted. A fiber, as it progresses through spaee, is effeetively a one-dimensional objeet. In the case of the PET fibers, there is no opportunity to limit the eontaet between fiber and drive train to a single surfaee. This is

possible in the case of a film, however, such that only one surface is ever exposed to friction at the rubber shaft, while the other is free to be modified.

In examining the film surfaces, it is obvious that LBL deposition results in significant modification (Figure A.9). The surfaces, however, are not smooth, but opaque to visual examination and appear scaly under SEM. In examining the deposited-film thickness, the PET is viewed edge-on (Figure A.10). This view reveals the presence of a two-layer architecture on the PET substrate (at bottom of the micrograph). A thin layer is evident, covered by a thick, covering layer. Because this thick layer does not exhibit any diffraction patterns in SAXS, it is assumed that the thick layer of material deposited onto the substrate is an amorphous gel. A similar structure can be produced by mixing a clay suspension with a PDDA solution and evaporating. The two electrolytes, thus, self-assemble in a disordered fashion. Observation of the deposition cycles reveals that the film surface becomes opaque after approximately 20 cycles, indicating a disordered assembly onto the substrate.

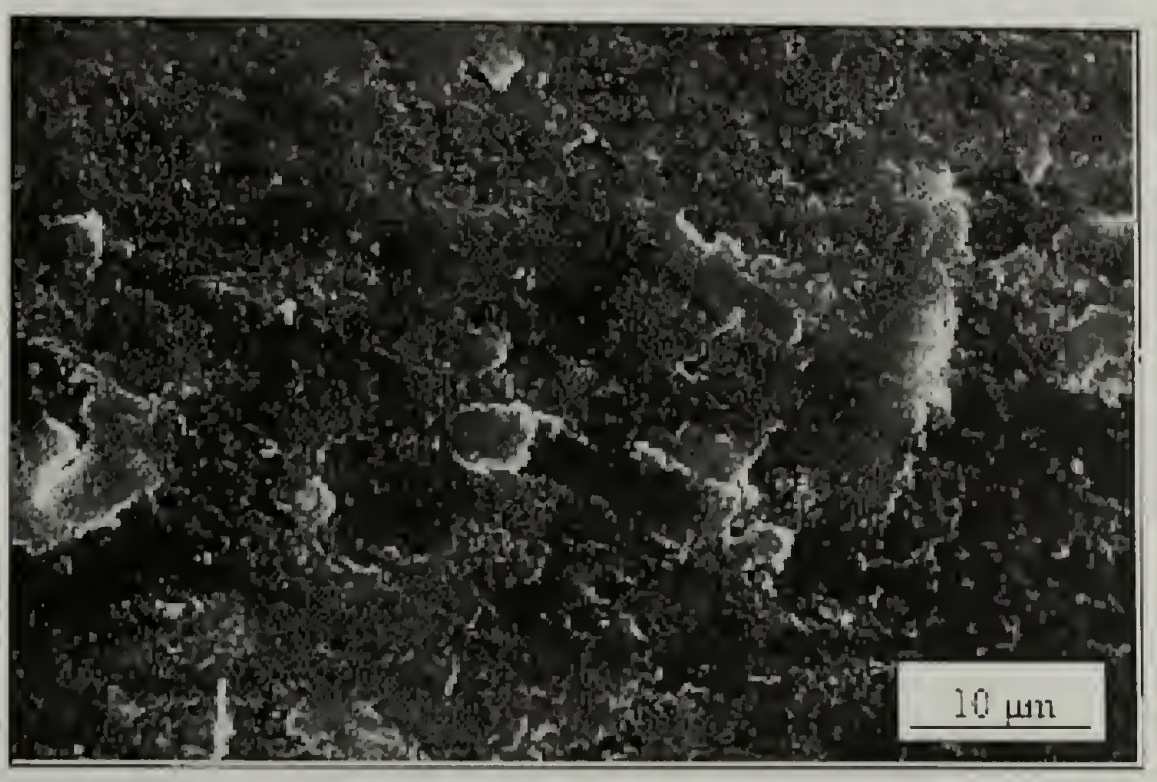

Figure A.9 Top-down view of PET film subjected to approximately 120 deposition cycles.

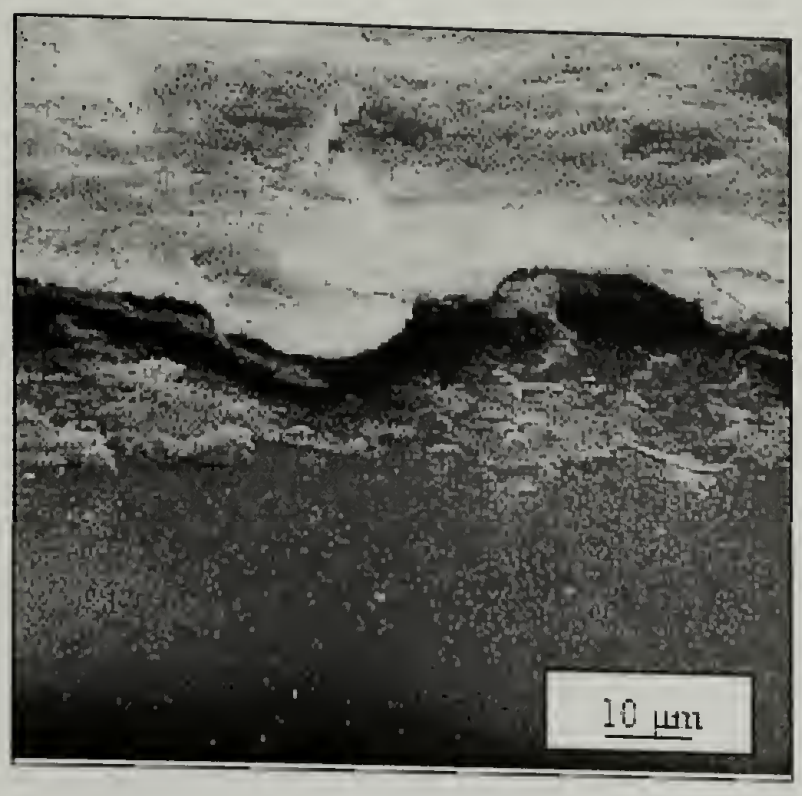

Figure A.10 Off-angle view of PET film subjected to 120 deposition cycles. A thin layer is visible beneath a thick layer of amorphous gel.

The formation of the amorphous gel is a result of incomplete charge negation during the LBL process. X-ray photoelectric spectroscopy (Figures A.11 and A.12) reveals a higher than expected concentration of silicate in the top portions of multilayer (Table A.1). As a result, it is unlikely that the structure of the film can be represented as an ideal alternating layer structure as depicted in Figure A.1. Rather, a significant amount of disorder is being introduced in the film. It is unknown whether this disordered layer formation is a result of the automation process, where the substrate is in constant motion, causing perturbations in the solutions as alternating layers are deposited. The result of this small disorder in the layer structure, however, is that each additional cycle adds to the imperfect order. Eventually it is not possible for the system to support even a layered architecture and the anionic silicates complex with the cationic polyelectrolyte to form gels that collapse upon drying.

Table A.1 Atomic composition of hydrolyzed and LBL-modified PET films as measured by XPS.

		Predicted		*Measured*	
		15°	75°	15°	75°
Hydrolyzed PET	*C*	62.5%	62.5%	60%	60%
	O	37.5%	37.5%	40%	40%
	Si	N/A	N/A	N/A	N/A
	Al	N/A	N/A	N/A	N/A
LBL Film	*C*	67%	50%	48%	35%
	O	23%	35%	35%	40%
	Si	6%	11.5%	13.6%	18%
	Al	2.7%	5%	3.7%	8%

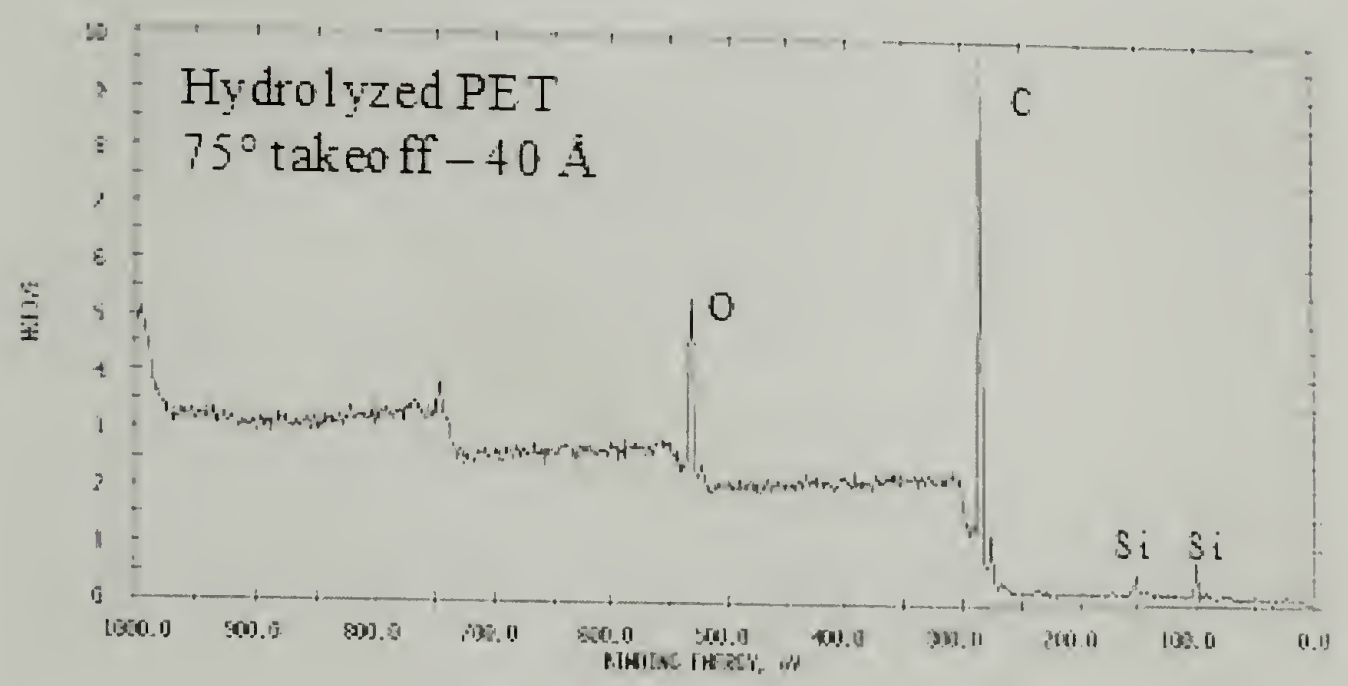

Figure A.11 X-ray photoelectron spectroscopy (XPS) spectrum of hydrolyzed PET. 75° takeoff angle, probing the top 40 Å of the substrate surface.

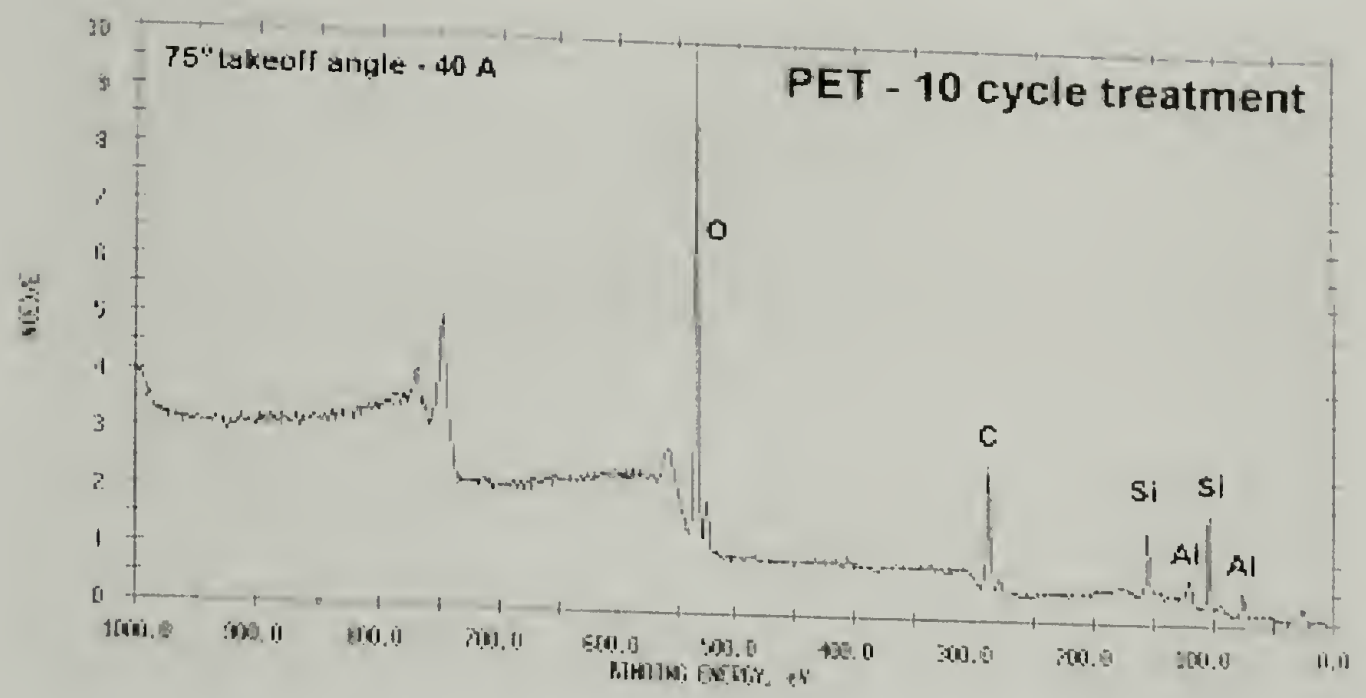

Figure A.12 XPS spectrum of PET film following ten deposition cycles. 75° takeoff angle, probing the top 40 Å of the substrate surface.

A.2 Conclusions

An attempt at implementing an automated LBL process for producing highly ordered intercalated silicate structures is described. The LBL deposition technique is often reported as a method for synthesizing multilayers of alternating charged species. In this investigation, however, the LBL technique is unable to support an ordered structure above approximately 20 repeat cycles. Instead, an amorphous gel is formed as the top surface becomes increasing disordered. The multilayers also demonstrate an inability to adhere strongly to each other as evidenced by the deposition of silicates onto the rubber drive shaft used to propel the PET-fiber substrate.

BIBLIOGRAPHY

(1) Christensen, R. M. *Mechanics of composite materials*; John Wiley & Sons: New York, 1979.

(2) Swanson, S. R. *Introduction to design and analysis with advanced composite materials*; Prentice Hall: Upper Saddle River, NJ, 1997.

(3) Timoshenko, S. P.; Gere, J. M. *Theory of Elastic Stability*; McGraw-Hill: NY, 1961.

(4) Pearson, R. A. In *Rubber Toughened Plastics*; Riew, C. K., Ed.; American Chemical Society: Washington, DC, **1993**; pp 405-425.

(5) Pearson, R. A.; Yee, A. F. *J. Mater. Sci.* **1991**, *26*, 3828-3844.

(6) Wu, S. *Polymer* **1985**, *24*, 43-46.

(7) Argon, A. S.; Cohen, R. E.; Mower, T. M. *Mater. Sci. Eng. A-Struct. Mater. Prop. Microstruct. Process*. **1994**, 176, 79-90.

(8) Bucknall, C. B.; Karpodinis, A.; Zhang, X. C. *J. Mater. Sci.* **1994**, *29*, 3377-3383.

(9) Sultan, J. N.; McGarry, F. J. *Polym. Eng. Sci.* **1973**, *13*, 29-34.

(10) Irwin, G. R. *Appl. Mat. Res.* **1964**, *3*, 65-81.

(11) Schroeder, L. R.; Cooper, S. L. *J. Appl. Polym. Sci.* **1976**, *47*, 4310-4317.

(12) Gillis, P. P. *J. Polym. Sci. A: Polym. Chem.* **1969**, *7*, 783-794.

(13) Jackson, W. J.; Caldwell, J. R. *J. Appl. Polym. Sci.* **1967**, *11*, 227-244.

(14) Jackson, W. J.; Caldwell, J. R. *J. Appl. Polym. Sci.* **1967**, *11*, 221-226.

(15) Makaruk, L.; Polanska, H.; Mizerski, T. *J. Appl. Polym. Sci.* **1979**, *23*, 1935-1942.

(16) Don, T. M.; Bell, J. P.; Narkis, M. *Polym. Eng. Sci.* **1996**, *36*, 2601-2613.

(17) Gupta, M. K.; Ripmeester, B.; Carlsson, D. J.; Wiles, D. M. *J. Polym. Sci. Polym. Lett. Ed.* **1983**, *21*, 211-215.

(18) Shuster, M.; Narkis, M.; Siegmann, A. *Polym. Eng. Sci.* **1994**, *34*, 1613-1618.

(19) Anderson, S. L. *Macromolecules* **1995**, *28*, 2944-2954.

(20) Mascia, L. *Polymer* **1978**, *19*, 325-328.

(21) Brous, S. L.; Semon, W. L. *Ind. Eng. Chem.* **1935**, 667-672.

(22) Sears, J.K.; Darby, J.R. *The technology of plasticizers*; Wiley: New York, 1982.

(23) Haldankar, G.; Shockey, E.; Garton, A. *Polym. Mater. Sci. Eng. Proc. ACS Div. Polym. Mater. Sci. Eng.* **1990**, *62*, 120-124.

(24) Daly, J.; Britten, A.; Garton, A. *J. Appl. Polym. Sci.* **1984**, *29*, 1403-1414.

(25) Khozin, V. G.; Farrakhov, A. G.; Voskresenskii, V. A. *Poly. Sci. U.S.S.R.* **1979**, *21*, 1757-1765.

(26) Shi, J. F.; Inglefield, P. T.; Jones, A. A.; Meadows, M. D. *Macromolecules* **1996**, *29*, 605-609.

(27) Heux, L.; Halary, J. L.; Laupretre, F.; Monnerie, L. *Polymer* **1997**, *38*, 1767-1778.

(28) Maeda, Y.; Paul, D. R. *J. Polym. Sci. B: Polym. Phys.* **1987**, *25*, 981-1003.

(29) Maeda, Y.; Paul, D. R. *J. Polym. Sci. B: Polym. Phys.* **1987**, *25*, 957-980.

(30) Vrentas, J. S.; Duda, J. L.; Ling, H.-C. *Macromolecules* **1988**, *21*, 1470-1475.

(31) Ruiz-Trevino, F. A.; Paul, D. R. *J. Polym. Sci. B: Polym. Phys.* **1998**, *36*, 1037-1050.

(32) Sears, J. K.; Darby, J. R. *The technology of plasticizers*; Wiley: New York, 1982.

(33) Zerda, A. S.; Lesser, A. J. *J. Appl. Polym. Sci.* **2001**, *84*, 302-309.

(34) Pinnavaia, T. J.; Lan, T. *Chem. Mat.* **1994**, *6*, 2216-2219.

(35) Giannelis, E. P.; Messersmith, P. B. *Chem. Mat.* **1994**, *6*, 1719-1725.

(36) Usuki, A.; Kojima, Y.; Kawasumi, M.; Okada, A.; Fukushima, Y.; Kurauchi, T.; Kamigaito, O. *J. Mater. Res.* **1993**, *8*, 1179-1184.

(37) Usuki, A.; Kojima, Y.; Kawasumi, M.; Okada, A.; Fukushima, Y.; Kurauchi, T.; Kamigaito, O. *J. Mater. Res.* **1993**, *8*, 1185-1189.

(38) Yano, K.; Usuki, A.; Okada, A.; Kurauchi, T.; Kamigaito, O. *J. Polym. Sci. Pol. Chem.* **1993**, *31*, 2493-2498.

(39) Giannelis, E. P.; Vaia, R. A.; Jandt, K. D.; Kramer, E. J. *Macromolecules* **1995**, *28*, 8080-8085.

(40) Pinnavaia, T. J.; Wang, Z. *Chem. Mat.* **1998**, *10*, 3769-3771.

(41) Wei, K. H.; Chen, T. K.; Tien, Y. I. *Polymer* **2000**, *41*, 1345-1353.

(42) Usuki, A.; Kawasumi, M.; Hasegawa, N.; Kato, M.; Okada, A. *Macromolecules* **1997**, *30*, 6333-6338.

(43) Giannelis, E. P.; Bergman, J. S.; Chen, H.; Thomas, M. G.; Coates, G. W. *Chem. Commun.* **1999**, *21*, 2179-2180.

(44) Giannelis, E. P.; Krishnamoorti, R.; Vaia, R. A. *Chem. Mat.* **1996**, *8*, 1728-1734.

(45) Qi, Z. N.; Zhang, G. Y.; Yi, G. Z.; Wu, L. H.; Xu, X.; Song, Q.; Yang, Y.; Jin, J.; Zhong, S. F. *Acta Polym. Sin.* **1999**, *3*, 309-314.

(46) Lee, A.; Lichtenhan, J. D. *J. Appl. Polym. Sci.* **1999**, *73*, 1993-2001.

(47) Pinnavaia, T. J.; LeBaron, P. C.; Wang, Z. *Appl. Clay Sci.* **1999**, *15*, 11-29.

(48) Berglund, L. A.; Kornmann, X.; Sterte, J. *Polym. Eng. Sci.* **1998**, *38*, 1351-1358.

(49) Chin, I. J.; Thurn-Albrecht, T.; Kim, H. C.; Russell, T. P.; Wang, J. *Polymer* **2001**, *42*, 5947-5952.

(50) Kachanov, M. In *Advances in Applied Mechanics*; Hutchinson, J. W., Wu, T. Y., Eds.; Academic Press, Inc.: Boston, 1994; Vol. 30.

(51) Jones, N. A.; Lesser, A. J. *J. Polym. Sci. B: Polym. Phys.* **1998**, *36*, 2751-2760.

(52) Heux, L.; Laupretre, F.; Halary, J. L.; Monnerie, L. *Polymer* **1998**, *39*, 1269-1278.

(53) Merritt, M. E.; Goetz, J. M.; Whitney, D.; Chang, C. P. P.; Heux, L.; Halary, J. L.; Schaefer, J. *Macromolecules* **1998**, *31*, 1214-1220.

(54) McLean, P. D.; Scott, R. F.; Garton, A. *Br. Polym. J.* **1983**, *15*, 66-70.

(55) Don, T. M.; Yeh, C. H.; Bell, J. P. *J. Appl. Polym. Sci.* **1999**, *74*, 2510-2521.

(56) Nanasawa, A.; Takayama, S.; Takeda, K. *J. Appl. Polym. Sci.* **1997**, *66*, 2269-2277.

(57) Walters, R. N.; Lyon, R. E. *Int SAMPE Symp Exhib* **1997**, *42*, 1335-1344.

(58) Westmoreland, P. R.; Inguilizian, T.; Rotem, K. *Thermochim. Acta* **2001**, *367*, 401-405.

(59) Brandrup, J.; Immergut, E. H., Eds. *Polymer Handbook*; 3rd ed.; John Wiley & Sons: New York, NY, 1989.

(60) Wurstlin, F.; Klein, H. *Makromolek. Chem.* **1955**, *16*, 1-9.

(61) Stickney, P. B.; Cheyney, L. E. *J. Polym. Sci* **1948**, *3*, 231-244.

(62) Dimarzio, E. A.; Gibbs, J. H. *J. Polym. Sci. Part A: Polym. Chem.* **1963**, *1*, 1417-1428.

(63) Ritehie, P. D., Ed. *Plasticizers, stabilizers and Fillers*; Iliffe Books, Ltd.: London, 1972.

(64) van Krevelen, D. W. *Properties of Polymers*; Elsevier Science Publ.: New York, 1990.

(65) Wang, C. S.; Lin, C. H. *J. Appl. Polym. Sci.* **2000**, *75*, 429-436.

(66) Wang, C. S.; Lin, C. H. *J. Polym. Sci. Pol. Chem.* **1999**, *37*, 3903-3909.

(67) Liu, Y. L.; Hsiue, G. H.; Chiu, Y. S. *J. Polym. Sci. Pol. Chem.* **1997**, *35*, 565-574.

(68) Liu, Y. L.; Hsiue, G. H.; Lee, R. H.; Chiu, Y. S. *J. Appl. Polym. Sci.* **1997**, *63*, 895-901.

(69) Derouet, D.; Morvan, F.; Brosse, J. C. *J. Appl. Polym. Sci.* **1996**, *62*, 1855-1868.

(70) Sankaran, K.; Vidya, V.; Viswanathan, K. S.; George, L.; Singh, S. *J. Phys. Chem. A* **1998**, *102*, 2944-2953.

(71) Wolfenden, R.; Williams, R. *JACS* **1983**, *105*, 1028-1031.

(72) Mateva, R. P.; Dencheva, N. V. *J. Appl. Polym. Sci.* **1993**, *47*, 1185-1192.

(73) Liu, Y. L.; Hsiue, G. H.; Chiu, Y. S.; Jeng, R. J.; Perng, L. H. *J. Appl. Polym. Sci.* **1996**, *61*, 613-621.

(74) Crawford, E.; Lesser, A. J. *J. Polym. Sci. Part B: Polym. Phys.* **1998**, *36*, 1371-1382.

(75) Kinloeh, A. J.; Williams, J. G. *J. Mater. Sci.* **1980**, *15*, 987-996.

(76) IUPAC *Pure Appl. Chem.* **1999**, *71*, 645-718.

(77) Flory, P. J. *Principles of Polymer Chemistry*; Cornell Univ. Press: Ithaea, NY, 1953.

(78) Lesser, A. J.; Kody, R. S. *J. Polym. Sci. B: Polym. Phys.* **1997**, *35*, 1611-1619.

(79) Lesser, A. J.; Crawford, E. *J. Appl. Polym. Sci.* **1997**, *66*, 387-395.

(80) Bellenger, V.; Morel, E.; Verdu, J. *J. Appl. Polym. Sci.* **1989**, *37*, 2563-2576.

(81) Sherman, L. M. In *Plastics Technology*, 1999; Vol. 45, pp 52-57.

(82) Lagaly, G. *Appl. Clay Sci.* **1999**, *15*, 1-9.

(83) Carrado, K. A. *Appl. Clay Sci.* **2000**, *17*, 1-23.

(84) Carrado, K. A.; Langqiu, X. *Chem. Mat.* **1998**, *10*, 1440-1445.

(85) Vaia, R. A.; Giannelis, E. P. *Macromolecules* **1997**, *30*, 8000-8009.

(86) Yee, A. F.; Sue, H. J. *J. Mater. Sci.* **1993**, *28*, 2975-2980.

(87) Pinnavaia, T. J.; Massam, J.; Wang, Z.; Lan, T.; Beall, G. *Abstr. Pap. Am. Chem. Soc.* **1998**, *215*, 206-208.

(88) Rosen, B. W. In *Fiber Composite Materials*; American Society for Metals: Metals Park, OH, 1987; pp 37-75.

(89) Weaver, C. E.; Pollard, L. D. *The Chemistry of Clay Minerals, v. 15*; Elsevier Scientific: New York, NY, 1973.

(90) Desimone, J. M.; Kendall, J. L.; Canelas, D. A.; Young, J. L. *Chemical Reviews* **1999**, *99*, 543-563.

(91) Shieh, Y.-T.; Su, J.-H.; Manivannan, G.; Lee, P. H. C.; Sawan, S. P.; Spall, W. D. *J. Appl. Polym. Sci.* **1996**, *59*, 707-717.

(92) Hobbs, T.; Lesser, A. J. *Polym. Eng. Sci.* **2001**, *41*, 135-144.

(93) Hobbs, T.; Lesser, A. J. *J. Polym. Sci. B: Polym. Phys.* **1999**, *37*, 1881-1891.

(94) Caskey, T. C.; Lesser, A. *J. Polym. Eng. Sci.* **2001**, *41*, 2259-2265.

(95) Watkins, J. J.; McCarthy, T. J. *Macromolecules* **1994**, *27*, 4845-4847.

(96) Watkins, J. J.; McCarthy, T. J. In *Polym. Mater. Sci. Eng. Proc. ACS Div. Polym. Mater. Sci. Eng.*: Chicago, IL, 1995; Vol. 73, p 158.

(97) Kung, E.; Lesser, A. J.; McCarthy, T. J. *Macromolecules* **1998**, *31*, 4160-4169.

(98) Vogt, B. D.; Brown, G. D.; Ramachandra, R.; S., V.; Watkins, J. J. *Macromolecules* **1999**, *32*, 7907-7912.

(99) Kumar, V.; Holl, M. R.; Garbini, J. L.; Murray, W. R. *J. Mater. Sci.* **1999**, *34*, 637-644.

(100) Wu, W.-L.; Orts, W. J.; van Zanten, J. H.; Fanconi, B. M. *J. Polym. Sci. B: Polym. Phys.* **1994**, *32*, 2475-2480.

(101) Fernandez, M. L.; Higgins, J. S.; Penfold, J.; Shackleton, C. S. *Poly. Comm.* **1990**, *31*, 124-127.

(102) Decher, G. In *Polymeric Materials Encyclopedia: Synthesis, Properties, and Applications*; Salamone, J. C., Ed.; CRC Press: Boca Raton, FL, 1996; Vol. 6, p 4540.

(103) Decher, G.; Hong, J. D.; Schmitt, J. *Thin Solid Films* **1992**, *210*, 831-835.

(104) Lvov, Y.; Decher, G.; Mohwald, H. *Langmuir* **1993**, *9*, 481-486.

(105) Kleinfeld, E. R.; Ferguson, G. S. *Science* **1994**, *265*, 370-373.

(106) van Duffel, B.; Schoonheydt, R. A.; Grim, C. P. M.; De Schryver, F. C. *Langmuir* **1999**, *15*, 7520-7529.

(107) Kotov, N. A.; Haraszti, T.; Turi, L.; Zavala, G.; Geer, R. E.; Dekany, I.; Fendler, J. H. *JACS* **1997**, *119*, 6821-6832.

(108) Fendler, J. H. *Chem. Mat.* **1996**, *8*, 1616-1624.

(109) Phuvanartnuruks, V.; McCarthy, T. J. *Macromolecules* **1998**, *31*, 1906-1914.

(110) Chen, W.; McCarthy, T. J. *Macromolecules* **1997**, *30*, 78-86.